University of Wollongong Theses Collection

University of Wollongong *Year* 2007

Investigation of the factors influencing the wettability of conducting polymers for fluid control in microfluidic devices

Jenny Halldorsson
University of Wollongong

INVESTIGATION OF THE FACTORS INFLUENCING THE WETTABILITY OF CONDUCTING POLYMERS FOR FLUID CONTROL IN MICROFLUIDIC DEVICES

A thesis submitted in fulfilment of the

requirements for the award of the degree

DOCTOR OF PHILOSOPHY

from

UNIVERSITY OF WOLLONGONG

by

JENNY HALLDORSSON, BSc (Hons)

DEPARTMENT OF CHEMISTRY

August, 2007

CERTIFICATION

I, Jennifer A. Halldorsson, declare that this thesis, submitted in fulfilment of the requirements for the award of Doctor of Philosophy, in the Department of Chemistry at the University of Wollongong, is wholly my own work unless otherwise referenced or acknowledged. The document has not been submitted for any qualifications at any other academic institution.

Jenny Halldorsson

August 2007

ACKNOWLEDGEMENTS

I would like to thank my supervisors, Prof. Geoff Spinks and Prof. Gordon Wallace, for their guidance, insight and support throughout the course of this project. The assistance of Prof. Peter Innis, Prof. Hugh Brown and Prof. Dermot Diamond with different areas of this project is also gratefully acknowledged.

I greatly appreciate the contributions of Dr. Yanzhe Wu, Dr. Shannon Stitzel, Sarah Brady and Ciarán Smyth in the laboratories of the National Centre for Sensor Research, Dublin City University, Ireland, to the fluid movement component of this study.

The assistance of Dr. Philip Whitten with AFM measurements, Dr. George Tsekouras and Adrian Gestos with SEM measurements, Mr. Greg Tillman with optical microscopy and thickness measurements and Mr. Adam Joyce in the laboratories of Prof. Deb Kane at Macquarie University with optical profilometry measurements is much appreciated. I would like to thank Dan Halldorsson for his help with many of the diagrams in this thesis.

My colleagues and friends at the Intelligent Polymer Research have offered help and support over the past seven years I have been a part of the group. In particular, I would like to thank Shannon Little, Adrian Gestos, Scott McGovern, Brianna Thompson, Jakub Mazurkiewicz, Carol Lynam, Magnus Gustavsson, Kaylene Atkinson and Fletcher Thompson for many helpful and interesting discussions, assistance with proof-reading and making my time in IPRI extremely enjoyable and memorable.

The financial support provided by the Australian Research Council in the form of an Australian Postgraduate Award and by Prof. Gordon Wallace for my PhD scholarship is gratefully acknowledged.

I would also like to thank Kaye Lowe and Robert Ashby for the enthusiasm and passion for learning they instilled in me.

Finally, the unending and loving support of my husband Dan, my parents, sisters and my friends has meant so much to me. Thank you.

PUBLICATIONS

Causley, J. A., Stitzel, S., Brady, S., Diamond, D. and Wallace, G. G. Electrochemically-induced fluid movement using polypyrrole, *Synthetic Metals,* 151 (2005) 60–64.

CONFERENCE PRESENTATIONS

Halldorsson, J. A., Spinks, G. M., Brown, H. and Wallace, G. G. Investigation of contact angle, wettability and surface energy of polyterthiophenes for fluid control in microfluidic devices. *Higher Degree Research Students Conference* (oral presentation), University of Wollongong, Wollongong, Australia, 2006.

Causley, J. A., Spinks, G. M. and Wallace, G. G. Investigation of conducting polymers for fluid control in microfluidic systems. *Connect* (oral presentation), Sydney, Australia, 2005.

Causley, J. A., Spinks, G. M., Diamond, D. and Wallace, G. G. Fluid control in microfluidic devices using polypyrrole. *Gordon Research Conference on The Physics and Chemistry of Microfluidics* (poster presentation), Magdlen College, Oxford, United Kingdom, 2005.

ABSTRACT

The advent of miniaturised analytical systems has the potential to revolutionise the way in which chemical and biological analyses are made, due to the benefits of reduced reagent consumption, increased sensitivity and decreased analysis times. With increasingly smaller device dimensions comes the need for more efficient methods of controlling fluid flow on the microscale. Electrokinetic techniques, such as electrophoresis and electroosmosis, are well suited for delivering analytes and reagents in microfluidic devices, however high driving voltages and power requirements limit the size to which the device may be miniaturised and thus limit the applicability of these flow control methods for portable, hand-held devices. In order to overcome this limitation, an elegant use of surface tension forces which dominate at the microscale is necessary.

Conducting organic polymers, such as polythiophene and polypyrrole, have found widespread use in recent years due to their attractive mechanical properties and processability, in addition to their ability to be reversibly switched between oxidised (conducting) and reduced (insulating) forms. This redox switching may be accompanied by a change in polymer properties such as wettability and surface energy which may be altered dramatically upon external stimulation, commonly in the form of a small applied electrical potential.

The effect of redox switching upon conducting polymer wettability for fluid control in microfluidic devices is the central theme which was explored in this thesis. In particular, the aims of this thesis were to characterise the wettability of conducting polymers and investigate the factors which influence it, as well as explore the use of

conducting polymers for fluid control in simple, dynamically controlled microfluidic devices, based on the change in wetting properties upon *in-situ* electrochemical redox switching. The role of polymer oxidation state, film thickness, polymerisation substrate and the configuration of the electrochemical cell used for fluid control were considered. Goniometry and tensiometry were used to characterise polymer wetting properties, while microscopy techniques (scanning electron microscopy, atomic force microscopy and optical profilometry) were used to probe the morphology of polymer and understand the role of roughness on conducting polymer wettability and fluid movement. The electrochemical properties of polymers were characterised by cyclic voltammetry, while Raman spectroscopy was employed to gain insight into the role of water and film thickness in determining the oxidation state of polyterthiophene in Chapter 3.

The insights gained during polymer wettability characterisations were extended to investigate surface tension-induced fluidic control using electrochemical cells in both channel-based and droplet-based configurations upon the application of a small voltage. The knowledge gained during the course of this study should form the basis for developing devices which will contribute to interesting solutions for improving flow control on the microscale.

ABBREVIATIONS AND NOTATION

θ	equilibrium contact angle
θ_a	advancing contact angle
θ_r	receding contact angle
$\Delta\theta$	contact angle hysteresis; $\theta_a - \theta_r$
γ_l	surface tension of a liquid
γ_s	surface tension of a solid
γ_{sl}	surface tension of the solid-liquid interface
γ_{sv}	surface tension of the solid in equilibrium with the saturated vapour pressure of the liquid
γ^-	surface tension arising from electron donation
γ^+	surface tension arising from electron accepting
γ^{AB}	surface tension arising from acid-base interactions
γ^d	surface tension arising from dispersive interactions
γ^{Debye}	surface tension arising from Debye interactions
γ^h	surface tension arising from hydrogen bonding
γ^{Keesom}	surface tension arising from Keesom interactions
γ^{London}	surface tension arising from London interactions
γ_{lv}	surface tension of the liquid-vapour interface
γ^{LW}	surface tension arising from Lifshitz-van der Waals interactions
γ^m	surface tension arising from metallic bonding
γ^p	surface tension arising from polar interactions
γ^{total}	total surface tension
κ	electrical conductivity

μTAS	micro total analysis systems
ρ	wetted perimeter of the sample in Wilhelmy balance tensiometry
ACN	acetonitrile
AFM	atomic force microscopy
ATR-FTIR	attenuated total reflection Fourier transform infrared spectrscopy
CDG	contact drop goniometry
CEW	continuous electrowetting
CH_2I_2	diiodomethane
DCM	dichloromethane
EDL	electrical double layer
EMI.TFSI	1-ethyl-3-methylimidazolium bis(trifluoromethyl)sulfonylimide
EWOD	electrowetting on dielectric
f	fraction of a solid in contact with a liquid
F	weight contribution from the meniscus in Wilhelmy balance tensiometry
F_b	buoyancy force
F_g	force due to gravity
F_w	wetting force
G	free energy
GC	glassy carbon
HREELS	high-resolution electron energy loss spectroscopy
ITO	ITO-coated glass
KCl	potassium chloride
NaDBS	sodium dodecylbenzenesulfoante
$NaNO_3$	sodium nitrate
NapTS	sodium *para*-toluenesulfonate

P3BT	poly-3-butylthiophene
P3HT	poly-3-hexylthiophene
P3MT	poly-3-methylthiophene
P3OT	poly-3-octylthiophene
PAn	polyaniline
PDMS	polydimethylsiloxane
PEDOT	poly-(3,4-ethylenedioxythiophene)
PMMA	polymethylmethacrylate
PNiPAAM	poly(*N*-isopropylacrylamide)
PPy	polypyrrole
PPy.DBS	polypyrrole doped with dodecylbenzenesulfonate
Pt	platinum sheet
Pt-PMMA	platinised polymethylmethacrylate
Pt-PVDF	platinised PVDF membrane
PTTh.ClO_4	polyterthiophene doped with perchlorate
PTTh-C_{60}.ClO_4	N-methyl-2-(2-[2′:5′,2″-terthiophen-3′yl]ethenyl)fullero[3,4] pyrolidine) doped with perchlorate
PTTh-DDO.ClO_4	poly-(4,4′-didecyloxy-2,2′:5′,2″-terthiophene) doped with perchlorate
PVDF	polyvinylidenedifluoride
r	roughness
SAM	self-assembled monolayer
SEM	scanning electron microscopy
SERS	surface enhanced Raman spectroscopy
SSIMS	static secondary ion mass spectrometry
TBA.ClO_4	tetrabutylammonium perchlorate

TiO_2	titanium dioxide
TPG	tilting plate goniometry
TTh	2,2′:5′,2″-terthiophene
TTh-C_{60}	N-methyl-2-(2-[2′:5′,2″-terthiophen-3′yl]ethenyl)fullero[3,4] pyrolidine
TTh-DDO	4,4′-didecyloxy-2,2′:5′,2″-terthiophene
W	measured weight (net force)
WBT	Wilhelmy balance tensiometry
XPS	X-ray photelectron spectroscopy
ZDOI	zero depth of immersion
ZnO	zinc oxide

TABLE OF CONTENTS

LIST OF FIGURES

CHAPTER 1

CHAPTER 2

CHAPTER 3

CHAPTER 4

CHAPTER 5

LIST OF TABLES

CHAPTER 1

CHAPTER 3

CHAPTER 4

CHAPTER 5

CHAPTER 1

INTRODUCTION

1.1 Wettability, contact angles and surface energy

1.1.1 Wettability

The effects of wettability pervade our lives in many ways in both the natural and technological realms. Wetting, and the interactions that govern it, is integral in many biological functions and as such is essential to the existence of life on earth. Consider water rolling off a ducks back, the printing of ink on paper, rain sticking to a glass window pane or a skimmer insect gliding effortlessly across the surface of a pond. These phenomena all result from the interaction between a liquid and a surface as they come into contact with each other. Thus, wettability is the extent to which a surface interacts with a liquid in contact with it. Different liquids will wet a given surface to different extents depending on the interactions between them. For example, a good adhesive may wet a surface by increasing the interactions between itself and the material by forming either a chemical or electrostatic bond, or by increasing the intermolecular forces between them. Wetting phenomena are of interest to a wide variety of industries, including the paint, fabric and printing industries, as well as biological and microfluidic technologies.

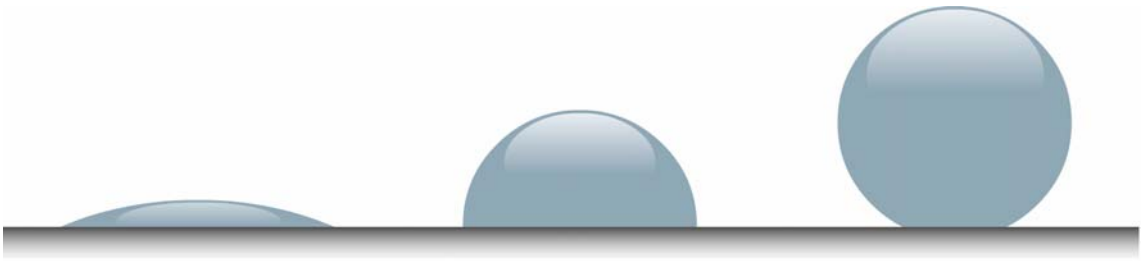

Figure 1. Diagram showing from left to right: highly wetting, partially wetting and non-wetting surfaces.

A diagrammatic depiction of wetting is shown in Figure 1. Surfaces may be described as completely wetting, partially wetting or non-wetting to a particular liquid. A convenient measure of wetting is the contact angle, described in the following section.

1.1.2 Contact angles

The extent of interaction between a liquid and a solid may be quantified by the contact angle (θ), which is the angle subtended by a tangent to the liquid drop at the point on the triple-phase contact line where the solid surface and the surrounding phase (vapour or liquid) meet. This is described by Young's equation (Equation 1), where θ is the equilibrium contact angle and the surface tension of the solid-liquid, solid-vapour and liquid-vapour interfaces are represented by γ_{sl}, γ_{sv} and γ_{lv}, respectively [1, 2]. This well-known relationship was first described by Thomas Young in 1805 and has been the subject of intensive research since.

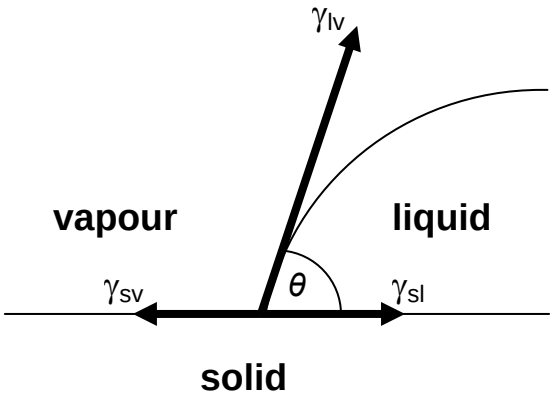

Figure 2. Schematic of the contact angle formed between a liquid and a solid in surrounding vapour phase.

Equation 1 $$\gamma_{sv} = \gamma_{sl} + \gamma_{lv} \cos\theta$$

$$\text{If } \gamma_{sv} - \gamma_{sl} > \gamma_{lv} \text{ then } \cos\theta = 1$$

This relation may also be described in terms of the work of adhesion, which is the work required when two interfaces of different materials are brought together and is described by the Young-Dupré equation [3] (Equation 2):

Equation 2 $$\Delta G_{sl} = - \gamma_{lv} (1 + \cos\theta);$$

where the free energy of the system per unit area (G) is proportional to the work done by the system to bring unit areas of two bodies into contact with a third medium [3, 4]. On a homogeneous solid surface, the contact angle is independent of volume (ignoring

gravity effects), but is influenced by ambient conditions. In particular, ambient humidity has a strong effect on the observed contact angle [5].

1.1.2.1 Wetting with water

The interaction of water with surfaces is of particular interest due to its ubiquitous nature and relevance to many aspects of our lives. Surfaces may be described as hydrophilic (water-'loving') if $\theta < 90$ °, or hydrophobic (water-'hating') if $\theta > 90$ °. Early experiments revealed that every liquid wets every solid to some extent, i.e. $\theta \neq 180^{o}$ [6]. In other words, there is always some adhesion of any liquid to any solid. However, Gao and McCarthy have recently reported the synthesis of a surface for which there is no interaction between itself and water, having a measured water contact angle of 180 ° [7]. Special cases exist where a liquid spontaneously spreads on a surface, resulting in complete wetting and a zero degree contact angle. This is referred to as superhydrophilicity when the liquid in question is water. Conversely, surfaces which are extremely non-wetting to water, exhibiting contact angles greater than 150 °, are known as superhydrophobic.

Superhydrophobicity is of interest industrially in applications where non-stick coatings [8, 9], self-cleaning surfaces [10] and biofouling prevention [11, 12] are important [13, 14]. Researchers in this area often look to nature for inspiration in designing non-sticking surfaces, where superhydrophobicity has already been perfected [15]. The leaves of some plants, including the widely investigated lotus leaf, strawberry and raspberry leaves, as well as cicada wings and the legs of water striders, exhibit superhydrophobicity [15-18]. Superhydrophobic materials possess microstructured textures which act to decrease their interaction with water. For instance, the highest measured contact angle for a highly hydrophobic smooth surface composed of close-

packed hexagonal —CF_3 groups is 119 ° [19]. For materials with water contact angles higher than this, the nanostructure of the material comes into play. The main chemical approach for increasing hydrophobicity is to incorporate fluorinated moieties into a coating, whereas the main geometric approach is to create fractal or rough surface structures [20], as described in Section 1.1.2.3.

Surfaces which are capable of being switched between hydrophobic and hydrophilic states are also of interest [21, 22]. Many routes have been investigated to create reversibly switchable surfaces which change properties under a range of external stimuli [23, 24]. Self-assembled monolayers (SAMs) have been thoroughly investigated, with changes in wettability observed upon application of electrical potential [25], light [26] or a change in pH [27, 28]. Thermally responsive poly(*N*-isopropylacrylamide) (PNIPAAm) undergoes a change in wettability when exposed to slight changes in temperature, due to the conformation of polymer chains switching from an expanded, hydrated form to a compact, non-hydrated form [29]. Metal oxides such as zinc oxide (ZnO; [30]) and titanium dioxide (TiO_2; [31]) exhibit a dramatic change in wettability upon exposure to UV light. TiO_2 surfaces exhibited complete wettability (i.e. a zero degree contact angle) for both water and oily liquids upon exposure to UV light. The transition of ZnO films from surperhydrophobic to superhydrophilic upon UV-exposure and dark storage is attributed to a change in surface free energy and roughness, the significance of which are paramount in determining a material's wettability. These surfaces have found use in devices where controllable wettability is necessary, such as self-cleaning windows, cell adhesion in biological processes and microfluidic devices.

1.1.2.2 Sessile drop goniometry

The technique by which contact angles of liquid drops are measured is called contact angle goniometry. A drop placed on a surface is illuminated with a back-light and the

contact angle measured either manually or using computer-controlled imaging software. The uppermost 0.5 – 1.0 nm of an ideal surface is probed, making it an extremely sensitive surface analysis technique [32, 33]. Several other techniques exist for characterising surfaces, including static secondary ion mass spectrometry (SSIMS), X-ray photoelectron spectroscopy (XPS), high-resolution electron energy loss spectroscopy (HREELS) and attenuated total reflection Fourier transform infrared spectroscopy (ATR-FTIR); however, these techniques are limited by their depth resolution or the qualitative nature of the data obtained [33]. Hence sessile drop goniometry is the most convenient surface-sensitive technique available [33-35]. In addition to liquid drops resting on a material, the contact angle of a captive bubble may also be determined for a sample immersed in a liquid using goniometry. Typically an air bubble or liquid drop of a second immiscible liquid is introduced to the underside of a sample using a hooked dosing needle. This technique is useful when investigating the interaction of air or a liquid that is less dense than the surrounding liquid with a surface.

Wettability determination of porous solids presents difficulties due to soaking of the liquid into the solid. The Washburn method is useful for measuring contact angles in such cases [36]. In this technique the solid is brought into contact with the probe liquid and the mass of liquid absorbed into the solid measured as a function of time. The contact angle can be determined if the viscosity, density and surface tension of the liquid are known [37-39].

1.1.2.3 Hysteresis of the contact angle

The wettability of a solid surface by a liquid is dictated by its chemical composition and its geometric structure. Young's equation (Equation 1) is based on ideal surfaces which are atomically smooth, chemically homogeneous, rigid and not prone to chemical

interaction with the liquid or vapour phase [4]. In such cases, a single unique contact angle exists. However for real surfaces it is generally accepted that a range of meta-stable contact angles may exist for the interaction of a liquid with a surface and as such, a single static contact angle is not sufficient to report. The difference between the maximum advancing angle (θ_a) and the minimum receding angle (θ_r) is known as the contact angle hysteresis ($\Delta\theta = \theta_a - \theta_r$). If θ_a and θ_r are not intentionally measured the angle determined will lie somewhere between the two extremes, often nearer to θ_a [4].

The primary causes of hysteresis are roughness, chemical heterogeneity or surface contamination (types of mechanical hysteresis) and molecular re-structuring (chemical hysteresis) [40]. Chemical heterogeneity may occur when a surface is composed of heterogeneous regions where the wettability of one area differs slightly from the adjacent region. When water advances across a surface, hydrophobic regions may obstruct the droplet's motion, increasing the local contact angle. Similarly, hydrophilic regions pin water drops as they trail across a surface. Hence it can be seen for water contact angle measurements, advancing angles are sensitive to hydrophobic domains and are related to the wettability of the surface, while receding angles are sensitive to hydrophilic areas and are related to the adhesion of the liquid to the material. Regions of chemical contamination behave the same as chemical heterogeneities.

Surface roughness presents similar barriers to wettability. Liquids may become attatched to the surface, particularly in deep valleys, and be difficult to remove [41, 42]. Roughness may also act to enhance the intrinsic wetting properties of material, i.e. if $\theta < 90°$ the observed contact angle will decrease with increasing roughness; if $\theta > 90°$ the observed contact angle will increase with increasing roughness. This effect will depend on whether the drop is in contact with the surface asperities or resting upon

them. These two different models have been described by Wenzel [43] and Cassie [44] (Figure 3).

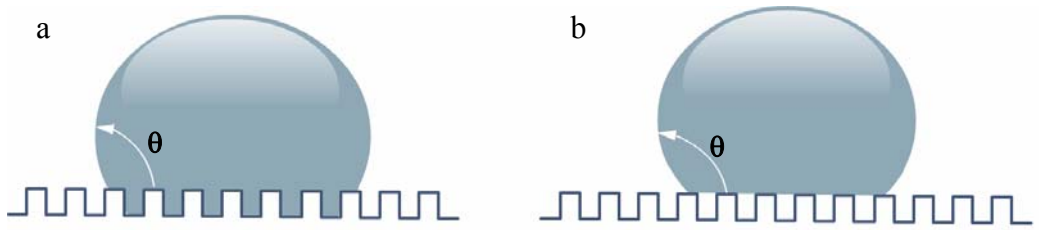

Figure 3. Two models of superhydrophobicity: a) the Wenzel state, where the liquid drop follows the surface asperities; and b) the Cassie state, where the liquid rests on top of the surface asperities [45].

In Wenzel's approach the natural hydrophobicity of a material is amplified by the increase in area due to surface textures. The observed roughness is related to the actual contact angle of the material via the surface roughness, *r*, which is the ratio of the actual surface area to the apparent surface area of a material, such that: $\cos\theta_{observed} = r \cos\theta_{actual}$ ($r > 1$). If a surface is in the Wenzel state, the contact angle hysteresis will be large, as trying to move a droplet results in it contacting itself, leading to a low receding contact angle [45]. In the Cassie state, drops are predominantly in contact with the top of the surface asperities, such that the contact angle is an average between the contact angle on air (i.e. 180 °) and that on the surface (θ), depending on the fraction (*f*) of the solid in contact with the liquid: $\cos\theta_{observed} = -1 + f(1 + \cos\theta)$ [45]. The contact angle hysteresis for surfaces in the Cassie state is quite low (ca. 5 – 10 °), as the contact of drops with the heterogeneities in the surface responsible for pinning is greatly reduced [42, 45].

The Wenzel and Cassie models of wetting rough or heterogeneous surfaces have been accepted for many years since their publication in 1936 and 1944 and have been cited by countless groups. However, in their recently published article titled '*How Wenzel*

and Cassie were wrong' [46], Gao and McCarthy argue that the interactions of the solid and liquid at the triple phase contact *line* solely determine the wetting behaviour of a liquid and that the contact *area* as used in Wenzel's and Cassie's equations is not relevant and in no way determines the contact angle of the liquid. This concept has been alluded to by the authors in other publications [7, 47, 48], as well as by other independent authors [49, 50]. Empirical data is presented that led to the following conclusion:

> Wettability (advancing and receding contact angles, and thus hysteresis) is a function of the activation energies that must be overcome in order for contact lines to move from one metastable state to another. Contact areas play no role in this. Wenzel's and Cassie's equations are valid only to the extent that the structure of the contact area reflects the ground-state energies of contact lines and the transition states between them [46].

These findings could bring about a dramatic change in the approach of determining the effect of roughness and heterogeneity on contact angle, and are sure to lead to some exciting discussions in this area. Gao and McCarthy have also shown that high advancing contact angles do not necessarily mean a surface is hydrophobic, and that hydrophobicity should be quantified in terms of the contact angle hysteresis [7].

Smooth chemically homogeneous surfaces can sometimes exhibit large hystereses, due to molecular reorganisation of the solid upon contact with liquid. For example, polar surface groups may form hydrogen bonds with water. This process is particularly prevalent in polymers, where surface-bound polymer chains are mobile [51]. Swelling of the solid, liquid penetration, chemical reactions and solutes in the liquid also contribute to wetting hysteresis. A hysteresis of 2 ° is considered negligible and within experimental uncertainty. A scatter of less than 1 ° is possible, although hystereses of greater than 10 or even 50 ° are observed on practical surfaces [4].

Contact line pinning, where the motion of a droplet is halted by a chemical, geometric or adsorptive heterogeneity is critical in applications where the motion of fluids is required, such as in microfluidic devices [52]. It has been shown theoretically that if the size of the heterogeneity or roughness features was larger than about 0.1 μm, the motion of the triple-phase contact line tended to be inhibited by the local surface defect and could not move unless an external force was introduced [53].

Knowledge of the contact angle hysteresis through determining the advancing and receding contact angles therefore enables one to discern whether the surface is in a Wenzel or a Cassie state, allowing insight into the surface morphology and adhesion properties of a material [45].

1.1.2.4 Measurement of dynamic contact angle data

The dynamic wetting properties of a material (i.e. θ_a, θ_r and $\Delta\theta$) may be measured by either goniometry or tensiometry. Two goniometric methods are widely used, namely sessile or captive drop goniometry (CDG) and tilting plate goniometry (TPG).

1.4.2.2.1 Contact Angle Goniometry

The goniometric methods for measuring advancing and receding contact angle data are conceptually simple. In the captive drop technique, a drop is dispensed from a syringe onto the sample. The advancing angle is measured by slowly adding liquid to the drop, causing the triple phase line to advance onto dry area of the solid until a steady value of θ_a is obtained (Figure 4a). The receding angle is measured by withdrawing liquid from the drop and receding the triple phase line over formerly wetted region of the surface until a steady value of θ_r is obtained (Figure 4b) [4, 54]. Alternately, a known, constant volume of liquid (e.g. 1 μL) may be dispensed into a drop and 'sucked' back into the

syringe to determine the advancing and receding contact angles, respectively [55, 56]. The latter method, whilst giving information about dynamic contact angle data, may not fully probe the extent of the hysteresis. The establishment of an accurate baseline is imperative when using the captive drop technique. Operator subjectivity in determining the maximum and minimum angles is of particular concern with this technique, leading some authors to recommended against its use [35, 57]. Despite this, the captive drop technique is still widely used due to its convenience, simplicity and ability to take measurements on-site in ambient conditions.

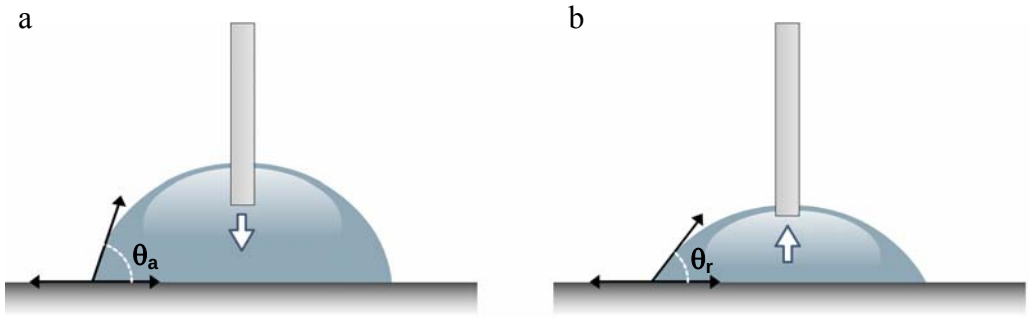

Figure 4. Advancing and receding contact angle measurement using captive drop goniometry. a) θ_a is measured by slowly adding liquid to a drop from a syringe until the triple phase contact line advances over previously unwet area. b) θ_r is measured by withdrawing liquid from a drop until the triple phase contact line recedes over previously wet surface.

An alternative goniometric method for the determination of dynamic contact angles is tilting plate goniometry. The sample is secured to a stage and tilted so that a drop resting on the surface accumulates at the leading (advancing) edge and is retained at the trailing (receding) edge. The maximum advancing and receding data are obtained when the drop is at a point of incipient motion [57]. The strong dependence of this technique on drop size, in addition to operator subjectivity in determining the point of incipient drop motion, have lead to this technique being considered inadequate for measuring advancing and receding contact angle data [57].

1.4.2.2.2 Tensiometry

Wilhelmy balance tensiometry (WBT) has become the method of choice for measuring dynamic contact angles in the polymer and biomaterial fields [35]. The wetting force between a liquid and a solid is determined by a microbalance as the sample is immersed in a liquid probe by an adjustable stage. The contact angle is related to the wetting force (the weight contribution from the meniscus; F) by Equation 3; where γ_{lv} refers to the liquid surface tension and ρ is the wetted perimeter of the sample.

Equation 3 $$F = \gamma_{lv} \rho \cos\theta$$

A balance of forces exist on a sample partially immersed in a liquid due to the force of gravity (F_g), the wetting force (F_w) and the buoyancy force, which acts in the opposite direction (F_b), so that the measured weight (net force) W is determined by:

Equation 4. $$W = F_g + F_w - F_b$$

As the sample is immersed and emersed, a relation develops between the measured weight and the density of the liquid, so that the advancing angle is due to the immersion and the receding angle to the emersion. Analysis of the resulting hysteresis plot allows for determination of the contact angle and is diagnostic of heterogeneities in surfaces.

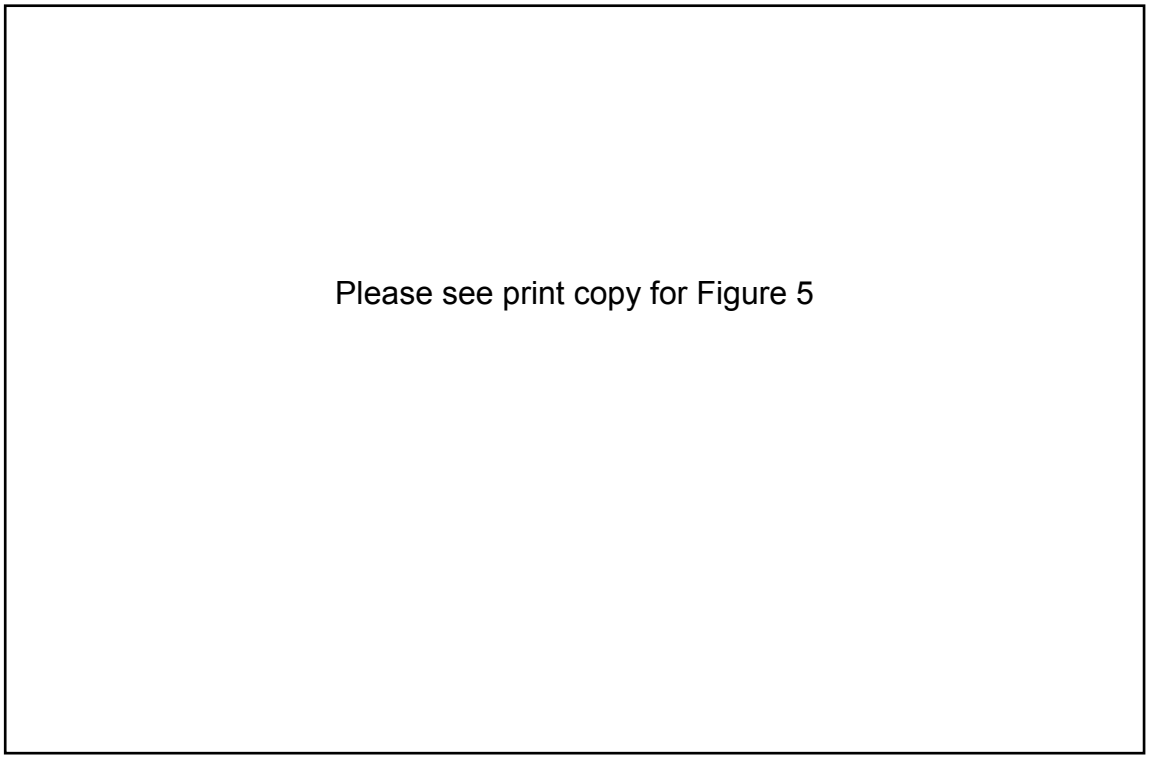

Figure 5. An idealised hysteresis loop for a wetting cycle of a non-ideal sample using Wilhelmy balance tensiometry, showing a plot of weight *vs.* immersion depth. The initial point of contact between the sample and the liquid is the zero depth of immersion [58].

A systematic comparison of the accuracy and precision of the above techniques for measuring dynamic contact angles revealed the WBT approach to be the most accurate and least subjective for measuring wetting hysteresis [35, 57]. Maximum θ_a and minimum θ_r values are determined as the triple phase line is in constant motion, while operator subjectivity is removed. Irreproducibility due to variation between randomly chosen sampling sites is reduced, as whole surfaces are simultaneously measured [58]. Accurate knowledge of the wetted perimeter and point of contact of the plate is necessary, in addition to the sample entering and exiting the fluid perpendicularly [57]. Samples may be cylindrical or flat plates, however if plates are used caution must be exercised so samples are coated evenly on both sides, unless the difference in sample wettability across both sides is sought after. Both CDG and WBT techniques have been employed to determine dynamic contact angle data in this thesis.

Contact angles are affected by the extent of interaction between a liquid and a solid. To understand the factors determining this, a discussion of the molecular forces which exist is pertinent.

1.1.3 Molecular interactions

Wettability is governed by molecular interactions between a liquid and the outermost surface groups of a material. All molecular interactions are electrostatic in origin and all molecules interact with each other (as well as with atoms and ions) to a certain degree [58, 59]. The existence of intermolecular forces is evident in condensation of the vapour phase of substances into a liquid, or the cohesion of a liquid drop. The majority of interfacial phenomena are influenced by forces with origins in atomic- and molecular-level interactions due to the induced or permanent polarities created in molecules by the electric fields of neighbouring molecules, or instantaneous dipoles caused by the distribution of electrons around the nuclei [60]. These forces, collectively known as van der Waals interactions, are important in determining material properties and governing interactions at surfaces.

Van der Waals forces consist of three types of interactions, namely Keesom interactions (permanent dipole-permanent dipole), Debye interactions (permanent dipole-induced dipole) and London interactions (induced dipole-induced dipole). The latter force is of particular note as it is always present in molecules, since it does not require the presence of a permanent polarity in the molecule. It is important in many phenomena including surface tension, physical adsorption, adhesion and the structure of biological and non-biological polymer molecules, as well as playing an important role in determining the properties of liquids, gases and solids [60]. There is an intrinsic connection between surface tension and van der Waals forces; hence, their role in wetting is of particular

note to the present study. London forces are also known as dispersion forces, due to the role that this type of interaction plays in the dispersion of light in the visible and ultraviolet wavelengths [60]. van der Waals forces are always attractive, except for one type of London force which is repulsive over long distances. van der Waals forces are long-ranged compared to other atomic- or molecular-level forces, exerting influence over 0.2 – 1.0 nm.

Molecules may undergo different types of interactions depending on the functional groups present and type of charge they carry. Ionic molecules carry an electric charge and donate or accept electrons during a reaction, polar molecules are neutral but have internal charge separation and non-polar molecules are neutral with no internal charge separation. The various interactions these functional groups may undergo are shown in Table 1.

Table 1. Molecular interactions occurring on ionic, polar and non-polar functional groups.

Interaction	Description
Ion-ion	Coulombic
Ion-dipole	Coulombic
Ion-induced dipole	Coulombic
Dipole-dipole	Keesom
Dipole-induced dipole	Debye
Induced dipole-induced dipole	London

A molecule may undergo the above interactions, depending on the type of functionality present. This leads to a range of chemical interactions responsible for the majority of

processes and reactions that chemicals undergo. Generally these chemical interactions may be classified as hydrogen bonding interactions, acid-base interactions, non-specific interactions and hydrophobic interactions [58], as discussed below.

Hydrogen bonding occurs when a hydrogen atom which is covalently bonded to a highly electronegative atom (such as nitrogen, oxygen or fluorine) non-covalently bonds with another highly electronegative atom. It is one of the most important interactions in nature, controlling important biological interactions in the human body and occurs in water that is in contact with polar surfaces consisting of nitrogen, oxygen or fluorine. Acid-base interactions occur between oppositely charged molecules which undergo ion-ion and ion-dipole molecular interactions, such as ion pair formation, ion-exchange behaviour, complexation and chelation [58]. Non-specific interactions are similar to acid-base (ion-ion) interactions but are weaker, as only partial charges are involved. They are wide-ranging and occur in neutral materials as induction and dispersion interactions (Debye, Keesom and London forces), but can also include ion-dipole interactions [58]. Hydrophobic interactions, more correctly called hydrophobic exclusions, are the tendency of neutral, non-polar molecules (such as hydrocarbons) to aggregate in aqueous solution to minimise their contact with water. This phenomenon is actually due to the effect of hydrocarbon groups on the water-water interaction in a manner synonymous with London dispersion forces, rather than repulsion between the neutral non-polar groups and water, as the name may suggest.

The surface energy of an interface may be considered as the summation of contributions arising from the various types of molecular interactions that exist at a materials interface. Thus determination of the surface energy of a material is possible through a consideration of the intermolecular forces and chemical interactions it undergoes.

1.1.4 Surface energy

Surface energy is a direct manifestation of intermolecular forces. Molecules at a surface or an interface of a solid or liquid are in a markedly different environment to molecules in the bulk, having fewer adjacent molecules which are predominantly anisotropic. Hence molecules at a surface are exposed to unbalanced forces and possess additional energy compared with molecules in the bulk. The magnitude of the surface energy depends on the number of broken bonds associated with the surface atoms and on the strength of the broken bonds [61]. New surfaces may be formed by either increasing the surface area or by stretching the pre-existing surface with a fixed number of atoms, thereby altering its strain. Hence the surface energy of a solid is the reversible work required per unit area to create a new surface, while the surface tension of a solid is the work required per unit area to elastically stretch a pre-existing surface [62].

In liquids, surface energy manifests as an internal force tending to reduce the surface area to a minimum. The term surface tension is used to describe this excess energy, as liquids cannot support any shear stresses and atoms in the liquid can diffuse quickly enough to accommodate any changes in the surface energy [61]. The word tension is used since the energy is equivalent to a line tension acting in all directions parallel to the surface [63]. Solids also possess additional free energy and a strong correlation exists between the surface energy of solids and their physical properties. Interfacial energy is analogous to surface energy and is the work per unit area to form a new interface at constant temperature and pressure [61]. Surface energy, surface tension and interfacial energy are all measured in units of force per length (mN/m) or energy per unit area (mJ/m^2). Quantitative knowledge of surface and interfacial energy is important in light of the role these parameters play in areas such as polymer adhesion and processing, printing, paint adhesion and fluid control in microfluidic devices [63, 64].

A lack of mobility of molecules at the surface of solids means that the excess energy is not directly observable and must be measured by indirect means. Contact angle goniometry (Section 1.1.2.2) is a convenient method of determining the interfacial tension of liquids on surfaces. The surface energy or surface tension of a solid may be calculated from the contact angle data of a series of liquids in contact with the surface. Surface energy theory has developed significantly since Thomas Young first described the balance of forces existing between a liquid and a solid at the triple-phase boundary (Equation 1). In this equation the parameters γ_{lv} and $\cos\theta$ are known. In order to determine the total surface energy, the unknown surface-liquid interfacial energy must be expressed in terms of the liquid and the solid surface energies. Historically, three main approaches have been used to do this. The first is to express γ_{sl} in terms of the solid and liquid surface energies then evaluate the unknown γ_{sv} using a mathematical formulation [65]. This is known as the equation of state approach, which was first published in 1898 and is still the subject of research [65, 66]. The second approach estimates the solid surface energy by determining the critical surface tension, below which spontaneous spreading of a liquid on a solid will occur [67]. This value is determined by measuring the contact angles of a series of homologous liquids (e.g. n-alkanes). The surface energy is equal to the critical surface tension if the interfacial tension at zero degree contact angle is zero. Deviation from linearity occurs when high surface tension (polar) liquids are used. This approach is best used for low surface energy polymers and organic films on high energy solids such as metals and glass, and is used extensively in the paint and adhesives industries [65]. The third approach is the surface tension component approach, where the total surface energy (γ_{sl}) depends not only on solid (γ_{sv}) and liquid (γ_{lv}) surface energies, but also on the specific molecular interactions (i.e. components of the surface energy) that they undergo. This approach is still currently in use today, as an extended version of the method initially presented by

Fowkes [68-70]; hence a discussion of the developments in this area will be presented in Sections 1.1.4.1 and 1.1.4.2. Sharma *et al.* [65] presents an excellent review detailing the chronological development of different approaches for the evaluation of solid surface energy using contact angle goniometry, while a thorough background of the theory behind the different surface energy measurement techniques is given by Good [4].

1.1.4.1 Summary of major developments in surface energy theory

Following the development of the Young-Dupré equation in 1869 (Equation 2) [3], measurement of surface tension returned to attention in the mid 1900's. The next important contribution was from Bangham and Razouk, who pointed out the importance of equilibrium film pressure or spreading pressure ($\pi_e = \gamma_s - \gamma_{sv}$), which is the reduction in γ_s resulting from vapour adsorption on the solid surface [71, 72]. However, if the contact angle is greater than zero, the spreading pressure may be regarded as negligible [4]; hence a term for the equilibrium spreading pressure does not need to be included in the Young equation [73].

The surface tension component approach views the contribution of attractive forces between liquids and solids to the total free energy to be additive. Individual components describe the surface tension of different interactions, such as those in polar liquids, hydrocarbons, low energy solids and liquid metals [65, 68-70], i.e. $\gamma = \gamma^d + \gamma^h + \gamma^m + \ldots$; where γ^d is the dispersive component, γ^h is the hydrogen bonding component (includes Keesom and Debye forces) and γ^m is the metallic bonding component, and so on. The dispersive component is also known as the apolar or Lifshitz-van der Waals component. It must be measured with an apolar liquid, such as diiodomethane or α-bromonaphthalene, which only undergoes dispersive interactions. Owens, Wendt [74]

and Kaeble [75] extended the Fowkes equation to a general form, where the polar (γ^p) and dispersive forces (γ^d) of a solid or a liquid were split into two components; i.e. $\gamma_l = \gamma_l^d + \gamma_l^p$ and $\gamma_s = \gamma_s^d + \gamma_s^p$. The energy of forces at the interface was determined by the geometric mean of the dispersive or non-dispersive components and the liquid [65], such that $\gamma_{sl} = \gamma_{sv} + \gamma_{lv} - 2\sqrt{\gamma_s^d \gamma_l^d} - 2\sqrt{\gamma_s^h \gamma_l^h}$. Two liquids, generally water and diiodomethane, are used to determine γ_s^d and γ_s^h. Wu [76, 77] used a similar method based on a two-liquid harmonic mean approach to combine the polar and dispersive components of the solid and the liquid surface energies.

1.1.4.2 Lifshitz-van der Waals-acid-base (LW-AB) theory

The Lifshitz-van der Waals-acid-base theory was established by van Oss, Good and Chaudhury in the late 1980's and has found extensive use since [78, 79]. A new polar term for Lewis acid and base interactions was introduced to explain an attraction observed between biopolymers and low energy solids [65]. Chaudhury [80] showed that surface tension components arising from the electrodynamic interactions present at an interface (i.e. Keesom, Debye and London interactions) should be grouped together, known as the Lifshitz-van der Waals (LW) interactions: $\gamma^{LW} = \gamma^{Keesom} + \gamma^{Debye} + \gamma^{London}$. Other contributions were considered polar, resulting from substances which undergo hydrogen bonding, have a dipole moment, are Lewis acid (electron acceptors) and/or Lewis bases (electron donors). The symbol γ^- was used to describe surface tension which is due to electron donation (or proton accepting) and γ^+ was used to describe surface tension which is due to electron accepting (or proton donation). The free energy of adhesion may be written as the sum of the Lifshitz-van der Waals (ΔG^{LW}) and acid-base (ΔG^{AB}) components:

Equation 5 $$\Delta G = \Delta G^{LW} + \Delta G^{AB}$$

The free energy of adhesion between two phases (1 and 2) may also be expressed as:

Equation 6 $$\Delta G_{12} = \gamma_{12} - \gamma_1 - \gamma_2;$$

where γ_1 and γ_2 are the surface energies of each phase and γ_{12} is the interfacial energy between the two phases. Hence the apolar (LW) energy of adhesion between 1 and 2 may be expressed as:

Equation 7 $$\Delta G_{12}^{LW} = -2\sqrt{\gamma_1^{LW}\gamma_2^{LW}}$$

At the solid and liquid interface the electron acceptors of the liquid will interact with electron donors of the solid and vice versa [65]. Hence, the acid-base component may be described as:

Equation 8 $$\Delta G^{AB} = -2\left(\sqrt{\gamma_1^+\gamma_2^-} + \sqrt{\gamma_2^+\gamma_1^-}\right)$$

Thus, combining Equation 1 (Young's equation) with Equation 7 and Equation 8, the free energy between a solid and a liquid may be described as:

Equation 9 $$(1+\cos\theta)\gamma_l = 2\sqrt{\gamma_l^{LW}\gamma_s^{LW}} + 2\sqrt{\gamma_l^+\gamma_s^-} + 2\sqrt{\gamma_l^-\gamma_s^+}$$

Therefore by measuring the contact angles of well-known polar and apolar liquids, the apolar Lifshitz-van der Waals surface tension component (γ^{LW}), the polar Lewis acid-base surface tension component (γ^{AB}), and the electron donating (γ^-) and accepting (γ^+) parameters of the latter may be determined for polar surfaces. The use of an apolar liquid with zero values for the γ^+ and γ^- components allows for a simplification of

Equation 9 to determine the γ^{LW} component, which then enables solving of two simultaneous equations to determine the remaining parameters. In order for a discernable contact angle to be measured and spontaneous spreading of the liquid on the solid not observed, test liquids normally have greater surface tension than that of the solid; i.e. $\gamma_l > \gamma_s$ [73]. For this reason, diiodomethane is frequently used as the apolar liquid. High surface tension polar liquids commonly used are water, glycerol, formamide and ethylene glycol. Surface tension components of these liquids are shown in Table 2.

Table 2. Surface energy components (mJ/m^2) at 20 °C of commonly used probe liquids in the Lifshitz-van der Waals-acid-base approach ([73] and references cited therein.)

Please see print copy for Table 2

The LW-AB theory has found extensive use since its advent 20 years ago in both academic and industrial realms, due to its applicability to polar surfaces and relative ease of use. However, several criticisms of the theory have arisen. There is an overwhelming tendency for the surface energy calculated for all surfaces to be basic. It has been suggested that this is due to the stronger basic component (γ^-) in comparison to the acidic component (γ^+) of common test liquids, as a result of the reference values chosen for water in the original theory, rather than some universal property of materials [81]. della Volpe and Siboni have suggested a new reference scale for water which

addresses this problem [81]. In addition, a mathematical instability of the model which returns negative values for the square root of acid-base parameters has been attributed to a lack of well characterised, high surface tension test liquids [82]. The selection of polar liquid pairs is also of importance, with the surface energy results found to depend strongly on the liquids chosen [81]. Tretinnikov [83] suggested the high sensitivity of test liquids to the surface energy results may be due to neglecting the polar component of halogenated hydrocarbons in the calculation. van Oss [73] summarised the conditions required for obtaining accurate and reproducible results. The polar liquid pairs must be chosen such that the ratio γ_l^+/γ_l^- of the two polar liquids is substantially different to each other, resulting in the recommendation of the pairs water-glycerol, water-formamide and water-ethylene glycol as suitable polar test liquids.

Despite the potential shortcomings of this method, with judicious choice of the surface energy test liquids and awareness of the tendencies of the model, consistent and reasonable results may be achieved using the Lifshitz-van der Waals-acid-base approach. This model is widely used in the surface energy assessment of polymers.

1.2 Conducting polymers

Conventional organic polymers are inextricably linked to many aspects of our lives. Polymers are insulators by nature, with conductivities of between 10^{-6} to 10^{-20} $\Omega^{-1}cm^{-1}$. The discovery of inherently conducting polymers [84, 85] created a stir in the scientific and engineering communities, as researchers became aware of the potential applications and benefits that conducting polymers could provide. This discovery was far-reaching, with many groups worldwide now investigating a myriad of conducting polymer aspects and applications. The basis of interest in conducting polymers lies in their

many desirable properties, many of which are inherited from their conventional polymer predecessors such as ease of processability, low cost and attractive mechanical properties. In addition to this, conducting polymers may be oxidatively doped to a conducting state, leading to a greatly increased conductivity. The maximum reported conductivity to date (greater than 10^5 S/cm) is comparable to that of copper and gold [86, 87]. Conducting polymers have been researched extensively for both academic and technological purposes. Many devices have been successfully commercialised and are proving useful for today's challenges, particularly in the areas of plastic solar cells for combating climate change [88, 89], smart textiles for advanced health care and numerous other applications [90] including interfacing biological devices with the human body for advanced medical treatment [91, 92]. The creation of novel, highly nanostructured composite materials, such as those with carbon nanotubes and biomaterials, promises to lead to an exciting future for conducting polymer research.

1.2.1 Structure and conductivity

Conducting polymers consist of a σ-bonded backbone with delocalised π electrons due to overlapping sp^2-hybridised orbitals, generally from aromatic units consisting of carbon and heteroatoms. Removal of a π bond from the conjugated backbone creates a charge carrier that enables electrons to be delocalised and the polymer to conduct electricity. Materials may be classed depending on their electrical conductivity, κ, namely conductors (10^4 – 10^6 $\Omega^{-1}cm^{-1}$), semi-conductors (10^{-4} – 10^2 $\Omega^{-1}cm^{-1}$) and insulators (10^{-6} – 10^{-20} $\Omega^{-1}cm^{-1}$) [63]. Conducting polymers are considered insulators in their neutral de-doped form and semi-conductors in their doped form.

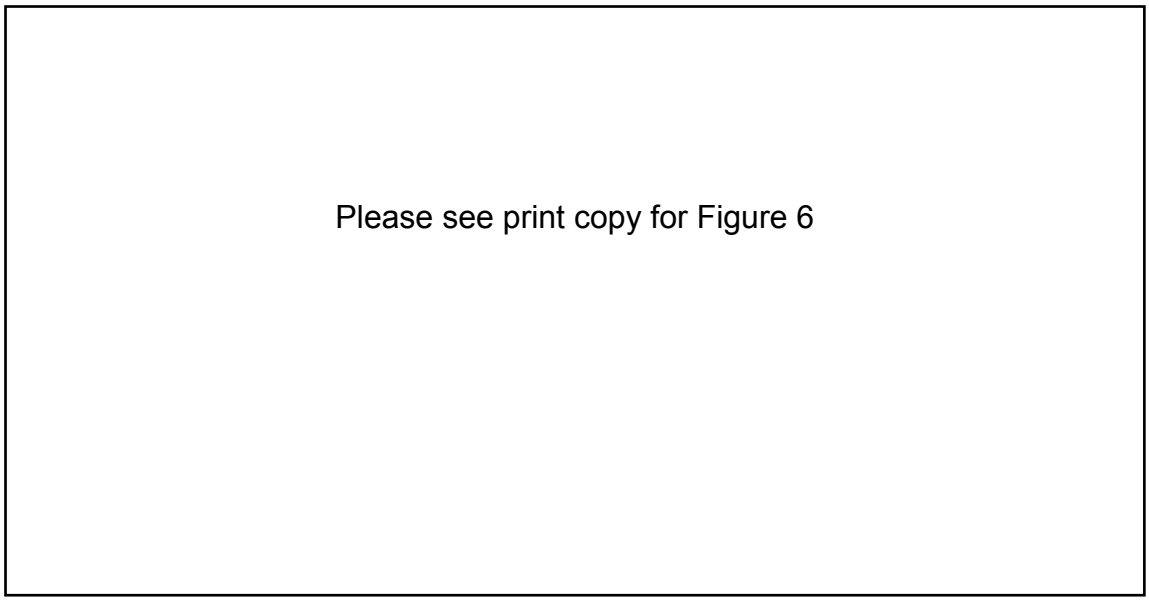

Figure 6. Schematic of the difference in band gap for insulators, semi-conductors and conductors [63].

The difference in conductivity of doped (conducting) and de-doped (insulating) polymers is explained by band theory (Figure 6). The term band gap refers to the difference in energy between the valance band, which is the highest occupied molecular orbital (i.e. the π orbital), and the conduction band, which is the lowest unoccupied band immediately above the valence band (i.e. the π^* orbital). Hence the band gap energy is defined as the energy of the π–π^* transition and determines the intrinsic electronic properties of the material. π electrons can be easily removed from (p-type doping) or added to (n-type doping) the polymer backbone without disrupting the σ bonds which hold the polymer together. The mechanism of conducting polymers has been thoroughly treated in an excellent article by Brédas and Street [93].

The most common form of charge carrier in a conducting polymer is formed via p-doping. Removal of a π electron from the polymer chain via oxidation or oxidative doping leads to the formation of a mobile charge carrier (electron or hole) on the polymer backbone known as a polaron. This is a radical cation with an associated spin, which is delocalised over several monomer units, typically four for polypyrrole [93]. Removal of a second electron from the polymer chain at the site of the polaron results in

the formation of a bipolaron, which is dicationic with no electron spin. This causes a further relaxation in polymer geometry, altering the energy levels (band gap) of the polymer. An increase in the doping level of the polymer leads to the generation of bipolaron energy levels within the gap. These bands are taken from the edges of the valence and the conduction bands and result in a widening of the gap. The position of these polaron or bipolaron energy levels and the transitions between them give rise to the absorptions present in the UV-Vis spectrum of a polymer. A fully reduced polymer exhibits only one absorption band at ca. 330 nm, corresponding to the benzenoid π–π^* transition (i.e. promotion of electrons from the valance band into the conducting band). Fully oxidised conducting polymers also exhibit a similar π–π^* transition, along with additional lower energy absorption bands corresponding to polaron–π^* (at ca. 430 nm). Absorbances at wavelengths typically greater than 800 nm are attributed to intraband transitions within half-filled polaron or bipolaron bands and are referred to a 'free carrier tail' [94].

Common conducting polymers include polythiophene (Figure 7), polypyrrole (Figure 8) and polyaniline, while many novel polymers have been synthesised for specific applications. The appending of functional groups to the monomer backbone (e.g. substitution of the monomer with hydrophobic alkyl chains) or judicious choice of polymerisation dopant may be used to tune properties, such as wettability [95-98], of the resulting polymer.

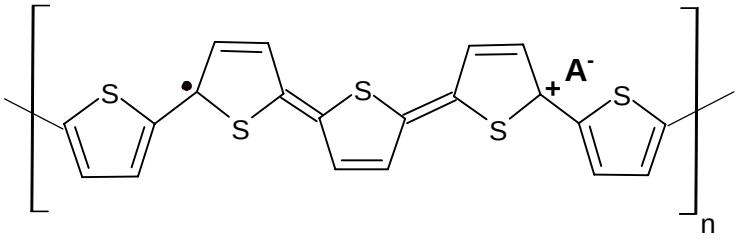

Figure 7. Electronic structure of partially doped polythiophene. A^- represents the dopant anion.

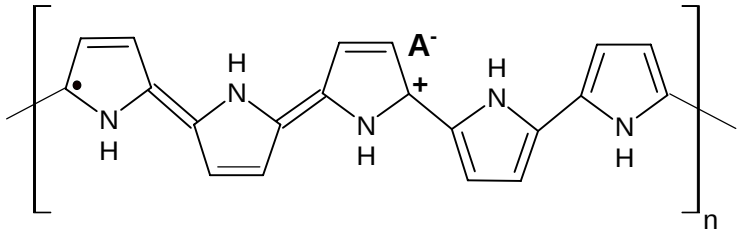

Figure 8. Electronic structure of partially doped polypyrrole. A^- represents the dopant anion.

1.2.2 Polymerisation

Conducting polymers are typically synthesised via oxidative polymerisation of a suitable monomer by chemical or electrochemical means. These processes are believed to involve initial formation of radical cations (polarons) on the monomers, followed by radical coupling and re-aromatisation, then chain propagation [99]. Polymer growth proceeds in solution until a critical molecular weight is exceeded, at which point the polymer precipitates (chemical oxidation) or deposits on the working electrode (electrochemical oxidation).

Chemical polymerisation involves the use of an oxidant such as ferric chloride to both oxidise an appropriate monomer and to provide dopant anions to balance the positive charges generated on the developing polymer backbone. The electrical conductivities of chemically prepared conducting polymers are typically slightly lower than electropolymerised polymer; however, this method allows greater control for the molecular weight and structural properties and is frequently used when large quantities of polymer are required, e.g. for commercial applications [100].

Electrochemical polymerisation is often the method of choice for the preparation of conducting polymers, as over-oxidation of the polymer (which chemical means are prone to) may be avoided by the use of controlled oxidation potentials. Monomer is

dissolved in a solvent containing an electrolyte salt, then a potential or current is applied to the solution in a two- or three-electrode cell configuration, causing the polymer to deposit on the working electrode. Galvanostatic (constant current) deposition involves the application of a constant current to the working electrode. The resulting plot of potential *vs*. time (chronopotentiogram) is indicative of the quality of the polymer, with an initial spike and a slight decrease in potential over time indicative of the formation of a conducting polymer. Potentiostatic (constant potential) deposition involves the application of a constant potential to the working electrode, with an increase in current in the resulting current-time plot (chronoamperogram) indicative of the formation of a conducting polymer. Cyclic voltammetric (potentiodynamic) methods are frequently used for both polymer growth and characterisaton of electroactivity. The potential is swept between an upper and lower potential and the current which is passed monitored. The reversibility of the reaction and the potentials at which oxidation and reduction of a polymer occur may be determined by inspection of the resulting cyclic voltammograms (current-potential plot).

1.2.3 Electroactivity

One particularly attractive feature inherent to conducting polymers is their ability to be reversibly switched between oxidised (conducting) and reduced (insulating) states. This feature is known as electroactivity and it may be controlled by the application of an external stimulus, which is generally chemical or electrochemical. The mechanism of ion movement for maintaining charge neutrality upon oxidation and reduction of the polymer depends on the size of the dopant and is shown in Figure 9 for polypyrrole. Anion expulsion is predominant upon reduction of the polymer for relatively small and mobile dopants such as chloride and nitrate (Figure 9a). Conversely, relatively large dopants such as polyelectrolytes or some surfactants are too bulky to be expelled easily

upon reduction of the polymer and remain enmeshed in the polymer matrix, with cation incorporation from the surrounding electrolyte being required in order to maintain charge neutrality (Figure 9b).

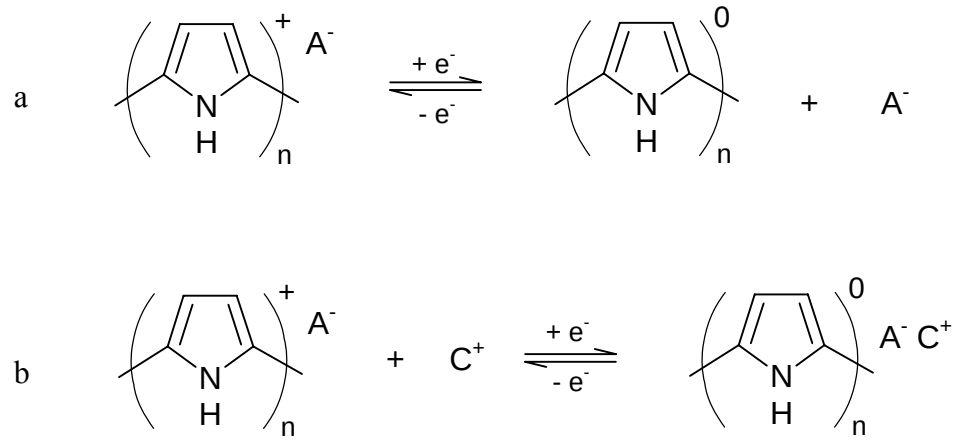

Figure 9. Mechanism for the maintenance of charge neutrality upon switching of polypyrrole between oxidised and reduced states. a) Anion (A^-) expulsion and incorporation occurs for small anions, while b) cation (C^+) insertion from the electrolyte occurs for large, immobile dopant anions.

Redox switching may be accompanied by a change in volume, colour and/or wettability, among other properties. Facile redox switching renders conducting polymers useful for applications where dynamic control of these properties is required, such as actuators [101, 102], controlled drug delivery [103-105], electrochromics [106, 107] and microfluidic devices [108-110]. The effect of redox switching upon conducting polymer wettability for fluid control in the target application of microfluidic devices is the central theme which will be explored in this thesis.

1.2.4 Chemical interactions

Conducting polymers undergo chemical interactions depending on their structure and the presence of functional groups. All conducting polymers comprise a hydrocarbon backbone which is electron rich and polarisable, due to the delocalisation of π electrons.

This allows the polymer to undergo acid-base interactions, with the π electrons behaving predominantly as a Lewis base. The heteroatom in the polymer backbone (i.e. nitrogen for polypyrrole and sulphur for polythiophene) is able to participate in hydrogen bonding, in addition to donating electrons and interacts through acid-base interactions. The de-doped (insulating) polymer backbone is likely to undergo hydrophobic interactions. Oxidation of the polymer to its conducting state results in a positive charge delocalised over several monomer units, enabling it to behave as a Lewis acid (i.e. able to accept electrons). Introduction of halogenated groups or other electrophilic sites, such as nitro groups, cause the polymer to behave as Lewis acids. Long alkyl chain functional groups will undergo hydrophobic interactions, while introduction of a counter-ion may cause the polymer to undergo ionic interactions and hydrogen bonding. A consideration of chemical interactions is therefore important when investigating the surface energy and wettability of conducting polymers.

1.2.5 Surface energy and wettability

Given the dynamic nature of conducting polymers and their change in chemical interactions when switched between conducting and insulating forms, it is reasonable to expect a change in wettability and/or surface energy to accompany oxidation and reduction. Oxidation of the polymer introduces positive charges onto the backbone, along with the incorporation of dopant anions for charge neutrality. This process introduces a dipole into the polymer backbone and is likely to increase the interaction of the polymer towards water in contact with it, and as such oxidised polymers are expected to be more hydrophilic than reduced polymers [95]. The nature of the counter-ion is believed to play an important role in determining the polymer wettability, depending on whether the dopant is mobile or immobile and dopant expulsion or cation incorporation is predominant upon reduction, respectively. Hence a change in oxidation

state of the polymer will effect the chemical interactions at the polymer surface, the extent of which may be monitored and quantified using goniometry or tensiometry. The mobility of polymer chains at the surface enables reorientation of the groups in response to the environment to which they are exposed. This rearrangement can occur within the time frame of contact angle measurements and can lead to spreading of the drop on the surface to minimise the interfacial free energy between two materials [51].

The study of conventional polymer wetting properties has been an integral part of surface science for many years. In contrast, investigations into factors affecting the wettability of conducting polymers are comparatively few, although there has been increased interest in recent years, due to the suitability of conducting polymers for various applications where control of wettability is necessary. Early studies by Teasdale found the substrate was important in governing the resulting polymer wetting properties [58]. Several studies into the effect of polymer oxidation state on wettability have been carried out. *In-situ* wettability measurements are desirable, as they give information regarding wetting the behaviour of the polymer in during an applied potential. Lee *et al*. measured the doping level of polypyrrole by *in-situ* Wilhelmy balance tensiometry [111, 112]. The force between the liquid and the polymer was found to increase upon doping, as a result of increased interaction between water and the oxidised polymer. This interaction decreased upon de-doping, however this process was slower. Hato *et al*. found the wettability of polyaniline doped with hydrochloric acid (PAn.HCl) increased as the polymer was oxidised [113]. Isaksson *et al*. showed that polyaniline doped with dodecylbenzenesulfonic acid (PAn.DBSA) increased in wettability upon reduction, thus revealing the importance of the role that the counter-ion plays in determining polymer wettability [108, 109]. Wang *et al*. carried out *in-situ* wettability measurements using Wilhelmy balance tensiometry [114]. They found the wettability of poly-3-

hexylthiophene (P3HT) to be directly related to oxidation state, as P3HT was more hydrophilic in the oxidised state, whereas poly(3,4-ethylenedioxythiophene) (PEDOT) was found to be less hydrophilic in the oxidised state.

Surface energy studies on conducting polymers have been carried out using several different methods. Chehimi *et al*. have used inverse gas chromatography of polypyrrole, polyaniline and polythiophene at infinite dilution to determine the dispersive and acid-base contributions to surface energy [115, 116]. They found the dispersive component of surface energy increased with doping level for polypyrrole powder. This factor was also dependent on time, decreasing as the film aged. The acid-base interactions, hydrophobic interactions and hydrogen bonding that conducting polymers undergo lends themselves well to being interpreted by the Lifshitz-van der Waals-acid-base approach of van Oss-Good-Chaudhury (described in Section 1.1.4.2). This has been successfully been applied to interpret the surface energy of various conducting polymers [56, 114, 117-119]. Fadda *et al*. found the Lewis base component was able to differentiate between the conducting and insulating forms of poly-3-octylthiophene. The above studies indicate that the surface energy and wettability of conducting polymers is dependant on oxidation state. An investigation of the factors affecting the wetting properties of conducting polymers, including oxidation state, film thickness, functional groups and substrate, is therefore warranted.

1.3 Microfluidic systems

The change in wettability upon dynamic switching of oxidation state renders conducting polymers useful for applications where dynamic control of wetting properties is required, such as in microfluidic devices. Microfluidic systems, also commonly referred to as micro total analysis systems (μTAS) or Lab-on-a-Chip devices, have

received much attention since their advent in the early 1990's [120, 121]. They are recognised as being one of the fastest emerging technologies of the new century, with many academic and industrial groups worldwide shifting their focus to include research in this exciting area. An increasing number of start-up companies have entered the market, which is a direct indication of the expected boom in microfluidics commercialisation in coming years, while the number of patents in microfluidic technologies continues to increase [122].

1.3.1.1 What are microfluidic devices?

Microfluidic devices are integrated systems composed of miniaturised fluidic channels which have at least one channel dimension less than 1 mm. The aim of such devices is to perform the biological and chemical analyses which are conventionally carried out on laboratory-sized equipment. Just as the microelectronics industry witnessed a decrease in the size of components, from vacuum tubes to transistors to silicon wafers over many years, the microfluidics world has followed a similar trend, with entire bench-top laboratory analysis systems being reduced to fit on devices smaller than the size of a credit card [123]. Many functions may be performed on a single chip, including sampling, separation, chemical reaction, fluid control, mixing and sample detection, in an integrated format similar to that of microelectronic circuits. Several excellent reviews exist on the many aspects of microfluidic design and implementation [124-129]. Miniaturisation of fluidic devices with channels of nanoscale dimension is also of interest. Interesting phenomena arise when device dimensions are similar to that of the molecules within them. Nanofluidic devices are now regularly researched [130-133]; however the discussion here will be restricted to microfluidic devices.

The intensive interest, both academically and industrially, in microfluidic devices has stemmed from the many benefits that exist upon miniaturisation. Reduced analysis times, reagent cost and sample volume requirement are gained due to the decreased size of the devices. Running costs are decreased due to cheap fabrication materials and the elimination of expensive instrumentation, as well as higher throughput and efficiency. The ability to carry out automated reactions with precision reduces the need of operator involvement and thus error. Hazardous substances may be handled safely due to the extremely low quantities required in the microscale [134].

1.3.1.2 Materials

Microfluidic devices have predominantly been fabricated out of 'hard' materials such as glass or silicon using micromachining techniques similar to those already well-established in the microelectronics industry [135, 136]. Despite the advantageous mechanical properties of glass and the ability to create three-dimensional features with dimensions of just a few microns [137, 138], the widespread interest in commercialising microfluidic devices for bioanalytical application has resulted in a drive to reduce costs. 'Soft' polymeric microfluidic devices, fabricated from materials such as polymethylmethacrylate (PMMA) [139] or polydimethylsiloxane (PDMS) [140-143], are significantly cheaper to produce and are fabricated using simplified manufacturing procedures, including laser ablation, soft-lithography, hot embossing or imprinting and injection molding [127]. Both plastic and glass are optically clear, allowing reactions to be monitored as they occur. PDMS is able to form a tight seal with both silicon and glass, making it particularly useful for hybrid soft-hard fluidic devices.

1.3.1.3 Applications

The advantages of miniaturisation have made microfluidic devices attractive for many different applications. They have found extensive use in the biotechnological and medical fields, where the increased reaction times and decreased reagent volume proves highly beneficial for high-throughput drug screening discovery, cell separation and sorting, DNA analysis and sequencing [52, 126, 143-146]. They are also proving useful for carrying out traditional chemical analyses and reactions on the microscale, with micro-chemical reactors [147, 148] and high-throughput HPLC [149] reported, while large scale deployment of autonomously operating devices have proved useful for environmental monitoring [150, 151]. One long-term goal of the microfluidics industry is to produce portable, hand-held diagnostic devices to be used at the point of care, in the home or for widespread deployment in developing countries. In order to enable this, low power and low voltage operation is required. Fully-integrated disposable devices have been reported for hand-held point of care clinical diagnostics [145, 152].

1.3.1.4 Channel- and droplet-based configurations

Microfluidic devices have typically been of composed tiny interconnected microchannels through which continuous streams of liquid are moved. However, channel-based microfluidic devices often have problems associated with leakage and bonding device components [153]. Droplet- or surface-based configurations have been increasingly investigated due to their ease of manufacture (planar surface compared to microfabricated channels) and the simplicity of introducing sample fluids into the device [129, 134, 144, 147, 154]. Some drawbacks to using droplet-based fluidic system exist, such as evaporation and contamination of the droplet or surrounding liquid, in addition to reagent concentration control. Both channel- and droplet-based paradigms will be considered in this thesis.

1.3.1.5 Surface tension forces on the microscale

A key aspect of microdevices is the beneficial scaling effects of surface tension that exist upon miniaturisation. Different physical forces affect liquids on the microscale compared to those in the macroscale, with surface tension forces that are generally insignificant on the macroscale, becoming dominant on the microscale [155]. Consider the way a skimmer insect is able to interact with water, resting on its surface as if a skin were present, in a way quite clearly different to what is observed if the same situation were present on the macroscale. One particularly elegant and fascinating example of the manipulation of surface tension upon going to small dimensions and volumes is that of the spider *Argyroneta aquatica*, or diving bell spider. This underwater-living, air breathing spider transports air from the surface in a thin layer of hairs around its legs and body, transferring it to an underwater net it has constructed from a fine layer of silk. The net is woven finely enough so that surface tension stops any air from escaping through any holes, based on the pressure difference at the air-water surface [156], enabling the spider to hunt, mate and rest under water. Other factors including surface roughness, electrical influences, van der Waals interactions and suspended particles (which may have similar dimensions to that of the microchannel) become important factors upon miniaturisation of device dimensions.

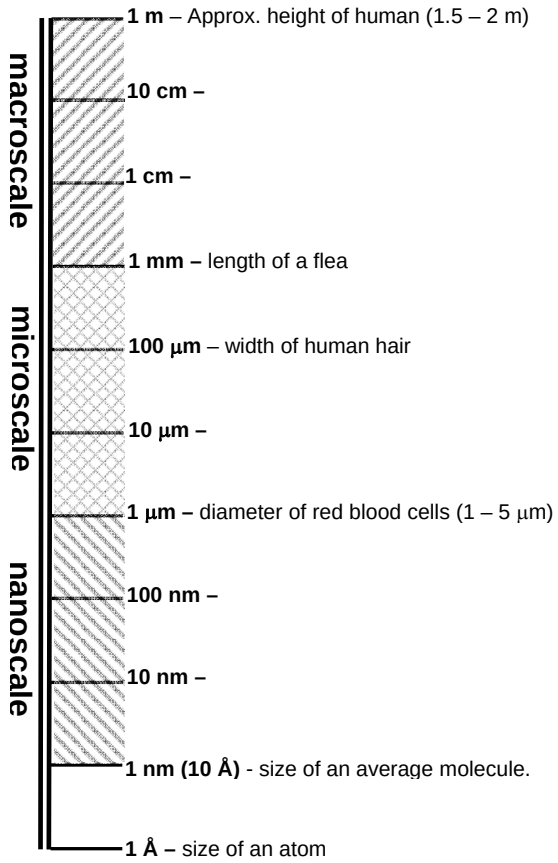

Figure 10. Schematic showing different length scales, from the macroscale to the microscale. Microfluidic devices have fluidic dimension from 1 – 1000 μm.

The beneficial scaling effects of surface tension forces upon miniaturisation of device dimensions lends itself well to being exploited for fluid control in microfluidic devices [52].

1.4 Fluid control techniques in microfluidic systems

With the advent of smaller devices and new technologies comes the need for more efficient control of the fluids within these microsystems. A crucial factor in the development of microfluidic devices is the means of moving analytes and reagents through channels or along surfaces, and much research has focussed on this area [157, 158]. Increasing complexity in microdevice design has led to the need of more efficient pumping systems. Fluid control techniques may be classified as either mechanical or non-mechanical.

1.4.1 Mechanical fluid control

Mechanical or pressure-driven flow uses physical means such as syringes, membranes and valves to drive fluids around a device [159-162]. These systems are generally inexpensive and able to generate large and reproducible flow rates, while being simple to control from off-chip sources. An excellent review on the development of micropumps is presented by Laser and Santiago [157]. However, micropumps are often complex to fabricate, may be accompanied by large external instrumentation to compensate for the high power consumption required to drive syringes and valves, and are limited by the lifetime of their parts (e.g. valves and diaphragms) which are prone to clogging and fatigue. Critically, they are unable to accurately deliver fluid volumes in the nanolitre per second range required for typical microchannel dimensions [163]. Concentrated samples may also be smeared by the drag exerted by the channel wall causing a parabolic flow profile. It is often difficult to integrate physical valves into an

on-chip format, limiting the size to which the device may be miniaturised. Non-mechanical systems, however, have no moving parts and are therefore not prone to routine mechanical failure.

1.4.2 Non-mechanical fluid control

There are many types of flow control which fall into the non-mechanical category. This is a wide and varied field of research, with many clever examples of non-mechanical means to drive fluid flow in microdevices. This includes electrokinetic, centrifugal [164], capillary techniques [165] and flow generated by changes in interfacial tension, including those which are electrically-induced. The electrokinetic control of fluids and surface-tension induced fluid control will be summarised below.

1.4.2.1 Electrokinetic

Electrokinetic methods have found extensive use in microfluidic devices for fluid delivery, mixing, separation, sample concentration and cell positioning [134]. It the most commonly used fluid control technique and has been the subject of several recent reviews [125, 126, 134, 158, 163, 166]. Electrophoresis and electroosmosis have found the most application in microdevices to date, among other electrokinetic techniques including electrocapillary, dielectrophoresis, electrowetting and electrohydrodynamic flow control.

1.4.2.1.1 Electroosmosis

Electroosmosis is the motion of an ionised liquid relative to a stationary charged surface upon an applied external voltage and has been used by many groups as a means of fluid control [167-172]. Electroosmosis relies on the generation of an electrical double layer (EDL) in a liquid at a channel or capillary surface, due to ionisation of the channel

walls. The thickness of this charged layer (the Debye layer) is related to the ion concentration in the bulk liquid and is commonly 1 – 100 nm in water [158]. When a potential is applied along the channels, the electrical double layer will move due to the electrostatic force, with the bulk fluid being pulled along with it. The directionality of the flow is controllable, as the potential may be applied simultaneously at different positions. Flow is maximised by a high channel surface area to volume ratio and exhibits a flat velocity profile ('plug'-like behaviour), as opposed to the drag exhibited at channel walls using pressure-driven flows, rendering it particularly useful for controlling sample injection in electrophoresis-based separations [134]. High driving voltages are often required to achieve practical flow velocities, with a potential difference of kilovolts per centimetre necessary for flow of several millimetres per second [158].

1.4.2.1.2 Electrophoresis

In electrophoresis, an external voltage is applied across a channel causing ions in the fluid to move towards ends of opposite polarity, moving the bulk fluid along with them. Extensive research in this field has occurred since the contribution of Manz and coworkers in the early 1990's [120, 121, 173-175]. Recently, rapid chiral analysis using microchip electrophoresis (MCE) with separations performed as fast as 2.5 seconds and commonly less than 1 minute have been demonstrated [176, 177]. Gel electrophoresis and capillary electrophoresis are used extensively for biological analyses including DNA fragment sizing, DNA sequencing and protein analysis [134]. Dielectrophoresis involves a similar process but with uncharged, polarisable particles which experience an induced dipole upon exposure to an electric field [148, 178, 179].

Electrophoretic flow control may also require similarly high driving voltages as electroosmotic flow (up to kV/cm), thus making ultra-miniaturisation of instrumental components difficult. In order to overcome this, an elegant use of the physics and forces on liquids in the microscale is required, where surface tension effects become increasingly important.

1.4.2.2 Surface tension-driven flow

The advantageous scaling effects of surface tension on the microscale have been exploited for passive fluid control in microfluidic devices. The flow of liquids caused by surface tension gradients is known as the Marangoni effect. Electrical analogies of this effect, known as electrocapillarity or electrowetting, are generally more energy efficient than thermal methods of controlling surface tension and are proving to be effective for fluid control on the microscale. Laminar flow dominates on the microscale, and is both controllable and predictable, meaning precise positioning of analytes is possible. Gradients in surface tension at a liquid-vapour or liquid-liquid interface may be generated by exposing that interface to an imbalance in surface temperature, chemical composition or charge density [52, 158], as summarised below.

1.4.2.2.1 Thermal control of surface tension

Thermocapillary-actuated fluid flow uses microfabricated heaters to generate a gradient in temperature, causing a local change in liquid surface tension [180, 181]. Darhuber *et al*. reported the development of a device with individually addressable microheater arrays, which were capable of moving, splitting, trapping and mixing nanolitre volumes without mechanically moving parts and with low operating voltages of 2-3 V, enabling operation of the device using conventional batteries [181]. However, thermally-controlled flow devices may have high power consumption and cause evaporation and heating of the liquid, which may present problems for biological samples.

1.4.2.2.2 Chemical control of surface tension

Active control of surface tension using chemically-initiated gradients are appealing as they often require no applied voltage or power. Significant work in this area has been carried out by Abbott and co-workers, who have demonstrated both UV-initiated and electrochemical surface tension gradients in solutions containing redox-active and UV-sensitive surfactants, such as ferrocenyl or azobenzene-based surfactants, for fluid control on the microscale [182-190]. Other authors have reported exploiting the photoisomerism in calixerenes [26] and spiropyrans [191] coated on surfaces upon exposure to UV and visible light for reversible control of liquid position. The difficulty in precisely controlling flow rate and possible depletion of reactant (depending on the configuration) may present drawbacks to chemically-controlled surface tension-driven flows.

1.4.2.2.3 Electrical control of surface tension

Electrically-controlled surface tension gradients are finding increasing use as a fluid control method in microfluidic devices due to the energy efficiency (compared to thermal) and long-lasting operation (compared to chemical) they afford. Electrocapillarity and electrowetting, the two main techniques in this group, are similar to but distinct from each other. Electrocapillarity typically refers to the change in surface tension of a liquid metal in an electrolyte under applied potential. It was first described by Lippmann in 1875 [192] for the change in surface tension of mercury in an electrolyte and has been used to generate flow in microfluidic devices, known as continuous electrowetting (CEW).

CEW is the flow generated by electrically changing the surface tension of a material, as a result of the electrocapillary effect [193]. Matsumoto and Colgate attempted to

exploit this phenomena in 1990 for micropump actuation using mercury [194]. Ni and co-workers first developed a micropump based on the surface tension change of mercury upon applied voltage across a mercury/electrolyte interface causing a change in height of the mercury plug, forming the basis of the pumping mechanism. Power consumption was only a few milliwatts over a potential difference of 1.4 V [195]. Lee and Kim were able to generate circular and linear flows based on the CEW phenomena of a mercury plug at voltages of around 3 V and low power consumption of 10 – 100 μW [193]. However the use of mercury in these devices is undesirable and less hazardous alternatives are sought after.

Electrowetting is the phenomenon whereby the wetting properties of a droplet on a substrate are modified by an electric field. It has been defined as "*a change in solid-electrolyte contact angle due to an applied potential difference between the solid and electrolyte* [196]." Drops of partially-wetting electrolyte usually less than 1 mm wide resting on planar surfaces either in air or an immiscible liquid such as oil [197] are grounded between two plates or using a thin metal electrode inserted into the drop [198]. Various scenarios where the droplet is conductive or where the droplet and surroundings are insulators have been demonstrated on both conducting and dielectric substrates [197-199]. Large numbers of droplets may be manipulated without the use of pumps and valves, eliminating the issue of part failure associated with mechanically driven devices. A gradient in surface energy may be generated, which can be used to direct the flow of a liquid on the electrode surface. Conventional electrowetting involves flow control of a liquid on a metal electrode, commonly gold or platinum, where potentials of around 1 – 2 V are sufficient to cause liquid motion as opposed to tens or hundreds of volts as required to move a liquid droplet on an insulating material**.**

Electrowetting-On-Dielectric (EWOD) is a type of electrowetting where an electrical potential is applied across dielectric-coated (insulating) electrodes with a liquid droplet between the electrodes, thus eliminating direct contact between the electrode and the liquid. It was introduced as a way to suppress electrolytic decomposition of water at voltages above several hundred millivolts. The surface tension of a drop is changed at one end, causing the droplet to move in the direction of lower surface tension. This technique has been used to move, combine, split and mix liquids in microfluidic devices and has the benefits of low power consumption and high reversibility [200, 201]. It is widely applicable to a variety of liquids, as electrically conducting liquids are not required. These devices still require somewhat higher driving voltages than other surface tension-driven techniques. Pollack *et al*. achieved initiation of droplet motion at around 48 V [202], while Cho and co-workers were able to initiate droplet movement at around 18 V [154]. If higher AC potentials of greater than 150 V were applied, transport speed of up to 250 mm/s was attainable. Despite exhibiting the lower power consumption common to non-mechanical pumping methods, further reduction of the operation voltage has yet to be realised and hence alternative fluid control methods are sought after.

1.4.3 Use of conducting polymers in microfluidic systems

1.4.3.1 General usage

The dynamically-controllable properties of conducting polymers make them suitable for varied applications in microfluidic devices. An integrated microfluidic device has been used for the *in-situ* polymerisation of polyaniline and polypyrrole nanowires for sensing applications [203]. The turbulent-free environment of microchannels affords wires with more well-defined morphologies than those deposited from the bulk solution. The nanowires were able to be used for sensing immediately after fabrication, for pH

detection in the case of polyaniline and ammonia detection to a concentration of 1 part per million (ppm) for polypyrrole. Polyaniline has been used for sealing polymeric (PMMA or polycarbonate) microfluidic devices [153], as sealing and bonding polymer-based microfluidic devices without destroying the integrity of patterned microstructures proves to be a challenging issue. Thin layers of polyaniline nanoparticles in an organic solvent were screen printed onto the substrate at the interface then welded using microwaves. The PMMA and polycarbonate substrates are virtually transparent to microwaves and therefore the integrity of the channels was not affected. A microfluidic electrochemical cell was described by Shim *et al*. for the synthesis of polypyrrole with various biomolecules as dopants on a single electrode, enabling rapid screening of novel polymers for nerve regeneration [204]. Polypyrrole has also been used in a microfluidic device as an electrochemical biosensor by registering a change in impedance upon interfacing with complex biological molecules [205], in addition to being used as a replacement for metal electrodes in an all-polymeric microfluidic device [206].

1.4.3.2 Use of conducting polymers for fluid control in microfluidic devices

The change in properties of conducting polymers upon oxidation and reduction renders them particularly useful for fluid control in microfluidic devices. The large out-of-plane thickness change (>30 %; [207]) of polypyrrole upon redox switching was exploited for valves to control the flow in microchannels [208]. Polypyrrole/gold bilayer hinges attached to a rigid polymer plate were secured to the bottom of microchannels and were able to greatly diminish fluid flow when the valves were in the closed position. The actuation properties of polypyrrole were also exploited for a micropump with a concentric tube-in-tube configuration [209]. Polypyrrole-coated polyvinylidenedifluoride (PVDF) tubes were arranged in such a way that peristaltic motion caused the flow of liquid through an inner tube upon the application of a low

voltage (1 V) with relatively low power consumption (8.7 mW). This configuration also had the benefit that the fluid moved was separate from the electrolyte used in the electrochemical cell, increasing the versatility of the micropump.

Several particularly elegant examples where conducting polymers have been used for fluid control in microfluidic devices have come from Isaksson and co-workers [95, 108-110]. A novel approach using an organic electronic wettability switch based on the change in surface energy of PAn.DBSA upon redox switching was reported [108]. The polymer was observed to undergo a change in wettability upon application of 2 or 5 V as it was switched from the oxidised to reduced forms, evidenced by the motion of a water drop to the more wettable reduced region of polymer. The use of a solid polymer electrolyte enabled the device to be operated in air. This concept was further developed so that both the initial contact angle and wetting gradient could be controlled for a drop resting on an electrode [109]. The change in wettability of P3HT of about 90 ° upon oxidation and reduction was also used to control the flow of water through a series of microchannel junctions using a low potential (typically 15 V but operational at 5 V) [110].

These findings show conducting polymers are providing useful solutions to some of the key issues associated with fluid control in microfluidic devices, including low cost materials, biocompatibility, minimisation of reagent volume and low power consumption enabling greater portability. Whilst there has been significant progress in the development of fluid control in microdevices, and many elegant examples of micropumping and exploiting surface tension forces at the microscale have been demonstrated, there is room for further contributions.

1.5 Thesis Aims

This thesis has two main objectives:

Objective 1: To characterise the wettability of conducting polymers and investigate the factors which influence it, and

Objective 2: To explore the use of conducting polymers for fluid control in simple, dynamically-controlled microfluidic devices, based on the change in wetting properties upon *in-situ* electrochemical redox switching.

These objectives were fulfilled in the following ways:

- The factors influencing the wettability and surface energy of poly-2,2′:5′,2″-terthiophene doped with perchlorate (PTTh.ClO_4) were investigated. This included a study into the role of polymer oxidation state, film thickness, polymerisation substrate and monomer functionalisation with groups of varying hydrophobicity (Objective 1).
- The change in wettability of PTTh.ClO_4 upon *in-situ* electrochemical redox switching was monitored by studying the contact angle of a captive water drop (Objective 1).
- Polypyrrole doped with dodecylbenzenesulfonate (PPy.DBS) was investigated for the control of organic and aqueous liquids in planar and channel configurations upon *in-situ* electrochemical redox switching (Objective 2).
- PPy.DBS was investigated in an integrated electrochemical cell for fluid movement of liquids *in air,* upon *in-situ* electrochemical redox switching without surrounding aqueous electrolyte (Objective 2).

The following characterisation techniques were used to gain insight into the factors influencing the wettability and fluid control capability of polyterthiophene and polypyrrole. Goniometry and tensiometry were used to characterise polymer wetting properties, which in turn enabled determination of the surface energy of select films. Raman spectroscopy was employed to explore the change in oxidation state through the depth of polyterthiophene films in Chapter 3. Scanning electron microscopy, atomic force microscopy and optical profilometry were used to probe the morphology of polymers and assist in understanding the role of roughness on conducting polymer wettability and fluid movement. Cyclic voltammetry was used to characterise the electrochemical properties of polymers.

General experimental details, including materials and instrumentation used in this thesis, are presented in Chapter 2. Further experimental details will be presented in the following individual chapters. Chapter 3 investigates the effect of various parameters on the wettability and surface energy of polyterthiophene films; in particular, the interaction of water with the polymer is explored. Chapter 4 describes the changes observed in an organic liquid immersed in a surrounding immiscible electrolyte upon *in-situ* electrochemical oxidation and reduction. A discussion of the unusual changes in droplet shape and contact angle observed is presented, as well as a proposed mechanism in light of the surface energy changes in the polymer. Chapter 5 details the characterisation of wetting properties and the implementation of polypyrrole into microchannels and on planar surfaces, for dynamic manipulation of wettability, to control the position of fluids. A final chapter summarises the achievements of each chapter and offers explanations for the results observed, as well as pointing to areas of future research.

1.6 References

1. Young, T., *Phil. Trans.*, 1805. **95** p. 65.
2. Young, T., *Phil. Trans.*, 1805. **95** p. 82.
3. Dupré, A., *Theorie mechanique de la chaleur*. 1869, Paris: Gauthier-Villars. p369.
4. Good, R.J., *Contact angle, wetting and adhesion: a critical review*, in *Contact angle, wettability and adhesion*, K.L. Mittal, Editor. 1993, VSP: Utrecht, The Netherlands. p. 3.
5. Muller, B., Riedel, M., Michel, R., De Paul, S.M., Hofer, R., Heger, D., and Grutzmacher, D., *J. Vac. Sci. Technol., B*, 2001. **19** p. 1715.
6. Fowkes, F.M., *Contact angle, wettability and adhesion:the Kendall award symposium honoring William A. Zisman, Los Angeles, Calif., April 2-3, 1963.* Advances in chemistry series. 1963, Washington: American Chemical Society.
7. Gao, L. and McCarthy, T.J., *Langmuir*, 2006. **22** p. 2966.
8. Saito, H., Takai, K., Takazawa, H., and Yamauchi, G., *Mater. Sci. Res. Int.*, 1997. **3** p. 216.
9. Kako, T., Nakajima, A., Irie, H., Kato, Z., Uematsu, K., Watanabe, T., and Hashimoto, K., *J. Mater. Sci.*, 2004. **39** p. 547.
10. Quere, D., *Rep. Prog. Phys.*, 2005. **68** p. 2495.
11. Schultz, M.P., Kavanagh, C.J., and Swain, G.W., *Biofouling*, 1999. **13** p. 323.
12. Scardino, A., De Nys, R., Ison, O., O'Connor, W., and Steinberg, P., *Biofouling*, 2003. **19** p. 221.
13. Ma, M. and Hill, R.M., *Curr. Opin. Colloid Interface Sci.*, 2006. **11** p. 193.
14. Li, X.M., Reinhoudt, D., and Crego-Calama, M., *Chem. Soc. Rev.*, 2007. **36** p. 1350.

15. Sun, T.L., Feng, L., Gao, X.F., and Jiang, L., *Accounts Chem. Res.*, 2005. **38** p. 644.

16. Erbil, H.Y., Demirel, A.L., Avci, Y., and Mert, O., *Science*, 2003. **299** p. 1377.

17. Coulson, S.R., Woodward, I., Badyal, J.P.S., Brewer, S.A., and Willis, C., *J. Phys. Chem. B*, 2000. **104** p. 8836.

18. Zhu, L.B., Xiu, Y.H., Xu, J.W., Tamirisa, P.A., Hess, D.W., and Wong, C.P., *Langmuir*, 2005. **21** p. 11208.

19. Nishino, T., Meguro, M., Nakamae, K., Matsushita, M., and Ueda, Y., *Langmuir*, 1999. **15** p. 4321.

20. Yan, H., Kurogi, K., Mayama, H., and Tsujii, K., *Angewandte Chemie International Edition*, 2005. **44** p. 3453.

21. Krupenkin, T.N., Taylor, J.A., Schneider, T.M., and Yang, S., *Langmuir*, 2004. **20** p. 3824.

22. Feng, X.J. and Jiang, L., *Advanced Materials*, 2006. **18** p. 3063.

23. Liu, Y., Mu, L., Liu, B., and Kong, J., *Chem. Eur. J.*, 2005. **11** p. 2622.

24. Lahann, J. and Langer, R., *MRS Bull.*, 2005. **30** p. 185.

25. Abbott, N.L., Gorman, C.B., and Whitesides, G.M., *Langmuir*, 1995. **11** p. 16.

26. Ichimura, K., Oh, S.K., and Nakagawa, M., *Science*, 2000. **288** p. 1624.

27. Sellergren, B., Swietlow, A., Arnebrant, T., and Unger, K., *Anal. Chem.*, 1996. **68** p. 402.

28. Auer, F., Schubert, D.W., Stamm, M., Arnebrant, T., Swietlow, A., Zizlsperger, M., and Sellergren, B., *Chem. Eur. J.*, 1999. **5** p. 1150.

29. Sun, T.L., Wang, G.J., Feng, L., Liu, B.Q., Ma, Y.M., Jiang, L., and Zhu, D.B., *Angew. Chem. Int. Ed.*, 2004. **43** p. 357.

30. Wang, R., Hashimoto, K., Fujishima, A., Chikuni, M., Kojima, E., Kitamura, A., Shimohigoshi, M., and Watanabe, T., *Advanced Materials*, 1998. **10** p. 135.

31. Feng, X.J., Feng, L., Jin, M.H., Zhai, J., Jiang, L., and Zhu, D.B., *JACS*, 2004. **126** p. 62.

32. Bain, C.D. and Whitesides, G.M., *Science*, 1988. **240** p. 62.

33. Tretinnikov, O.N., *Wettability and microstructure of polymer surfaces: stereochemical and conformational aspects*, in *Apparent and microscopic contact angles*, J. Drelich, J.S. Laskowski, and K.L. Mittal, Editors. 2000, VSP. p. 111.

34. Holmes-Farley, S.R., Reamey, R.H., Nuzzo, R., McCarthy, T.J., and Whitesides, G.M., *Langmuir*, 1987. **3** p. 799.

35. Lander, L.M., Siewierski, L.M., Brittain, W.J., and Vogler, E.A., *Langmuir*, 1993. **9** p. 2237.

36. Washburn, E.W., *Phys. rev.*, 1921. **17** p. 273.

37. van Oss, C.J., Giese, R.F., Li, Z., Murphy, K., Norris, J., Chaudhury, M.K., and Good, R.J., *J. Adhes. Sci. Technol.*, 1992. **6** p. 413.

38. Chibowski, E. and Holysz, L., *Langmuir*, 1992. **8** p. 710.

39. Brugnara, M., Degasperi, E., Della Volpe, C., Maniglio, D., Penati, A., and Siboni, S., *Wettability of porous materials II: Can we obtain the contact angle from the Washburn equation?* in *Contact angle, wettability and adhesion*, K.L. Mittal, Editor. 2006, VSP: Leiden. p. 143.

40. de Gennes, P.G., *Rev. Mod. Phys.*, 1985. **57** p. 827.

41. Lafuma, A. and Quere, D., *Nat. Mater.*, 2003. **2** p. 457.

42. Dettre, R.H. and Johnson, J.R.E., *Adv. Chem. Ser.*, 1964. **43** p. 136.

43. Wenzel, R.N., *Ind. Eng. Chem*, 1936. **28** p. 988.

44. Cassie, A.B.D. and Baxter, S., *Trans. Faraday Soc.*, 1944. **40** p. 546.

45. Callies, M. and Quere, D., *Soft Matter*, 2005. **1** p. 55.

46. Gao, L.C. and McCarthy, T.J., *Langmuir*, 2007. **23** p. 3762.

47. Chen, W., Fadeev, A.Y., Hsieh, M.C., Oner, D., Youngblood, J., and McCarthy, T.J., *Langmuir*, 1999. **15** p. 3395.

48. Oner, D. and McCarthy, T.J., *Langmuir*, 2000. **16** p. 7777.

49. Bartell, F.E. and Shepard, J.W., *J. Phys. Chem.*, 1953. **57** p. 455.

50. Extrand, C.W., *Langmuir*, 2003. **19** p. 3793.

51. Garbassi, F., Morra, M., and Occhiello, E., *Surface energetics and contact angle*, in *Polymer surfaces: from physics to technology*. 1998, John Wiley & Sons Ltd: West Sussex. p. 169.

52. Darhuber, A.A. and Troian, S.M., *Annu. Rev. Fluid Mech.*, 2005. **37** p. 425.

53. Drelich, J., *Instability of the three-phase contact region and its effect on contact angle relaxation*, in *Apparent and microscopic contact angles*, J. Drelich, J.S. Laskowski, and K.L. Mittal, Editors. 2000, VSP. p. 27.

54. Kamusewitz, H. and Possart, W., *The static contact angle hysteresis and Young's equilibrium contact angle*, in *Contact angle, wettability and adhesion*, K.L. Mittal, Editor. 2006, VSP: Leiden. p. 101.

55. Radelczuk, H., Holysz, L., and Chibowski, E., *J. Adhes. Sci. Technol.*, 2002. **16** p. 1547.

56. Azioune, A., Chehimi, M.M., Miksa, B., Basinska, T., and Slomkowski, S., *Langmuir*, 2002. **18** p. 1150.

57. Krishnan, A., Liu, Y.H., Cha, P., Woodward, R., Allara, D., and Vogler, E.A., *Colloids Surf., B*, 2005. **43** p. 95.

58. Teasdale, P.R., *Characterisation of the chemical properties of polypyrrole and polyaniline*, in *Intelligent Polymer Research Institute*. 1993, University of Wollongong: Wollongong.

59. Stranks, D.R., Heffernan, M.L., Lee Dow, K.C., McTigue, P.T., and Withers, C.R.A., *Chemistry: A structural view*. 1973, Clayton: Wilke and Company.

60. Hiemenz, P.C. and Rajagopalan, R., *Principles of colloid and surface chemistry*. 3rd ed. 1997, New York: Marcel Dekker.

61. Howe, J.M., *Interfaces in Materials: Atomic Structure, Kinetics and Thermodynamics of Solid-Vapor, Solid-Liquid and Solid-Solid Interfaces*. 1997, New York: John Wiley & Sons.

62. Cuenot, S., Fretigny, C., Demoustier-Champagne, S., and Nysten, B., *Physical Review B*, 2004. **69**.

63. van Krevelen, D.W., *Properties of polymers*. 3rd ed. 1997: Elsevier Science.

64. Klammer, I., Hofmann, M.C., Buchenauer, A., Mokwa, W., and Schnakenberg, U., *J. Micromech. Microeng.*, 2006. **16** p. 2425.

65. Sharma, P. and Hanumantha Rao, K., *Adv. Colloid. Inter. Sci.*, 2002. **98** p. 341.

66. Siboni, S., Della Volpe, C., Maniglio, D., and Brugnara, M., *J. Colloid Interface Sci.*, 2004. **271** p. 454.

67. Fox, H.W. and Zisman, W.A., *J. Colloid Interface Sci.*, 1952. **7** p. 428.

68. Fowkes, F.M., *Ind. Eng. Chem*, 1964. **56** p. 40.

69. Fowkes, F.M., *Contact angle, wettability and adhesion*. Advances in chemistry series. Vol. 43. 1964, Washington: American Chemical Society. 99.

70. Fowkes, F.M., McCarthy, D.C., and Mostafa, M.A., *J. Colloid Interface Sci.*, 1980. **78** p. 200.

71. Bangham, D.H. and Razouk, R.I., *Trans. Faraday Soc.*, 1937. **33** p. 1459.

72. Bangham, D.H. and Razouk, R.I., *Proc. R. Soc. London, Ser. A.*, 1938. **166** p. 572.

73. van Oss, C.J., *J. Adhes. Sci. Technol.*, 2002. **16** p. 669.

74. Owens, D.K. and Wendt, R.C., *J. Appl. Polym. Sci.*, 1969. **13** p. 1741.

75. Kaeble, D.H., *Physical Chemistry of Adhesion*. 1971, New York: Wiley Interscience.

76. Wu, S., *J. Polym. Sci. C*, 1971. **34** p. 19.

77. Wu, S., *Polymer Interface and Adhesion*. 1982, New York: Marcel Dekker.

78. van Oss, C.J., Chaudhury, M.K., and Good, R.J., *Adv. Coll. Inter. Sci.*, 1987. **28** p. 35.

79. van Oss, C.J., Good, R.J., and Chaudhury, M.K., *Sep. Sci. Tech.*, 1987. **22** p. 1.

80. Chaudhury, M.K., *Short-range and long-range forces in colloidal and macroscopic systems*. 1984, State University of New York, SUNY: Buffalo.

81. Della Volpe, C. and Siboni, S., *J. Adhes. Sci. Technol.*, 2000. **14** p. 235.

82. Hollander, A., *J. Colloid Interface Sci.*, 1995. **169** p. 493.

83. Tretinnikov, O., *J. Colloid Interface Sci.*, 2000. **229** p. 644.

84. Chiang, C.K., Fincher, C.R., Park, Y.W., Heeger, A.J., Shirakawa, H., Louis, E.J., Gau, S.C., and Macdiarmid, A.G., *Phys. Rev. Lett.*, 1977. **39** p. 1098.

85. Shirakawa, H., Louis, E.J., Macdiarmid, A.G., Chiang, C.K., and Heeger, A.J., *J. Chem. Soc., Chem. Commun.*, 1977 p. 578.

86. Naarrmann, H. and Theophilou, N., *Synth. Met.*, 1987. **22** p. 1.

87. Tsukamoto, J., Takahashi, A., and Kawasaki, K., *Jpn. J. Appl. Phys.*, 1990. **29** p. 125.

88. Brabec, C.J., Sariciftci, N.S., and Hummelen, J.C., *Adv. Funct. Mater.*, 2001. **11** p. 15.

89. Kamat, P.V., *J. Phys. Chem. C*, 2007. **111** p. 2834.

90. Coyle, S., Wu, Y.Z., Lau, K.T., De Rossi, D., Wallace, G., and Diamond, D., *MRS Bull.*, 2007. **32** p. 434.

91. Wallace, G. and Spinks, G., *Soft Matter*, 2007. **3** p. 665.

92. Richardson, R.T., Thompson, B., Moulton, S., Newbold, C., Lum, M.G., Cameron, A., Wallace, G., Kapsa, R., Clark, G., and O'Leary, S., *Biomaterials*, 2007. **28** p. 513.

93. Brédas, J.L. and Street, G.B., *Acc. Chem. Res.*, 1985. **18** p. 309.

94. Xia, Y., Wiesinger, J.M., and Macdiarmid, A.G., *Chem. Mater.*, 1995. **7** p. 443.

95. Robinson, L., Isaksson, J., Robinson, N.D., and Berggren, M., *Surf. Sci.*, 2006. **600** p. L148.

96. Nicolas, M., Guittard, F., and Geribaldi, S., *Langmuir*, 2006. **22** p. 3081.

97. Nicolas, M., Guittard, F., and Géribaldi, S., *Angewandte Chemie International Edition*, 2006. **45** p. 2251.

98. Xu, L.B., Chen, W., Mulchandani, A., and Yan, Y.S., *Angew. Chem. Int. Ed.*, 2005. **44** p. 6009.

99. Diaz, A.F. and Bargon, J., *Handbook of conducting polymers*, T.A. Skotheim, Editor. 1986, Marcel Dekker: New York. p. 81.

100. Cho, S.H., Song, K.T., and Lee, J.Y., *Recent advances in polypyrrole*, in *Handbook of conducting polymers*. 2007, CRC Press: New York. p. 8.

101. Madden, J.D., Cush, R.A., Kanigan, T.S., Brenan, C.J., and Hunter, I.W., *Synth. Met.*, 1999. **105** p. 61.

102. Careem, M.A., Vidanapathirana, K.P., Skaarup, S., and West, K., *Solid State Ionics*, 2004. **175** p. 725.

103. Xu, H., Wang, C., Wang, C.L., Zoval, J., and Madou, M., *Biosens. Bioelectron.*, 2006. **21** p. 2094.

104. Wadhwa, R., Lagenaur, C.F., and Cui, X.T., *J. Control. Release*, 2006. **110** p. 531.

105. Low, L.M., Seetharaman, S., He, K.Q., and Madou, M.J., *Sens. Actuators, B*, 2000. **67** p. 149.

106. Gurunathan, K., Murugan, A.V., Marimuthu, R., Mulik, U.P., and Amalnerkar, D.P., *Mater. Chem. Phys.*, 1999. **61** p. 173.

107. Jagur-Grodzinski, J., *Polymers for Advanced Technologies*, 2002. **13** p. 615.

108. Isaksson, J., Tengstedt, C., Fahlman, M., Robinson, N., and Berggren, M., *Advanced Materials*, 2004. **16** p. 316.

109. Isaksson, J., Robinson, N.D., and Berggren, M., *Thin Solid Films*, 2006. **515** p. 2003.

110. Robinson, L., Hentzell, A., Robinson, N., Isaksson, J., and Berggren, M., *Lab Chip*, 2006. **6** p. 1277.

111. Lee, M.-H., *Mol. Cryst. Liq. Cryst.*, 1998. **316** p. 329.

112. Lee, M.-H., Kim, S.S., Rhee, J.M., and Kang, Y., *Polymer (Korea)*, 1998. **22** p. 619.

113. Hato, M., *Chem. Lett., Chem. Soc. Japan*, 1988 p. 1959.

114. Wang, X., Ederth, T., and Inganas, O., *Langmuir*, 2006. **22** p. 9287.

115. Chehimi, M.M., Abel, M.L., Sahraoui, Z., Fraoua, K., Lascelles, S.F., and Armes, S.P., *Int. J. Adhes. Adhes.*, 1997. **17** p. 1.

116. Chehimi, M.M., Abel, M.-L., Perruchot, C., Delamar, M., Lascelles, S.F., and Armes, S.P., *Synth. Met.*, 1999. **104** p. 51.

117. Chehimi, M.M., Pigoislandureau, E., and Delamar, M., *J. Chim. Phys. Phys.-Chim. Biol.*, 1992. **89** p. 1173.

118. Chehimi, M.M., Abel, M.L., Pigoislandureau, E., and Delamar, M., *Synth. Met.*, 1993. **60** p. 183.

119. Fadda, E. and Clarisse, C., *Synth. Met.*, 1995. **72** p. 99.

120. Manz, A., Graber, N., and Widmer, H.M., *Sens. Actuators*, 1990. **B1** p. 244.

121. Manz, A., Miyahara, Y., Miura, J., Watanabe, Y., Miyagi, H., and Sato, K., *Sens. Actuators*, 1990. **B1** p. 249.

122. *Nat. Biotechnol.*, 2003. **21** p. 333.

123. Gould, P., *Mater. Today*, 2004. **7** p. 48.

124. Whitesides, G.M., *Nature*, 2006. **442** p. 368.

125. Reyes, D.R., Iossifidis, D., Auroux, P.A., and Manz, A., *Anal. Chem.*, 2002. **74** p. 2623.

126. Beebe, D.J., Mensing, G.A., and Walker, G.M., *Annu. Rev. Biomed. Eng.*, 2002. **4** p. 261.

127. Becker, H. and Locascio, L.E., *Talanta*, 2002. **56** p. 267.

128. Abgrall, P. and Gue, A.M., *J. Micromech. Microeng.*, 2007. **17** p. R15.

129. Fair, R., *Microfluid. Nanofluid.*, 2007. **3** p. 245.

130. Karlsson, R., Karlsson, M., Karlsson, A., Cans, A.S., Bergenholtz, J., Akerman, B., Ewing, A.G., Voinova, M., and Orwar, O., *Langmuir*, 2002. **18** p. 4186.

131. Tas, N.R., Berenschot, J.W., Lammerink, T.S.J., Elwenspoek, M., and van den Berg, A., *Anal. Chem.*, 2002. **74** p. 2224.

132. Fan, R., Yue, M., Karnik, R., Majumdar, A., and Yang, P., *Phys. Rev. Lett.*, 2005. **95** p. 86607(4).

133. Karnik, R., Fan, R., Yue, M., Li, D.Y., Yang, P.D., and Majumdar, A., *Nano Lett.*, 2005. **5** p. 943.

134. Wong, P.K., Wang, T.H., Deval, J.H., and Ho, C.M., *IEEE-ASME T. Mech.*, 2004. **9** p. 366.

135. Manz, A., Harrison, D.J., Verpoorte, E.M.J., Fettinger, J.C., Paulus, A., Ludi, H., and Widmer, H.M., *J. Chromatogr.*, 1992. **593** p. 253.

136. Harrison, D.J.F., K., Seiler, K., Fan, Z.H., Effenhauser, C.S., and Manz, A., *Science*, 1993. **261** p. 895–897.

137. Peterson, K.E., *Proc. IEEE*, 1982. **70** p. 420.

138. Verpoorte, E.M.J., *Trends in anal. chem.*, 2000. **19** p. 350.

139. Locascio, L. and Michael, G., *Anal. Chem.*, 1997. **69** p. 4783.

140. Unger, M.A., Chou, H.P., Thorsen, T., Scherer, A., and Quake, S.R., *Science*, 2000. **288** p. 113.

141. Duffy, D.C. and C., M.J., *Anal. Chem.*, 1998. **70** p. 4974.

142. Thorsen, T., Maerkl, S.J., and Quake, S.R., *Science*, 2002. **298** p. 580.

143. Sia, S.K. and Whitesides, G.M., *Electrophoresis*, 2003. **24** p. 3563.

144. Fair, R.B., Khlystov, A., Tailor, T.D., Ivanov, V., Evans, R.D., Griffin, P.B., Srinivasan, V., Pamula, V.K., Pollack, M.G., and Zhou, J., *IEEE Des. Test Comput.*, 2007. **24** p. 10.

145. Weston, D.F., Smekal, T., Rhine, D.B., and Blackwell, J., *J. Vac. Sci. Technol. B*, 2001. **19** p. 2846.

146. Lee, L.J., *J. Chin. Inst. Chem. Eng.*, 2003. **34** p. 25.

147. Dubois, P., Marchand, G., Fouillet, Y., Berthier, J., Douki, T., Hassine, F., Gmouh, S., and Vaultier, M., *Anal. Chem.*, 2006. **78** p. 4909.

148. Jeffrey, R.M., Ketan, H.B., Brian, G.P., and Orlin, D.V., *Nat. Mater.*, 2005. **4** p. 98.

149. Eeltink, S., Decrop, W.M.C., Rozing, G.P., Schoenmakers, P.J., and Kok, W.T., *J. Sep. Sci.*, 2004. **27** p. 1431.

150. Marle, L. and Greenway, G.M., *TrAC Trends in Analytical Chemistry*, 2005. **24** p. 795.

151. McGraw, C.M., Stitzel, S.E., Cleary, J., Slater, C., and Diamond, D., *Talanta*, 2007. **71** p. 1180.

152. Ahn, C.H., Choi, J.W., Beaucage, G., Nevin, J.H., Lee, J.B., Puntambekar, A., and Lee, J.Y., *Proceedings Of The Ieee*, 2004. **92** p. 154.

153. Yussuf, A.A., Sbarski, I., Solomon, M., Tran, N., and Hayes, J.P., *J. Mater. Process. Technol.*, 2007. **189** p. 401.

154. Cho, S.K., Moon, H.J., and Kim, C.J., *J. Microelectromech. Syst.*, 2003. **12** p. 70.

155. Zhao, B., Moore, J.S., and Beebe, D.J., *Anal. Chem.*, 2002. **74** p. 4259.

156. De Bakker, D., Baetens, K., Van Nimmen, E., Gellynck, K., Mertens, J., Van Langenhove, L., and Kiekens, P., *Belg. J. Zool.*, 2006. **136** p. 137.

157. Laser, D.J. and Santiago, J.G., *J. Micromech. Microeng.*, 2004. **14** p. R35.

158. Stone, H.A., Stroock, A.D., and Ajdari, A., *Annu. Rev. Fluid Mech.*, 2004. **36** p. 381.

159. Cardenas-Valencia, A.M., Dlutowski, J., Bumgarner, J., Munoz, C., Wang, W., Popuri, R., and Langebrake, L., *Sens. Actuators, A*, 2007. **136** p. 374.

160. Cardenas-Valencia, A.M., Fries, D.P., Langebrake, L.C., and Benson, R.F. *Rapid design, fabrication and optimization of a single shot thermo-pneumatic micro-actuation for the delivery of minute amounts of liquids*. in *Proc. of the Intern. Conf. on Microchannels and Minichannels*. 2003. NY, USA.

161. Griss, P., Andersson, H., and Stemme, G. *Liquid handling using expandable microspheres*. in *The Fifteenth IEEE International Conference on Micro Electro Mechanical Systems*. 2002.

162. Felton, M., *Anal. Chem.*, 2003. **75** p. 429A–432A.

163. Bousse, L., Cohen, C., Nikiforov, T., Chow, A., Kopf-Sill, A.R., Dubrow, R., and Parce, J.W., *Annu. Rev. Biophys. Biomol. Struct.*, 2000. **29** p. 155.

164. Madou, M.J., Lee, L.J., Daunert, S., Lai, S., and Shih, C.-H., *Biomed. Microdev*, 2001. **3** p. 245.

165. Juncker, D., Schmid, H., Drechsler, U., Wolf, H., Wolf, M., Michel, B., de Rooij, N., and Delamarche, E., *Anal. Chem.*, 2002. **74** p. 6139.

166. Squires, T.M. and Quake, S.R., *Rev. Mod. Phys.*, 2005. **77** p. 977.

167. Schasfoort, R.B.M., Schlautmann, S., Hendrikse, L., and van den Berg, A., *Science*, 1999. **286** p. 942.

168. Polson, N.A. and Hayes, M.A., *Anal. Chem.*, 2000. **72** p. 1088.

169. Lazar, I.M. and Karger, B.L., *Anal. Chem.*, 2002. **74** p. 6259.

170. McKnight, T., E., Culbertson, C.T., Jacobson, S.C., and Ramsey, J.M., *Anal. Chem.*, 2001. **73** p. 4045.

171. Barker, S.L.R., Ross, D., Tarlov, M.J., Gaitan, M., and Locascio, L.E., *Anal. Chem.*, 2000. **72** p. 5925.

172. Moorthy, J., Khoury, C., Moore, J.S., and Beebe, D.J., *Sens. Actuators, B*, 2001. **75** p. 223.

173. Regnier, F.E., He, B., Lin, S., and Busse, J., *Tib Tech*, 1999. **17** p. 101.

174. Woolley, A.T., Lao, K.Q., Glazer, A.N., and Mathies, R.A., *Anal. Chem.*, 1998. **70** p. 684.

175. Liu, J., Enzelberger, M., and Quake, S., *Electrophoresis*, 2002. **23** p. 1531.

176. Ludwig, M. and Belder, D., *Electrophoresis*, 2003. **24** p. 2481.

177. Ludwig, M., Kohler, F., and Belder, D., *Electrophoresis*, 2003. **24** p. 3233.

178. Gascoyne, P.R.C., Vykoukal, J.V., Schwartz, J.A., Anderson, T.J., Vykoukal, D.M., Current, K.W., McConaghy, C., Becker, F.F., and Andrews, C., *Lab Chip*, 2004. **4** p. 299.

179. Jones, T.B., Gunji, M., Washizu, M., and Feldman, M.J., *J. Appl. Phys.*, 2001. **89** p. 1441.

180. Kataoka, D.E. and Troian, S.M., *Nature*, 1999. **402** p. 794.

181. Darhuber, A.A., Valentino, J.P., Davis, J.M., Troian, S.M., and Wagner, S., *Appl. Phys. Lett.*, 2003. **82** p. 657.

182. Gallardo, B.S., Gupta, V.K., Eagerton, F.D., Jong, L.I., Craig, V.S., Shah, R.R., and Abbott, N.L., *Science*, 1999. **283** p. 57.

183. Abbott, N.L., *Colloid Polym. Sci.*, 1997. **103** p. 300.

184. Aydogan, N., Gallardo, B.S., and Abbott, N.L., *Langmuir*, 1999. **15** p. 722.

185. Shin, J.Y. and Abbott, N.L., *Langmuir*, 1999. **15** p. 4404.

186. Rosslee, C.A. and Abbott, N.L., *Curr. Opin. Colloid Interface Sci.*, 2000. **5** p. 81.

187. Aydogan, N. and Abbott, N.L., *Langmuir*, 2001. **17** p. 5703.

188. Abbott, N.L., *AICHE Journal*, 2001. **47** p. 2634.

189. Aydogan, N., Rosslee, C.A., and Abbott, N.L., *Colloids Surf., A*, 2002. **201** p. 101.

190. Aydogan, N., Aldis, N., and Guvenir, O., *Langmuir*, 2003. **19** p. 10726.

191. Rosario, R., Gust, D., Hayes, M., Jahnke, F., Springer, J., and Garcia, A.A., *Langmuir*, 2002. **18** p. 8062.

192. Lippmann, G., *Ann. Chim. Phys.*, 1875. **5** p. 494.

193. Lee, J. and Kim, C.-J., *J. Microelectromech. Syst.*, 2000. **9** p. 171.

194. Colgate, E. and Matsumoto, H., *J. Vac. Technol.*, 1990 p. 3625.

195. Ni, J., Zhong, C.J., Coldiron, S.J., and Porter, M.D., *Anal. Chem.*, 2001. **73** p. 103.

196. Beni, G. and Hackwood, S., *Appl. Phys. Lett.*, 1981. **38** p. 207.

197. Kuo, J.S., Spicar-Mihalic, P., Rodriguez, I., and Chiu, D.T., *Langmuir*, 2003. **19** p. 250.

198. Mugele, F. and Baret, J.C., *J. Phys.-Condes. Matter*, 2005. **17** p. R705.

199. Quilliet, C. and Berge, B., *Curr. Opin. Colloid Interface Sci.*, 2001. **6** p. 34.

200. Welters, W.J.J. and Fokkink, L.G.J., *Langmuir*, 1998. **14** p. 1535.

201. Yoon, J.-Y. and Garrell, R.L., *Anal. Chem.*, 2003. **75** p. 5097.

202. Pollack, M.G., Fair, R.B., and Shenderov, A.D., *Appl. Phys. Lett.*, 2000. **77** p. 1725.

203. Wang, J., Bunimovich, Y.L., Sui, G., Savvas, S., Wang, J., and Guo, Y., *Chem. Commun.*, 2006 p. 3075.

204. Shim, J., Cui, X., Matrin, D.C., and Takayama, S., *Proceedings of the Second Joint EMBS/BMES Conference (IEEE)*, 2002 p. 1684.

205. Gill, A., Lillie, G., Farace, G., and Vadgama, P., *Int. J. Environ. Anal. Chem.*, 2005. **85** p. 699.

206. Kastantin, M.J., Li, S., Gadre, A.P., Wu, L.-Q., Bentley, W.E., Payne, G.F., Rubloff, G.W., and Ghodssi, R., *Sens. Mater.*, 2003. **15** p. 295.

207. Smela, E., *Advanced Materials*, 2003. **15** p. 481.

208. Pettersson, P.K., Jager, E.W.H., and Inganäs, O., *Surface micromachined polymer actuators as valves in PDMS microfluidic system*, in *IEEE-EMBS Special Topic Conf. on Microtechnologies in Medicine and Biology*. 2000: Lyon, France.

209. Wu, Y., Zhou, D., Spinks, G.M., Innis, P.C., Megill, W.M., and Wallace, G.G., *Smart Mater. Struct.*, 2005. **14** p. 1511.

CHAPTER 2

GENERAL EXPERIMENTAL

2.1 Introduction

General experimental details of materials and techniques used in this thesis are described in this chapter. Information pertaining to specific procedures is presented in the experimental section of the relevant chapters.

2.2 Reagents and materials

2.2.1 Reagents

Acetonitrile (ACN; Univar, APS, 99.7 %), sodium dodecylbenzenesulfonate (NaDBS; Sigma), sodium nitrate ($NaNO_3$; Ajax), sodium *p*-toluenesulfonate (NapTS; Sigma), tetrabutylammonium perchlorate ($TBA.ClO_4$; Fluka), diiodomethane (CH_2I_2; Sigma) glycerol (Sigma), formamide (Sigma), ethylene glycol (Sigma), potassium ferricyanide ($K_3Fe(CN_6)$; Ajax), potassium chloride (KCl; Ajax), methyl methacrylate (MMA; Sigma), tetraethylene glycol diacrylate (TEGDA; Sigma) and benzoyl peroxide (BPO; Sigma) were used as received. Dichloromethane (DCM; Ajax) was purified by rotary evaporation and the clear fraction retained. Pyrrole (Py; Merck, > 97 %) was distilled and stored below -20 ° C under nitrogen. All aqueous solutions were prepared using deionised MilliQ® water (18 MΩcm).

2.2.2 Electrodes

Working electrode materials were indium tin oxide coated glass (ITO; $\leq 10\ \Omega\ sq^{-1}$, Delta Technologies Ltd (USA)), glassy carbon (GC; BAS), platinum sheet (Pt sheet; AGR Matthey) and platinised polyvinylidenedifluoride (PVDF) membrane (Pt-PVDF; Durapore (pore size 0.45 μm; hydrophobic)). These electrodes were generally cut to 1 cm x 1.5 cm pieces. A Pt disk electrode (BAS MF-2013; 1.76 mm^2) was used for cyclic voltammetric studies. Pt disk, GC and Pt sheet electrodes were polished sequentially

using 1.0, 0.3 and 0.05 μm alumina powder on felt polishing cloth and were sonicated in MilliQ® water for 10 min to remove excess alumina from the electrode surface. All electrodes were gently washed in acetonitrile to remove any surface contamination and dried under a nitrogen stream prior to use.

Pt-PVDF was prepared by sputtering a thin layer of platinum onto PVDF membrane using a Dynavac Magnetron sputter coater (Model SC100MS). Sputtering was performed using an argon pressure of 2 x 10^3 mBar and a sputtering current of 30 mA for a duration of 20 min. This resulted in a platinum layer with conductivity of 26 – 47 S/cm, using a linear four point conductivity probe (Jandel). The platinum coating on the Pt-PVDF membrane was measured to be ca. 10 μm in thickness using a micrometer. For the preparation of the integrated trilayer electrochemical cell configuration used in Chapter 4 and Chapter 5, the PVDF membrane was sputter-coated on both sides and the membrane trimmed to size using a scalpel. The deposition of polypyrrole on the integrated trilayer membrane electrodes is further discussed in Section 2.3.2.

2.3 Electrochemical polymerisation of conducting polymers

2.3.1 Instrumentation

Electrochemical depositions and characterisations were carried out using an EG&G PAR 363 potentiostat/galvanostat and a MacLab 400, employing Chart (v 5.2.11) and EChem (v 2.0.7) software. For all depositions and cyclic voltammetric characterisations a conventional three-electrode cell was employed, consisting of a working electrode (Pt sheet, Pt-PVDF, GC, ITO, Pt disk, Pt-glass or Pt-coated channel) and a cylindrical platinum mesh counter electrode surrounding the working electrode. A schematic of the three-electrode cell is given in Figure 1.

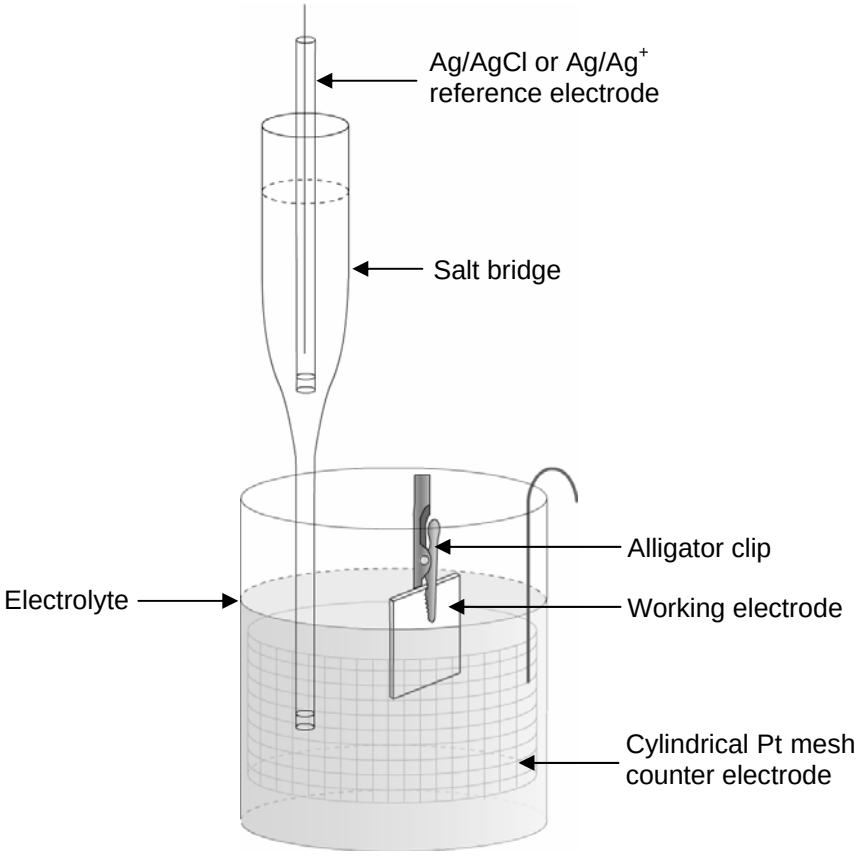

Figure 1. Schematic of three-electrode electrochemical cell used for all polymerisations and electrochemical characterisation of polymers.

An organic reference electrode (Ag/Ag^+ reference electrode in 0.01 M $AgNO_3$ and 0.1 M $TBA.ClO_4$ in ACN) was used in all studies employing organic electrolytes (Chapter 3), whereas a Ag/AgCl reference electrode in 3.0 M KCl was used for all aqueous studies (Chapter 4 and Chapter 5). Specific deposition conditions for individual polymers are given in the relevant chapters.

2.3.2 Trilayer integrated membrane configuration

The following configuration was used in *in-situ* electrochemical fluid movement experiments in Chapter 4 and Chapter 5. This configuration was pursued to ensure the maximum efficiency of the electrochemical redox reactions due to the close proximity of the working and counter electrodes and the ability for the membrane to be contained

within the membrane pores, while simplifying the structure of the electrochemical cell by integrating the counter electrode (Figure 2). PVDF membrane which had been coated on either side with a layer of platinum (described in Section 2.2.2) was coated with polypyrrole doped with dodecylbenzenesulfonate (PPy.DBS) on both sides to form working and counter electrodes, which were electrically insulated from each other by trimming the edges with a scalpel. The PPy.DBS working and counter electrodes were deposited using a current density of 1 mA/cm^2 for 90 s (working electrode) and 180 s (counter electrode), to form a thicker counter electrode than the working electrode. This configuration was then implemented for *in-situ* electrochemical fluid control studies in external aqueous electrolytes (Chapter 4) and with electrolyte integrated into the pores of the membrane, without the need for surrounding electrolyte in Chapter 5, where further details will be given.

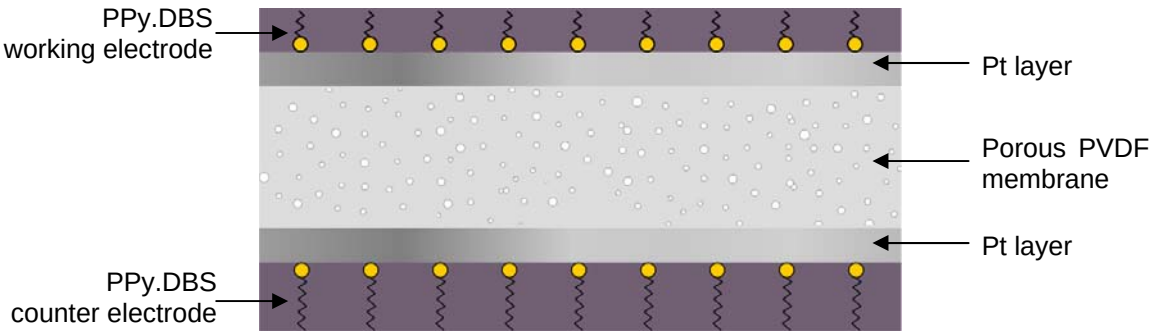

Figure 2. Integrated trilayer electrochemical cell configuration: PPy.DBS deposited on both sides of Pt-PVDF membrane to form a working electrode (1 mA/cm^2, 90s) and a thicker counter electrode (1 mA/cm^2, 180s). Membrane pores were filled with aqueous electrolyte from the surrounding liquid (0.1 M $NaNO_3$) in Chapter 4 and with ionic liquid-based electrolytes in Chapter 5.

2.4 Characterisation techniques

All polymer preparation and characterisations were carried out at ambient temperature (ca. 20 ° C) in a laboratory with variable humidity.

2.4.1 Electrochemical characterisation

The electrochemical properties of polymers were investigated post-deposition using cyclic voltammetry. Films were prepared on an appropriate working electrode using conditions specified in individual chapters. The same three-electrode cell used for deposition of polymers (Figure 1) was employed with an appropriate electrolyte and reference electrode for all cyclic voltammetric studies. The potential was swept between suitable upper and lower potentials while the current was monitored. The resulting cyclic voltammogram was diagnostic of the electrochemical characteristics of the polymer.

2.4.2 Scanning Electron Microscopy

A Leica-Stereo SS440 scanning electron microscope (SEM) with a secondary electron detector was employed to investigate the surface morphology of polymers at high magnification. Polymers were mounted on a stage and sputter-coated with a thin layer of gold to avoid charging of polymer samples and in order to obtain clear images. An accelerating voltage of 20 kV was used for all SEM examinations.

2.4.3 Wettability and surface energy measurements

A DataPhysics OCA20 goniometer utilising SCA21 software was used for all sessile drop contact angle measurements, surface energy analyses and dynamic contact angle analyses in Chapter 3 and Chapter 4 using captive drop goniometry (described in Chapter 1, Section 1.4.2.2.1) employed. Wilhelmy balance tensiometry (described in Chapter 1, Section 1.4.2.2.2) was used for dynamic contact angle measurement of polymers in Chapter 5, where it will be discussed further.

2.4.3.1 Contact angle goniometery of sessile drops

Contact angle measurements of sessile drops were carried out in ambient laboratory conditions (in air). Typically the contact angles of 2 μL droplets of test liquid were measured in at least five different positions on each film. This was carried out on at least triplicate films, with the total contact angle and standard deviation (SD) reported in the format θ ± SD. (e.g. 50.0 ± 2.4 º). Contact angles were measured after polymer deposition, electrochemical oxidation or electrochemical reduction using the conditions described in individual chapters. The contact angles reported for sessile drops were recorded just as the liquid motion had ceased and may be regarded as the 'recently advanced' angle. A slight downwards tilt in the camera viewing angle was necessary to accurately determine the baseline.

Surface energy measurements of polymers were carried out according to the Lifshitz-van der Waals Acid-Base theory of van Oss, Good and Chaudhury, discussed in Chapter 1, Section 1.1.4.2. Contact angle measurements of surface energy test liquids, typically water, glycerol and diiodomethane, were carried out using the method described above for sessile drops. Note that 1 μL drops of CH_2I_2 were used as 2 μL drops spread too far across the film for multiple measurements to be made. The surface energy components were determined from the contact angles of test liquids with known surface tension components (Chapter 1, Section 1.1.4.2, Table 2) using DataPhysics SCA21 software. The total surface energy of a material was regarded as the combination of the apolar Lifshitz-van der Waals component (LW; intermolecular force term) and polar Lewis acid-base (AB) component, where the latter term consists of the electron donating (γ^-) and accepting (γ^+) parameters of the material, as described by Equation 1:

Equation 1 $$(1+\cos\theta)\gamma_l = 2\sqrt{\gamma_l^{LW}\gamma_s^{LW}} + 2\sqrt{\gamma_l^{+}\gamma_s^{-}} + 2\sqrt{\gamma_l^{-}\gamma_s^{+}}$$

2.4.3.2 Dynamic contact angle analyses

Captive drop goniometry was used to investigate the dynamic wetting properties of polymers in Chapter 3. The advancing (θ_a) and receding (θ_r) contact angles of polymers were determined by placing a 2 μL water drop on the film surface and gently inserting the dosing syringe into the top of the drop. A set volume of water (~1 μL) was then added to, and withdrawn, from the droplet to determine θ_a and θ_r, respectively, immediately after the volume had been dispensed or withdrawn, according to the method of Radelczuk *et al*. [1]. This scenario was depicted diagrammatically in Chapter 1, Section 1.4.2.2.1, Figure 4.

2.5 References

1. Radelczuk, H., Holysz, L., and Chibowski, E., *J. Adhes. Sci. Technol.*, 2002. 16 p. 1547.

CHAPTER 3

WETTABILITY AND SURFACE ENERGY OF POLYTERTHIOPHENES

3.1 Introduction

The wettability and surface energy of materials has long been investigated and many surfaces, including polymers, have been characterised. Conducting polymers are of particular interest due to their dynamic nature and inherent ability to respond to changes in their environment. Of the studies carried out (see Chapter 1, Section 1.2.5 for more detail), few have focused on polythiophenes (PTh) and none, to the best of the candidate's knowledge, on those prepared from the 2,2′:5′,2″-terthiophene monomer (TTh; Figure 1). Electrochemical deposition of polythiophene from the terthiophene monomer occurs at a lower oxidation potential than if thiophene or bithiophene monomers were used [1], resulting in a decreased likelihood of irreversible over-oxidiation of the polymer and thereby improving the reversible nature of the electroactivity of the resultant polymer.

3.1.1 Wettability studies on polythiophenes and their application in microdevices

The inherent change in wettability and surface energy of conducting polymers upon electrochemical oxidation and reduction suggests they may be useful for fluid control in microdevices, as discussed in Chapter 1, Section 1.4.3.2. Several recent examples of this using polythiophenes include a microfluidic chip with gates which control the path of water by switching poly-3-hexylthiophene (P3HT)-coated channels between hydrophilic and hydrophobic [2], an electrochemical switching device based on P3HT [3] and P3HT-coated glass slides in an electrochemical cell configuration capable of moving the level of electrolyte up against gravity [4]. Of the wettability studies on polythiophene, most have been concerned with the effect of polymer functionalisation on the resulting wettability by water. A summary of published wettability data and surface energy components, where applicable, is given in Table 1. Surface energy components were defined in Chapter 1, Section 1.1.4.

Table 1. Contact angle (°) and surface energy components (mJ/m^2) for various polythiophenes published in the literature.

	Contact angle (°)			Surface energy components (mJ/m^2)					
Polymer	**Water**	**L1**	**L2**	γ_s	γ^{LW}	γ^{AB}	γ^+	γ^-	**Ref.**
PTh$^{0\,a}$	86	54 [b]							[c] [5]
PTh$^{+\,a}$	83	58 [b]							
P3MT$^{0\,a}$	90	42 [b]							
P3MT$^{+\,a}$	88	40 [b]							
P3OT^0				ca. 23	23	<1			[d] [6]
P3OT$^+$				ca. 31	26	ca. 5			
P3OT^0					34.2				[e] [7]
P3OT^0	105								[2]
P3OT$^+$	96								
P3HT^0	102								
P3HT$^+$	89								
P3BT^0	88								
P3BT$^+$	71								
P3HT^0	97	67 [b]	25 [g]	27	25	2.3	0.4	3.6	[h] [4]
PEDOT$^{+\,f}$	34	11 [b]	5 [g]	47	27	20	2.1	48	
PTh-F$^{0\,i}$	108	96 [k]	78 [g]	11.8	9.5	2.3			[m] [8]
PTh-F$^{0\,j}$	153	137 [k]	135 [g]	[l]	[l]	[l]			
PTh-F$^{0\,n}$	134								[9]
PTh-F$^{0\,o}$	82								

L1: test liquid 1; L2: test liquid 2; PTh: polythiophene; P3MT: poly-3-methylthiophene; P3OT: poly-3-octylthiophene; P3HT: poly-3-hexylthiophene; P3BT: poly-3-butylthiophene; PEDOT: poly(3,4-ethylenedioxythiophene); PTh-F: fluorinated PTh. a: electrodeposited; b: ethylene glycol; c: spreading coefficients (not shown) calculated by Fox-Zisman method; d: calculated using Lifshitz-van der Waals-Acid-Base theory; e: measured by inverse gas chromatography; f: vapour phase polymerised; g: n-hexadecane; h: calculated using Lifshitz-van der Waals-Acid-Base theory; i: chemically deposited; j: electrodeposited; k: diiodomethane; l: too low to be measured by Owens-Wendt-Fowkes method; m: calculated using Owens-Wendt-Fowkes method; n: microtubules; o: flat. *Polymer superscripts:* 0: polymer is in reduced state; +: polymer is in oxidised state.

Early studies included a comparison of the effect of oxidation state on the surface energy of PTh and P3MT, with only a small difference in the wettability of neutral and oxidised films apparent [5]. More recent studies have investigated the surface energy and wettability of P3OT and found the surface energy to be on the order of 23 mJ/m^2 for de-doped films and 31 mJ/m^2 for doped films [6]. The dispersive component of P3OT was determined to be 34 mJ/m^2 by inverse gas chromatography [7]. Robinson *et al.* investigated the effect of chain length on the water contact angle of oxidised and reduced alkyl-functionalised polythiophenes using an *in-situ* electrochemical switching device [10]. A change in wettability of 9, 13 and 17 ° upon redox switching was observed between the oxidised and reduced states of P3OT, P3HT and P3BT, respectively. P3HT was then employed for gating the flow of aqueous liquids in microfluidic devices [2]. A comprehensive study on the wettability of P3HT and PEDOT at different potentials during *in-situ* oxidation and reduction, as well as the surface energy of oxidised and reduced polymer *ex-situ* the electrochemical cell was carried out by Wang *et al*. [4]. It was shown that hydrophobic P3HT had a low surface energy dominated by non-polar interactions in the neutral state (27 mJ/m^2), while PEDOT was higher in surface energy (47 mJ/m^2) in the native oxidised state due to the predominant acid-base interactions at the surface.

Other studies have focused on creating highly hydrophobic polythiophene by use of a fluorinated dopant or functionalised monomer. Nicolas *et al.* prepared ultrahydrophobic polythiophene, exhibiting a water contact angle greater than 150 ° and an oil contact angle of 130 ° by polymerisation of a fluorinated thiophene monomer using electrochemical means [8, 11]. Other examples included preparation of hydrophobic PTh microtubules exhibiting a water contact angle of 134 ° [9].

Very few reports of advancing (θ_a) and receding (θ_r) contact angle measurements (as discussed in Chapter 1, Section 1.1.2.3) have been carried out for polythiophene. In one study, chemically prepared poly(fluorinated thiophene) was been found to possess a water contact angle hysteresis of > 70 °, while electrochemically prepared poly(fluorinated thiophene) had a significantly lower wetting hysteresis of < 10 ° [8]. An investigation into the effect of substrate and film thickness on the surface energy and wettability of polythiophenes is lacking.

Of the methods used to determine the surface energy of materials (see Chapter 1, Section 1.1.4 for an in-depth discussion), the van Oss-Good-Chaudhury approach has found repeated use for conducting polymers based on the interpretation of the polymer in terms of non-polar and acid-base interactions [4, 12]. The electron loss and gain that occurs during oxidation and reduction of conducting polymers lends itself to being interpreted by the Lewis acid-base terms of the van Oss-Good-Chaudhury method. There is precedent for using this approach, as previous studies have shown its usefulness for conducting polymers [4, 12].

3.1.2 Raman spectroscopic analysis of polythiophenes

The wettability of a material is strongly influenced by its surface composition and topography (Chapter 1). To probe these surface properties, Raman spectroscopy, AFM, SEM and optical profilometry have been used to characterise the PTTh films investigated in this thesis. The Raman vibrations of polythiophenes have been well documented [13-24], with peaks in the 1450 cm^{-1} region particularly useful in identifying changes in the structure of the polymer backbone during oxidative doping. There have also been few Raman studies for polythiophene prepared from the 2,2′:5′,2″-terthiophene monomer [1], though reports on the Raman vibrations of the terthiophene monomer itself are more common [25-30]. Raman spectroscopy is a useful technique

for probing the oxidation state of conducting polymers, due to its ease of use, instant feedback and non-destructive nature. Peak assignments for Raman bands of polythiophene are shown in Table 2 and are a combination of several assignments reported in the literature [15, 18, 19, 23, 31]. Several studies have looked at the change in Raman bands of polythiophene upon doping. Surface Enhanced Raman Scattering (SERS) measurements have been extensively studied for polythiophene [19, 21, 32] and have allowed insight into the vibrations of the oxidised state. The SERS technique provides selective enhancement of the Raman bands for the oxidised species of polythiophene. Unfortunately this selectivity masks changes in the doping level of polythiophene [23], and as a consequence has not been actively pursued in this study.

Table 2. Raman peak assignments for polythiophene [18].

Please see print copy for Table 2

There have been several different descriptions of the most intense Raman band for polythiophene, that is the symmetric C_α=C_β ring stretching (ν_2), whose position and intensity are an indicator of polymer oxidation state. The treatment of Shi *et al*. [31] has been followed in this thesis, where the ν_2 band is separated into two components due to quinoidic radical cations (polarons) and dications (bipolarons), denoted Q_1 and Q_2, respectively. In addition to the above peaks, a shoulder at ca. 1040 cm^{-1} adjacent to the ν_5 C_β-H bending and a peak at ca. 1100 cm^{-1} were present in the spectra; however these do not appear in the literature and were left out of spectral deconvolution for ease of analysis. A very weak peak at 1410 cm^{-1} was also present, but was also omitted from analyses as it has not been reported in previous studies for polythiophene, and its inclusion affected the intensity of the Q_1 peak.

3.1.3 Chapter Aims

This chapter details the characterisation of novel polyterthiophenes functionalised with different hydrophobic substituents and compares them with unsubstituted polyterthiophene (PTTh). Monomer structures for the hydrophobic-functionalised terthiophenes 4,4′-didecyloxy-2,2′:5′,2″-terthiophene (TTh-DDO) and N-methyl-2-(2-[2′:5′,2″-terthiophen-3′-yl]ethenyl)fullero[3,4]pyrolidine (TTh-C_{60}) are shown in Figure 2 and Figure 3, respectively. These particular monomers were chosen as they were available for the study.

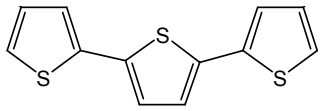

Figure 1. 2,2′:5′,2″-terthiophene (TTh).

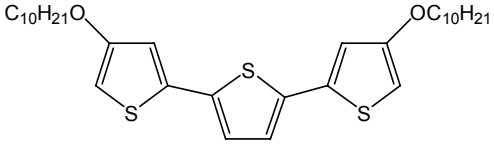

Figure 2. 4,4′-didecyloxy-2,2′:5′,2″-terthiophene (TTh-DDO).

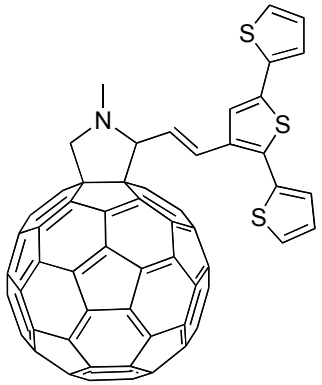

Figure 3. N-methyl-2-(2-[2′:5′,2″-terthiophen-3′-yl]ethenyl)fullero[3,4]pyrolidine (TTh-C_{60}).

Sessile drop goniometry was used to determine the water contact angles of polymer films prepared under varying conditions, along with the contact angles of test liquids for the determination of polymer surface energy. The effect of oxidation state, film thickness, roughness and substrate upon the wettability of the polymer was investigated. Raman spectroscopy was used to elucidate changes in the oxidation state throughout the thickness of the polymer, with the results correlated to the work function of the electrode substrate. These characterisations were carried out with a view to investigating the dynamic surface properties of polyterthiophenes, which may have application in fluid control in microfluidic devices.

Working electrode substrates were chosen so that a range of different morphologies and work functions could be investigated. Platinum sheet (Pt sheet) and glassy carbon (GC) have been used extensively as electrodes for the deposition of conducting polymers, while possessing well-known electrochemistries and smooth, polishable surfaces. ITO-coated glass (ITO) is frequently used for the deposition of polythiophene in solar cells. Platinised PVDF membrane (Pt-PVDF) was chosen as it has a similar work function to that of platinum, but has a highly microstructured morphology, so the effect of induced roughness upon the resulting properties of the polymer could be explored.

The objectives of this chapter may therefore be summarised as follows:

- To investigate surface energy and wettability of PTTh films in different oxidation states, prepared on various substrates to different thicknesses, by the use of contact drop goniometry;
- To investigate the dynamic switching of water contact angle on PTTh films by electrochemically controlling the oxidation state;
- To investigate the effect of substituents on contact angle and surface energy of PTTh.

An experimental section will be followed by presentation of the results, then discussion and conclusions will be presented.

3.2 Experimental methods

3.2.1 Reagents and materials

Additional reagents and materials are detailed in Chapter 2. 2,2′:5′,2″-terthiophene (TTh, Aldrich; Figure 1) was used as received. TTh-DDO (Figure 2) and TTh-C_{60} (Figure 3) were synthesised in the laboratories of Prof. David Officer at Massey University, New Zealand and were used as received. Details of the synthesis and characterisation of these novel monomers has been published elsewhere [33, 34].

3.2.2 Electrochemical deposition and parameters

The electrochemical polymerisation conditions for all three polymers are summarised in Table 3. Films of polyterthiophene doped with perchlorate (PTTh.ClO_4) were deposited from a solution containing 10 mM TTh monomer (Figure 1) and 0.1 M TBA.ClO_4 in DCM, using a current density of 0.5 mA/cm^2 for 100 or 20 s until 50 or 10 mC/cm^2 of charge had been passed. Poly-(4,4′-didecyloxy-2,2′:5′2″-terthiophene) doped with perchlorate (PTTh-DDO.ClO_4) was deposited from a solution containing 1 mM TTh-

DDO monomer (Figure 2) and 0.1 M TBA.ClO_4 in a 1:1 mixture of DCM and ACN by constant current, using a current density of 0.1 mA/cm^2 for 500 and 100 s until 50 or 10 mC/cm^2 of charge had been passed, respectively. Poly-(N-methyl-2-(2-[2′:5′,2″-terthiophen-3′-yl]ethenyl)fullero[3,4]pyrolidine) doped with perchlorate (PTTh-C_{60}.ClO_4) films were deposited from a solution of 1 mM TTh-C_{60} monomer (Figure 3) and 0.1 M TBA.ClO_4 in DCM at a constant current density of 0.5 mA/cm^2 for 100 or 20 s until 50 or 10 mC/cm^2 of charge had been passed, respectively. All films were washed gently in an acetonitrile bath after deposition to remove any excess monomer before being dried under a gentle nitrogen stream. All films were stored in a covered Petri dish prior to analysis to minimise surface dust contamination. Certain films were reduced in monomer-free deposition solution at a potential of 0 V *vs.* Ag/Ag^+ for PTTh.ClO_4 or -0.5 V *vs.* Ag/Ag^+ for PTTh-DDO.ClO_4 and PTTh-C_{60}.ClO_4 (as detailed in Table 3) until the current reached a steady state close to 0 mA.

Table 3. Deposition conditions of polyterthiophenes from various monomers.

	TTh	**TTh-DDO**	**TTh-C_{60}**
[Monomer] (mM)	10	1	1
Dopant	0.1 M TBA.ClO_4	0.1 M TBA.ClO_4	0.1 M TBA.ClO_4
Solvent	DCM	1:1 ACN:DCM	DCM
Applied I (mAcm^{-2})	0.5	0.1	0.5
Monomer used (μg)	12.04	2.81	5.23
Reduction E (V)	0.0	-0.5	-0.5

3.2.3 Instrumentation and characterisation

For additional instrumental parameters refer to Chapter 2.

3.2.3.1 Determination of reduction potential (E^0) for PTTh.ClO_4

Films of PTTh.ClO_4 were galvanostatically deposited onto freshly polished and rinsed Pt-disk electrodes, applying current densities of 50 and 10 mC/cm^2 using the conditions

described in Table 3. The E^0 value of the polymers was determined by cycling the films in monomer-free deposition solution using cyclic voltammetry from an initial potential of +0.8 V *vs.* Ag/Ag^+. Cyclic voltammograms were conducted at a slow scan rate of 10 mV/s with the potential being initially swept in the cathodic direction.

3.2.3.2 UV-Visible spectroscopy

UV-Visible spectra of as-deposited, oxidised and reduced polymers deposited on ITO-coated glass were recorded using Shimadzu 1601 UV-Visible spectrophotometer between 350 and 1100 nm. As-deposited polymers were typically prepared galvanostatically, while oxidised polymers were prepared by applying an appropriate potential to the as-deposited polymer. Reduced films were prepared by applying a suitable reducing potential to as-deposited polymer.

3.2.3.3 Atomic Force Microscopy

A Veeco Digital Instruments Dimension 3100 atomic force microscope (AFM) operating in contact mode was used to probe the surface morphology of polymer films.

3.2.3.4 Optical profilometry

The morphology and roughness of films was probed using a Veeco Wyko NT3300 optical profiler in the laboratories of Prof. Deborah Kane at Macquarie University. Measurements were made at several points on the film in order to obtain a representative roughness value. Further detail regarding the roughness determination is given in Section 3.3.1.3.

3.2.3.5 Thickness determination of $PTTh.ClO_4$

Thickness measurements of $PTTh.ClO_4$ deposited on ITO-coated glass were carried out using optical microscopy. Polymer-coated electrodes were mounted vertically in a

holder and cast in a resin containing a fluorescent dye for colour contrast. The resin and hardener were allowed to cure for 24 hours, after which the resin-substrate-polymer block was ground down using 1200 grade sand paper on a polishing wheel, followed by 0.3 μm alumina powder on a felt polishing cloth. An optical microscope (Leica DMR) calibrated using a stage micrometer was employed to determine the cross-sectional thickness of the polymer at 200 x magnification. The thicknesses of PTTh.ClO_4 films on ITO were also determined by SEM. The ITO slides were scored 3 mm from the end opposite the solution edge and broken to reveal the polymer cross section. Samples were gold-sputtered and SEM images were taken at varying magnifications.

3.2.3.6 Raman spectroscopy

Raman spectra of polymers deposited on working electrode substrates were measured using a Jobin Yvon Horiba HR800 Raman spectrometer with LabSpec software. A 632.8 nm laser was employed and peaks were deconvoluted using Gaussian fitting. Raman intensity was reported in arbitrary units, denoted as 'a.u.'. Raman mapping (Section 3.3.3.3.1) was carried out by rastering the laser over a given area of film, with an x-y resolution of 1 μm.

3.2.3.6.1 Depth profiling studies

The change in oxidation state throughout the thickness of a PTTh.ClO_4 film deposited on a substrate (using the conditions described in Section 3.2.2) was probed by confocal Raman spectroscopy (Section 3.3.3.3.2). A pinhole of 150 μm was typically used, corresponding to a sampling volume of ca. 5 μm^3 (ca. 0.6 μm diameter sample spot). The laser was focused on the film surface then at 2 μm intervals into the thickness of the polymer by moving the z-stage on which the polymer rested. The z-stage was then moved 2 μm so that the laser was sampling deeper into the film. This process was

repeated so the polymer was sampled throughout its thickness, from the surface layer through to polymer adjacent to the substrate.

3.2.3.6.2 Raman measurement through water drops

The interaction of water with PTTh.ClO_4 was probed using Raman spectroscopy. The difference in polymer oxidation state was determined by comparing the Raman spectrum of dry, untouched polymer with that of polymer which had a water drop resting on its surface. The laser was focussed on the surface of the water drop and then the z-stage moved so the laser was approximately focussed on the polymer surface.

3.2.3.7 *In-situ* electrochemical contact angle of captive water drop on PTTh.ClO_4

In-situ electrochemical contact angle measurements were carried out using the DataPhysics goniometer described in Chapter 2 and a modified electrochemical cell (Figure 4). Films of PTTh.ClO_4 were deposited onto Pt sheet for 20 and 100 s as per Section 3.2.2. The resulting PTTh.ClO_4-coated Pt sheet was held horizontally using tweezers, within a glass cell containing 0.1 M TBA.ClO_4 in DCM electrolyte that was placed upon the goniometer stage. A hooked dosing needle (not shown) was used to introduce a 2 μL MilliQ water droplet to the underside of the film (required as water is less dense than DCM). The cell was aligned so that the droplet could be viewed side-on by the video camera, and the drop shape recorded using the goniometer software. A three-electrode cell configuration was employed where the PTTh.ClO_4 on Pt sheet was the working electrode, Pt mesh was the counter electrode and potentials were measured *vs.* a Ag/Ag^+ reference electrode. The potential of the working electrode was switched between oxidising (+0.8 V *vs.* Ag/Ag^+) or reducing (0 V *vs.* Ag/Ag^+) and the change in drop shape noted.

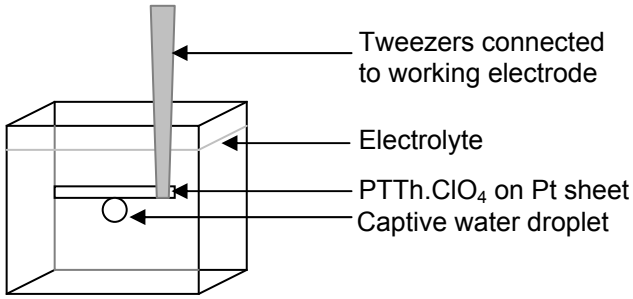

Figure 4. Set-up for *in-situ* electrochemical contact angle measurement of captive drop. PTTh.ClO_4-coated Pt sheet (working electrode) was held horizontally by tweezers in a glass cell containing 0.1 M TBA.ClO_4 in DCM electrolyte. A hooked dosing needle (not shown) was used to introduce water droplets to the underside of the electrode. The polymer-coated Pt sheet, Pt mesh counter electrode (not shown) and Ag/Ag^+ reference electrode (not shown) were connected in a three-electrode cell configuration and the potential was switched between oxidising and reducing potentials (+0.8 V *vs.* Ag/Ag^+ and 0 V *vs.* Ag/Ag^+, respectively).

3.3 Results

3.3.1 General characterisation of PTTh.ClO_4, PTTh-DDO.ClO_4 and PTTh-C_{60}.ClO_4

Initial characterisations of polyterthiophenes were carried out using electrochemistry, UV-Vis spectroscopy and optical microscopy techniques. The terms 'thick' and 'thin' will be used hereafter to denote polymers deposited using a charge density of 50 mC/cm^2 (ca. 5 – 10 μm) or 10 mC/cm^2 (ca. 1 – 2 μm) , respectively. The measurement of polymer thickness will be discussed in more detail in Section 3.3.1.3.1. Note that the descriptors thick and thin are relative and are only of significance for comparisons within this thesis.

3.3.1.1 Electrochemical deposition and characterisation

3.3.1.1.1 PTTh.ClO_4

Electrodeposition of PTTh.ClO_4 was carried out galvanostatically using an applied current of 0.5 mA/cm^2 from dichloromethane electrolyte containing TBA.ClO_4, as per

Table 3. The polymerisation proceeded at a constant potential of ca. +0.85 to 0.90 V on all substrates for both thin and thick films, indicating the deposition of conductive films. As-deposited films were dark black-blue immediately after deposition and developed faint green hues after a short time in air. Reduced films were bright orange, as is typical for polythiophene [35]. Polymer was observed to initially deposit at the edge of the substrates and hence appeared slightly thicker at the edges than in the centre. Therefore contact angles were measured over a range of positions on the film to determine an average value, as well as over several months to sample a variety of ambient humidity and temperatures. The polymerisation conditions for PTTh.ClO_4 (Table 3) were in alignment with those used by Tsekouras *et al.* [36] and Bazzaoui *et al*. [19].

Cyclic voltammetry (CV) was used to determine the oxidation and reduction potentials of PTTh.ClO_4 in conjunction with UV-Vis spectrometry (Section 3.3.1.2.1). A cathodic peak was evident at ca. +0.35 V in post-growth cyclic voltammograms (Figure 5), whereas no anodic peak was present. This is consistent with observations by Tsekouras [37], where the use of an upper potential limit sufficiently high enough to show an oxidation peak resulted in polymer degradation, as evidenced by an irreversible change in the polyterthiophene from orange to orange-brown.

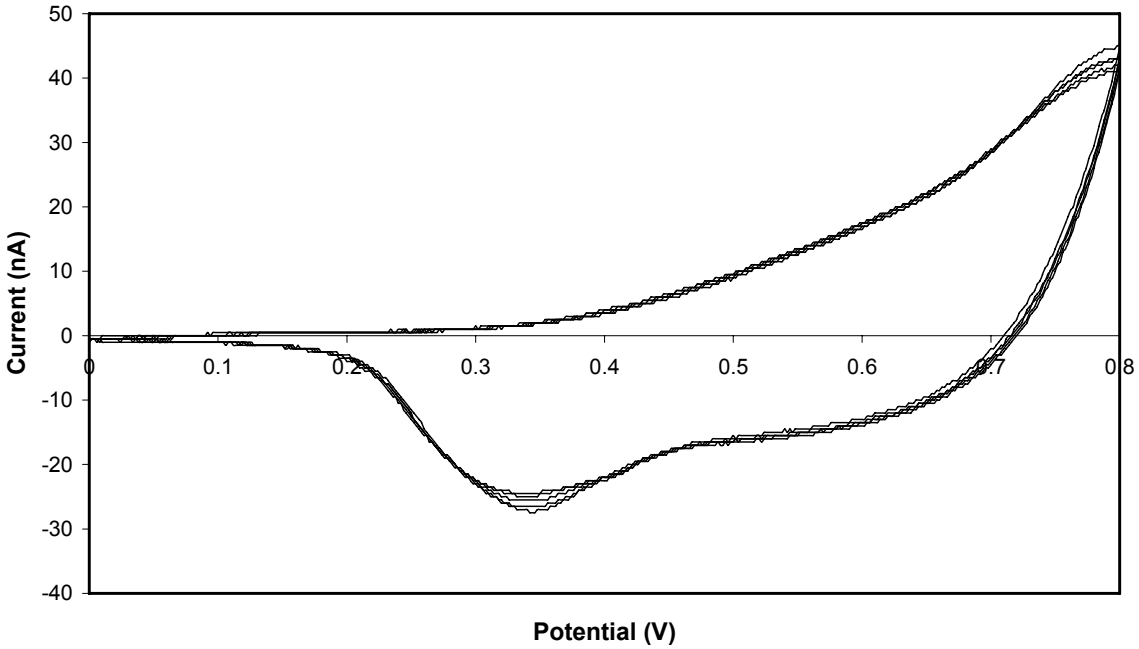

Figure 5. Cyclic voltammogram of thick (50 mC/cm^2 charge density) PTTh.ClO_4 on Pt disk in 0.1 M TBA.ClO_4 in DCM. The potential was scanned from 0 to +0.8 V *vs*. Ag/Ag$^+$ using a platinum counter electrode at a scan rate of 50 mV/s for 5 cycles.

Cyclic voltammograms were featureless at potentials below 0 V and did not change upon decreasing the lower potential limit, hence 0 V was used as the reduction potential in further studies. Upon redox cycling with upper potential limits of greater than +0.8 V, the anodic peak was present at ca. +0.8 V (not shown). There was no increase in the amount of charge passed upon repeated cycling in monomer-free deposition solution, indicating the films were in a highly-doped state when prepared, as well as being composed predominantly of polymerised oligomers [23] and containing a minimal amount of unpolymerised monomer [1].

The reduction potentials of thick and thin PTTh.ClO4 were determined to be ca. 0.447 V (vs. Ag/Ag+) and 0.427 V (vs. Ag/Ag+), respectively, using slow scan rate (10 mV/s) cyclic voltammetry in monomer-free deposition solution, immediately after polymerisation (Figure 6). The higher potential (more positive) peak was taken to be the initial reduction potential, although the splitting of the cathodic peak into two shoulders indicated the presence of two types of material with slightly different E^0 values.

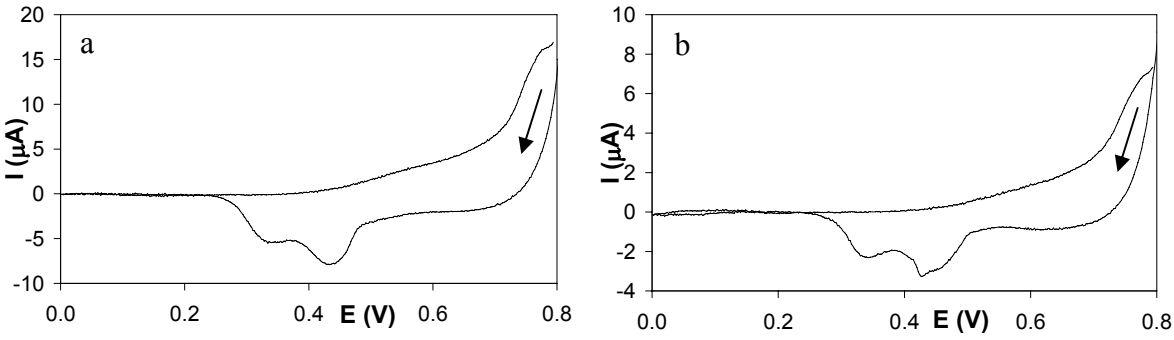

Figure 6. Cyclic voltammograms to determine E^0 of a) thick (50 mC/cm^2 charge density) and b) thin (10 mC/cm^2 charge density) PTTh.ClO_4 immediately after deposition on Pt disk, in 0.1 M TBA.ClO_4 in DCM at 10 mV/s *vs.* Ag/Ag^+ in a three-electrode cell configuration. Arrow indicates direction of initial sweep.

3.3.1.1.2 PTTh-DDO.ClO_4

PTTh-DDO.P was chosen as a functionalised polyterthiophene worthy of investigation as the presence of long alkyl chains on the TTh-DDO monomer (Figure 2) was expected to introduce hydrophobicity into the polymer backbone. PTTh-DDO.ClO_4 was initially deposited using conditions analogous to employed for the deposition of PTTh.ClO_4 (Table 3). However the polymer did not adhere well to the electrode when DCM was used as the solvent, hence a mixed solvent of 1:1 ACN:DCM was employed. The initial current density applied was 0.5 mA/cm^2, as for PTTh.ClO_4; however the potential was observed to increase significantly during deposition (up to ca. 2 V) at this current density and the polymer did not adhere to the electrode. Monomer concentrations of 10 and 5 mM were investigated; however the resulting films appeared to leach into the deposition solution, had poor mechanical properties and washed off in acetonitrile post-deposition. Solutions containing 1 mM monomer with an applied current of 0.1 mA/cm^2 were used thereafter, producing films which adhered well and evenly coated the substrate. Charge densities of 50 and 10 mC/cm^2 were again used to provide consistency with the results for PTTh.ClO_4, so that a comparison of the polymer's wettability and surface energy at similar thicknesses could be made. Polymerisation

occurred at an initial potential of +0.9 V, gradually increasing to +1.1 V over the course of 500 s, indicating the deposition of a slightly resistive layer. Films were pale blue in the as-deposited state and bright purple after electrochemical reduction at -0.5 V *vs.* Ag/Ag^+, which was lower than the reduction potential of unsubstituted PTTh.ClO_4. The reduction potential of -0.5 V was in alignment with conditions used by Wang *et al.* [38]. Post-growth cyclic voltammetry revealed two redox couples at -0.13 and -0.03 V (*vs.* Ag/Ag^+) and 0.16 V and 0.33 V (*vs.* Ag/Ag^+), as shown in Figure 7.

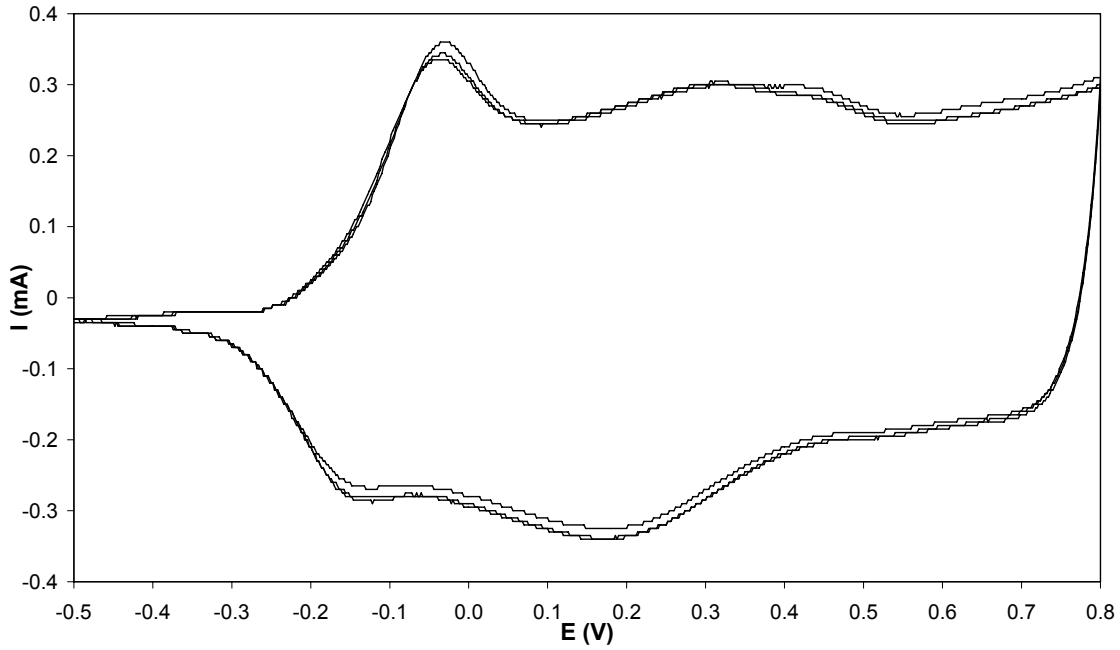

Figure 7. Cyclic voltammogram of thick (50 mC/cm^2 charge density) PTTh-DDO.ClO_4 on Pt disk in 0.1 M TBA.ClO_4 in 1:1 ACN/DCM. The potential was scanned from -0.5 to +0.8 V *vs.* Ag/Ag^+ using a platinum counter electrode at a scan rate of 50 mV/s for 5 cycles.

3.3.1.1.3 PTTh-C_{60}.ClO_4

Further investigation into the effect of terthiophene monomer-functionalisation upon the resulting wettability was carried out using buckyball-substituted polyterthiophene (TTh-C_{60}; Figure 3). The combination of the inherently hydrophobic buckyball substituent with the polyterthiophene backbone was hoped to provide some interesting insights into the factors controlling wetting of polyterthiophene. A current density of 0.5 mA/cm^2

was applied in a solution containing 1 mM TTh-C_{60} in 0.1 M TBA.ClO_4, resulting in the deposition of mottled-yellow polymers with charge densities of 50 and 10 mC/cm^2, analogous to those for PTTh-DDO.ClO_4. Polymer growth proceeded at an initial potential of 1.1 V, gradually increasing to ca. 1.3 V over 100 s, indicating the deposition of a slightly resistive polymer. Upon reduction of the polymer at -0.5 V, the current did not return to 0 mA, despite applying the reducing potential for greater than 20 minutes. .

Post-growth characterisation of PTTh-C_{60}.ClO_4 on a platinum disk electrode by cyclic voltammetry in monomer-free deposition solution revealed no clear anodic or cathodic peaks (Figure 8). This was in contrast to observations by Tsekouras [37], where a cathodic peak occurred at +0.65 V, suggesting the reversible electroactivity of the PTTh-C_{60}.ClO_4 polymer in the present study was questionable.

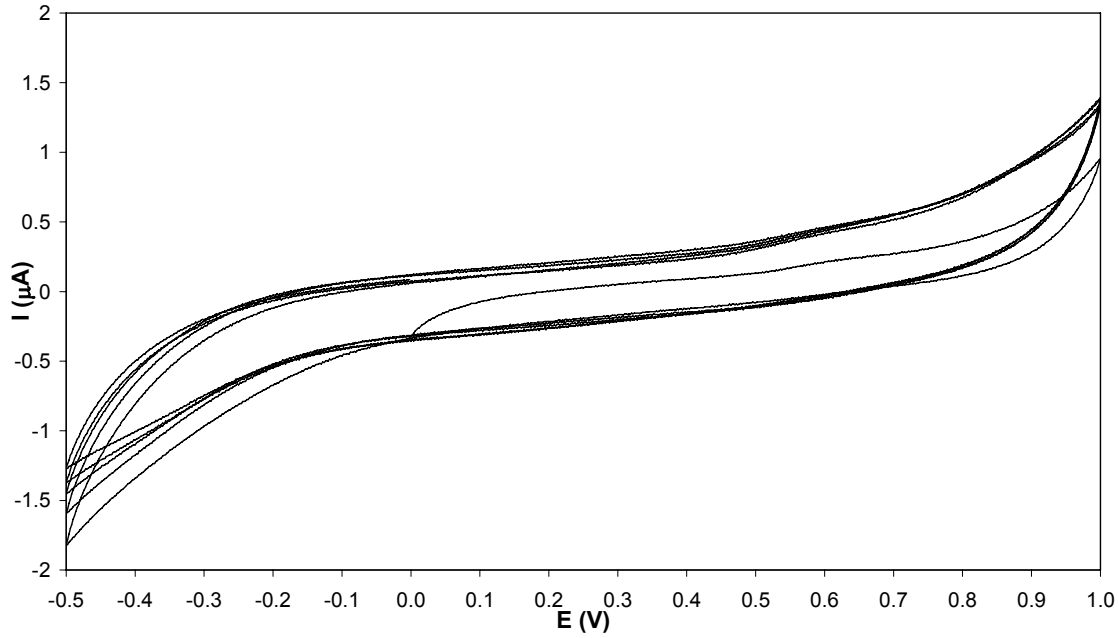

Figure 8. Cyclic voltammogram of thick (50 mC/cm^2 charge density) PTTh-C_{60}.ClO_4 on Pt disk in 0.1 M TBA.ClO_4 in DCM. Potential was scanned from -0.5 to +1.0 V *vs*. Ag/Ag$^+$ using a scan rate of 50 mV/s for 5 cycles.

3.3.1.2 UV-Vis spectroscopy

3.3.1.2.1 PTTh.ClO_4

The oxidation and reduction potentials determined for PTTh.ClO_4 using cyclic voltammetry were corroborated by inspection of the UV-Vis spectra of as-deposited and reduced films, and those electrochemically oxidised subsequent to deposition (by applying +0.8 V for 30 s). There was little difference between spectra obtained for as-deposited films and those electrochemically oxidised post-deposition, suggesting the as-deposited films were in a similarly highly doped state as the intentionally oxidised films (Figure 9).

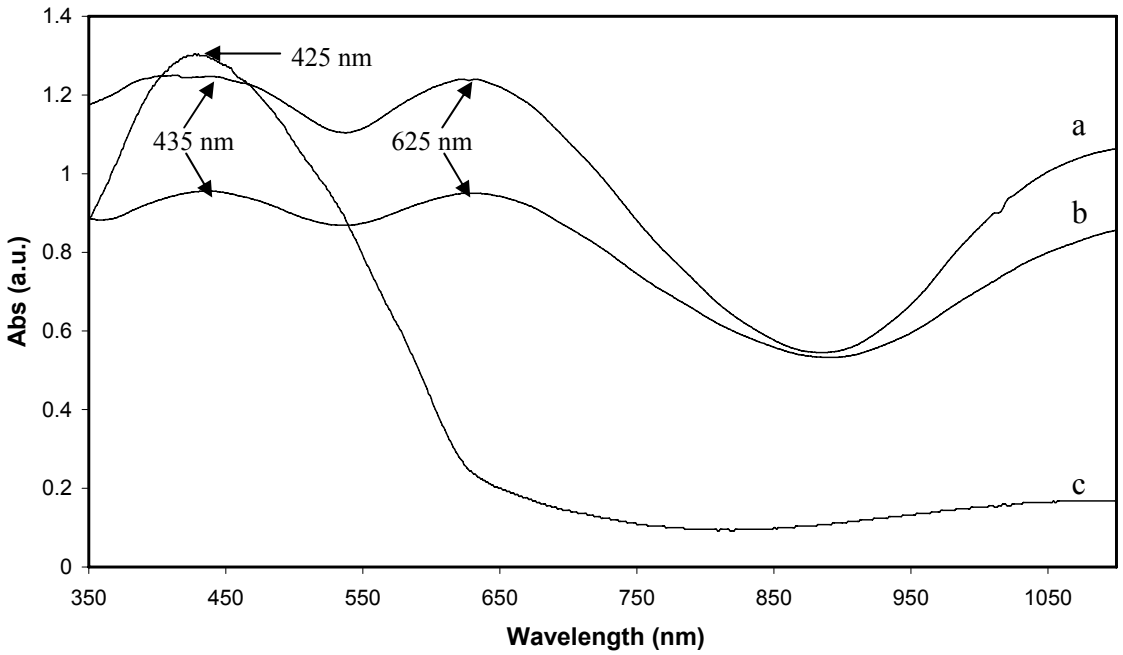

Figure 9. UV-Vis spectra of thick (50 mC/cm^2 charge density) PTTh.ClO_4 on ITO-coated glass; a) as-deposited, b) after oxidation at +0.8 V *vs.* Ag/Ag$^+$ and c) after reduction at 0 V *vs.* Ag/Ag$^+$.

Bands observed at 435 and 625 nm were attributed to $\pi \rightarrow \pi^*$ and polaron $\rightarrow \pi^*$ transitions of polyterthiophene, respectively, with a free carrier tail present at wavelengths greater than 900 nm. The presence of these peaks (at 435 nm and 625 nm) as two distinct bands indicates a lower degree of conjugation than PTTh.ClO_4 which had been deposited from acetonitrile, and is consistent with the formation of oligomers rather than polymers [39]. The spectra of PTTh.ClO_4 reduced at 0 V is consistent with

previously published observations, with the lack of a free carrier tail indicating the polymer was in the non-conductive form [1, 37, 39]. Hence +0.8 V and 0 V were used as potentials of oxidation and reduction, respectively, in subsequent studies on PTTh.ClO_4.

3.3.1.2.2 PTTh-DDO.ClO_4

A comparison of as-deposited and reduced PTTh-DDO.ClO_4 films exhibited strikingly different UV-Vis spectra, while films in the same oxidation state but prepared using different charge densities (50 and 10 mC/cm^2) had spectra that were quite similar to each other (Figure 10). A significant free carrier tail was observed for as-deposited films, indicative of a high level of doping, with a $\pi \rightarrow \pi^*$ transition of polyterthiophene evident at ca. 400 nm. The reduced films exhibited a broad polaron $\rightarrow \pi^*$ band centred at ca. 590 nm, which quickly dropped off to low absorbance in the near-infra red region, consistent with reduced polythiophene.

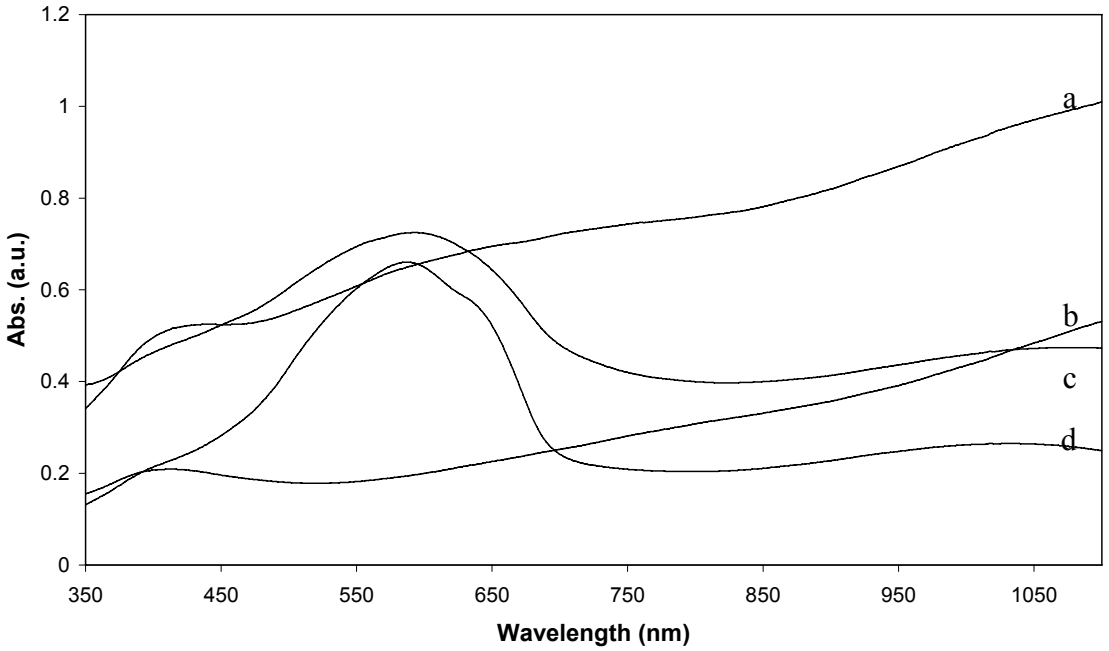

Figure 10. UV-Vis spectra of PTTh-DDO.ClO_4 on Pt sheet; a) thick (50 mC/cm^2 charge density) as-deposited film, b) thin (10 mC/cm^2 charge density) as-deposited film, c) after reduction of thick (50 mC/cm^2 charge density) film at -0.5 V *vs.* Ag/Ag$^+$ and d) after reduction of thin (10 mC/cm^2 charge density) film at -0.5 V *vs.* Ag/Ag$^+$.

3.3.1.2.3 PTTh-C_{60}.ClO_4

The UV-Vis absorbances of as-deposited and reduced PTTh-C_{60}.ClO_4 grown using both 50 and 10 mC/cm^2 charge densities were similar, with peaks at ca. 330 nm and 420 nm attributable to absorption by the C_{60} moiety and the $\pi - \pi^*$ transition of terthiophene, respectively [37]. A lack of free carrier tail absorbance indicated that all films, both as-deposited and electrochemically reduced, were in the reduced state (Figure 11).

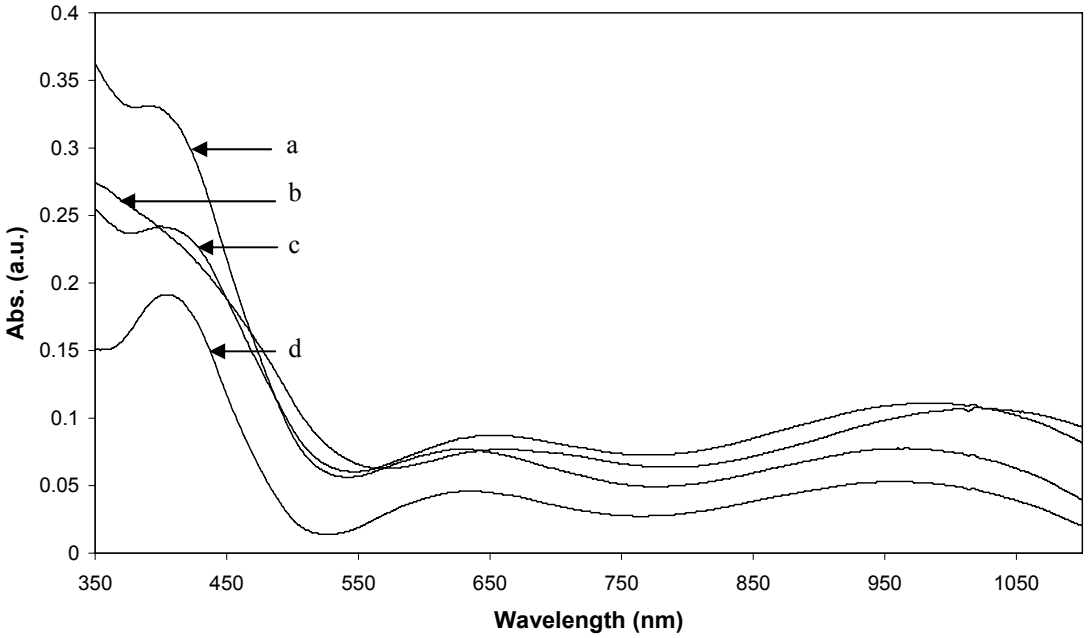

Figure 11. UV-Vis spectra of PTTh.ClO_4 on ITO-coated glass; a) thin (10 mC/cm^2 charge density) as-deposited film, b) thick (50 mC/cm^2 charge density) as-deposited film, c) thick (50 mC/cm^2 charge density) film after reduction at -0.5 V *vs.* Ag/Ag^+ and d) thin (10 mC/cm^2 charge density) film after reduction at -0.5 V *vs.* Ag/Ag^+.

The above spectra of as-deposited films are different to those previously reported for PTTh-C_{60}.ClO_4 by Chen *et al.*, which exhibited a broad absorbance at 700 nm [37] and a free carrier tail at wavelengths greater than 700 nm [33]. Tsekouras [37] has previously observed that in co-polymers made with varying proportions of TTh and TTh-C_{60} monomer, those with higher proportions of the C_{60}-substitued terthiophene were found to be more susceptible to auto-reduction in ambient laboratory conditions, thus making it difficult to isolate the oxidised form. This is believed to be due to the

high electron affinity of the buckyball substituent. The poor electrochemistry and inability to isolate oxidised polymer led to further characterisation of PTTh-C_{60}.ClO_4 wetting properties not being pursued.

3.3.1.3 Optical characterisations

3.3.1.3.1 PTTh.ClO_4

The roughness, morphology and thickness of 50 and 10 mC/cm^2 charge density PTTh.ClO_4 films were probed using SEM (Figure 12), AFM (Figure 13) and optical profilometry (Figure 14). As-deposited films were generally found to be quite porous, whereas reduced films had a more compact 'peaked'-type structure. PTTh.ClO_4 on Pt sheet appeared to have the smoothest, most compact morphology of all substrates, in both as-deposited and reduced states and for both film thicknesses (Figure 12a). Films on Pt-PVDF membrane were highly microstructured, as a result of the underlying porous membrane. Interestingly, a small area of as-deposited thick PTTh.ClO_4 on glassy carbon (Figure 12c) showed a peaked-type structure typical of the reduced film. From the SEM images it can be seen that the polymers possessed a range of surface morphologies, imparted by the underlying substrates.

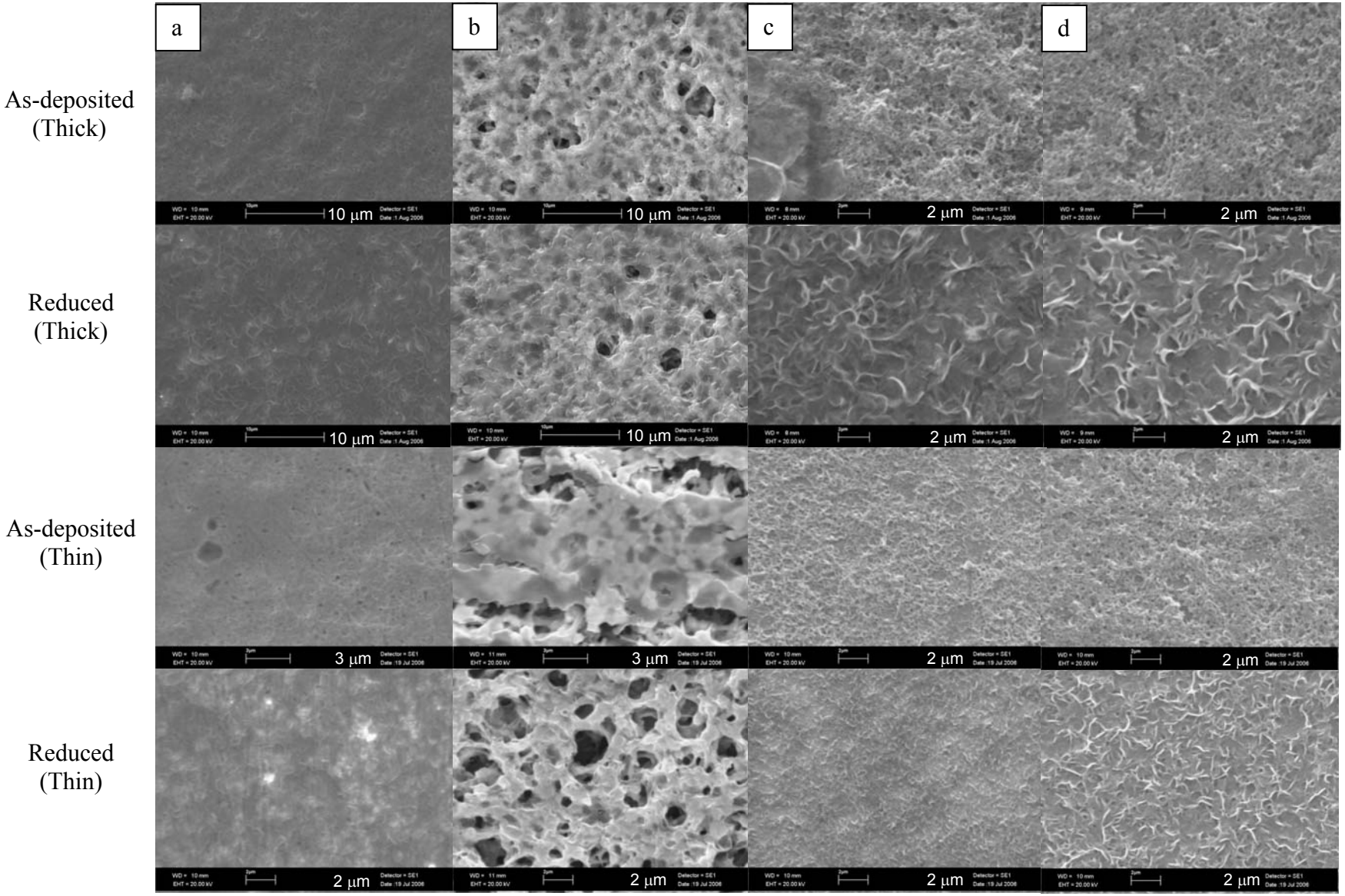

Figure 12. SEM images of thick (50 mC/cm^2 charge density) and thin (10 mC/cm^2 charge density) PTTh.ClO_4 in the as-deposited or electrochemically reduced states, on a) platinum sheet, b) platinised PVDF membrane, c) glassy carbon and d) ITO-coated glass.

Atomic force microscopy (AFM) corroborated the image of the PTTh.ClO_4 surface morphology obtained by SEM. The PTTh.ClO_4 films of differing oxidation states were found to have different surface morphologies, with the as-deposited (oxidised) film exhibiting the 'cauliflower'-type morphology that is common for conducting polymers, whereas the reduced film had a more 'wavy' and peaked-type appearance, as shown in Figure 13.

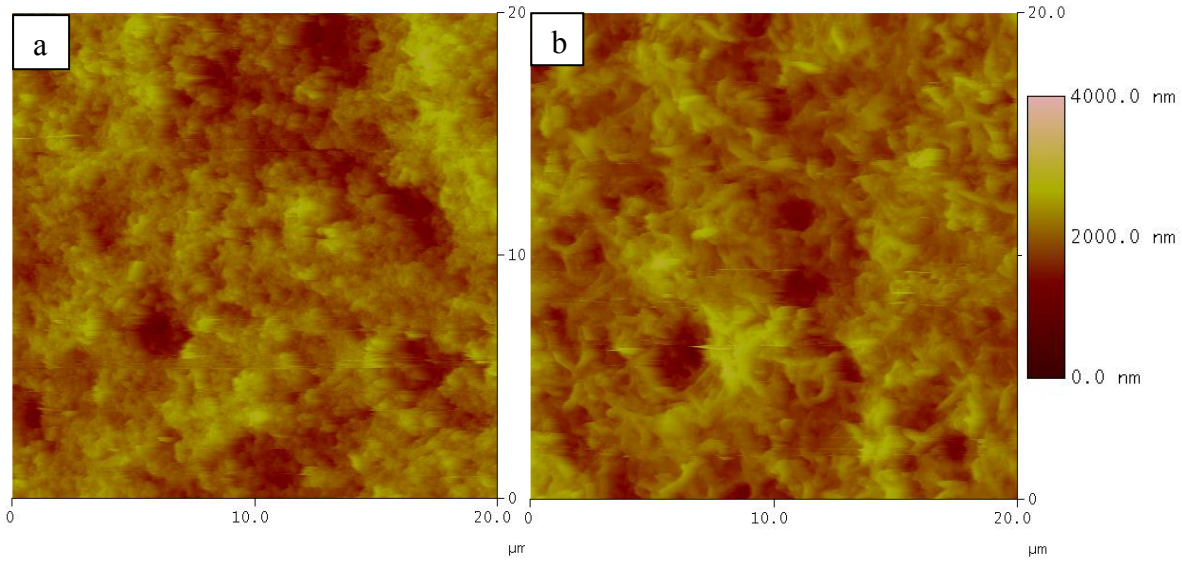

Figure 13. AFM images of thick (50 mC/cm^2 charge density) PTTh.ClO_4 films in the a) as-deposited and b) reduced states (0 V *vs* Ag/Ag^+).

Polymer roughness was determined by optical profilometry, as it was found that polymers were scratched off with the stylus when using traditional contact profilometry. The roughness value (r) reported is the ratio of the actual surface area to the scan area;

i.e.:
$$r = \frac{A_{real}}{A_{geom}}$$

where A_{real} is the surface area determined by the software by means of triangulation over 4 data points, and A_{geom} is the geometric area of the sample (namely 13 µm^2) [40]. The roughness data reported for PTTh.ClO_4 on various substrates are representative of the measurement made at several points on the film (Figure 14; Table 4).

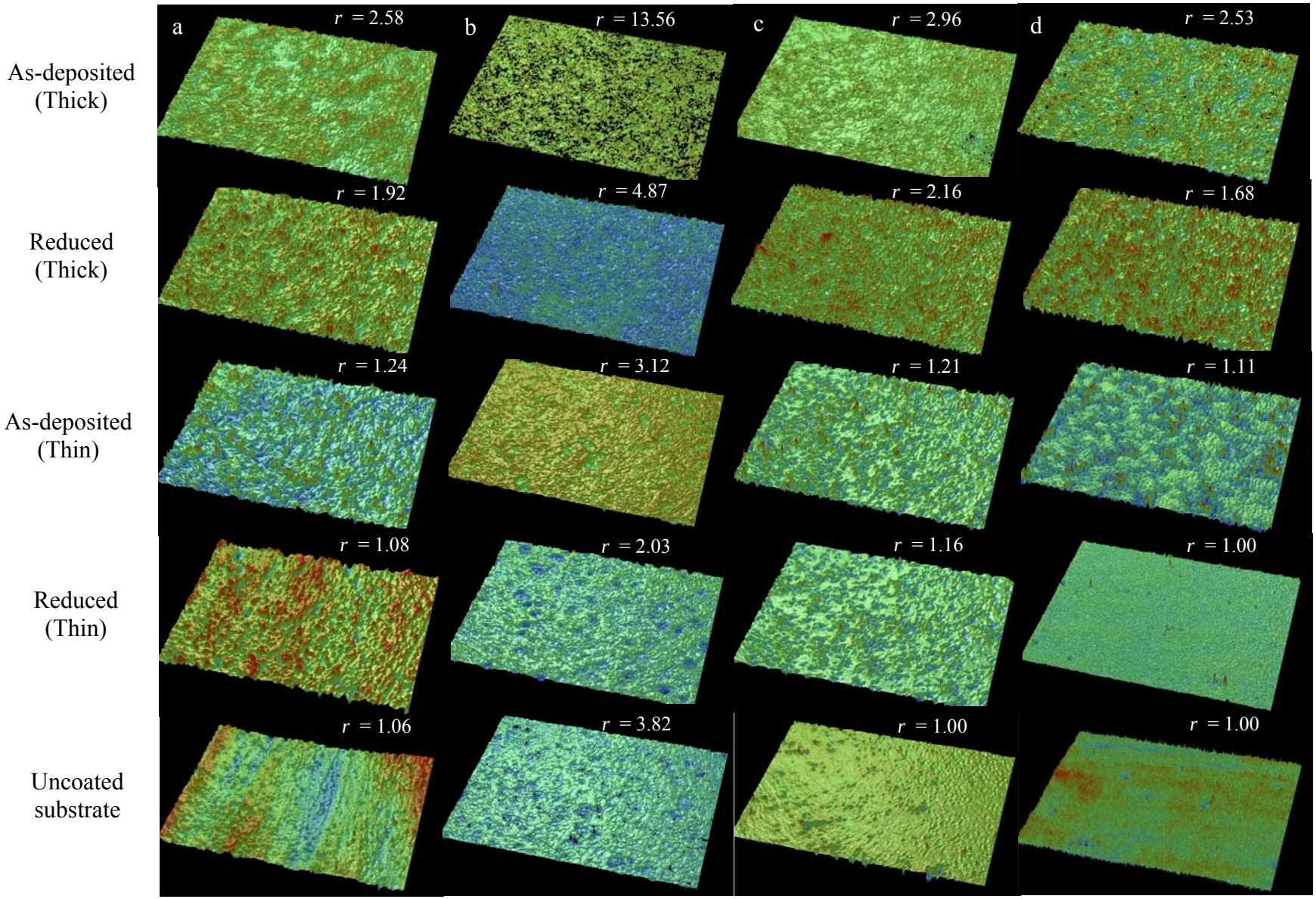

Figure 14. Optical profilometry images of thick (50 mC/cm^2 charge density) and thin (10 mC/cm^2 charge density) PTTh.ClO_4 films in the as-deposited or electrochemically reduced states and uncoated substrate; a) Pt sheet, b) Pt-PVDF membrane, c) glassy carbon and d) ITO-coated glass, at 50 x magnification. *r* denotes roughness.

Table 4. Roughness (*r*) measurements of PTTh.ClO_4 films deposited on various substrates at 50 x magnification.

Substrate	Polymer thickness	Oxidation state	*r*
Pt sheet	**Thick**	as-deposited	2.58
		reduced	1.92
	Thin	as-deposited	1.24
		reduced	1.08
		uncoated	1.06
Pt-PVDF	**Thick**	as-deposited	13.56
		reduced	4.87
	Thin	as-deposited	3.12
		reduced	2.03
		uncoated	3.82
Glassy carbon	**Thick**	as-deposited	2.96
		reduced	2.16
	Thin	as-deposited	1.21
		reduced	1.16
		uncoated	1.00
ITO	**Thick**	as-deposited	2.53
		reduced	1.68
	Thin	as-deposited	1.11
		reduced	1.00
		uncoated	1.00

As-deposited films were consistently rougher than their reduced counterpart of the same thickness (e.g. r = 2.58 and 1.92 for thick as-deposited and reduced PTTh.ClO_4 on Pt sheet, respectively), while thick films were consistently rougher than their thin

counterparts (e.g. r = 2.58 and 1.24 for thick and thin as-deposited PTTh.ClO_4 on Pt sheet, respectively). This effect was observed across all substrates. Substrates were generally smoother than the polymers deposited on them, as may have been predicted. The exception to this was uncoated Pt-PVDF, which had a higher r value (3.82) than the thin as-deposited and reduced PTTh.ClO_4 deposited on it (3.12 and 2.03, respectively). Glassy carbon (1.00) and ITO-coated glass (1.00) were the smoothest substrates, with Pt sheet slightly rougher (1.06).

The thickness of 50 and 10 mC/cm^2 charge density polyterthiophene films on ITO-coated glass was determined using optical microscopy and SEM. The films were cast in resin and polished down to reveal the polymer cross-section as described in Section 3.2.3. Thick (50 mC/cm^2 charge density) films were determined to be 5 – 10 μm thick (Figure 15) and thin (10 mC/cm^2 charge density) films were determined to be 1 - 2 μm in thickness.

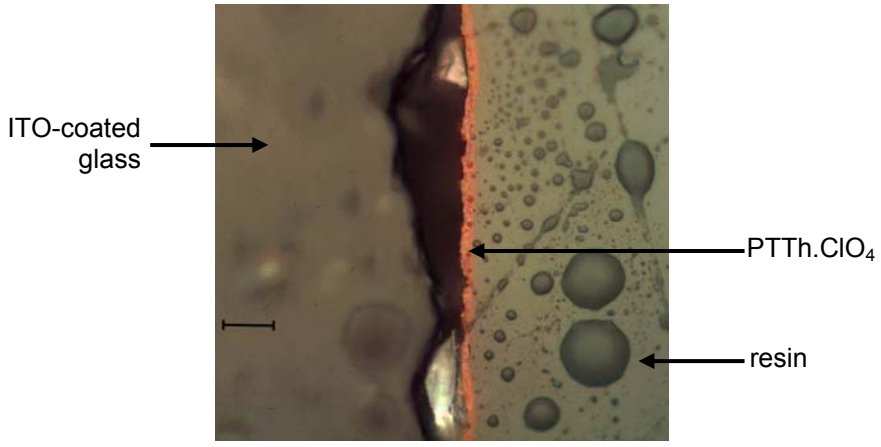

Figure 15. Optical microscope image of thick (50 mC/cm^2 charge density) PTTh.ClO_4 film on ITO-coated glass, cast in resin and polished to reveal polymer cross-section. Scale bar represents 38 μm.

As-deposited films were observed to instantaneously reduce upon addition of the resin, presumably due to the amine in the resin hardener. Thicknesses were therefore only determined for reduced films, which are known to be more compact than oxidised films due to the loss of dopant anions upon de-doping [41]. The thicknesses of films on other

substrates were also measured using the same method, but it was often difficult to obtain a clear image. Thus PTTh.ClO_4 on alternate substrates would invariably have had different thicknesses to those reported for ITO-coated glass; hence the thickness measurements reported here may only be regarded as an estimation. There is some discrepancy between the PTTh thickness determined by optical microscopy in this study and the thickness calculated by the commonly cited equation relating the amount of charge passed during deposition to the thickness of polythiophene and its derivatives [42]. A linear charge thickness relationship of 10 Å/mC cm^2 has been used to characterise polymers of Angstrom to millimetre thickness. When applied to the present study, films of 50 or 10 mC/cm^2 charge density equate to 50 and 10 nm thick polymers, respectively, which is significantly lower than the thicknesses determined above by optical methods. This discrepancy may result from the many factors involved with the deposition of conducting polymers, including monomer and dopant concentration, applied current density during deposition, substrate and so on, and suggests a generalised equation for thickness determination is not applicable.

3.3.1.3.2 PTTh-DDO.ClO_4

SEM and optical profilometry was used to probe the morphology of PTTh-DDO.ClO_4 films deposited on Pt sheet (Figure 16 and Figure 17). Thinner films were found to be smooth and possess vastly different surface morphology to thicker films, which had roughened surface features. The difference in morphology is believed to be due to the method of polymer formation during electrodeposition. Thin films are thought to be formed by an initial 2-dimensional nucleation of PTTh-DDO.ClO_4 chains, followed by the growth of chains in three dimensions at longer deposition times [43-45]. Optical profilometry (Figure 16, Table 5) confirmed the increased roughness of thicker films, which had *r* values of 3.93 and 2.16 for as-deposited and reduced thick films, while thinner films had roughness values similar to that of uncoated Pt sheet (1.06).

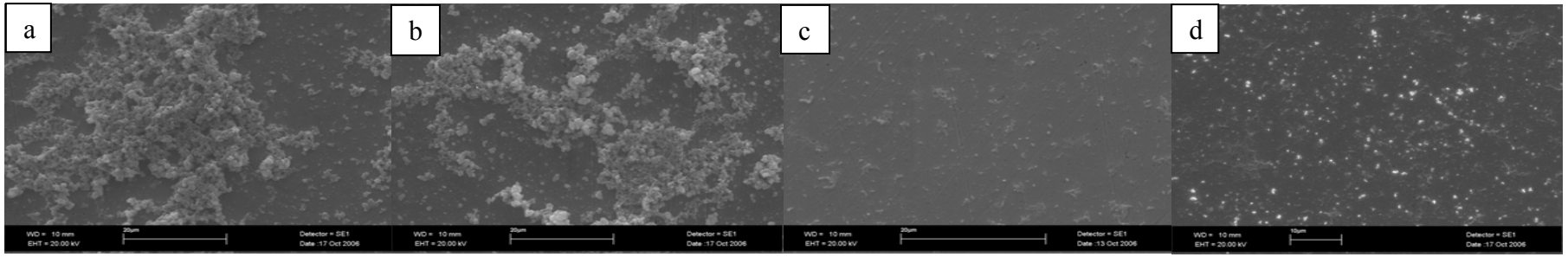

Figure 17. SEM images of PTTh-DDO.ClO_4 deposited on Pt sheet (5000 x magnification); a) thick (50 mC/cm^2 charge density) as-deposited films, b) thick (50 mC/cm^2 charge density) reduced films, c) thin (10 mC/cm^2 charge density) as-deposited films and d) thin (10 mC/cm^2 charge density) reduced films.

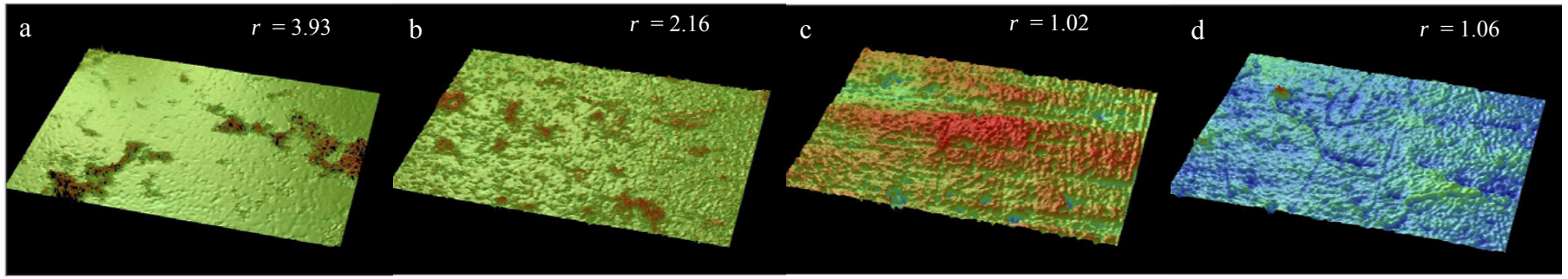

Figure 16. Optical profilometry images of PTTh-DDO.ClO_4 deposited on Pt sheet (50 x magnification); a) thick (50 mC/cm^2 charge density) as-deposited films, b) thick (50 mC/cm^2 charge density) reduced films, c) thin (10 mC/cm^2 charge density) as-deposited films and d) thin (10 mC/cm^2 charge density) reduced films. *r* denotes roughness.

Table 5. Roughness measurements of PTTh-DDO.ClO_4 films deposited on platinum sheet at 50 x magnification

Substrate	Polymer thickness	Oxidation state	*r*
Pt sheet	Thick	as-deposited	3.93
		reduced	2.16
	Thin	as-deposited	1.02
		reduced	1.06
		uncoated	1.06

3.3.2 Wettability and surface energy of PTTh films

After initial characterisations which allowed insight into the electrochemistry and morphology of non-substituted PTTh and PTTh functionalised with long hydrophobic alkyl chains (PTTh-DDO.ClO_4), contact angle measurements of water and the probe liquids glycerol and diiodomethane were carried out to gain insight into the impact of thickness, morphology and substrate on the polymers' wettabilities and surface energies.

3.3.2.1 Uncoated substrates

The effect of substrate pre-treatment upon the resulting wettability and surface energy was initially investigated. The four different working electrode substrates, namely Pt sheet, Pt-PVDF, glassy carbon and ITO-coated glass, were washed in an acetonitrile bath and dried under a nitrogen stream prior to use, in order to ensure a homogeneous pre-treatment across substrates. The water contact angles of substrates before and after acetonitrile-washing are shown in Table 6.

Table 6. Effect of washing bare substrates on resulting water contact angle (°).

Substrate	Before washing (°)	After ACN wash (°)
Pt-sheet	42 ± 2	0 – 5
Pt-PVDF	127 ± 1	120 ± 2
Glassy carbon	57 ± 3	61 ± 5
ITO-coated glass	97 ± 1	78 ± 3

Washing with acetonitrile had varied effects on substrate wettability, with minimal change observed for Pt-PVDF and glassy carbon. ITO-coated glass exhibited a slight decrease in water contact angle while, notably, the wettability of Pt sheet increased dramatically as a result of the ACN treatment, suggesting the majority of organic contaminants were removed from the surface.

The surface energy of uncoated substrates was determined so that a comparison to PTTh-coated electrodes may be drawn (Table 7). A range of γ_s values were obtained ranging from 36 – 62 mJ/m^2, with Pt sheet possessing the highest surface energy (62 mJ/m^2) and ITO-coated glass the lowest (36 mJ/m^2), which is somewhat lower than has been reported in the literature for ITO (48 mJ/m^2; [46]). The Lewis acid (γ^-) component was particularly pronounced for Pt sheet and GC, consistent with the delocalised electrons and sp^2 hybridised electrons, respectively, of these materials.

Table 7. Contact angle (°) and surface energy data (mJ/m^2) for test liquids on uncoated working electrode substrates.

Substrate	Water	CH_2I_2	Glycerol	γ_s	γ^{LW}	γ^{AB}	γ^+	γ^-
Pt	~5	28 ± 8	19 ± 3	62	45.0	17.4	1.6	48.1
Pt-PVDF	120 ± 2	21 ± 2	86 ± 18	48	47.4	0.5	0.0	6.9
GC	63 ± 7	16 ± 3	67 ± 6	56	48.9	7.4	0.6	22.9
ITO	81 ± 6	48 ± 0	77 ± 12	36	35.2	1.0	0.0	9.2

3.3.2.2 PTTh.ClO_4

3.3.2.2.1 Thick films

The use of as-deposited PTTh.ClO_4 as a representative of the oxidised state was tested by comparing the water contact angle of as-deposited and electrochemically oxidised (at +0.8 V for 10 s) films on ITO-coated glass. As-deposited films were found to have a water contact angle of 68 ± 10 ° (presented in Table 8), whereas electrochemically oxidised films had a water contact angle of 64 ± 10 °. This comparable wettability implied a similar level of doping, as was also indicated by UV-Vis spectroscopy (Section 3.3.1.2.1). In the interest of avoiding over-oxidation of the polymer and maintaining the integrity of the films (subsequent oxidation after deposition caused some of the films to peel off), the as-deposited polymers were used in further studies where oxidised PTTh was investigated.

Wettability studies of PTTh.ClO_4 were carried out on as-deposited and electrochemically reduced films of two different thicknesses, namely thick (50 mC/cm^2; present Section) and thin (10 mC/cm^2; Section 3.3.2.2.2). Static (recently advanced) water contact angles (θ_s) for thick as-deposited (denoted 'as-dep.') and electrochemically-reduced (denoted 'red.') PTTh.ClO_4 are shown in Table 8, along with advancing (θ_a), receding (θ_r) and hysteresis ($\Delta\theta = \theta_a - \theta_r$) data (as discussed in Chapter 1, Section 1.1.2.3).

Table 8. Contact angles of water droplets on thick PTTh.ClO_4 films deposited on various substrates. All contact angles are reported in degrees (°).

Substrate	Ox'n state	θ_s	$\theta_{red} - \theta_{as\text{-}dep}$	θ_a	θ_r	$\Delta\theta$
Pt sheet	**As-dep.**	54 ± 16	75	101 ± 1	68 ± 5	33
	Red.	129 ± 4		140 ± 3	132 ± 3	8
Pt PVDF	**As-dep.**	63 ± 26	39	125 ± 4	100 ± 21	25
	Red.	102 ± 7		112 ± 9	86 ± 8	26
GC	**As-dep.**	65 ± 15	61	113 ± 8	68 ± 7	45
	Red.	126 ± 7		130 ± 2	115 ± 5	15
ITO	**As-dep.**	68 ± 10	61	94 ± 14	57 ± 12	37
	Red.	129 ± 3		142 ± 1	133 ± 2	9

Thick PTTh.ClO_4 films were found to exhibit a dramatic change in wettability between the as-deposited and reduced states when measured in air (*ex-situ* the electrochemical cell) in ambient laboratory conditions. The water contact angle values ranged from 54 – 68 ° and 102 – 129 ° for as-deposited and reduced films, respectively. The difference in wettability of the reduced and as-deposited films (39 – 75 °) is significantly higher than those previously reported in the literature (Table 1). Representative images of water contact angles on as-deposited and electrochemically reduced PTTh.ClO_4 are shown in Figure 18 - Figure 21. A decrease in droplet contact angle and volume over time was observed as evaporation occurred, thus contact angle measurements were carried out immediately after the cessation of any spreading of the water on the polymer.

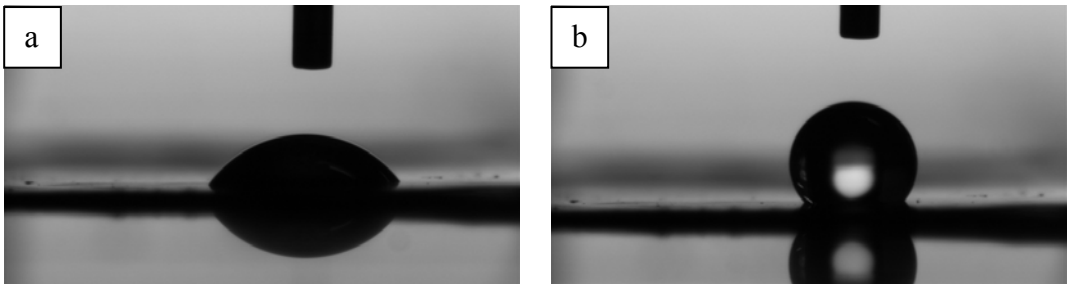

Figure 18. Water drop on surface of PTTh.ClO_4 on Pt sheet; a) as-deposited thick (50 mC/cm^2 charge density) films and b) electrochemically-reduced thick (50 mC/cm^2 charge density) films.

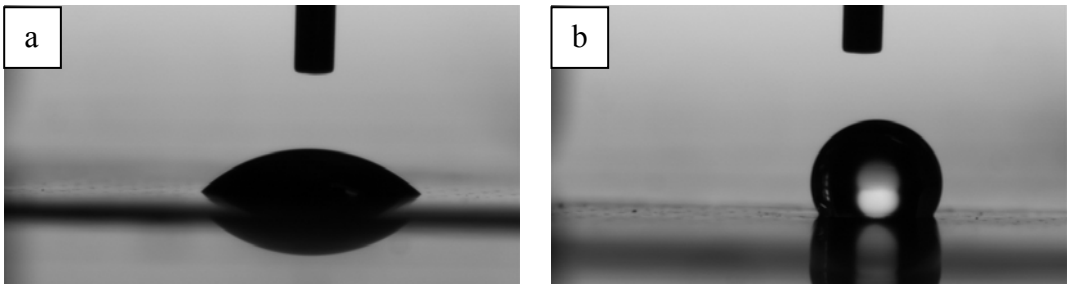

Figure 19. Water drop on surface of PTTh.ClO_4 on Pt-PVDF; a) as-deposited thick (50 mC/cm^2 charge density) films and b) electrochemically-reduced thick (50 mC/cm^2 charge density) films.

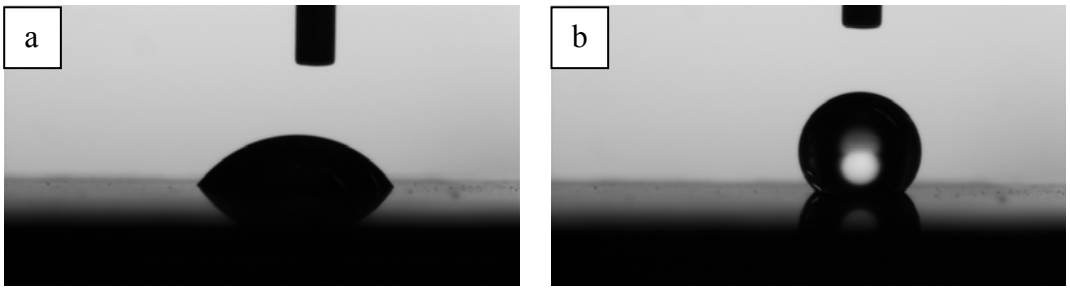

Figure 20. Water drop on surface of PTTh.ClO_4 on GC; a) as-deposited thick (50 mC/cm^2 charge density) films and b) electrochemically-reduced thick (50 mC/cm^2 charge density) films.

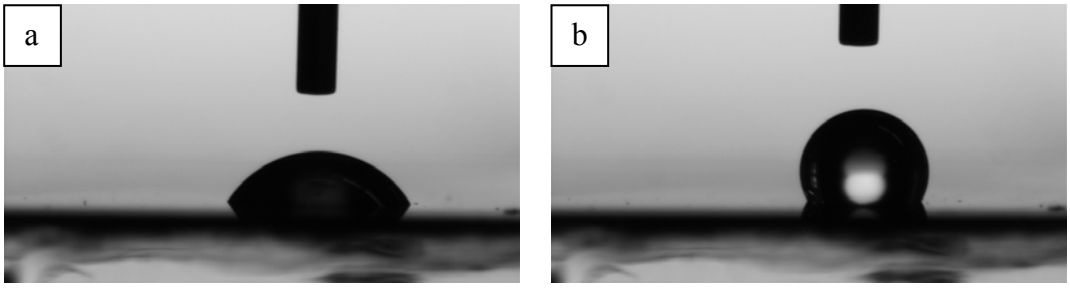

Figure 21. Water drop on surface of PTTh.ClO_4 on ITO; a) as-deposited thick (50 mC/cm^2 charge density) films and b) electrochemically-reduced thick (50 mC/cm^2 charge density) films.

The advancing and receding contact angles are a measure of a material's hydrophobicity and hydrophilicity, respectively. A high hysteresis is indicative of a strong interaction between the liquid and the solid, while a low hysteresis indicates the liquid does not interact significantly with to the material. As-deposited thick PTTh.ClO_4 ($\Delta\theta$ = 33 – 45 °) had a higher hysteresis on all substrates than their reduced counterparts ($\Delta\theta$ = 8 – 15 °). The one exception to this was as-deposited and reduced thick PTTh.ClO_4 on Pt-PVDF, both of which had a hysteresis of ca. 25 °. Of note is the fact that the θ_r values for as-deposited films were often greater than the equilibrium contact angle (θ_s) measured. This is believed to be due to the fact that the method used to determine θ_a and θ_r (described in Chapter 2, Section 2.4.3.2) did not fully probe the minimum receding angle, as the value of liquid withdrawn from the drop during receding contact angle measurements was fixed (i.e. 1 μL; according to the method of Radelczuk *et al.* [47]), rather than receding the triple phase line over previously wetted area, as is more typically carried out. Hence the θ_r value reported in this study may not represent the true dynamic wetting properties of the materials investigated.

The surface energy of PTTh.ClO_4 films was calculated using the treatment of van Oss-Good-Chaudhury, as described in Chapter 1. Ethylene glycol and formamide are among the commonly used polar liquids for surface energy determinations using the Lifshitz-van der Waals acid-base theory and were initially chosen as polar test liquids. However, both of these liquids were found to instantaneously reduce the as-deposited polymer. This was evidenced by the area of film underneath the test liquid becoming orange, in contrast with the black-blue of the surrounding as-deposited polymer, suggesting localised reduction of the PTTh.ClO_4 by the test liquid during the time frame of the measurement. Glycerol and water were thus chosen as polar surface energy test

liquids. Reduction of as-deposited PTTh.ClO_4 was also observed on some substrates while using glycerol and water as test liquids (typically on as-deposited thin PTTh.ClO_4 films); however it was much slower than when using formamide or ethylene glycol. The effect of interaction of these test liquids with the polymer undoubtedly influences the calculated surface energy and will be discussed in Section 3.4.2.

Table 9. Contact angle (°) and surface energy data (mJ/m^2) for test liquids on thick as-deposited and electrochemically-reduced PTTh.ClO_4 films on various substrates.

Substrate	Ox'n state	Water	CH_2I_2	Glycerol	γ_s	γ^{LW}	γ^{AB}	γ^+	γ^-
Pt	**As-deposited**	54 ± 16	[a]	46 ± 3					
	Reduced	129 ± 4	[a]	113 ± 4					
Pt-PVDF	**As-deposited**	63 ± 26	10 ± 1	59 ± 4	50	50.0	0.5	0.0	15.8
	Reduced	102 ± 7	[a]	90 ± 10					
GC	**As-deposited**	65 ± 15	7 ± 2	53 ± 5	53	50.5	2.8	0.2	10.9
	Reduced	126 ± 7	[a]	105 ± 3					
ITO	**As-deposited**	68 ± 10	[a]	48 ± 3					
	Reduced	129 ± 3	[a]	108 ± 2					

N.B. [a] is indicative of spontaneous spreading of the liquid, in which case the surface energy components were not calculated.

The contact angle and surface energy data for thick PTTh.ClO_4 on all substrates and oxidation states are shown in Table 9. The most striking observation from the surface energy measurements is that the apolar test liquid diiodomethane (CH_2I_2) was observed to spread spontaneously on the surface of both as-deposited and reduced PTTh.ClO_4 on almost all substrates. Discernable CH_2I_2 contact angles were only measured for thick as-deposited PTTh.ClO_4 on Pt-PVDF and GC, and even then the films were still highly wet by the CH_2I_2 (~10 °). Such spontaneous spreading invalidates the use of contact

angle data from the spread liquid in the calculation of surface energy components, and as such only the surface energy of films with non-zero contact angles was calculated. The scientific importance of measuring both advancing and receding contact angles of surface energy test liquids for determining the limits of hydrophobicity and hydrophilicity is recognised [48, 49]; however spreading of CH_2I_2 prevented the determination of dynamic contact angle data using contact drop goniometry. The interactions on thick PTTh.ClO_4 were predominantly non-polar, as evidenced by the large γ^{LW} component.

3.3.2.2.2 Thin films

The wettability and surface energy of thin PTTh.ClO_4 films was characterised to establish the effect of polymer thickness. Water contact angles of thin PTTh.ClO_4 films are shown in Table 10.

Table 10. Contact angles of water droplets on thin PTTh.ClO_4 films deposited on various substrates. All contact angles are reported in degrees (°).

Substrate	Ox'n state	θ_s	$\theta_{red} - \theta_{as\text{-}dep}$	θ_a	θ_r	$\Delta\theta$
Pt sheet	**As-dep.**	71 ± 5	36	77 ± 6	64 ± 6	13
	Red.	107 ± 10		139 ± 2	129 ± 3	10
Pt PVDF	**As-dep.**	91 ± 7	12	102 ± 3	72 ± 5	30
	Red.	103 ± 2		100 ± 12	76 ± 3	24
GC	**As-dep.**	96 ± 10	18	117 ± 5	84 ± 11	33
	Red.	114 ± 9		110 ± 2	90 ± 5	20
ITO	**As-dep.**	75 ± 11	31	94 ± 5	53 ± 2	41
	Red.	106 ± 9		111 ± 4	91 ± 6	10

As-deposited thin films had contact angles ranging from 71 – 96 °, while reduced thin film contact angles ranged from 103 – 114 °. The difference between the as-deposited and reduced polymer ranged from 12 – 36 °, with the largest change observed for

PTTh.ClO_4 on Pt sheet. As was the case for thick PTTh.ClO_4, as-deposited thin PTTh.ClO_4 films had higher wetting hystereses than their reduced counterparts, though the trends were less clear and the hysteresis for as-deposited and reduced films on Pt sheet (13 ° and 10 °, respectively) and Pt-PVDF (30 ° and 24 °, respectively) was quite similar. Contact angles of test liquids and calculated surface energy parameters of thin PTTh.ClO_4 films are shown in Table 11.

Table 11. Contact angle (°) and surface energy data (mJ/m^2) for test liquids on thin as-deposited and electrochemically-reduced PTTh.ClO_4 films on various substrates.

Substrate	Ox'n state	Water	CH_2I_2	Glycerol	γ_s	γ^{LW}	γ^{AB}	γ^+	γ^-
Pt	**As-dep.**	71 ± 5	11 ± 4	57 ± 6	52	49.9	2.1	0.2	6.8
	Red.	107 ± 10.	[a]	78 ± 2					
Pt-PVDF	**As-dep.**	91 ± 7	13 ± 9	79 ± 2	52	49.5	2.1	0.6	1.9
	Red.	103 ± 2	[a]	~88					
GC	**As-dep.**	96 ± 10	[a]	57 ± 12					
	Red.	114 ± 9	[a]	86 ± 2					
ITO	**As-dep.**	75 ± 14	[a]	51 ± 5					
	Red.	106 ± 9	10 ± 5	85 ±	51	50.1	0.9	0.4	0.5

N.B. [a] is indicative of spontaneous spreading of the liquid, in which case the surface energy components were not calculated.

Spontaneous spreading of CH_2I_2 on thin PTTh.ClO_4 films was again evident, thus invalidating its use for surface energy determination. Only as-deposited PTTh.ClO_4 on both Pt sheet and Pt-PVDF, and reduced PTTh.ClO_4 on ITO-coated glass exhibited discernable contact angles, and all were approximately 10 °. As for thick films, non-polar interactions were predominant on thin PTTh.ClO_4, again as evidenced by the large γ^{LW} component, with results being comparable to those of the thicker films (Table 9).

3.3.2.3 PTTh-DDO.ClO_4

In order to further explore the factors influencing the wettability of polyterthiophenes, novel functionalised polymers were characterised using analogous methods to those described for the non-functionalised PTTh.ClO_4. The dopant anion was kept constant for consistency and so that the effect of functionalising the polymer backbone with different substituents could be probed. Pt sheet was chosen as the substrate for further investigation of the functionalised monomers for several reasons:

a) It had the lowest contact angle after acetonitrile washing, indicating that the majority of organic contaminants had been removed.
b) The SEMs of PTTh.ClO_4 were the smoothest on Pt sheet, suggesting that the effect of roughness can be minimized in our assumptions regarding the contact angle, so the CA is based mainly on the chemical composition rather than the roughness.
c) The largest change in contact angle between as-deposited and reduced states for PTTh.ClO_4 was observed on platinum sheet (i.e. 75 °), despite its smoothness.

There is little in the literature on PTTh-DDO.ClO_4 and to the best of the author's knowledge this is the first wettability study of this novel substituted-polyterthiophene. An investigation of the water contact angle results revealed a striking difference between the wettability of PTTh-DDO.ClO_4 (Table 12) and the unsubstituted PTTh.ClO_4 presented in the preceding section.

Table 12. Contact angles of water droplets on thick and thin PTTh-DDO.ClO_4 films (50 and 10 mC/cm^2 charge density, respectively) deposited on Pt sheet in the as-deposited and reduced states. All contact angles are reported in degrees (°).

Polymer thickness	Ox'n state	θ_s	$\theta_{red} - \theta_{as\text{-}dep}$	θ_a	θ_r	$\Delta\theta$
Thick	**As-dep.**	145 ± 4	4	136	128	8
	Red.	150 ± 4		151 ± 3	147 ± 3	4
Thin	**As-dep.**	125 ± 6	13	119 ± 11	99 ± 12	20
	Red.	112 ± 4		113 ± 3	99 ± 7	14

As-deposited and reduced thick PTTh-DDO.ClO_4 films were found to have similarly high water contact angles (145 ° and 150 °, respectively). Thin films were less hydrophobic than their thicker counterparts, with water contact angles of 125 ° and 112 ° observed for the as-deposited and reduced films, respectively.

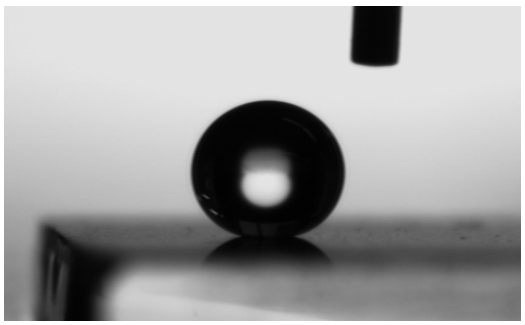

Figure 22. Water drop on the surface of reduced thick (50 mC/cm^2 charge density) PTTh-DDO.ClO_4 with contact angle of ca. 150 °.

Of particular note is the extremely hydrophobic nature of the thick reduced PTTh-DDO.ClO_4 films (Figure 22). Films with a water contact angle greater than 150 ° and a low hysteresis ($\Delta\theta$ < 5 °) may be classified as superhydrophobic. During contact angle analyses of this material, the water drop would not detach from the syringe onto the polymer surface, due to the extreme hydrophobicity of the material, and had to be tapped off the end of the syringe onto the polymer so contact angle measurements could be made.

Table 13. Contact angle (°) and surface energy data (mJ/m^2) for test liquids on thick and thin (50 and 10 mC/cm^2 charge density, respectively) as-deposited and electrochemically reduced PTTh-DDO.ClO_4 on Pt sheet.

Polymer thickness	Ox'n state	Water	CH_2I_2	Glycerol	γ_s	γ^{LW}	γ^{AB}	γ^+	γ^-
Thick	As-dep.	145 ± 4	52 ± 1	147 ± 3	36	33.4	3.0	13.3	0.2
	Red.	150 ± 4	50 ± 2	140 ± 9	42	34.4	8.0	10.0	1.6
Thin	As-dep.	125 ± 6	55 ± 2	122 ± 4	34	31.7	1.9	6.0	0.1
	Red.	112 ± 4	58 ± 2	103 ± 4	31	29.7	1.2	1.1	0.3

The surface energy was determined using an analogous approach to that used for PTTh.ClO_4, with the various components reported in Table 13. Unlike for PTTh.ClO_4, CH_2I_2 formed discrete contact angles on all PTTh-DDO.ClO_4 films, with no spontaneous spreading exhibited. This tendency allowed for valid surface energy calculations using all three liquids to be carried out. All films of PTTh-DDO.ClO_4 were of significantly lower surface energy (31 – 42 mJ/m^2) than PTTh.ClO_4 (ranging from 50 – 53 mJ/m^2; Table 9 and Table 11) consistent with the influence of the hydrophobic alkyl substituents. Both as-deposited and reduced thin films (31 and 34 mJ/m^2) had lower surface energies than that of thicker films (36 and 42 mJ/m^2). Interestingly, reduced thick PTTh-DDO.ClO_4 was the most hydrophobic film (150 °), yet it had the highest surface energy (42 mJ/m^2). Similarly, the thin reduced film was the most hydrophilic (112 °), yet it was calculated to have the lowest surface energy (31 mJ/m^2). These results will be discussed in Section 3.4.3.

3.3.2.4 Summary of valid contact angle data for surface energy determination of PTTh

A comparison of the surface energy components calculated from valid (i.e. non-zero) contact angles is summarised in Table 14. In the interest of legibility, the following

abbreviations have been used: *Polym.*: polymer; *Thick.*: polymer thickness; *Substr.*: substrate; *Ox state*: oxidation state; *PTTh* denotes PTTh.ClO_4; *DDO* denotes PTTh-DDO.ClO_4.

Table 14. Summary of contact angle (°) and surface energy data (mJ/m^2) for test liquids on PTTh.ClO_4 and PTTh-DDO.ClO_4 with measurable contact angles for all test liquids.

Polym.	Thick.	Substr.	Ox state	Water	CH_2I_2	Glycerol	γ_s	γ^{LW}	γ^{AB}	γ^+	γ^-
		Pt	**-**	~5	28 ± 8	19 ± 3	62	45.0	17.4	1.6	48.1
		Pt-PVDF	**-**	120 ± 2	21 ± 2	86 ± 18	48	47.4	0.5	0.0	6.9
		GC	**-**	63 ± 7	16 ± 3	67 ± 6	56	48.9	7.4	0.6	22.9
		ITO	**-**	81 ± 6	48 ± 0	77 ± 12	36	35.2	0.9	0.0	9.2
PTTh	**Thick**	**Pt-PVDF**	**As-dep.**	63 ± 26	10 ± 1	59 ± 4	50	50.0	0.5	0.0	15.8
PTTh	**Thick**	**GC**	**As-dep.**	65 ± 15	7 ± 2	53 ± 5	53	50.5	2.8	0.2	10.9
PTTh	**Thin**	**Pt**	**As-dep.**	71 ± 5	11 ± 4	57 ± 6	52	49.9	2.1	0.2	6.8
PTTh	**Thin**	**Pt-PVDF**	**As-dep.**	91 ± 7	13 ± 9	79 ± 2	52	49.5	2.1	0.6	1.9
PTTh	**Thin**	**Pt-PVDF**	**Red.**	106 ± 9	10 ± 5	85± 2	51	50.1	0.9	0.4	0.5
DDO	**Thick**	**Pt**	**As-dep.**	145 ± 4	52 ± 1	147 ± 3	36	33.4	3.0	13.3	0.2
DDO	**Thick**	**Pt**	**Red.**	150 ± 4	50 ± 2	139 ± 9	42	34.4	8.0	10.0	1.6
DDO	**Thin**	**Pt**	**As-dep.**	125 ± 6	55 ± 2	122 ± 4	34	31.7	1.9	6.0	0.1
DDO	**Thin**	**Pt**	**Red.**	112 ± 4	58 ± 2	103 ± 4	31	29.7	1.2	1.1	0.3

PTTh-DDO.ClO_4 films had the lowest surface energy of the three polyterthiophenes investigated in this study (31 – 42 mJ/m^2). This was significantly lower than the surface energy of the Pt sheet on which they were coated (62 mJ/m^2). The surface energy of PTTh.ClO_4 films were between 50 - 53 mJ/m^2, with no apparent correlation to the substrate, thickness or oxidation state. Further discussion into the reasons behind this will be presented in Section 3.4.2.3.

3.3.3 Interaction between water and PTTh.ClO_4 films

3.3.3.1 Spreading of water drops on as-depostited PTTh.ClO_4

The interaction of water with PTTh.ClO_4 was observed in several ways. Spreading of sessile water drops on as-deposited PTTh.ClO_4 was typically observed immediately upon contact with the surface, equilibrating very quickly to the reported 'recently advanced' angle of ca. 60 ° for thick films and 70 – 96 ° for thin films. Consecutive still images of the droplet spreading were captured using the video capability of the goniometer software (Figure 23). These images often revealed a high initial water contact angle at the moment of contact (ca. 120 °), however the angle was observed to decrease rapidly to the final value of ca. 60 °. This behaviour was only observed on as-deposited films as the spreading of water droplets was generally not observed on electrochemically reduced films. These findings point to the different interactions of water with as-deposited and reduced PTTh.ClO_4.

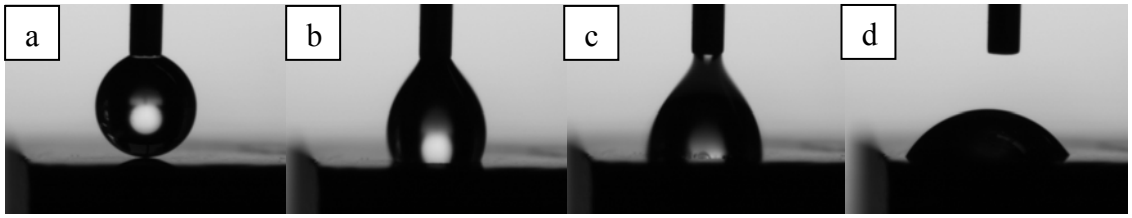

Figure 23. Sequential still images captured from a video of a water drop spreading upon contact with as-deposited thick (50 mC/cm^2 charge density) PTTh.ClO_4 on Pt sheet. A high initial contact angle of 120 ° (image b) was observed to quickly decrease to the final measured contact angle of 60 ° (image d). a) t = 0.00s; b) t = 0.08 s; c) t = 0.32 s; d) t = 0.52 s.

3.3.3.2 The 'watermark effect' on as-deposited PTTh.ClO_4

A striking example of the interaction of water with PTTh.ClO_4 was observed during contact angle measurements of films. An initial water drop on as-deposited thick PTTh.ClO_4 was observed to spread to a typical value of ca. 60 ° (Table 8), after which

point the drop was 'wicked' away from the surface using a lint-free (KimWipe) tissue. A clearly observable change in appearance of the film was noted where the initial droplet had contacted the film. A second water drop, immediately placed in exactly the same position as the previous drop, exhibited a dramatic change in wettability with contact angles of ca. 125 °, consistent with that of reduced thick PTTh.ClO_4. This phenomenon is shown in Figure 24 and shall subsequently be referred to as the watermark effect.

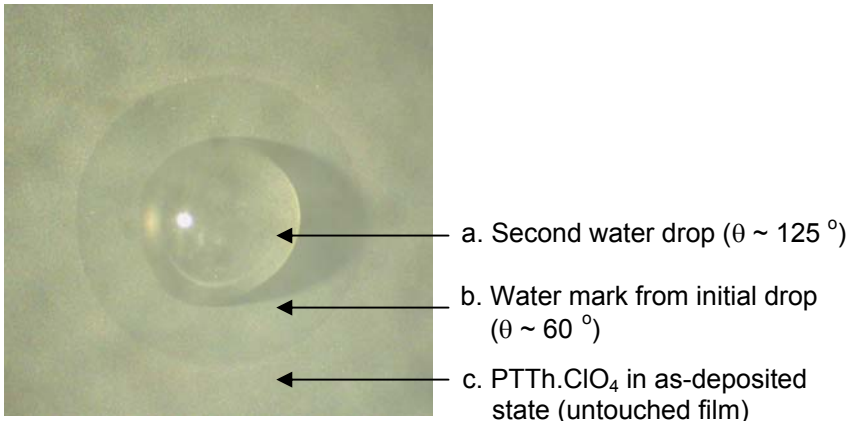

Figure 24. Optical microscope image of a) water drop placed in b) water mark of previous droplet on c) as-deposited thick PTTh.ClO_4 film.

A similar effect was also present on thin films but the change in contact angle of the second water drop was somewhat diminished. Initial drops spread to ca. 70 – 96 ° (Table 10), while water drops placed inside the watermark of the first drop had contact angles of ca. 110 °, consistent with reduced thin PTTh.ClO_4. In addition to the watermark effect, thin as-deposited PTTh.ClO_4 films (blue-black in colour) often became orange beneath the water drop during the time frame of water contact angle measurement, indicating a reduction of the polymer by water.

3.3.3.3 Raman spectroscopic investigation of $PTTh.ClO_4$ oxidation state

3.3.3.3.1 Surface and 'scratched' polymer

Raman spectroscopy was used to provide insight into the interaction between water and $PTTh.ClO_4$. An area of as-deposited thick $PTTh.ClO_4$ film which had been scratched to expose underlying layers was studied by Raman mapping (Figure 25). Inspection of the film surface and 'scratched off' areas of film revealed a dramatic change in the polymer oxidation state, from reduced at the polymer surface to oxidised in underlying layers, with a sharp difference observable at a distance of just 1 μm across the surface/scratched polymer interface. The measure of oxidised or reduced character was determined by the position and intensity of key Raman vibrations, namely the Q_1 and D_3 peaks at 1435 and 1161 cm^{-1}, respectively. The Raman spectra on which the mapping was based (not shown here) were consistent with previously published doped and de-doped polythiophene [31].

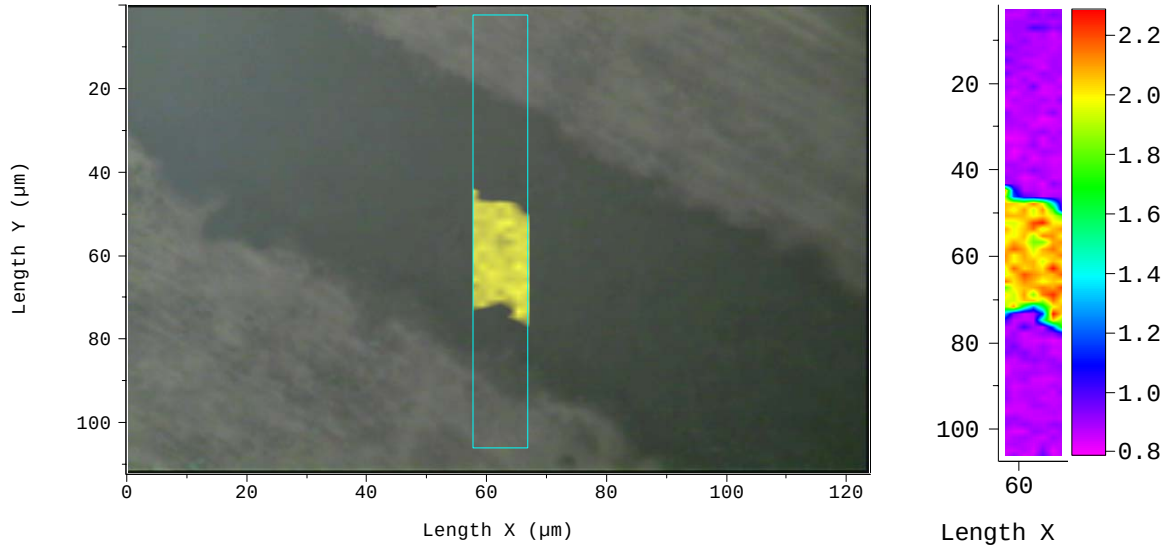

Figure 25. Optical image of an area of thick (50 mC/cm^2 charge density) as-deposited $PTTh.ClO_4$ film which had been scratched to reveal underlying layers. Raman spectra were measured over the area in the rectangle at 1 μm intervals. The surface layer was found to be reduced while underlying layers in the scratch were oxidised, as indicated by the light band in the centre of the rectangle.

The unexpected Raman findings showed that the surface of the as-deposited film was in the reduced state, rather than the oxidised state formed by electrochemical polymerisation of the TTh monomer. As reported in Section 3.3.1.2.1, UV-Vis studies have shown that the bulk of the film was predominantly oxidised in the as-deposited state. The Raman studies suggest that the reduced layer was confined to the film-air interface. It was initially thought that the surface of the polymer possibly became reduced upon rinsing of the film in acetonitrile post-deposition as the dopant may be washed out from surface layers by the non-anhydrous solvent being used [50]. However, Raman spectra of as-deposited PTTh.ClO_4 films which were not rinsed after deposition had surfaces that were still found to be in the reduced state.

3.3.3.3.2 Depth profiling of as-deposited PTTh.ClO_4

The presence of strongly oxidised and reduced PTTh.ClO_4 in the same film was interesting and warranted further investigation. The heterogeneity in oxidation state was probed with depth profiling using confocal Raman microscopy with a 632.8 nm laser and a 150 μm pinhole. The 632.8 nm laser was used due to its ability to give structural information about oxidised and reduced states of polythiophene simultaneously [22, 23]. Confocal microscopy is a useful technique for probing depth as it allows for greater depth accessibility than other depth profiling techniques (up to 100 μm), such as X-ray Photoelectron Spectroscopy (XPS) or Attenuated Total Reflection (ATR) spectroscopy, in addition to its non-destructive nature and rapid analysis times [51].

The sampling volume of the analysing laser was dependant on the size of the pinhole and refractive index of the material, but is typically ca. 5 μm^3 [51, 52]. This volume corresponds to a sphere with a diameter of approximately 0.6 to 1 μm at the focal plane

selected by the optics and pin-hole combination. The spectral depth intervals reported in the following sections, for thick and thin PTTh.ClO_4, refer to the distance moved by the z-stage objective which does not directly correlate to the actual sampling depth within the polymer film. For example, thick polymer films were on the order of 5 - 10 μm thick and the z-stage could be moved by 30 μm (i.e. 15 x 2 μm steps) with a signal still obtained. This apparent inflation in film thickness can be explained by the fact that even though the "in-focus" laser spot was ca. 0.6 to 1 μm, scattered Raman shifted laser interactions could still be observed at other focal planes within the sample.

Spectral aberrations due the incongruity of refractive indices at the polymer/air interface may be treated using a normalisation equation [51, 53] or the use of an oil immersion objective, whereby the refractive index of the polymer is matched to that of surrounding oil [52]. However, the added complications of oil absorption in the spectra and possible interaction of the oil with the polymer may be introduced. Given the dynamic nature of conducting polymers and their interaction with various liquids already observed in this study, confocal Raman investigations were carried out conventionally in air, with awareness of the possible distortions.

As-deposited thick PTTh.ClO_4

The effect of substrate (Pt sheet, Pt-PVDF, GC and ITO) on the oxidation state and extent of surface reduction of thick as-deposited PTTh.ClO_4 was investigated (Figure 26 - Figure 29). Depth profiling was carried out using the procedure described in Section 3.2.3.6.1). Spectra were normalised with respect to the 1046 cm^{-1} peak, corresponding to the C-H bend of the thiophene ring which is present in both the neutral and oxidised forms of polythiophene.

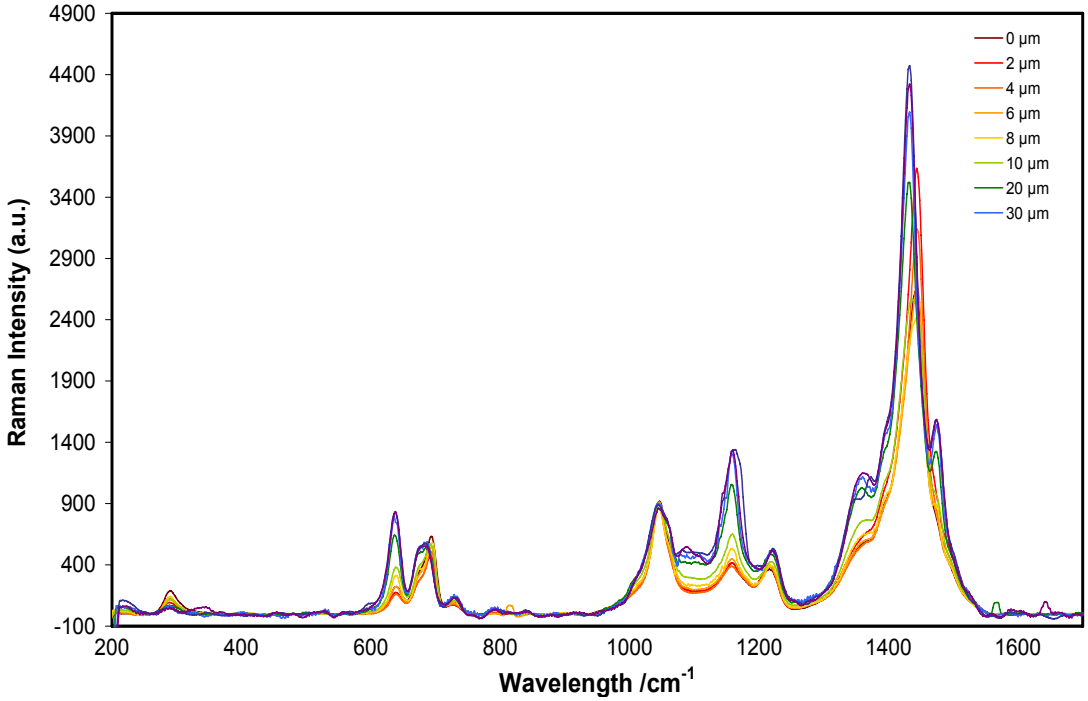

Figure 26. Confocal Raman depth profiling through thickness of as-deposited thick (50 mC/cm^2 charge density) PTTh.ClO_4 on Pt sheet. Spectral intervals refer to the distance moved by the z-stage, with 0 µm corresponding to the laser focussed on the film surface.

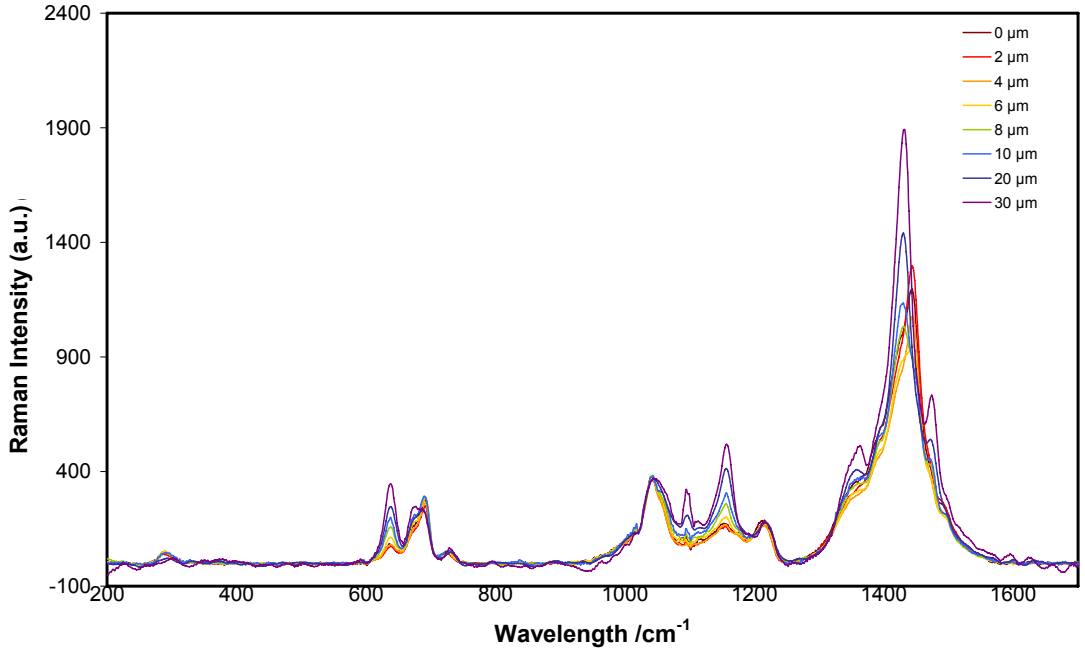

Figure 27. Confocal Raman depth profiling through thickness of as-deposited thick (50 mC/cm^2 charge density) PTTh.ClO_4 on Pt-PVDF. Spectral intervals refer to the distance moved by the z-stage, with 0 µm corresponding to the laser focussed on the film surface.

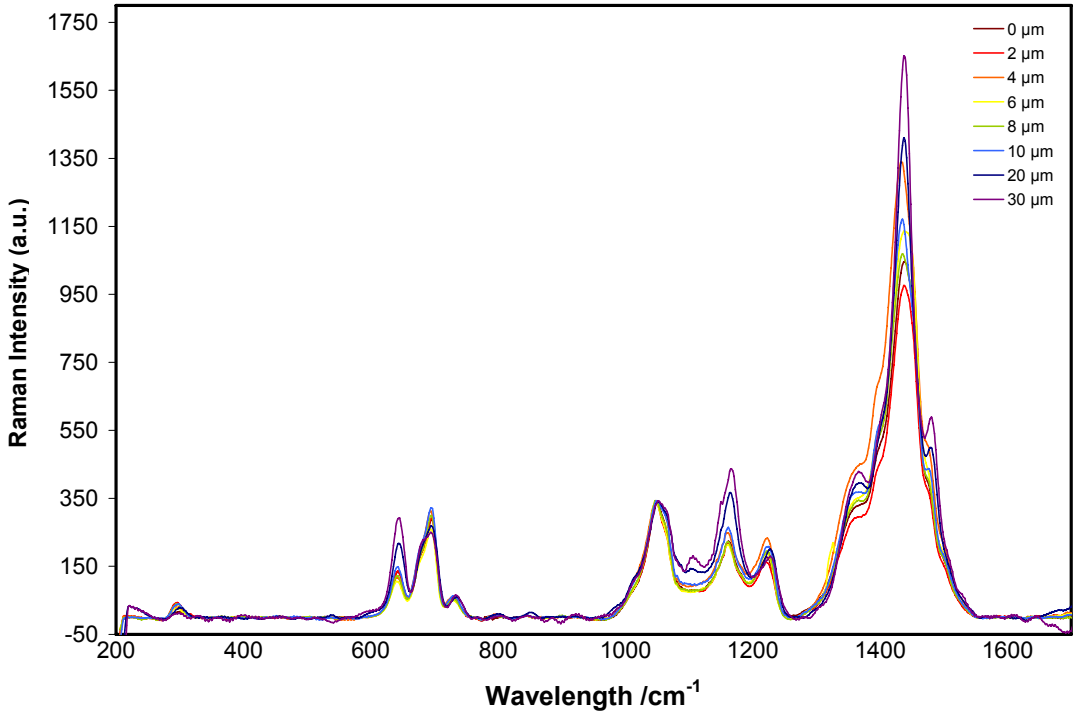

Figure 28. Confocal Raman depth profiling through thickness of as-deposited thick (50 mC/cm^2 charge density) PTTh.ClO_4 on glassy carbon. Spectral intervals refer to the distance moved by the z-stage, with 0 µm corresponding to the laser focussed on the film surface.

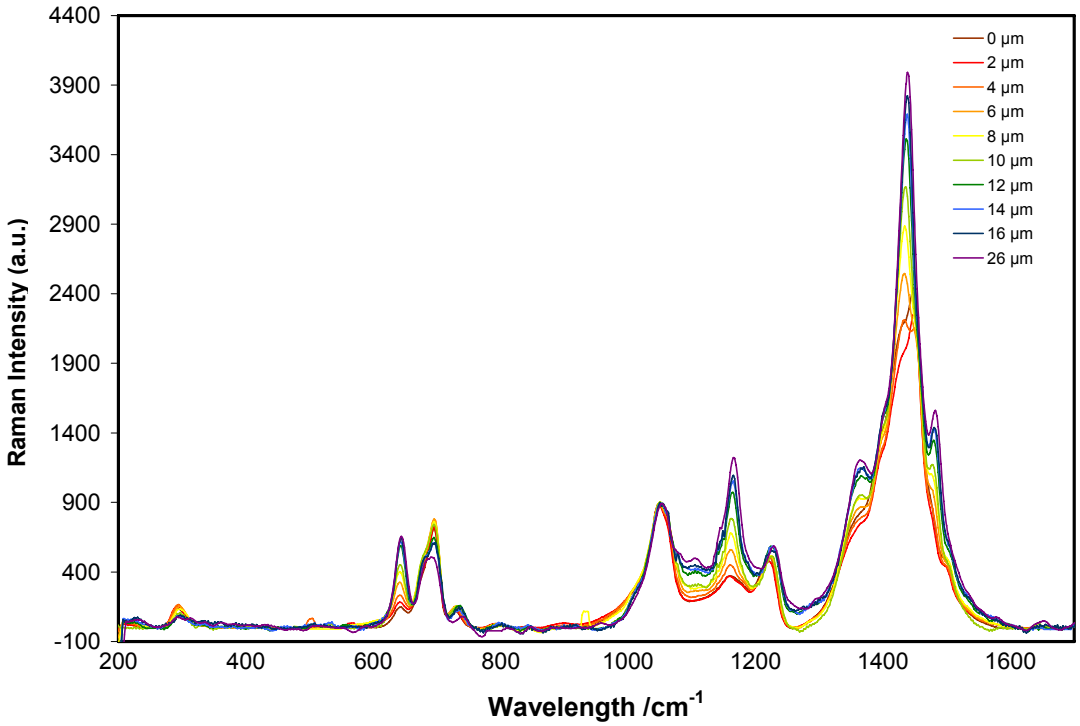

Figure 29. Confocal Raman depth profiling through thickness of as-deposited thick (50 mC/cm^2 charge density) PTTh.ClO_4 on ITO-coated glass. Spectral intervals refer to the distance moved by the z-stage, with 0 µm corresponding to the laser focussed on the film surface.

The PTTh.ClO_4 oxidation state gradually changed throughout the thickness of the as-deposited thick polymer. Films were reduced at the surface and became more oxidised as spectra were sampled deeper into the polymer film. This phenomenon was observed to a similar extent across all substrates and will be discussed in Section 3.4.1.1.1.

As-deposited thin PTTh.ClO_4

Further investigation into the heterogeneity in oxidation state throughout PTTh.ClO_4 samples was carried out by Raman depth profiling of as-deposited thin films. Such films were observed to be in the oxidised state throughout the entire polymer thickness, with little or no change in the spectra as the laser was focused deeper into the polymer and spectra mostly overlaying each other (Figure 30- Figure 33). The exception to this was PTTh.ClO_4 on Pt sheet, which was observed to undergo a slight change in oxidation state, with the film increasing in oxidised character as the stage was moved focussing deeper into the film. The stability of the peak intensities was due to the minimal change in doping levels in the material sampled in the thin (1 – 2 μm) films.

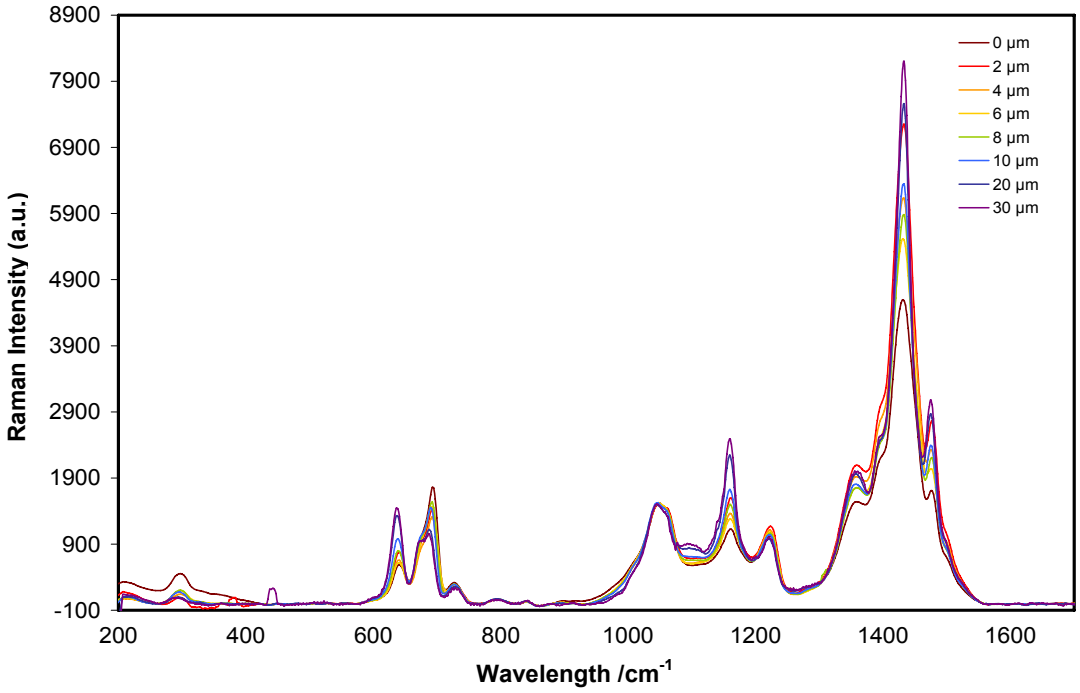

Figure 30. Confocal Raman depth profiling through thickness of as-deposited thin (10 mC/cm^2 charge density) PTTh.ClO_4 on Pt sheet. Spectral intervals refer to the distance moved by the z-stage, with 0 μm corresponding to the laser focussed on the film surface.

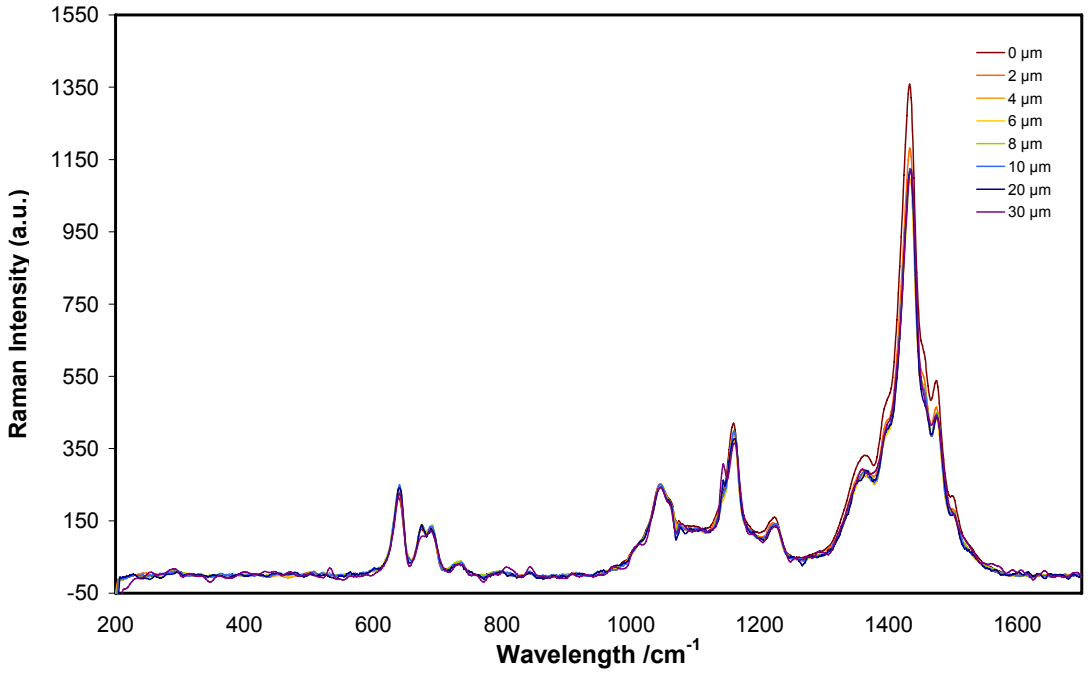

Figure 31. Confocal Raman depth profiling through thickness of as-deposited thin (10 mC/cm^2 charge density) PTTh.ClO_4 on Pt-PVDF. Spectral intervals refer to the distance moved by the z-stage, with 0 µm corresponding to the laser focussed on the film surface.

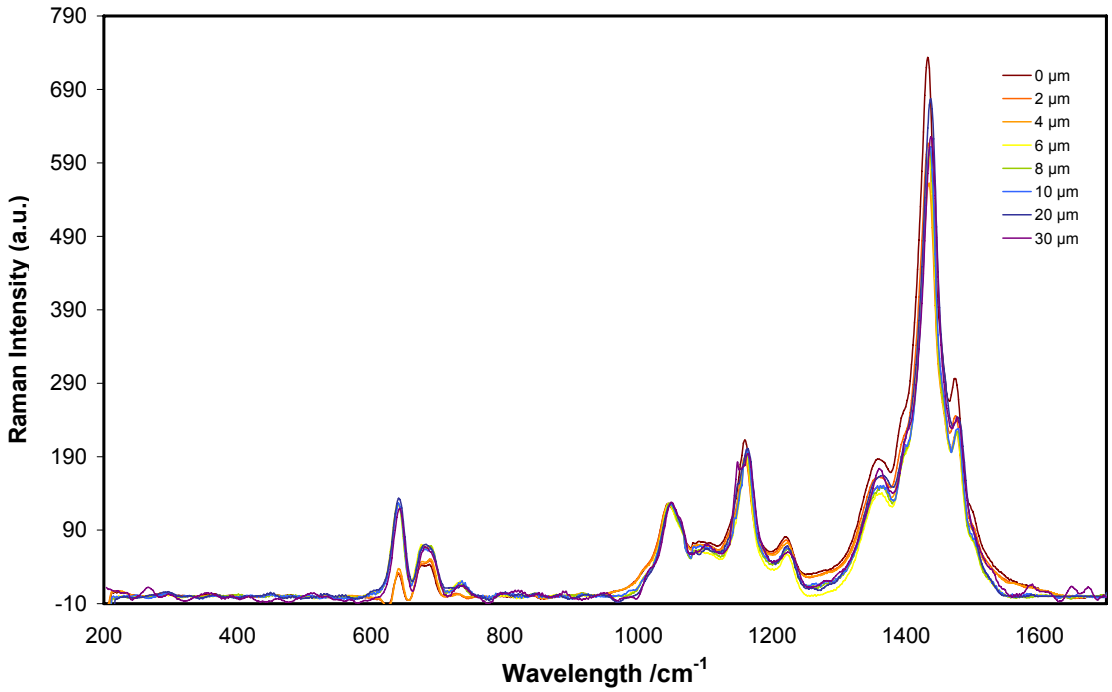

Figure 32. Confocal Raman depth profiling through thickness of as-deposited thin (10 mC/cm^2 charge density) PTTh.ClO_4 on glassy carbon. Spectral intervals refer to the distance moved by the z-stage, with 0 µm corresponding to the laser focussed on the film surface.

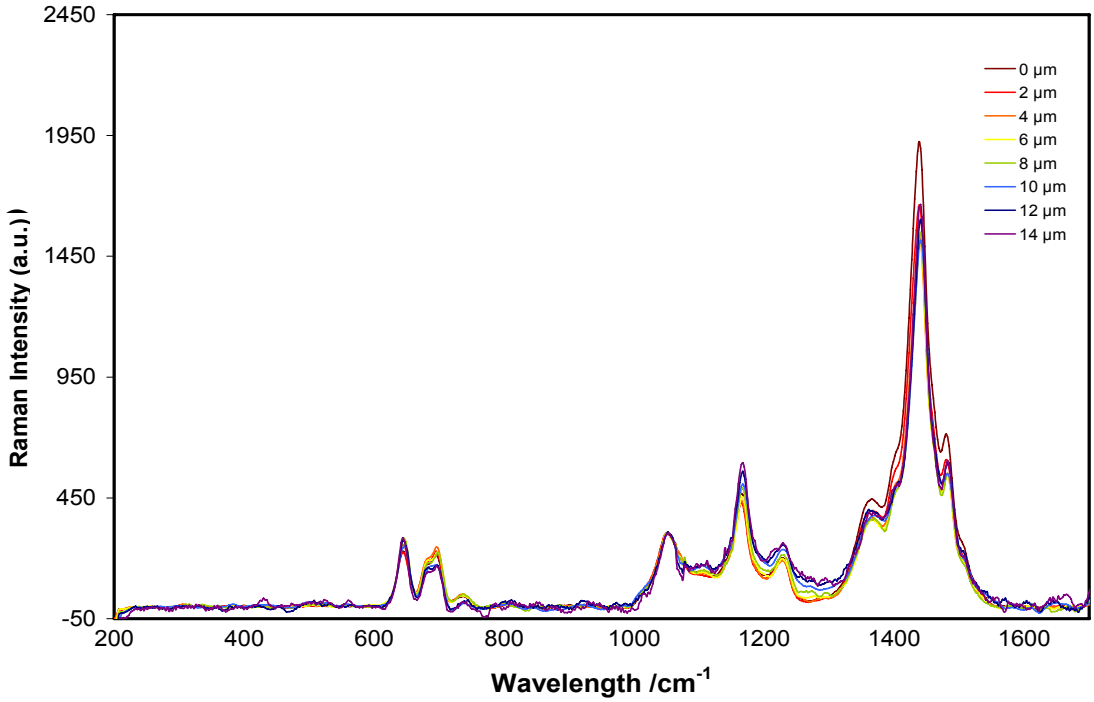

Figure 33. Confocal Raman depth profiling through thickness of as-deposited thin (10 mC/cm^2 charge density) PTTh.ClO_4 on ITO-coated glass. Spectral intervals refer to the distance moved by the z-stage, with 0 µm corresponding to the laser focussed on the film surface.

3.3.3.3.3 Raman investigation of the watermark effect

In light of the differences in polymer oxidation state for thin and thick PTTh.ClO_4 films, Raman spectroscopy was used to further investigate the watermark effect on as-deposited PTTh.ClO_4 films. Raman spectra were measured at the surface of the film on previously un-wet polymer, in the watermark produced during contact angle measurement of the initial water drop and through the second water drop inside the watermark (Figure 34 and Figure 35).

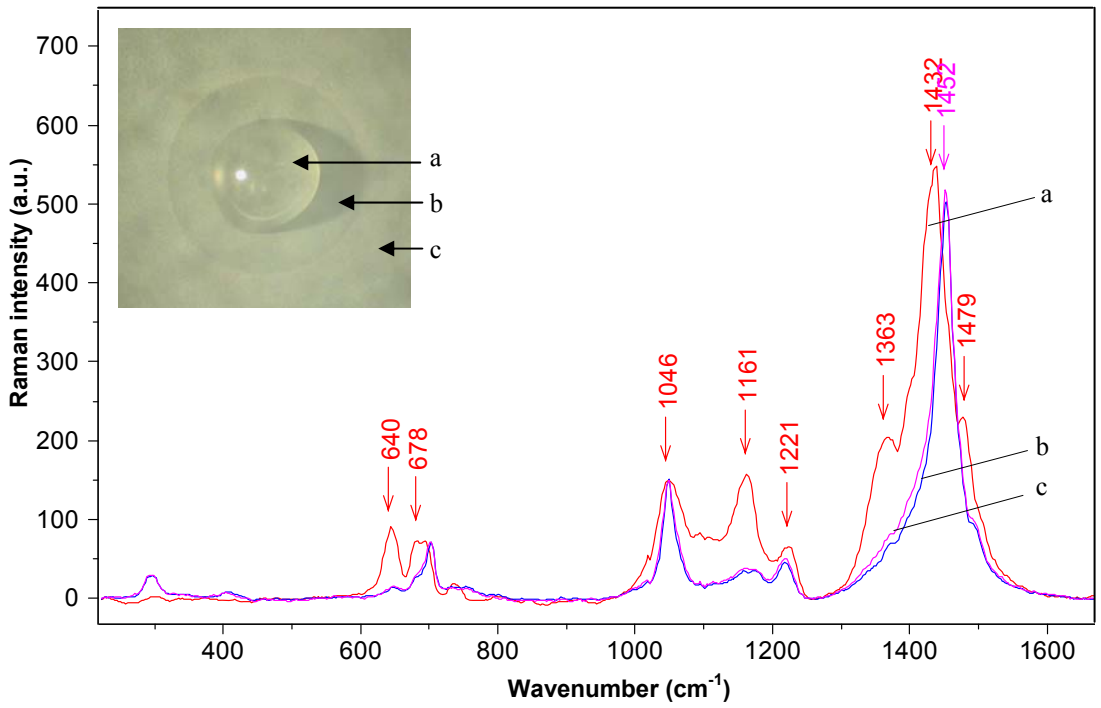

Figure 34. Raman spectra at different positions on as-deposited thick (50 mC/cm^2 charge density) PTTh.ClO_4 film. a) Through water drop (red spectrum; oxidised), b) in watermark of previous droplet (blue spectrum; reduced) and c) on as-deposited surface of film (purple spectrum; reduced).

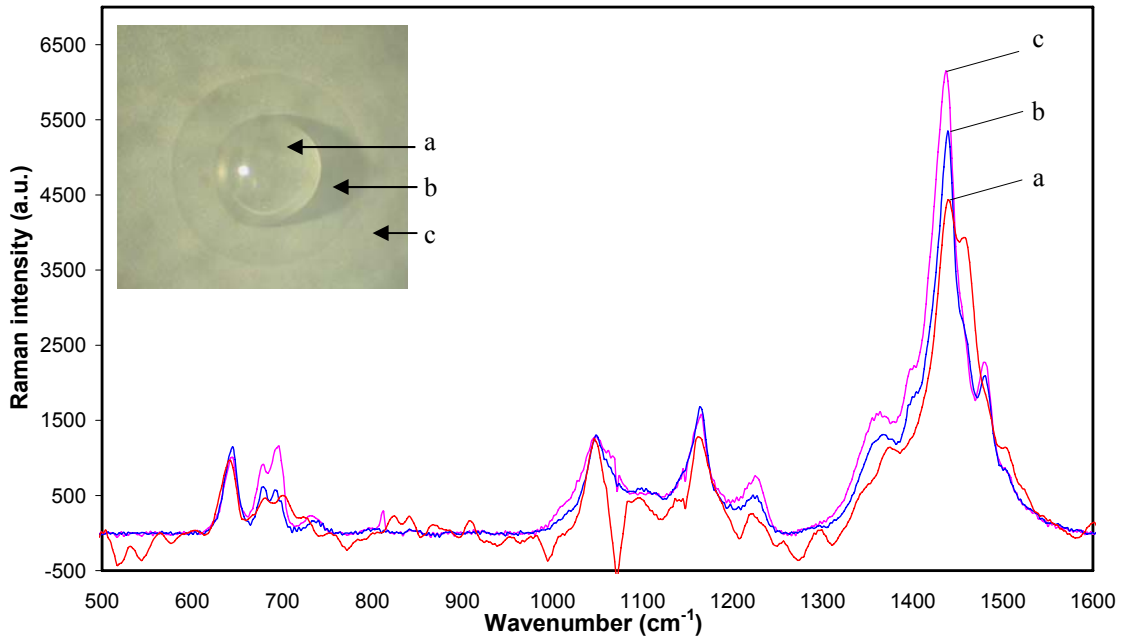

Figure 35. Raman spectra at different positions on as-deposited thin (10 mC/cm^2 charge density) PTTh.ClO_4 film. a) Through water drop (red spectrum; oxidised), b) in watermark of previous droplet (blue spectrum; reduced) and c) on as-deposited surface of film (purple spectrum; reduced).

Marked differences between thick (~5 – 10 μm) and thin (1 – 2 μm) PTTh.ClO_4 films were observed. The surface of previously un-wet thick PTTh.ClO_4 was in the reduced state, consistent with observations for as-deposited thick PTTh.ClO_4 investigated in depth profiling and Raman mapping studies. Interestingly, the area of film under the water drop was found to be predominantly oxidised; however the extent of oxidation was less than that for thick PTTh.ClO_4 films close to the substrate (Figure 26 - Figure 29), based on the ratio of the 1046:1161 cm^{-1} peaks, which are indicative of the degree of polymer oxidation [31]. An inspection of the Raman spectra for thin PTTh.ClO_4 revealed markedly different oxidation states of films at varying positions. The most notable difference is that the surface of the thin films were oxidised and had not undergone surface reduction as the thicker films had. In addition to this feature, polymer underneath the water drop was observed to be partially oxidised/partially reduced. This was evidenced by the splitting of the main peak at ca. 1450 cm^{-1} into two peaks attributable to the Q_1 and v_2 vibrations at 1440 and 1458 cm^{-1}, respectively, and indicated the presence of both oxidised and reduced material underneath the water drop on the as-deposited thin PTTh.ClO_4 film.

The effect of the water drop on the oxidation state of both thin and thick electrochemically-reduced PTTh.ClO_4 was also explored using Raman spectroscopy. The area underneath the water drop on films of both thicknesses remained in the reduced state, in contrast with observations of the effect of water on the oxidation state of as-deposited PTTh.ClO_4.

3.3.4 Raman spectroscopy of functionalised polyterthiophene PTTh-DDO.ClO_4

Raman spectroscopy of as-deposited and reduced PTTh-DDO.ClO_4 films of both thicknesses was carried out at film surfaces (Figure 36 and Figure 37). Confocal depth profiling was attempted, however little change in oxidation state was observed

throughout the thickness of the polymer, as the surface of as-deposited films was already in a highly doped state and had not reduced, in contrast to the results obtained for PTTh.ClO_4.

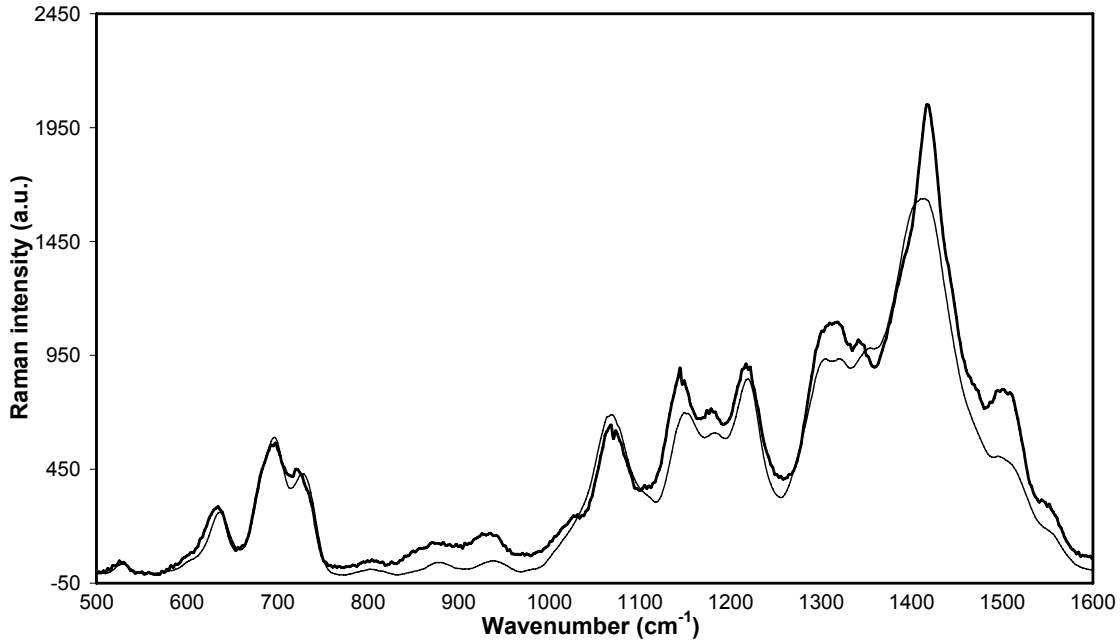

Figure 36. Raman spectra of as-deposited thick (50 mC/cm^2 charge density; —— bold line) and thin (10 mC/cm^2 charge density; —— thin line) PTTh-DDO.ClO_4 on platinum sheet.

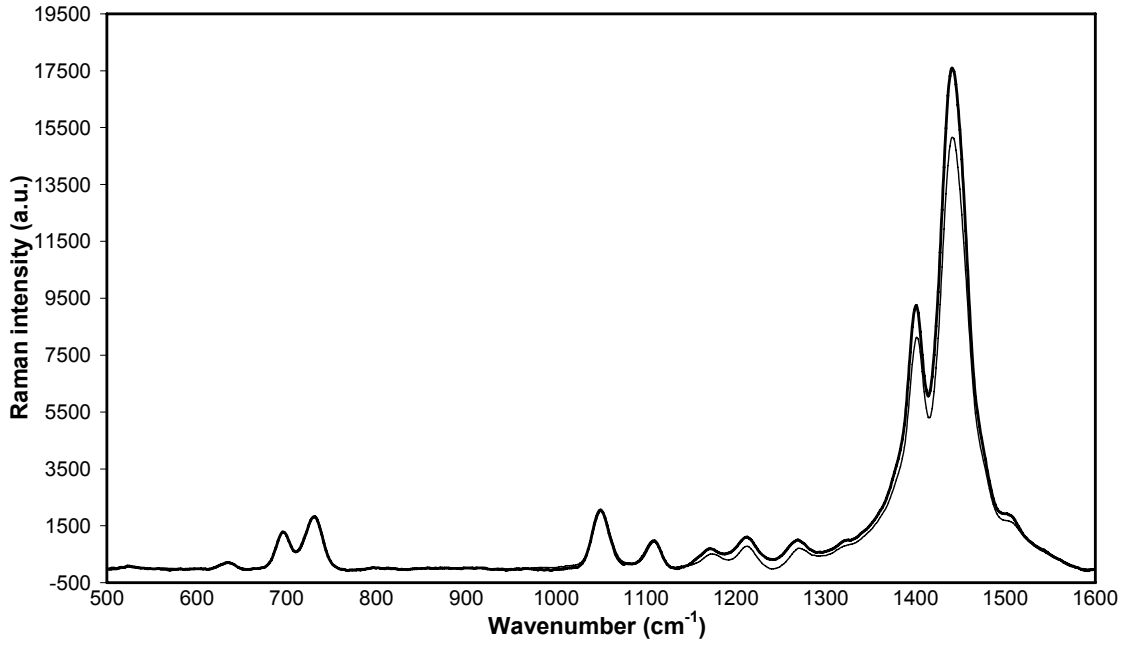

Figure 37. Raman spectra of reduced thick (50 mC/cm^2 charge density; —— bold line) and thin (10 mC/cm^2 charge density; —— thin line) PTTh-DDO.ClO_4 (reduction potential of -0.5 V *vs*. Ag/Ag^+) on platinum sheet.

3.3.5 *In-situ* electrochemically-induced contact angle changes

The dramatic change in wettability of thick PTTh.ClO4 films in ambient laboratory conditions (i.e. *ex-situ* the electrochemical cell) led to an examination of water contact angle change upon *in-situ* electrochemical redox switching, using the set-up described in Section 3.2.3.7; Figure 4. Contact angles of captive water drops were monitored during oxidation and reduction of the polymer to determine if a similar change in wettability was present. Interestingly, no change in water drop shape or contact angle was observed upon redox switching. The observation of a reversible PTTh.ClO_4 colour change from orange to blue indicated that the electrochemical set-up was working correctly and redox switching of the polymer was occurring. In addition, drops of water were difficult to adhere to polymer-coated Pt sheet and had contact angles of ca. 150 ° on both thin and thick PTTh.ClO_4 (Figure 38), whereas they easily adhered to non-polymer coated Pt sheet.

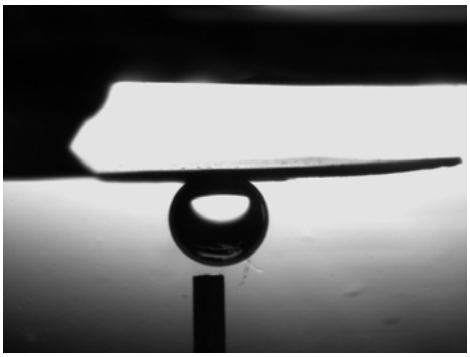

Figure 38. Electrochemical contact angle measurement of captive water bubble resting on the underside of PTTh.ClO_4-coated Pt sheet. The potential was switched between +0.8 and 0 V *vs.* Ag/Ag^+.

3.4 Discussion

3.4.1 Effect of water on oxidation state of PTTh.ClO_4

The surface reduction observed for as-deposited thick PTTh.ClO_4 films in Raman depth profiling and mapping studies has been described in the literature as an auto-reduction effect. It has been observed for polythiophenes and in particular a large body of

research has been carried out into the auto-de-doping of poly-3-alkylthiophenes (P3AT) [54-59]. The rate of de-doping and loss of conductivity has been found to depend on the dopant molecule [60, 61], degree of doping and temperature [54] as well as humidity [56, 57] and ambient lighting [58, 62]. There has been some discrepancy regarding the role of parameters such as dopant size, with Pei *et al.* [55] reporting that larger dopants were expelled more easily than smaller ones, which is in contrast with the findings of Ciprelli *et al.* [61] who found that dopant size was not important in the de-doping rate. The length of the side group in P3ATs was also found to be important in determining stability, as polymers with longer side chains were less stable. Chemically deposited polymers were slightly more stable than those which were electrochemically deposited [60].

The role of water in de-doping P3ATs [58, 60, 63] and polythiophene [64, 65] has been identified, with the increased reactivity of the oxidised state to the water deemed responsible for the auto-reduction. Indeed, the rate of de-doping has been observed to increase upon exposure of the polymer to water vapour [55]. Upon de-doping the polymer, the counter-ion is believed to form ion pairs with the H^+ or OH^- in the ambient water. A discussion of the redox potentials involved in such reactions is presented in Section 3.4.1.1.3. However, as de-doping of P3AT has been reported to occur under dry nitrogen atmosphere [54] and vacuum [66], other factors are also believed to be involved.

3.4.1.1 Influence of substrate and film thickness on PTTh.ClO_4 surface auto-reduction

3.4.1.1.1 Thick films

Substrate and film thickness were found to have a marked effect on the extent of auto-reduction in PTTh.ClO_4, as evidenced by depth profiling studies. As-deposited thick

PTTh.ClO_4 films exhibited a dramatic change in oxidation state as the laser was focused deeper into the polymer (Figure 26 - Figure 29). Significant increases in the defect bands (D_1 – D_7) and enhancement of ν_3 (C-C stretching) and ν_1 (asymmetric C=C stretching) modes with depth indicated a transition from reduced polymer at the surface to oxidised polythiophene in underlying layers [21]. This observation was supported with a decrease in intensity of the ν_2 C=C ring stretching peak at 1458 cm^{-1} with a concurrent increase in the quinoidic bipolaron band Q_2 at 1435 cm^{-1}. As-deposited thick PTTh.ClO_4 films remained black, despite the Raman spectra indicating the surface was reduced. This observation supports the notion that the surface reduced layer was very thin. The change in Raman intensity with nominal depth into as-deposited thick PTTh.ClO_4 on various substrates for several peaks diagnostic of oxidation state, namely Q_1 (quinoidic radical cations), D_1 (distorted kink), D_3 (distorted kink), ν_2 (symmetric C_α=C_β ring stretching) and D_5 (distorted kink), is shown in Figure 39 i - iv.

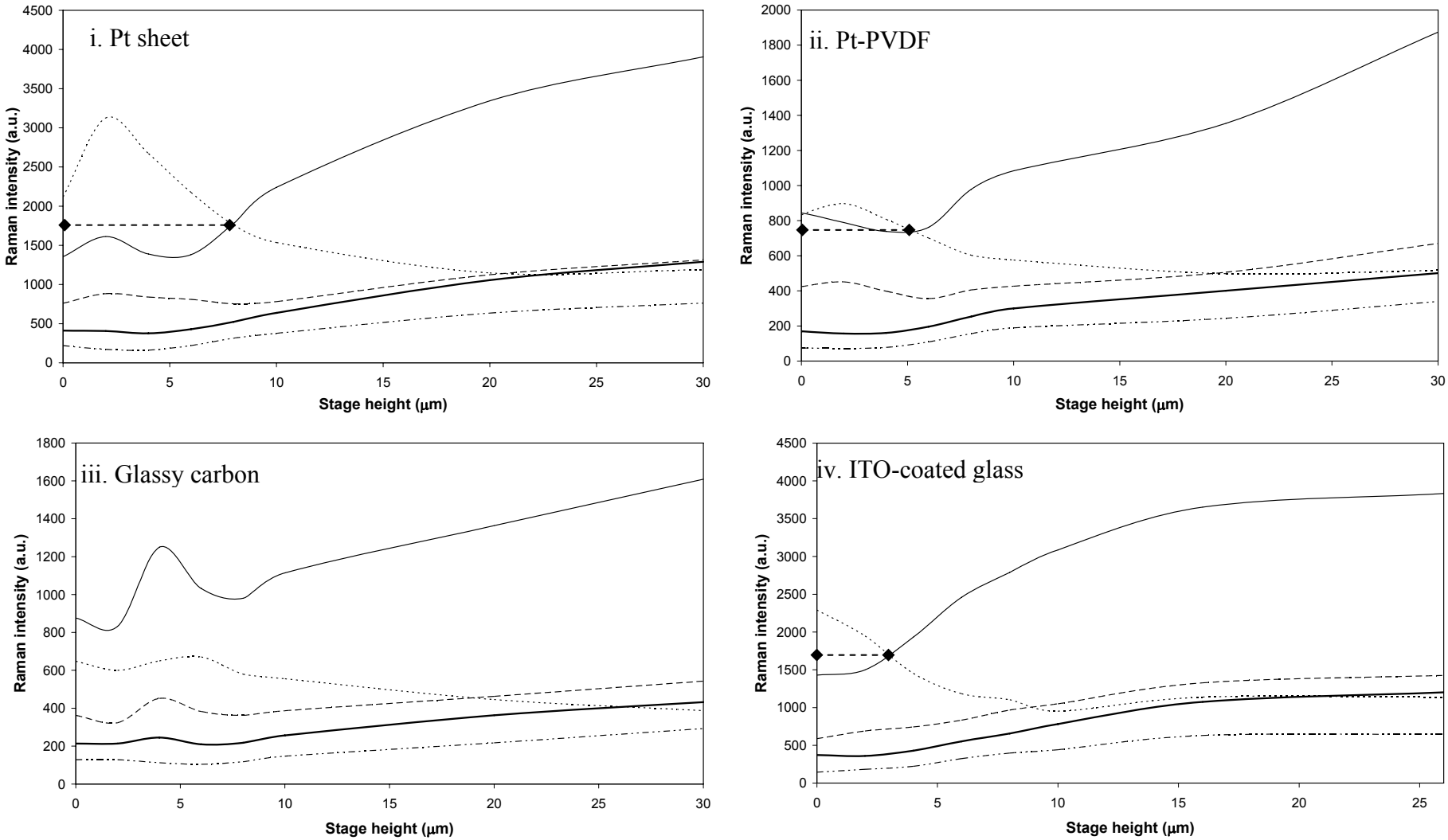

Figure 39. Raman intensity of various bands with respect to distance z-stage moved shifting the focal point into as-deposited thick PTTh.ClO_4 on i) platinum sheet, ii) platinised PVDF membrane, iii) glassy carbon and iv) ITO-coated glass. Intensity of bands shown: —— Q_1: quinoidic radical cations; - - - - D_1: distorted kink; —— D_3: distorted kink; ····· ν_2: symmetric C_α=C_β ring stretching and — · — · D_5: distorted kink. ◆ - - - - ◆ denotes area of film which is reduced.

An increase in intensity of the dication Q_1 band at 1428 cm^{-1} with movement of the z-stage shifting the laser focal point into the polymer, attributable to oxidised polythiophene species [18], was clearly evident for all substrates (depicted by solid thin line in Figure 39). The slope of this curve is an indicator of the extent of change in doping level throughout the polymer. For as-deposited thick PTTh.ClO_4 on ITO (Figure 39 iv), the intensity of the band continued to increase until it had reached a plateau at an ca. 15 μm shift in the z-stage. The intensity of the Q_1 band reached a plateau more gradually for as-deposited thick PTTh.ClO_4 on Pt sheet (Figure 39 i), while for Pt-PVDF and glassy carbon the intensity was still increasing after 30 μm movement of the z-stage into the film (Figure 39 ii and iii, respectively). An anomaly present in the spectra for PTTh.ClO_4 glassy carbon (50 mC/cm^2 charge density) at 4 μm z-stage movement (manifested as a sharp increase in the intensity of the Q_1 band) may be explained by certain inaccuracies that exist for confocal spectra, due to the difference in refractive indices at the polymer-air interface, as outlined by Gallardo *et al*. [53].

The area of film where the intensity of v_2 is greater than Q_1 may be used as an indicator of the oxidation state of the polymer; that is, if $I_{v2} > I_{Q1}$, then the film is likely to have a more reduced character [31]. For Pt sheet, Pt-PVDF and ITO, the I_{v2}:I_{Q1} ratio changed through the thickness of the film suggesting that the surface layers were less oxidised, while the intensity of the Q_1 band was always greater than the v_2 band for as-deposited thick PTTh.ClO_4 on glassy carbon, suggesting this film was in the oxidised state through the entire thickness.

Table 15. Work function of substrates (eV) and the depth into PTTh.ClO_4 where I_{v2} > I_{Q1} (μm).

Substrate	Work function	Distance moved by z-stage where $I_{v2} > I_{Q1}$
Pt-sheet	5.6	8
Pt-PVDF	~5.6	6
ITO-coated glass	~4.7	3
Glassy carbon	4.0	[a]

[a] I_{Q1} always > I_{v2}, suggesting entire film is in doped state (ca. 30 μm depth in z-direction)

The extent of polymer surface reduction may be correlated to the work function of the electrode, which is shown in Table 15 for all substrates. The work function of a material is defined as the energy required to remove an electron from the surface to a point directly outside and adjacent to the surface. Low work function materials require less energy to remove electrons than high work function materials, and as such the oxidation state of the polymer coated onto the substrate may be affected by variation in electrode work functions. When two materials with different work functions come into contact, electrons will flow from the one with the lower work function to the other until the Fermi levels of the materials equilibrate. The material having a higher work function gains electrons and charges negatively, while the material having the lower work function loses electrons and charges positively [67, 68]. The differing extents of surface reduction of PTTh.ClO_4 may be correlated to the work function of the underlying electrode substrate as materials with higher work functions caused adjacent PTTh.ClO_4 layers to have a more oxidised character. For example, Pt sheet possesses the highest work function at 5.6 eV [69], hence the polymer adjacent to the electrode was more oxidised than that of the polymer at the air-polymer interface. This was evident in the Raman spectra of PTTh.ClO_4 on Pt sheet which exhibited the greatest section of reduced polymer at the surface (i.e. 8 μm moved by z-stage). Pt-PVDF is expected to

have a similar work function to Pt sheet, but vastly different morphology and higher interfacial surface area, leading to a slightly smaller thickness of reduced polymer (i.e. 6 μm moved by z-stage into polymer). ITO-coated glass has a work function of ca. 4.7 eV, but values of between 4.1 – 5.5 eV have been reported [70, 71]. The work function of glassy carbon is the lowest at ca. 4.0 eV [72], hence the polymer at the surface was found to be in a doped state, with the oxidised character increasing steadily throughout the thickness of the polymer. The existence of polymer with varying oxidation states may be facilitated by the reduction of the polymer with ambient moisture, as discussed in Section 3.4.1.1.3. There was no apparent correlation between film roughness (Table 4) and the extent of PTTh.ClO_4 surface reduction, indicating the influence of the substrate work function was the overriding effect.

The ratio of certain peaks is characteristic of polyterthiophene doping level, namely the quinoidic radical cation (Q_2), dication (Q_1) and symmetric C=C ring stretch (ν_2) [20, 21, 31]. The change in ratio of the above peaks ($I_{Q1}/I_{\nu 2}$, $I_{Q2}/I_{\nu 2}$ and I_{Q2}/I_{Q1}) is shown in Figure 40 i - iv. Since the ratio of the intensity of the Q_2 band to that of the Q_1 is less than 0.5, it is reasonable to assume that the oxidised species were mainly radical cations (polarons) and not dications (bipolaron) [31, 73, 74]. The ratios of bands $I_{Q1}/I_{\nu 2}$ and $I_{Q2}/I_{\nu 2}$ represent the probabilities of polaron and bipolaron states, respectively [22]. These ratios have been found to be up to 2.0 [75], whereas in the present study the ratios are around 3 – 4 as the laser was focussed closer to the substrate for the as-deposited thick PTTh.ClO_4 (Figure 40).

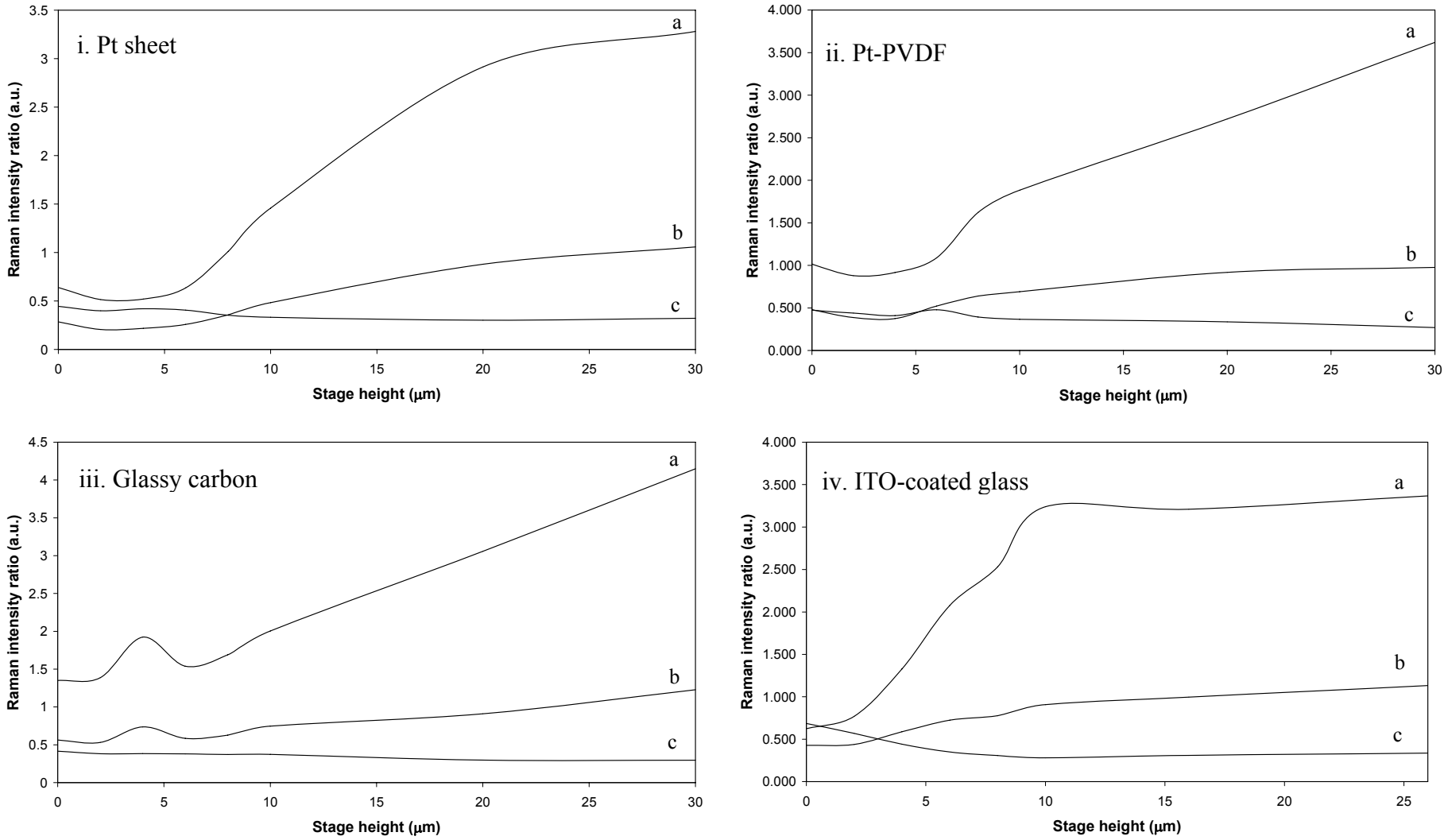

Figure 40. Raman intensity ratios of various bands with respect to distance z-stage moved shifting the laser focal point into as-deposited thick PTTh.ClO_4 on i) platinum sheet, ii) platinised PVDF membrane, iii) glassy carbon and iv) ITO-coated glass. Intensity ratio of bands shown: a) Q_1/ν_2, b) Q_2/ν_2 and c) Q_2/Q_1.

3.4.1.1.2 Thin films

An inspection of Raman band intensities *vs.* depth into polymer (Figure 41) reveals minimal change in the intensity of the diagnostic Q_1 (quinoidic radical cation) band, which decreased slightly upon probing the polymer depth. Also, the intensity of the Q_1 band was always greater than the ν_2 band, which indicated there was no reduced portion of the polymer and it was entirely in the oxidised state. High, stable doping levels were also present (Figure 42), with the intensity ratios $I_{Q1}/I_{\nu 2}$, $I_{Q2}/I_{\nu 2}$ and I_{Q2}/I_{Q1} remaining fairly constant throughout the thickness of the polymer. Intensity ratio $I_{Q1}/I_{\nu 2}$ values were approximately 3 – 4 across all substrates, in comparison to the values for as-deposited thick PTTh.ClO_4 films (0.5 – 1.5 at the surface (0 μm) to 3 – 4 into the depth of the polymer), suggesting a high and consistent level of doping for as-deposited thin PTTh.ClO_4.

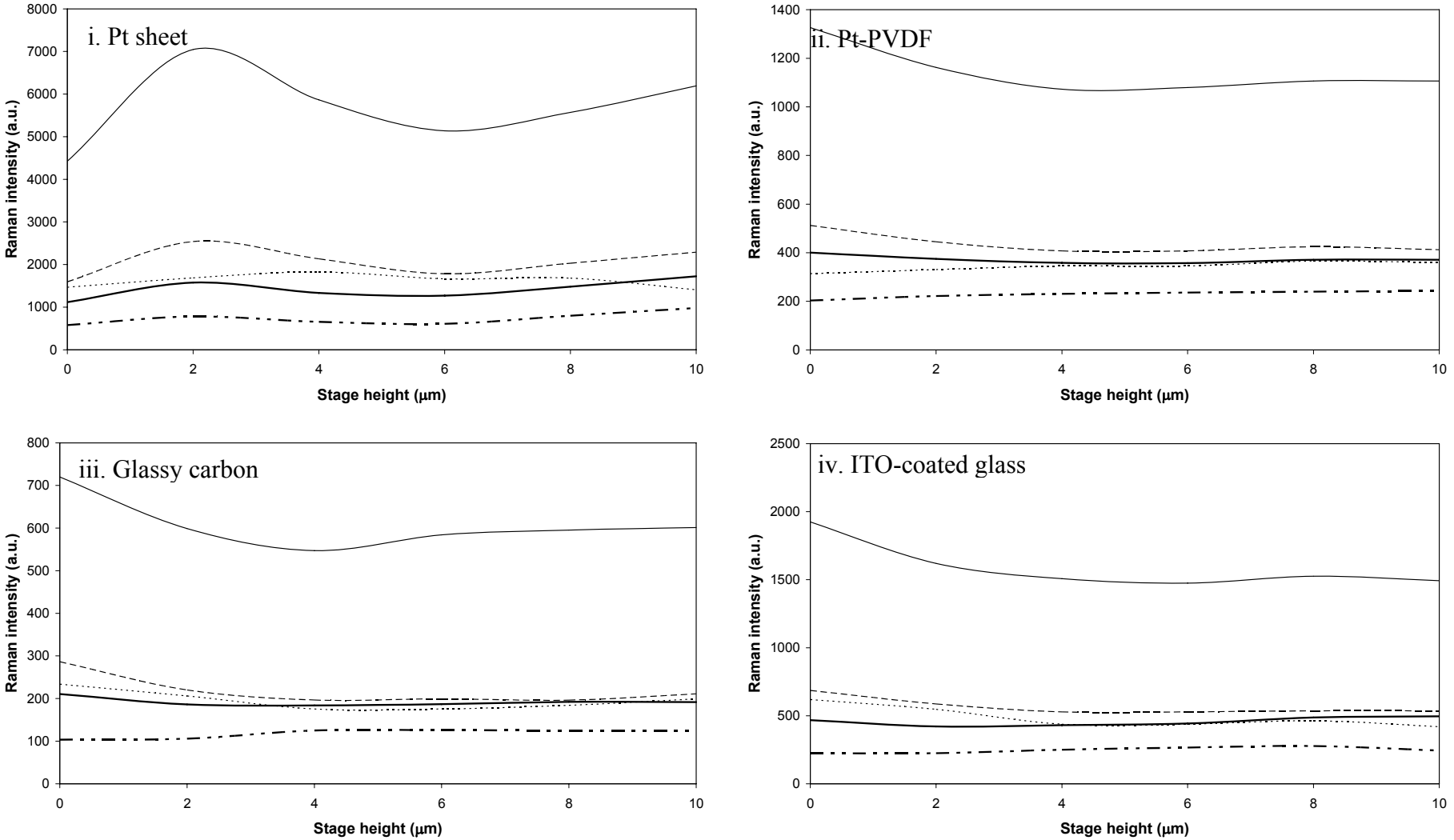

Figure 41. Raman intensity of various bands with respect to distance z-stage moved shifting the laser focal point into as-deposited thin (10 mC/cm^2 charge density) PTTh.ClO_4 on i) platinum sheet, ii) platinised PVDF membrane, iii) glassy carbon and iv) ITO-coated glass. Intensity of bands shown: —— Q_1: quinoidic radical cations; - - - - D_1: distorted kink; ——— D_3: distorted kink; ····· ν_2: symmetric C_α=C_β ring stretching and — · D_5: distorted kink.

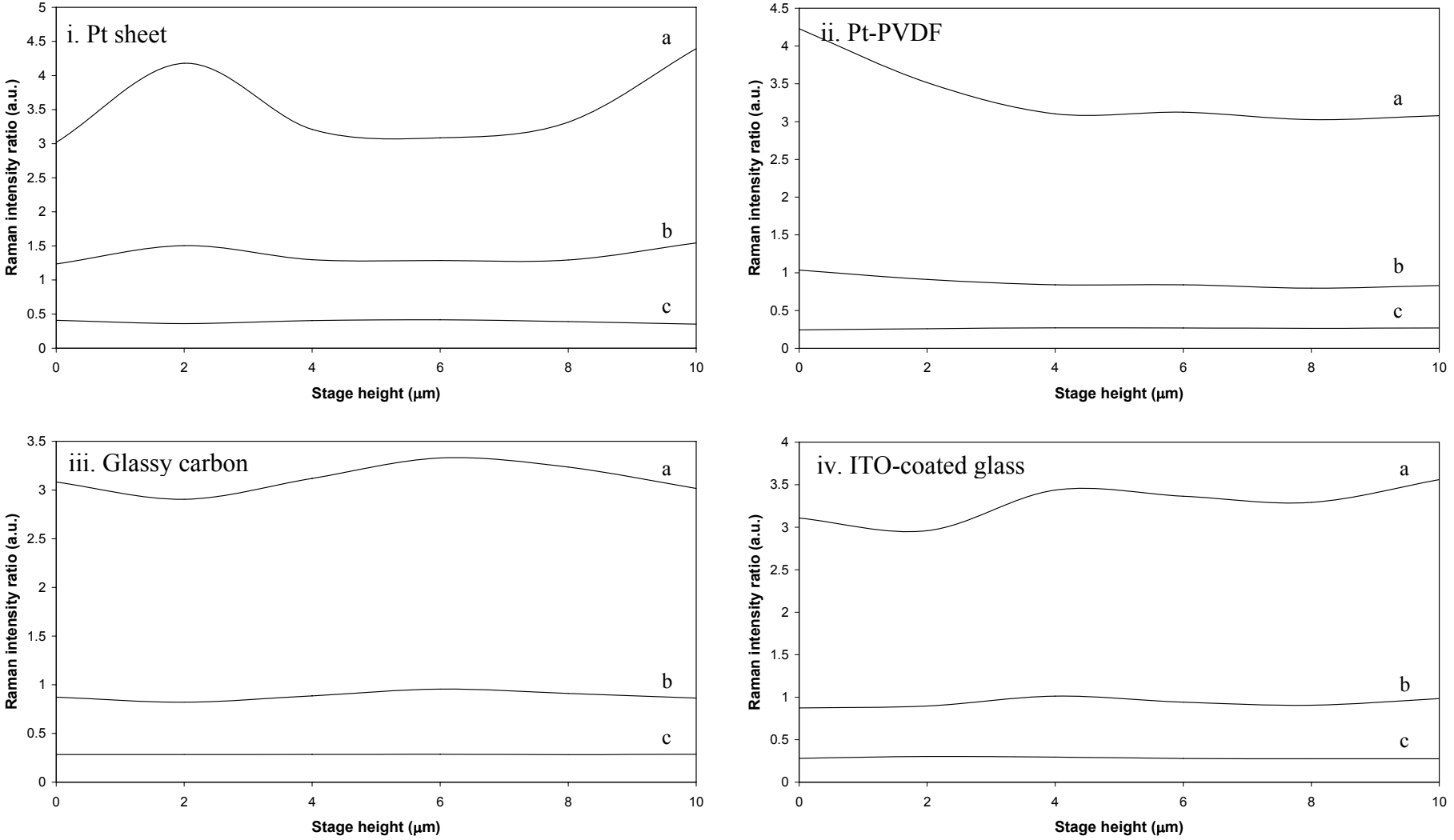

Figure 42. Raman intensity ratios of various bands with respect to distance z-stage moved shifting the laser focal point into as-deposited thin PTTh.ClO_4 on i) platinum sheet, ii) platinised PVDF membrane, iii) glassy carbon and iv) ITO-coated glass. Intensity ratio of bands a) Q_1/ν_2, b) Q_2/ν_2 and c) Q_2/Q_1, are an indicator of doping level.

3.4.1.1.3 Effect of film thickness on PTTh.ClO_4 reduction potential and extent of surface auto-reduction

The difference in surface auto-reduction observed for as-deposited PTTh.ClO_4 using depth profiling studies may be explained by consideration of the polymer reduction potential (E^0). Reduction of thick and thin as-deposited PTTh.ClO_4 films was found to occur at ca. 0.447 and 0.427 V (vs. Ag/Ag^+), respectively, by cyclic voltammetry (Figure 6). When coupled with the reduction reaction of water (which occurs at 0.429 V vs. Ag/Ag^+ at pH = 7), it becomes apparent that water may facilitate the reduction of the thicker polymer, while causing the oxidation of the thinner polymer. This situation is depicted schematically in a plot of the reduction potentials of water against thick and thin PTTh.ClO_4 (Figure 43). Table 16 lists standard reduction potentials for thick and thin PTTh.ClO_4 measured in this study and water.

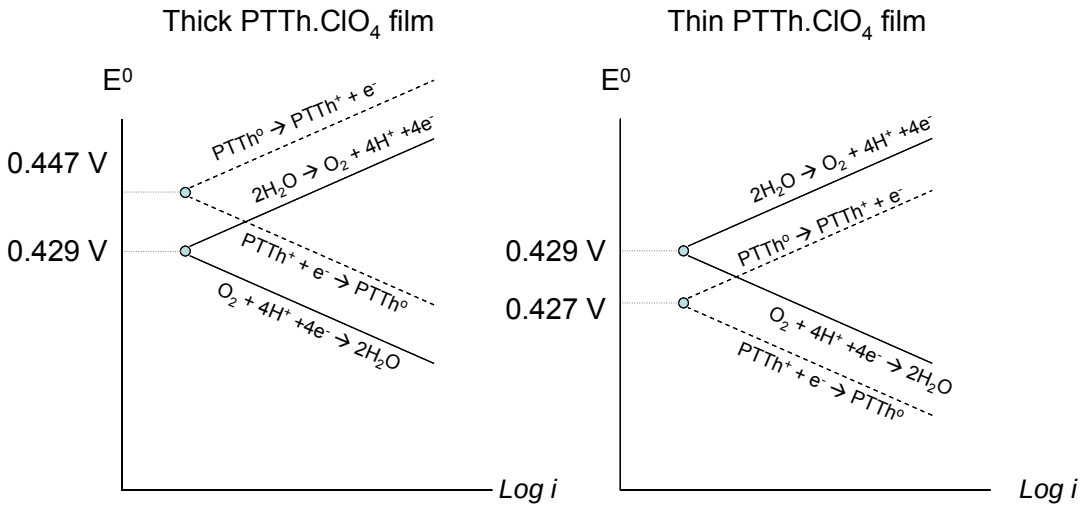

Figure 43. Schematic Evans diagram showing PTTh.ClO_4 oxidation and reduction reactions with O_2/H_2O redox processes. E^0 values for reduction reactions are *vs.* Ag/Ag^+. Not drawn to same scale.

Table 16. Electrode potentials of thick and thin PTTh.ClO_4 and water

Reduction reaction	**E^0 (V *vs.* Ag/Ag^+)**
Thick $PTTh^+ + e^- \rightarrow PTTh^0$	0.447
$O_2 + 4H^+ + 4e^- \rightarrow 2H_2O$	0.429
Thin $PTTh^+ + e^- \rightarrow PTTh^0$	0.427

The higher reduction potential of thick PTTh.ClO_4 (0.447 V *vs.* Ag/Ag^+) compared to water (0.429 V *vs.* Ag/Ag^+) means water may act as a reducing agent for PTTh.ClO_4, causing the surface auto-reduction observed for as-deposited films where the polymer is in contact with air and ambient H_2O. In the case of thin PTTh.ClO_4 (0.427 V) the electrode potential is very close to that of water, hence it is reasonable to expect that thin PTTh.ClO_4 is stable in air, resulting in consistently oxidised as-deposited thin PTTh.ClO_4 showing no evidence of auto-reduction [64].

3.4.1.2 Explanation of watermark effect

Observable colour changes as well as unusual contact angle measurements suggest chemical interactions occurred between water drops and PTTh.ClO_4 during water contact angle measurements. A second drop placed within the 'watermark' on a thick as-deposited PTTh.ClO_4 film was found to cause oxidation of the previously auto-reduced surface. The cause of this oxidation may be due to a galvanic coupling between underlying oxidised layers and the reduced surface of PTTh.ClO_4, causing oxidation of the polymer under the water drop. The water was thought to act as an electrolyte, facilitating the movement of dopant anions and allowing the galvanic coupling reaction to proceed. The level of doping underneath the water drop was not as high as for underlying layers of thick as-deposited PTTh.ClO_4, based on a comparison of the intensities of the 1046:1161 cm^{-1} peaks. The peak intensities were approximately 1:1 for the film underneath the water drop (curve (a) in Figure 34); while highly doped PTTh.ClO_4 had a 1046:1161 cm^{-1} peak intensity ratio of ca. 1:2 (refer to 30 μm stage height trace in Figure 30).

A different mechanism was believed to be responsible for the effects observed on as-deposited thin PTTh.ClO_4. Raman depth profiling revealed the bulk of the polymer to

be oxidised (Figure 30 to Figure 33) showing that atmospheric water could not reduce the polymer. Water drops were again observed to increase in contact angle when placed in the watermark of a preceding drop, while Raman spectroscopy indicated the area under the water drop was partially oxidised/partially reduced (curve (a) in Figure 35). Polymer colour change under the water drop from dark blue-black to orange supported a somewhat partial reduction of the film by the water drop. These phenomena may be explained by the similarity of the polymer's reduction potential with that of H_2O/O_2. The precise E^0 values for the reversible reactions

$$PTTh^+ + e^- \rightleftharpoons PTTh^0$$

$$O_2 + 4H^+ + 4e^- \rightleftharpoons 2H_2O$$

depend on the activities of the species involved. The E^0 value for the O_2/H_2O reaction will be different when liquid water is present compared with humid air. Similarly, the E^0 values of the PTTh will be sensitive to the molecular structure. Any slight variations in E^0 values may produce opposite effects such that the polymer may either be oxidised or reduced by the presence of O_2 and H_2O.

An inspection of the cyclic voltammograms for determining the E^0 values of thick and thin PTTh.ClO_4 (Figure 6) revealed a splitting of the reduction peak into two shoulders, indicating the presence of materials with slightly different properties spanning a range of reduction potentials. The deposition of conducting polymers has been recognised to occur in two steps: a thin, well-ordered first layer initially polymerises at the surface of the electrodes, followed by the deposition of less ordered polymer layers as the distance from the electrode is increased [44, 45, 76]. The morphological differences inherent to the structurally different layers may lead to the deposition of polymers with slightly different reduction potentials, manifested as the peak splitting observed. Hence it is

plausible that the slightly different structured PTTh.ClO_4 with similar E^0 values, in addition to the reduction potential of water being extremely similar to that of both thick and thin PTTh.ClO_4, may enable atmospheric water to reduce as-deposited thick PTTh.ClO_4 and water drops to reduce thin polymer. This is shown diagrammatically in Figure 44 and Figure 45.

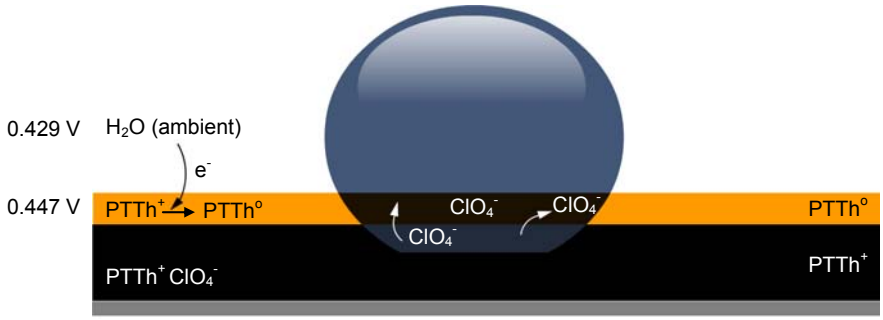

Figure 44. Schematic for the interaction of water with as-deposited thick PTTh.ClO_4. Atmospheric water reduces the surface of oxidised PTTh.ClO_4. The water drop facilitates the oxidation of $PTTh^0$ by providing a medium for the movement of dopant anions. Electrode potentials are *vs*. Ag/Ag^+.

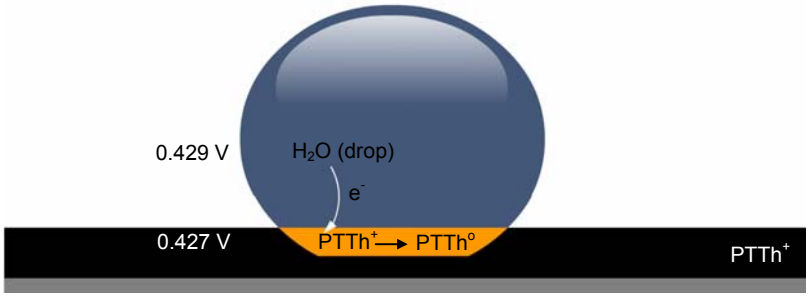

Figure 45. Schematic for the interaction of water with as-deposited thin PTTh.ClO_4. The film is stabilised in the oxidised state by the similar E^0 values of thin PTTh and water. The water drop partially reduces $PTTh^+$ due to slight variations in thin PTTh E^0 value. Electrode potentials are *vs*. Ag/Ag^+.

Raman studies through water drops on electrochemically reduced PTTh.ClO_4 revealed a different interaction than as-deposited films. Both thin and thick electrochemically reduced PTTh.ClO_4 films were found to remain in the reduced state when studied through a water drop on the film's surface. Since these films were in the reduced state through the entire film thickness, there was no opportunity to generate a galvanic cell

by ingress of water. This observation supports the argument that oxidation of the as-deposited thick PTTh.ClO_4 was caused by galvanic coupling and the motion of dopant ions from underlying layers.

Previous studies have found the nature of the working electrode to affect the degree of oxidation of polythiophene [20]. Films of polythiophene on platinum were found to be more oxidised than those on oxidisable metals such as Zn, Al and Fe, whose low redox potentials (lower than that of the polythiophene coating) meant the polymers tended towards the reduced state. The present study is the first, to the authors' knowledge, where confocal Raman spectroscopy was used to probe the change in oxidation state throughout the depth of polythiophene films. Others have used confocal Raman spectrometers [22] but did not probe the difference in doping level throughout the depth of the polymer. A recent study on P3MTh nanotubules [75] used confocal Raman spectroscopy to investigate the variation in doping level at different positions along the nanotubules, though a scan through the depth of the polymer was not carried out.

3.4.2 Effect of chemical interactions on contact angle and surface energy values

3.4.2.1 Spontaneous change in contact angle of water on as-deposited PTTh.ClO_4

The interaction between water and polyterthiophene discussed in the previous section may be used to explain the spreading of water drops on as-deposited PTTh.ClO_4 films. The spreading is believed to be due to the molecular interactions that arise upon contact of the water with oxidised polymer. As noted previously, UV-Vis studies have shown the as-deposited polymer is predominantly oxidised and that the surface reduced layer is confined to the film-air interface. As such, the water drop placed on the as-deposited film during contact angle measurement is expected to soak through the surface reduced layer and contact oxidised polymer. The presence of a delocalised positive charge on

the oxidised polymer backbone enables it to behave as a Lewis acid, thereby increasing its polar interactions with water. The perchlorate dopant ion is also able to interact with the water drop through hydrogen bonding and ionic interactions. The mobility of the polymer chains at the polymer-water interface allows rearrangement upon contact with water, increasing the hydrogen bonding between the oxidised polymer and dopant with water. These interactions result in a spreading of the water upon contact with the films, as the polymer undergoes reorganisation to minimise the energy between itself and the water [77], resulting in a higher standard deviation for as-deposited films compared to reduced films. Conversely, water drops were generally not observed to spread on electrochemically reduced PTTh.ClO_4, a fact that may be attributed, not only to the absence of positive charges on the polymer backbone and dopant anions, but also to the predominantly hydrophobic interactions that exist between long hydrocarbon chains. These hydrophobic interactions act to minimise the energy of the hydrocarbon groups by excluding water. Hence it may be seen that the difference in behaviour of water drops on oxidised and reduced PTTh.ClO_4 are a result of the different interactions the polymer undergoes.

3.4.2.2 Watermark effect

The watermark effect may be explained by the chemical interaction upon contact of the water drop with the film. The first water drop spread due to penetration of the liquid through the thin surface-reduced layer providing contact with underlying oxidised layers with inherently higher wettability (Table 8). The water drop then reduced the deeper layers, in a similar fashion to the reduction of the as-deposited thick PTTh.ClO_4 by atmospheric water presented in Figure 43. This caused the subsequent drop placed in the same area to have a high contact angle, analogous to that of reduced thick PTTh.ClO_4 (Figure 46). This phenomenon may be explained by a consideration of the

thermodynamics of the interactions of the film with the first and second water drops. In addition to the surface tension of the components (i.e. γ_{sv}, γ_{lv} and γ_{sl}), the contact angle of the first drop with dry as-deposited PTTh.ClO_4 is determined by its reaction with the polymer, and as such involves a thermodynamic energy term for the reaction, $\Delta G_{reaction}$. The contact angle of the second drop is only affected by γ_{sv}, γ_{lv} and γ_{sl}, since there is no reaction between the reduced PTTh.ClO_4 and the water drop.

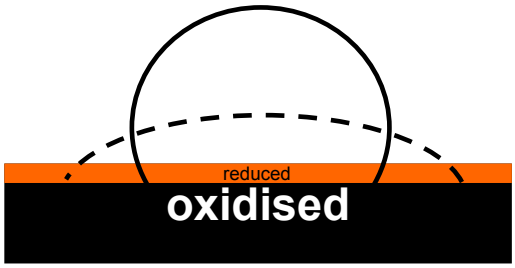

Figure 46. Schematic of the watermark effect on as-deposited thick PTTh.ClO_4. The dashed line represents the interaction of a first drop with the film, soaking through a thin surface reduced layer. The second drop placed in the watermark of the first drop has a higher contact angle due to the film now being reduced.

3.4.2.3 Analysis of valid surface energy results

The determination of surface energy using the Lifshitz-van der Waals-Acid-Base theory (van Oss-Good-Chaudhury method) assumes an atomically flat, non-reactive surface. In addition to this, the surface tension of the liquid (γ_l) must be greater than that of the solid (γ_s), otherwise spontaneous spreading of the liquid will occur on polar surfaces [78, 79]. Diiodomethane has found extensive use as an apolar liquid for surface energy analyses due to its particularly high surface tension compared to other apolar liquids such as hexadecane (γ_l = 27.1 mJ/m^2) or α-bromonaphthalene (γ_l = 44.4 mJ/m^2). However, in the present study the diiodomethane was found to spread on most PTTh.ClO_4 films. In such cases, the data cannot be reasonably used to determine surface energy components, and indeed the instability of negative numbers in

calculations has been highlighted as a deficiency of the van Oss-Good-Chaudhury treatment [80]. In a similar study on polypyrrole doped with chloride (PPy.Cl), diiodomethane and α-bromonaphthalene were observed to spontaneously spread on the polymer surface, thus the surface energy components were determined using the contact angles of the polar liquids water, formamide and glycerol solved by three simultaneous equations [12]. This approach was considered in the present study to determine the relevant surface energy components; however, as has previously been discussed, alternate commonly used polar surface energy test liquids were observed to instantly reduce as-deposited polymer. Herein lies one of the complications uncovered while trying to determine the surface energy of conducting polymer films. The inherent reactivity and dynamic nature of conducting polymers is beneficial in many applications, and indeed is one reason they have found such widespread usage since their discovery. However their interaction with probe liquids, by its very nature, influences the observed contact angle made with the conducting polymer. There are inherent problems using water to determine a conducting polymer's wettability, as water undoubtedly interacts with the polymer during the contact angle determination. Reactive wetting, whereby a liquid is deliberately chosen to interact with the material in question, has been studied and indeed explored as a means for moving droplets in microfluidic devices [81-83]. However, the analysis of reactive wetting was outside the scope of this study. Hence, obtaining quantitative information from the surface energy data in the present study was not always possible due to the interaction of the test liquids with the polyterthiophene during the contact angle measurement. This aspect of conducting polymers has rarely been discussed in the literature; therefore these measurements point to the factors one must be aware of when attempting to measure the surface energy of conducting polymers.

3.4.3 Effect of PTTh composition and morphology on contact angle and surface energy

3.4.3.1 Surface energy of polyterthiophenes with valid contact angle data

A comparison of surface energy components may be carried out for polymers and uncoated substrates with valid contact angle data (Table 14). The extreme wettability by water of uncoated Pt sheet was consistent with its high γ_s value (62 mJ/m^2). The high Lewis base (γ^-) component for both uncoated Pt sheet and glassy carbon (48 and 23 mJ/m^2) was considerably higher than for PTTh-coated substrates (0 – 16 mJ/m^2), as a result of the greater electron donating capacity of the delocalised electrons of Pt sheet and sp^2 hybridised electrons of glassy carbon.

PTTh.ClO_4 films with valid surface energy data all had similar γ_s values (50 – 53 mJ/m^2) and were dominated by non-polar interactions (γ^{LW}; ca. 50 mJ/m^2), with only a minor contribution from acid-base interactions (γ^{AB}; 0 – 3 mJ/m^2). There was no particular correlation apparent between substrate, thickness or oxidation state and surface energy. A lack of meaningful data meant that a detailed comparison into the effect of these parameters on the surface energy of PTTh.ClO_4 was not possible.

PTTh-DDO.ClO_4 was the only polymer for which a complete set of valid contact angle data was obtained (i.e. both thin and thick as-deposited and reduced films). These data allowed some insight into the factors contributing to the surface energy of polyterthiophene. Consideration of thin PTTh-DDO.ClO_4, which had similarly low roughness data for as-deposited and reduced polymer (1.02 and 1.06, respectively; Table 5) meaning the effect of roughness was minimised, revealed the γ_s of the reduced polymer to be slightly lower than that of the as-deposited polymer (31 and 34 mJ/m^2, respectively). This result was consistent with the absence of a charged polymer

backbone and dopant molecule in the reduced film that would be expected to decrease its surface energy. However, reduced thick PTTh-DDO.ClO_4 was found to have a higher γ_s (42 mJ/m^2) than as-deposited thick PTTh-DDO.ClO_4 (36 mJ/m^2). A comparison of the surface energy with water contact angle data revealed, interestingly, reduced thick PTTh-DDO.ClO_4 was the most hydrophobic film (150 °), yet it had the highest apparent surface energy out of the PTTh-DDO.ClO_4 films. Similarly, thin reduced PTTh-DDO.ClO_4 was the least hydrophobic (112 °), yet it had the lowest γ_s (31 mJ/m^2). Polymer roughness is believed to be the source of this incongruity. Thicker films were significantly rougher (3.93 and 2.16 for as-deposited and reduced, respectively) than thin films (1.02 and 1.06) (Figure 16, Figure 17 and Table 5). Interestingly, reduced thick PTTh.ClO_4 films were significantly less rough (2.16) than as-deposited thick films (3.93). If surface energy was based on roughness alone, as-deposited thick PTTh-DDO.ClO_4 would be expected to have the highest γ_s value. Similarly, if surface energy were based on hydrophobicity alone, reduced thick PTTh-DDO.ClO_4 would be expected to have the lowest surface energy (highest water contact angle (150 °), lowest water contact angle hysteresis (3 °) and lowest CH_2I_2 contact angle (50 °)); instead it had the highest surface energy for PTTh-DDO.ClO_4. These observations point to the complex interplay between roughness, dynamic chemical composition and surface energy and suggest the interaction between water and the polymer is strongly dependent on these factors.

Determination of the effect of PTTh functionalisation on surface energy was one of the objectives of this study. A comparison of γ_s for PTTh.ClO_4 and PTTh-DDO.ClO_4 reveals the incorporation of the hydrophobic didecyloxy chains onto the terthiophene monomer backbone dramatically reduced the γ_s (31 – 42 mJ/m^2) in comparison to PTTh.ClO_4 (50 – 53 mJ/m^2). As was the case for PTTh.ClO_4 films, the interactions on

PTTh-DDO.ClO_4 were predominantly non-polar; however the thicker films exhibited a stronger Lewis acid (γ^+) component (10 and 13 mJ/m^2 for as-deposited and reduced films, respectively) than thin films (1 and 6 mJ/m^2, for as-deposited and reduced films, respectively). This result was consistent with the thick films possessing a highly microstructured morphology (SEM images; Figure 17) primarily composed of hydrophobic alkyl chains, which are slightly electron withdrawing in nature. Hence, functionalisation of polyterthiophene with hydrophobic alkyl chains resulted in lower surface energy polymers, strongly influenced by nanoscale roughness.

All PTTh.ClO_4 films were found to have surface energies considerably higher than those reported in literature for chemically polymerized P3OT (28-34 mJ/m^2) [6, 7] and for P3HT (27 mJ/m^2 in neutral state) [4], though they were similar to that of PEDOT (47 mJ/m^2 in oxidised state). The thin reduced PTTh-DDO.ClO_4 film (31 mJ/m^2) had a surface energy similar to the aforementioned poly-3-alkylthiophenes in the literature, which is not surprising given the nature of long alkyl chains present. These authors did not measure the surface energy of polymers in both their oxidised and reduced states; hence this comparison may not be drawn to the present study. Predominantly non-polar interactions were observed for the hydrophobic neutral P3HT [4], as was observed in this study.

3.4.3.2 Effect of oxidation state on water contact angles

An investigation into the effect of polyterthiophene oxidation state on its wettability by water was one of the primary goals of this chapter. The water wettability will be discussed for both thick and thin PTTh.ClO_4 films, as well as the functionalised PTTh-DDO.ClO_4.

3.4.3.2.1 Thick PTTh.ClO_4 films

The dramatic change of wettability for thick PTTh.ClO_4 films upon changing the oxidation state (39 – 75 °; Table 8) may be explained at least partially by the difference in polarity of oxidised and reduced polyterthiophene. An increase in polarity occurs upon oxidation of the polymer due to the formation of polarons on the polymer backbone, coupled with the incorporation of charged dopant anions, and causes the wettability of the polymer to increase. Conversely, reduction of the polymer to its neutral state was accompanied with a decrease in polarity, reflected by the inherent hydrophobicity of the fully conjugated polymer backbone. This change in wettability is notably higher than that observed for a series of P3AT's [2] (Table 1), which exhibited differences of 9 – 17 ° when the films were maintained in the oxidised and the reduced state using an electrochemical switching device, depending on the length of the alkyl chain.

The higher contact angle hysteresis typical for as-deposited films (33 – 45 °) reveals a greater adhesion of water to the polymer than for reduced films (8 – 15 °), consistent with greater charge mobility of the doped polymer. The advancing angles of as-deposited films (94 – 113 °) were significantly higher than the equilibrium 'recently advanced' angle (54 – 68 °), indicating the present of hydrophobic portions on the polymer backbone, which was to be expected in light of the polymer's structure. In comparison, the advancing angle of the reduced films (130 – 140 °) were closer to that of the equilibrium contact angle (100 – 129 °), consistent with the films already being in a highly hydrophobic state. The lower receding angle of as-deposited films (57 – 68 °) than the reduced films (115 – 132 °) indicated better adhesion of water to the as-deposited polymer, which was expected due to charge mobility. The exception for all of these cases was PTTh.ClO_4 on Pt-PVDF, for which the data was not included in the

above comparisons. The hysteresis of both as-deposited and reduced films was ca. 26 °, with advancing (125 ° and 112 °, respectively) and receding contact angles (100 ° and 86 °, respectively) similar for both films. This result indicated the porous microstructure of the PVDF membrane was the dominant factor in determining the interaction of water with the polymer, rather than its oxidation state. As-deposited films had consistently higher roughness values than their reduced counterparts, across all substrates and thicknesses (Table 4). This roughness is also believed to be responsible for the higher hysteresis observed for as-deposited films, consistent with the widely accepted idea that roughness increases contact angle hysteresis [84, 85].

It should be noted that the standard deviation for contact angle measurements on some films was high (up to 25 °). This was particularly prevalent for thick as-deposited PTTh.ClO_4 in comparison to their analogous reduced counterparts (Table 8). Measurements were taken over many months in a laboratory which was not humidity or temperature controlled; however the use of these conducting polymers in any devices would also most likely be in areas of varying ambient humidity and temperature. Wettability measurements depend on ambient conditions, with humidity having a strong effect on the resulting contact angles measured [86]. Hence, the effect of humidity must be taken into consideration when characterising the wettability of conducting polymers. Variation in wettability of as-deposited films may also have been due to a slightly different degree of doping due to galvanostatic polymerisation [1]. Teasdale ***et al.*** observed a decrease in the standard deviation of wettability measurements on polypyrrole films upon potentiostatic deposition, as compared to constant current deposition [87]. This was noted in the preliminary stages of the study, however galvanostatic deposition was preferred due to the ability to standardise the amount of polymer deposited. It is most likely that the cause of the large standard deviation for as-

deposited PTTh.ClO_4 was due to reduction of the polymer to differing extents by ambient water [64]. Measurements made in warmer humid summer months were more likely to be subject to greater auto-reduction of the films, resulting in higher water contact angles. Increased auto-reduction of polyterthiophene due to higher humidity is a consideration when characterising its wettability.

3.4.3.2.2 Thin PTTh.ClO_4 films

Thin as-deposited PTTh.ClO_4 films (71 – 96 °) were more wettable than reduced films (103 – 114 °), for the reasons detailed above for thick PTTh.ClO_4 films. Advancing and receding contact angle data were also similar to thick PTTh.ClO_4, in that as-deposited films generally had higher hystereses than their reduced counterparts, though the trends were less clear for thin films. Again, PTTh.ClO_4 on Pt-PVDF exhibited similar hystereses for both the as-deposited and reduced films (30 °), pointing to the role of the film microstructure in determining dynamic wetting properties.

3.4.3.2.3 PTTh-DDO.ClO_4

The wettability of PTTh-DDO.ClO_4 was very similar in as-deposited and reduced states for both thicknesses (145 ° and 150 ° for thick films, respectively, and 112 ° and 125 ° for thin films, respectively). This result was interesting, as UV-Vis studies indicated significant difference in their doping levels (Figure 10). Raman spectroscopy also revealed vastly different spectra for as-deposited and reduced films of both thicknesses, indicating they were in significantly different oxidation states. This observation suggests the morphology and roughness of the films, in addition to the presence of the hydrophobic alkyl chains, had a more significant impact on wettability than the oxidation state had. Contact hystereses for as-deposited and reduced films were quite low (3 – 15 °), suggesting water did not adhere well to the polymer in either oxidation

state as a result of the presence of the hydrophobic alkyl chains. The contact angle hysteresis was particularly low for reduced thick PTTh.ClO_4 (3 °). This low hysteresis coupled with the high water contact angle of the film (150 °) allows the material to be classified as superhydrophobic. Previous reports of superhydrophobic conducting polymers have been based on fluorination of the polymer backbone [8] or incorporation of a fluorinated dopant [88]. This material is the first superhydrophobic conducting polymer, to the author's knowledge, prepared without incorporation of a fluorinated moiety, rendering it useful for applications where fluorinated compounds are not appropriate, e.g. biofouling prevention in environmental applications.

3.4.3.3 Effect of polymer functionalisation on water contact angle

One of the main aims of this chapter was to determine the effect of functionalisation with hydrophobic groups on the wetting properties of polyterthiophene. A comparison of the wetting properties of PTTh-DDO.ClO_4 with unfunctionalised PTTh.ClO_4 clearly exemplifies this effect. Significantly, a dramatic increase in hydrophobicity of the as-deposited polymer was observed in comparison to unsubstituted PTTh.ClO_4 films, with water contact angles of 145 ° (compared to 54 ° for thick PTTh.ClO_4 films) and 125 ° (compared to 72 ° for thin PTTh.ClO_4 films) measured for thick and thin PTTh-DDO.ClO_4, respectively. This difference equated to a 91° increase in the water contact angle for thick films, while an increase of 53 ° was evident for thin films. Hence, the presence of the hydrophobic alkyl chains significantly decreased the wettability of polyterthiophene in the as-deposited state for both film thicknesses, as may be predicted by a comparison of the monomer's molecular structures (Figure 1 and Figure 2). Reduced thick PTTh-DDO.ClO_4 (150 °) films only exhibited a ca. 21 ° increase in contact angle as compared to non-functionalised PTTh.ClO_4 (129 °), as a result of the inherent hydrophobicity of the terthiophene backbone. Interestingly, reduced thin

PTTh-DDO.ClO_4 films (112 °) were of a similar wettability to the unsubstituted analogue on Pt sheet (107 °). The highly roughened surface of thick PTTh-DDO.ClO_4, coupled with the inherently hydrophobic alkyl chains, was believed to be the primary factor in the significant decrease in polymer wettability.

Hence the substitution of the polyterthiophene backbone with hydrophobic alkyl chains led to dramatically different wetting properties from the parent unsubstituted PTTh.ClO_4 upon oxidation and reduction. The many variables involved when preparing conducting polymers results in a complex interplay between different factors which all contribute to their wetting properties.

3.4.3.4 Effect of film thickness on water contact angle

3.4.3.4.1 PTTh.ClO_4

A notable difference existed in the wettability of thick and thin PTTh.ClO_4 films. A comparison of the water contact angles of thick and thin PTTh.ClO_4 for as-deposited and reduced films is shown in Table 17. Roughness data determined by optical profilometry (initially presented in Table 4) is shown in brackets for each polymer for ease of comparison.

Table 17. Comparison of water contact angles for thick and thin PTTh.ClO_4 (°), for as-deposited and reduced films. Polymer roughness (*r*) is shown in brackets.

	As-deposited		Reduced	
Substrate	**Thick**	**Thin**	**Thick**	**Thin**
Pt	54 (2.58)	71 (1.24)	129 (1.92)	107 (1.08)
Pt-PVDF	63 (13.56)	91 (3.12)	102 (4.87)	103 (2.03)
GC	65 (2.96)	96 (1.21)	126 (2.16)	114 (1.16)
ITO	68 (2.53)	75 (1.11)	129 (1.68)	106 (1.00)

It can immediately be seen that reduction in polymer thickness caused a dramatic decrease in the variation of polymer wettability between the as-deposited and reduced states. The as-deposited films became less hydrophilic (71 – 96 ° compared to 54 – 68 ° for thicker films) and the reduced films less hydrophobic (103 – 114 ° compared to 102 – 129 ° for thicker films). The difference in wettability between as-deposited and reduced films on the same substrate also decreased, from 39 – 75 ° (Table 8) for thick films to 12 – 36 ° for thin films (Table 10). Thus, the reduction in polymer thickness resulted in a significant decrease in the difference in water contact angle between as-deposited and reduced films upon going to thinner polymer across all substrates.

A direct correlation between film thickness and roughness was evident. Thick films were consistently of higher roughness than thin films for both as-deposited and reduced polymer (Table 17). Roughness is known to increase with polythiophene thickness [18], with the results in the present study supporting this finding. The presence of surface roughness may amplify the wettability in the direction of wetting, so for materials with contact angles less than 90 °, the presence of surface roughness makes films more wettable, whereas for hydrophobic films roughness can act to amplify the hydrophobicity [89]. This is consistent with the observations for PTTh.ClO_4 in the present study and suggests the results obtained for thin PTTh.ClO_4 are closer to the actual wettability of this polymer.

Water drops were only in contact with oxidised polymer during goniometry of as-deposited thin films, as opposed to the reduced surface layer and underlying oxidised layers present in thicker films. The use of thinner films resulted in a lower degree of wettability (i.e. thin PTTh.ClO_4 polymers exhibited 30 – 40 ° less difference between as-deposited and reduced films than thick films), therefore the layers of polymer

responsible for the greater difference in wettability between as-deposited and reduced states were removed. Thus, this decrease in wettability change is believed not to be due to the chemistry of the layers (as the thinner, more oxidised films should have an inherently lower contact angle based on the nature of the charged backbone and dopant incorporation.), but the role of porosity and roughness. Thin films were found to be more compact than thicker PTTh.ClO_4 films, which were more porous in nature (SEM images; Figure 12). Porosity is known to affect contact angle by means of the liquid soaking into or resting upon the material, depending on the geometry of the pores. The contact angle of porous materials may be determined by the Washburn equation (described in Chapter 1), and indeed the wettability of many porous materials have been characterised using this approach [90, 91]. Although characterisation using this technique was outside the scope of this project, the effect of polymer porosity on the resulting wettability must be considered.

3.4.3.4.2 PTTh-DDO.ClO_4

The effect of film thickness and hence roughness on polymer wettability was examined for PTTh-DDO.ClO_4. The water contact angles of thick and thin PTTh-DDO.ClO_4 for as-deposited and reduced films are shown in Table 18. Roughness data determined by optical profilometry (initially presented in Table 5) is shown in brackets for each polymer for ease of comparison.

Table 18. Water contact angles for thick and thin PTTh-DDO.ClO_4 (°) deposited on Pt sheet for as-deposited and reduced films. Polymer roughness (*r*) is shown in brackets.

	As-deposited		**Reduced**	
Polymer	**Thick**	**Thin**	**Thick**	**Thin**
PTTh-DDO	145 (3.93)	125 (1.02)	150 (2.16)	112 (1.06)

Roughness and nanostructure played an important role in determining the wettability of thick and thin PTTh-DDO.ClO_4 films. As was the case for PTTh.ClO_4, both as-deposited and reduced thick PTTh-DDO.ClO_4 films were consistently rougher than thin films. The superhydrophobicity of the reduced thick film was due to the nanostructured surface of the polymer and was therefore related to film thickness, in conjunction with the ordering of the hydrophobic alkyl chains. It may be assumed that the superhydrophobicity was entirely due to the chemical composition and morphology of the polymer, as the smooth Pt sheet did not impart microstructured morphology to the polymer. Thin PTTh-DDO.ClO_4 film better represent the actual wettability of the polymer, as the contribution of roughness is removed.

3.4.3.5 Effect of substrate on water contact angle of PTTh.ClO_4

An investigation into the effect of substrate on the wettability of PTTh.ClO_4 was one of the objectives of this chapter, and as such a range of electrode materials with different properties were chosen. Pt sheet and Pt-PVDF were interesting to compare, given their similar work functions and chemical properties but vastly different morphologies, allowing insight into the impact of substrate roughness on resulting wettability. A comparison of the change in PTTh.ClO_4 wettability between as-deposited and reduced films yielded interesting results. The most significant change in wettability between thick as-deposited and reduced films was observed on Pt sheet (difference of 75 °), which possessed smooth morphology (SEM images, column (a); Figure 12) and low roughness values (2.58 and 1.92 for as-deposited and reduced thick PTTh.ClO_4, respectively). The smallest change in wettability between as-deposited and reduced thick films was observed on Pt-PVDF (change of ca. 40 °), which possessed highly nanostructured morphology (SEM images, column (b); Figure 12) and the highest roughness values (13.56 and 4.87 for as-deposited and reduced thick PTTh.ClO_4,

respectively). Analogous trends were observed for thin PTTh.ClO_4. The largest difference in contact angle between as-deposited and reduced thin films was on Pt sheet (36 °), while the smallest change in wettability was on Pt-PVDF (12 °). Roughness was observed to enhance wettability (in the direction of wetting) in the case of thick films compared to thin films of the same oxidation state (Section 3.4.3.4); however when considering the effect of substrate, an increase in roughness diminished the change in wettability between as-deposited and reduced films. The roughness of the PTTh.ClO_4 on Pt-PVDF membrane was quite different to that formed by PTTh.ClO_4 films on flat Pt sheet. Hence, the wettability of the Pt-PVDF coated membranes is likely to be dominated by the porous nature of the membrane.

PTTh.ClO_4 on GC and ITO-coated glass had similar differences in wettability between the as-deposited and reduced state (ca. 62 ° for thick films; 18 ° (GC) and 32 ° (ITO) for thin films), in line with their similar roughness values to Pt sheet. Reduced thick PTTh.ClO_4 films on Pt-PVDF were the roughest of the reduced films (4.87) but were also the least hydrophobic (102 °), indicating the roughness contributed to decreasing the hydrophobicity of the polymer, which may be explained by the capillary effect [89]. In contrast, reduced thick PTTh.ClO_4 with the lowest roughness value (i.e 1.68 for ITO-coated glass) actually possessed the highest contact angle. Hence the inherent roughness of the underlying substrate influenced the resulting wetting properties of PTTh.ClO_4.

3.4.3.6 *In-situ* electrochemical contact angle measurements of captive water drop on PTTh.ClO_4

The determination of the change in contact angle of a captive water drop resting on the underside of PTTh.ClO_4 on Pt sheet connected to a three-electrode cell was pursued due

to the large change in wettability of PTTh.ClO_4 films observed in ambient laboratory conditions. The lack of a change in water contact angle upon redox switching in dichloromethane electrolyte, despite successful oxidation and reduction of the film, was believed to be due to the different interfacial tensions that exist upon the introduction of another liquid as the surrounding phase. The difficulty in bringing water drops into contact with the polymer, compared to the ease with which they adhered to non-polymer coated Pt sheet, suggests the surface of the polymer was completely wet with dichloromethane and that the interfacial tension at the PTTh.ClO_4/DCM interface more favourable than that of water with PTTh.ClO_4.

The environment in which wettability measurements are made has been recognised to be a variable in the surface characterisation of conventional polymers [77]. Given the dynamic nature of conducting polymers, reorganisation of surface molecules upon immersion in a different liquid phase undoubtedly occurs. These observations enforce the comments made by Teasdale [87] that correlation between the structure and properties observed in one environment cannot be used to predict the behaviour in a different environment, as has been done for conventional polymers. There is precedent for determining the wetting properties of conducting polymers in air, as scientifically useful information regarding polymer composition and the various factors that effect wettability may be obtained. However, when considering a conducting polymer for use in a microfluidic device, characterisation of the surface in the environment in which it is to be used is more pertinent.

3.5 Conclusions

Several factors influencing the wettability and surface energy of polyterthiophene films, including polymer oxidation state, substrate, functionalisation of the polymer backbone and thickness, were investigated by contact angle goniometry (sessile and dynamic) of water drops and the surface energy test liquids glycerol and diiodomethane. A dramatic difference in the wettability of as-deposited and reduced thick PTTh.ClO_4 was evident across all substrates, with the increased wettability of as-deposited films due to charge on the polymer backbone. This effect was diminished upon investigation of thin films, due to the removal of roughened, porous layers responsible for the enhancement of polymer wettability. The wetting data of thin PTTh.ClO_4 on flat substrates (Pt sheet, GC and ITO-coated glass) were believed to be a more accurate representation of the wettability of PTTh.ClO_4. Surface energy measurements were affected by chemical interactions of the test liquids with the polymer. A lack of valid data meant a thorough comparison into the effect of various factors on surface energy could not be carried out. In general, PTTh.ClO_4 was dominated by non-polar Lifshitz-van der Waals interactions, with surface energy ranging from 50 – 53 mJ/m^2.

Functionalisation of the polyterthiophene backbone with hydrophobic alkyl chains was found to have a dramatic effect on the polymer's wettability and surface energy. Incorporation of the hydrophobic didecyloxy chains to the polymer backbone (PTTh-DDO.ClO_4) resulted in a dramatic decrease in polymer wettability in comparison to PTTh.ClO_4, particularly for as-deposited films. The roughness inherent to thicker films, in addition to decreased surface energy due to the hydrophobic alkyl chains, was believed to be responsible for their high water contact angles and low wetting hysteresis in comparison to PTTh.ClO_4 (31 – 42 mJ/m^2).

Polyterthiophene functionalised with a hydrophobic buckyball substituent (PTTh-C_{60}.ClO_4) was found to have poor electroactivity, with cyclic voltammograms of the polymer post-deposition not showing any defined redox peaks. In addition to this, as-deposited films exhibited UV-Vis spectra analogous to polymer which had been electrochemically reduced, suggesting the polymer had instantaneously de-doped in air. An investigation into the wetting properties of PTTh-C_{60}.ClO_4 was therefore not pursued.

Water was found to interact with PTTh.ClO_4 in a number of ways. The impact of film thickness on the auto-reduction of as-deposited PTTh.ClO_4 was probed using confocal Raman depth profiling. As-deposited thick PTTh.ClO_4 was found to undergo surface reduction with atmospheric water, leading to a thin layer of reduced polymer upon underlying oxidised layers. As-deposited thin PTTh.ClO_4 was maintained in the oxidised state from deposition due to its similar reduction potential as water. The slight variations in reduction potential for thick and thin PTTh.ClO_4 enabled different interactions of water drops, with water facilitating the oxidation of PTTh.ClO_4 by forming a galvanic cell with underlying oxidised layers for thick PTTh.ClO_4, while water drops partially reduced the area of as-deposited thin PTTh.ClO_4 film under the water drop.

The change in contact angle of captive water drops on the underside of PTTh.ClO_4-coated Pt sheet in a three-electrode cell configuration during *in-situ* electrochemical redox switching was pursued based on the significant change in polymer wettability when investigated in air. The lack of a change in water contact angle was believed to be due to a lack of contact between the water drop and the polymer, as a result of the more favourable interaction of the polymer with the dichloromethane electrolyte.

These findings point to the many factors which must be considered when determining the wettability of conducting polymers. Development of a microfluidic device employing conducting polymers would benefit from an initial study into the factors affecting polymer wettability *ex-situ* the electrochemical cell, to gain a deeper understanding of the polymer structure and various interactions it may undergo. Subsequent implementation of the polymer into a device where the wettability may be tested during *in-situ* electrochemical redox-switching should reveal the role of the external environment on the wetting properties of the polymer.

Some generalised suggestions are proposed for future investigation into the wetting properties of conducting polymers. Roughness-induced wettability enhancement may be avoided by investigating thin, flat polymers with roughness (r) values close to 1. Caution must be exercised when using any probe liquid to determine the wettability of a film, given the dynamic nature of conducting polymers. Surface energy measurements must be carried out with liquids which do not interact with the polymer surface, particularly for films where spontaneous spreading of the liquid is observed. The Lifshitz-van der Waals acid-base theory [12] may be used with three polar liquids if spontaneous spreading of the apolar liquid occurs, employing liquids which do not interact with the polymer (this was not possible with common polar test liquids in the present study).

Future work could include an investigation into the effect of incorporating molecules with differing hydrophobicities into PTTh.ClO_4 as dopants, to determine the effect on polymer wettability. Investigation of the change in work function of polymers through their depth may be carried out using a Kelvin probe, to further explore the effect of substrate on polymer oxidation state and the extent of auto-reduction.

3.6 References

1. Eales, R.M. and Hillman, A.R., *J. Mater. Sci.*, 1990. **25** p. 3806.
2. Robinson, L., Hentzell, A., Robinson, N., Isaksson, J., and Berggren, M., *Lab Chip*, 2006. **6** p. 1277.
3. Isaksson, J., Tengstedt, C., Fahlman, M., Robinson, N., and Berggren, M., *Advanced Materials*, 2004. **16** p. 316.
4. Wang, X., Ederth, T., and Inganas, O., *Langmuir*, 2006. **22** p. 9287.
5. Hernandez, R., Diaz, A.F., Waltman, R., and Bargon, J., *J. Phys. Chem.*, 1984. **88** p. 3333.
6. Fadda, E. and Clarisse, C., *Synth. Met.*, 1995. **72** p. 99.
7. Chehimi, M.M., Abel, M.-L., Perruchot, C., Delamar, M., Lascelles, S.F., and Armes, S.P., *Synth. Met.*, 1999. **104** p. 51.
8. Nicolas, M., Guittard, F., and Geribaldi, S., *Langmuir*, 2006. **22** p. 3081.
9. Zhang, Z.P., Qu, L.T., and Shi, G.Q., *J. Mater. Chem.*, 2003. **13** p. 2858.
10. Robinson, L., Isaksson, J., Robinson, N.D., and Berggren, M., *Surf. Sci.*, 2006. **600** p. L148.
11. Nicolas, M., Guittard, F., and Géribaldi, S., *Angewandte Chemie International Edition*, 2006. **45** p. 2251.
12. Azioune, A., Chehimi, M.M., Miksa, B., Basinska, T., and Slomkowski, S., *Langmuir*, 2002. **18** p. 1150.
13. Poussigue, G. and Benoit, C., *J. Phys.-Condes. Matter*, 1989. **1** p. 9547.
14. Poussigue, G., Benoit, C., Sauvajol, J.L., Lereporte, J.P., and Chorro, C., *J. Phys.-Condes. Matter*, 1991. **3** p. 8803.
15. Akimoto, M., Furukawa, Y., Takeuchi, H., Harada, I., Soma, Y., and Soma, M., *Synth. Met.*, 1986. **15** p. 353.
16. Furukawa, Y., Akimoto, M., and Harada, I., *Synth. Met.*, 1987. **18** p. 151.

17. Bukowska, J. and Jackowska, K., *Science*, 1990. **35** p. 143.

18. Bazzaoui, E.A., Marsault, J.P., Aeiyach, S., and Lacaze, P.C., *Synth. Met.*, 1994. **66** p. 217.

19. Bazzaoui, E.A., Levi, G., Aeiyach, S., Aubard, J., Marsault, J.P., and Lacaze, P.C., *J. Phys. Chem.*, 1995. **99** p. 6628.

20. Bazzaoui, E.A., Aubard, J., Elidrissi, A., Ramdani, A., and Levi, G., *J. Raman Spectrosc.*, 1998. **29** p. 799.

21. Bazzaoui, E.A., Aubard, J., Felidj, N., Laurent, G., and Levi, G., *J. Raman Spectrosc.*, 2005. **36** p. 817.

22. Chen, F., Shi, G., Fu, M., Qu, L., and Hong, X., *Synth. Met.*, 2003. **132** p. 125.

23. Fu, M.X., Shi, G.Q., Chen, F.G., and Hong, X.Y., *Phys. Chem. Chem. Phys.*, 2002. **4** p. 2685.

24. Chiu, W.W., Travas-Sejdic, J., Cooney, R.P., and Bowmaker, G.A., *J. Raman Spectrosc.*, 2006. **37** p. 1354.

25. Ehrendorfer, C. and Karpfen, A., *Vib. Spectrosc*, 1995. **8** p. 293.

26. Compagnini, G., De Bonis, A., Cataliotti, R.S., and Marletta, G., *Phys. Chem. Chem. Phys.*, 2000. **2** p. 5298.

27. Compagnini, G., De Bonis, A., and Cataliotti, R.S., *Mater. Sci. Eng., C*, 2001. **15** p. 37.

28. Alaverdyan, Y., Johansson, P., and Kall, M., *Phys. Chem. Chem. Phys.*, 2006. **8** p. 1445.

29. Clarke, T.M., Gordon, K.C., Chan, W.S., Phillips, D.L., Wagner, P., and Officer, D.L., *Chemphyschem*, 2006. **7** p. 1276.

30. Svedberg, F., Alaverdyan, Y., Johansson, P., and Kall, M., *J. Phys. Chem. B*, 2006. **110** p. 25671.

31. Shi, G., Xu, J., and Fu, M., *J. Phys. Chem. B*, 2002. **106** p. 288.

32. Holze, R., *Synth. Met.*, 1991. **40** p. 379.

33. Chen, J., Tsekouras, G., Officer, D.L., Wagner, P., Wang, C.Y., Too, C.O., and Wallace, G.G., *J. Electroanal. Chem.*, 2007. **599** p. 79.

34. Ballantyne, A.M., Belcher, W.J., Grant, D.K., Wagner, P., Wagner, K., Jolley, K.W., Hall, S.B., Clarke, T.M., Gordon, K.C., Misoska, V.J., Wallace, G.G., and Officer, D.L., *Manuscript in preparation*, 2007.

35. Aizawa, M., Watanabe, S., Shinohara, H., and Shirakawa, H., *J. Chem. Soc. Chem. Commun.*, 1985. **25** p. 264.

36. Tsekouras, G., Too, C.O., and Wallace, G.G., *Electrochim. Acta*, 2005. **50** p. 3224.

37. Tsekouras, G., *Electrochemical and photovoltaic properties of polythiophenes*, in *Intelligent Polymer Research Institute*. 2005, University of Wollongong: Wollongong.

38. Wang, C.Y., Tsekouras, G., Wagner, P., Too, C.O., Officer, D.L., and Wallace, G.G., *Submitted to J. Power Sources*, 2007.

39. Little, S.J., *Preparation, characterisation and applications of novel redox-functionalised conducting polymers*, in *Intelligent Polymer Research Institute*. 2006, University of Wollongong: Wollongong.

40. Kamusewitz, H. and Possart, W., *The static contact angle hysteresis and Young's equilibrium contact angle*, in *Contact angle, wettability and adhesion*, K.L. Mittal, Editor. 2006, VSP: Leiden. p. 101.

41. Otero, T.F. and Boyano, I., *Chemphyschem*, 2003. **4** p. 868.

42. Tourillon, G., *Polythiophene and its derivatives*, in *Handbook of Conducting Polymers*, T.A. Skotheim, Editor. 1986, Marcel Dekker: New York. p. 293.

43. Officer, D.L., *Personal communication.*

44. Schrebler, R.G., P., Cury, P., Veas, C., Merino, M., Gomez, H., Cordova, R., and del Valle, M.A., *J. Electroanal. Chem.*, 1997. **430** p. 77.

45. Budevski, E., Staikov, G., and Lorenz, W.J., *Electrochemical Phase Formation and Growth*. 1996, Wenheim: VCH.

46. Cho, J.H., Lee, H.S., Hwang, M., Choi, H.H., Kim, W.K., Lee, J.L., and Cho, K., *Electrochem. Solid St.*, 2007. **10** p. H156.

47. Radelczuk, H., Holysz, L., and Chibowski, E., *J. Adhes. Sci. Technol.*, 2002. **16** p. 1547.

48. Brugnara, M., Degasperi, E., Della Volpe, C., Maniglio, D., Penati, A., Siboni, S., Toniolo, L., Poli, I., Invernizzi, S., and Castelvetro, V., *Colloids Surf., A*, 2004. **241** p. 299.

49. Siboni, S., Della Volpe, C., Maniglio, D., and Brugnara, M., *J. Colloid Interface Sci.*, 2004. **271** p. 454.

50. Abou-Elenien, G.M., El-Maghraby, A.A., and El-Abdallah, G.M., *Synth. Met.*, 2004. **146** p. 109.

51. Spells, S.J., Reinecke, H., Sacristan, J., Yarwood, J., and Mijangos, C., *Macromol. Symp.*, 2003. **203** p. 147.

52. Fleming, O.S., Stepanek, F., and Kazarian, S.G., *Macromol. Chem. Phys*, 2005. **206** p. 1077.

53. Gallardo, A., Navarro, R., Reinecke, H., and Spells, S., *Opt. Express*, 2006. **14** p. 8706.

54. Loponen, M.T., Taka, T., Laakso, J., Vakiparta, K., Suuronen, K., Valkeinen, P., and Osterholm, J.E., *Synth. Met.*, 1991. **41** p. 479.

55. Pei, Q., Inganas, O., Gustafsson, G., Granstrom, M., Andersson, M., Hjertberg, T., Wennerstrom, O., Osterholm, J.E., Laakso, J., and Jarvinen, H., *Synth. Met.*, 1993. **55** p. 1221.

56. Andersson, M.R., Pei, Q., Hjertberg, T., Inganas, O., Wennerstrom, O., and Osterholm, J.E., *Synth. Met.*, 1993. **55** p. 1227.

57. Magnoni, M.C., Gallazzi, M.C., and Zerbi, G., *Acta Polymerica*, 1996. **47** p. 228.

58. Wu, C.G., Chan, M.J., and Lin, Y.C., *J. Mater. Chem.*, 1998. **8** p. 2657.

59. Wu, C.G., Yeh, Y.R., and Chien, L.N., *Polymer*, 2000. **41** p. 5839.

60. Wang, Y. and Rubner, M.F., *Synth. Met.*, 1990. **39** p. 153.

61. Ciprelli, J.L., Clarisse, C., and Delabouglise, D., *Synth. Met.*, 1995. **74** p. 217.

62. Abdou, M.S.A. and Holdcroft, S., *Chem. Mat.*, 1994. **6** p. 962.

63. Yoshino, K., Morita, S., Uchida, M., Muro, K., Kawai, T., and Ohmori, Y., *Synth. Met.*, 1993. **55** p. 28.

64. Li, Y. and Qian, R., *Synth. Met.*, 1993. **53** p. 149.

65. Billingham, N.C., Calvert, P.D., Foot, P.J.S., and Mohammad, F., *Polym. Degrad. Stab.*, 1987. **19** p. 323.

66. Szabo, L., Cik, G., and Lesny, J., *Synth. Met.*, 1996. **78** p. 149.

67. Ahn, Y.C., Kim, D.H., Kim, S.C., Hwang, E.G., Lee, C.G., Kim, G.T., Shin, H.S., Lee, J.K., and Lee, S.H., *Part. Sci. Technol.*, 2004. **22** p. 305.

68. Mukherjee, A., *Characterisation and separation of charged particles*, in *School of Advanced Studies of the Illinois Institute of Technology*. 1987.

69. *Handbook of Chemistry and Physics*. 61st ed, ed. R.C. Weast. 1980-1981, Boca Raton, Florida: CRC Press.

70. Tang, C.W. and VanSlyke, S.A., *Appl. Phys. Lett.*, 1987. **51** p. 913.

71. Lin, Y.-J., You, C.-F., and Tsai, C.-L., *Appl. Surf. Sci.*, 2007. **253** p. 3957.

72. Fomenko, V.S., *Emission Properties of Materials*. 1972, Washington, D. C.: U.S. Department of Commerce.

73. Salaneck, W.R., Friend, R.H., and Bredas, J.L., *Phys. Rep.*, 1999. **319** p. 231.

74. Van Haare, J.A.E.H., Havinga, E.E., Van Dongen, J.L.J., Janssen, R.A.J., Cornil, J., and Bredas, J.L., *Chem.sEur. J.*, 1998. **4** p. 1059.

75. Kim, H.-J., Kim, D.-C., Kim, R., Kim, J., Park, D.-H., Kim, H.-S., Joo, J., and Suh, Y.D., *J. Appl. Phys.*, 2007. **101** p. 053514.

76. Biscarini, F., Murgia, M., Dinelli, F., Cavallini, M., Levy, P., and De Leeuw, D. in *E-MRS 2002 Spring Meeting*. 2002. Strasbourg, France.

77. Garbassi, F., Morra, M., and Occhiello, E., *Surface energetics and contact angle*, in *Polymer surfaces: from physics to technology*. 1998, John Wiley & Sons Ltd: West Sussex. p. 169.

78. van Oss, C.J., *J. Adhes. Sci. Technol.*, 2002. **16** p. 669.

79. Sharma, P. and Hanumantha Rao, K., *Adv. Colloid. Inter. Sci.*, 2002. **98** p. 341.

80. Greiveldinger, M. and Shanahan, M.E.R., *J. Colloid Interface Sci.*, 1999. **215** p. 170.

81. Bain, C.D., *Chemphyschem*, 2001. **2** p. 580.

82. Dos Santos, D.F. and Ondarcuhu, T., *Phys. Rev. Lett.*, 1995. **75** p. 2972.

83. Shanahan, M.E.R. and deGennes, P.G., *C.R. Acad. Sci., Ser. IIb: Mec., Phys., Chim., Astron.*, 1997. **324** p. 261.

84. de Gennes, P.G., *Rev. Mod. Phys.*, 1985. **57** p. 827.

85. Kamusewitz, H. and Possart, W., *Appl. Phys. A*, 2003. **76** p. 899.

86. Muller, B., Riedel, M., Michel, R., De Paul, S.M., Hofer, R., Heger, D., and Grutzmacher, D., *J. Vac. Sci. Technol., B*, 2001. **19** p. 1715.

87. Teasdale, P.R., *Characterisation of the chemical properties of polypyrrole and polyaniline*, in *Intelligent Polymer Research Institute*. 1993, University of Wollongong: Wollongong.

88. Xu, L.B., Chen, W., Mulchandani, A., and Yan, Y.S., *Angew. Chem. Int. Ed.*, 2005. **44** p. 6009.

89. Kamusewitz, H., Possart, W., and Paul, D., *Colloids Surf., A*, 1999. **156** p. 271.

90. Chibowski, E. and Holysz, L., *Langmuir*, 1992. **8** p. 710.

91. Brugnara, M., Degasperi, E., Della Volpe, C., Maniglio, D., Penati, A., and Siboni, S., *Wettability of porous materials II: Can we obtain the contact angle from the Washburn equation?* in *Contact angle, wettability and adhesion*, K.L. Mittal, Editor. 2006, VSP: Leiden. p. 143.

CHAPTER 4

REVERSIBLE FLUID CONTROL OF ORGANIC LIQUIDS USING POLYPYRROLE

4.1 Introduction

The previous chapter highlighted some complexities and factors involved when measuring the wettability and surface energy of conducting polymers. Despite the complex factors involved, significant changes in polymer wettability were observed upon redox switching. The current chapter aims to explore the use of conducting polymers for fluid control upon *in-situ* electrochemical oxidation and reduction, based on the change in wettability and surface energy. Specifically, polypyrrole doped with dodecylbenzenesulfonate (PPy.DBS) will be used to control the shape and position of dichloromethane in aqueous electrolyte upon redox-switching the polymer. Polypyrrole was chosen as the active polymer in this study since it can be operated in aqueous electrolytes, unlike polythiophenes. Aqueous systems are more common in practical microfluidic devices.

Among the different methods used to control fluid flow in microdevices (described in Chapter 1, Section 1.4), modulation of the surface tension of solids and liquids has been intensively investigated in recent years due to the advantageous scaling effects which exist upon miniaturisation of devices. Thermocapillary, electrocapillary and solutocapillary effects involve the generation of surface tension gradients at fluid-fluid interfaces by thermal, electrical and species concentration gradients, respectively [1]. Each are examples of Marangoni or surface tension-generated flows and have proved useful in controlling fluid flow on the microscale. Only fluid motion driven by solutocapillary effects will be discussed in this introduction; for a review of surface tension controlled-fluid movement using other techniques refer to Chapter 1, Section 1.4.2.2.

4.1.1 Solutocapillary-driven flow

Solutocapillary flows arise when a gradient in species concentration exists at an interface, causing a local change in interfacial tension of the liquid which induces droplet motion (Marangoni flow). It commonly refers to the gradient in surface tension at a liquid-liquid interface, but recently examples of controlling liquid-solid interfacial tension have been used to drive fluids in microfluidic devices [2-4]. Otherwise, solutocapillary effects have remained largely unexplored for driving fluid flow in microdevices, due to the difficulty in controlling gradients in surfactant species concentration, as highlighted in an excellent review by Squires and Quake [1]. Much of the work in this area has been carried out by Abbott and co-workers [5-10], who have explored the use of light [2, 11] and electrochemistry [4] to control UV and redox-active molecules which can be switched between surfactant and non-surfactant states. Induced differences in surface tension at opposing ends of drops caused a gradient capable of propelling the droplets. Solutocapillary effects, when harnessed properly, are therefore well suited for driving fluid flow on the microscale, where surface tension becomes the dominant force.

4.1.2 Droplet-based microfluidic devices

Droplet-based microfluidic devices have been investigated as an alternative to channel-based configurations, as they address some of the problems present in channel-based devices such as leakage and bonding of device components. In addition, no moving parts are required, so the energy requirements of devices are decreased [12]. Droplet-based digital microfluidic circuits have been demonstrated in which the motion of drops is driven by optical [13], thermal [14, 15] or electrical [16-19] means. Applications for such devices have included actuators for pumping or mixing flows, individual chemical reactors or the formation of emulsions with controlled drop size [20]. Several excellent

reviews have been written on the subject [20-22]. Moving liquids in external fluids is beneficial as frictional forces are overcome more easily, leading to faster flow rates and enabling more precise control of droplet position. The ability to manipulate droplets on the microscale has been exploited for individual micro-scale chemical reactors [23, 24] and this continues to be a promising area for research. Chen *et al*. recently reported a clever use of surface morphology to control the wettability of liquids by electrostatic forces separated from the liquid, enabling droplets to remain free of contaminants or modification upon manipulation [23]. Isaksson *et al*. [25, 26] reported the use of conducting polymers to control the position of droplets in microfluidic devices. The change in wettability of polyaniline doped with dodecylbenzenesulfonic acid (PAn.DBSA) upon reduction has previously been exploited to induce movement of water placed on its surface, with the droplet observed to move its centre of mass in the direction of reduced polymer [25, 26].

4.1.3 Wettability studies of polypyrrole and sodium dodecylbenzenesulfonate

The wettability and surface energy of conducting polymers, in particular polypyrrole, with various dopants has been studied in recent years, with a summary of findings detailed in Chapter 1, Section 1.2.5. Dopants and doping level were found to greatly influence the wettability and surface energy of conducting polymers investigated. The dynamic change in polypyrrole properties upon reduction and oxidation of the conducting polymer has rendered it useful for microdevices with various applications (see Chapter 1, Section 1.4.3 for a discussion); however exploitation of the wetting change present in polypyrrole for fluid control in microdevices remains largely unexplored.

Sodium dodecylbenzenesulfonate (NaDBS) has been widely studied as a dopant for polypyrrole due to its usefulness as an actuator material [27, 28] and the fact that the resulting polymer is highly stable in ambient conditions [29]. Surprisingly, there has been only one report regarding wettability measurements of PPy.DBS, to the author's knowledge [30]. The dopant concentration used during synthesis was found to have an impact on polymer wettability. Increasing dopant concentration in the polymerisation solution to the critical micellar concentration of NaDBS led to a water contact angle up to 85 °, after which point increasing NaDBS concentration led to a decrease in water contact angle. Despite the demonstration of the dependence of polymer wettability on dopant concentration, dynamic control of PPy.DBS wettability has yet to be explored. The surfactant nature of DBS renders it well-suited to produce solutocapillary flow upon generation of a surface tension gradient in the polymer by dynamically tuning the oxidation state.

4.1.4 Chapter Aims

This chapter aims to exploit the expected change in PPy.DBS (Figure 1) wettability upon *in-situ* electrochemical redox switching, along with the favourable scaling effects of surface tension at small dimensions, for the control of movement of immiscible droplets (typically dichloromethane) on the polymer's surface. The study is based on the premise reported in the literature that conducting polymers undergo a change in wettability and surface energy upon oxidation and reduction due to an inherent change in the polarity of the conducting polymer backbone, in addition to the incorporation and expulsion of dopants with varying charges. It is recognised that droplet position and speed can be controlled on the microscale by modulating the interfacial energy between solid and liquid phases by means of gradients in chemical surface composition [22]. Therefore surface tension effects should cause liquids in contact with PPy.DBS films to

move upon the generation of surface energy gradient in the polymer. The surfactant nature of the DBS dopant expected to bring about large changes in polymer wettability upon redox cycling. Polypyrrole may also be electrochemically cycled in aqueous solutions, removing the complication of operating in organic electrolytes, which is necessary for polymers such as polyterthiophene. Polypyrrole-based devices are, therefore, more suited to practical microfluidic systems.

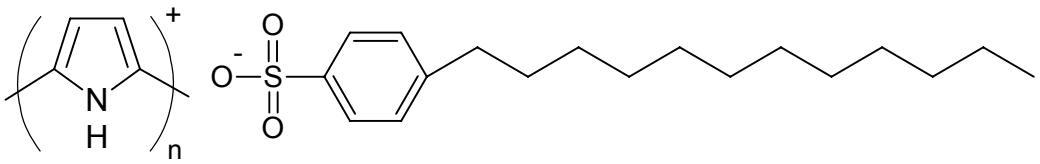

Figure 1. Structure of polypyrrole doped with dodecylbenzenesulfonate (PPy.DBS).

Factors of interest included the various configurations of the electrochemical cell, the extent of contact angle change and lateral translation of the droplet upon redox switching, the electrode substrates employed and the fluids that were to be moved.

Initial wettability characterisations of PPy.DBS deposited on two platinum substrates of varying roughness's, i.e. platinum sheet (Pt sheet) and platinised PVDF (Pt-PVDF), were carried out in air, removed from the electrochemical cell. Subsequently, PPy.DBS-coated Pt-PVDF and PPy.DBS-coated Pt sheet were implemented as working electrodes in an *in-situ* aqueous electrochemical cell, where the shape and position of immiscible dichloromethane droplets were analysed upon redox switching of the polymer. An integrated configuration was investigated, whereby PPy.DBS was coated on alternate sides of Pt-PVDF membrane forming a trilayer structure similar to that used for actuators [31-35]. This configuration was described in Chapter 2, Figure 2. The versatility of the electrochemical cell is increased by integrating the working and counter electrodes into one unit, removing the need for an external counter electrode

and rendering it more widely applicable for fluid control in a variety of devices. The porous nature of the membrane also provided a substrate in which the electrolyte could be stored, enabling the potential for the integrated cell to operate in air, as will be discussed in Chapter 5.

The objectives of this chapter may therefore be summarised as follows:

- To characterise the water wetting properties of PPy.DBS on Pt sheet and Pt-PVDF *ex-situ* (removed from the synthesis electrochemical cell).
- To investigate the use of an integrated trilayer configuration on Pt-PVDF membrane, where PPy.DBS coatings on opposite sides of the membrane formed the working and counter electrodes, and to establish the suitability of this configuration for a fully-integrated electrochemical cell for fluid control in surrounding aqueous electrolyte.
- To investigate fluid control of dichloromethane droplets by exploiting the expected change in PPy.DBS wettability upon *in-situ* electrochemical redox switching using Pt-PVDF and Pt sheet substrates in surrounding aqueous electrolyte.

A brief experimental section will be followed by a presentation of a combined results and discussion section. Characterisation of PPy.DBS wettability and morphology *ex-situ* is presented prior to the *in-situ* electrochemical characterisations of the trilayer integrated Pt-PVDF electrode configuration and the investigation of PPy.DBS for fluid control capabilities upon redox switching in surrounding aqueous electrolyte. Finally, conclusions and future work will be summarised.

4.2 Experimental methods

4.2.1 Reagents and materials

Additional materials and reagents are described in Chapter 2. Platinum sheet (Pt sheet), platinised PVDF membrane (Pt-PVDF) and platinised glass (Pt-glass) were used as electrode substrates in fluid movement studies. Pt-glass was prepared using the Dynavac sputter coater described in Chapter 2. A sputtering current of 30 mA and argon pressure of 2 x 10^{-3} mBar were applied for 5 min. Electrical connection was made to the platinum coating with a platinum wire and conducting epoxy, with the Pt wire/epoxy area sealed using insulating sealant spray. Electrical connection was made to Pt sheet used in *in-situ* fluid movement experiments by spot-welding Pt wire to the corner. MilliQ water was used to determine the wettability of PPy.DBS films in air during initial studies. Dichloromethane (DCM) was primarily used as an immiscible test droplet for *in-situ* electrochemical contact angle measurement; however other chlorinated solvents were tested as alternative droplets, along with silicone oil, glycerol, ethylene glycol and the ionic liquid 1-ethyl-3-methylimidazolium bis(trifluoromethyl)sulfonylimide (EMI.TFSI).

4.2.2 Electrochemical preparation of polymers

The electrochemical polymerisation cell is described in Chapter 2. Deposition solutions containing 0.2 M pyrrole (Py) in 0.2 M NaDBS dopant were degassed for 10 min prior to use and a blanket of nitrogen was maintained over the solution during polymerisation. Films were washed in acetonitrile after deposition and air-dried. Polymers were deposited in the oxidised state using a constant current of 1 mA/cm^2 for 90 s on both Pt sheet and Pt-PVDF working electrodes. Relevant films were reduced in 0.2 M NaDBS using a potential of -0.8 V *vs*. Ag/AgCl. For *ex-situ* wettability measurements, the polymers were removed from the electrochemical cell and water

contact angles of as-deposited and reduced films measured. The preparation of the integrated trilayer Pt-PVDF membrane was described in Chapter 2, Section 2.3.1. In order to explore the role of dopant on polypyrrole fluid movement capability, 0.2 M sodium chloride (NaCl) was used as an alternate polymerisation dopant. Analogous deposition conditions as were used for NaDBS dopant were used to prepare polypyrrole doped with chloride (PPy.Cl).

4.2.3 Cyclic voltammetric studies

Cyclic voltammetry was used to determine the optimum potential ranges for redox switching. The three-electrode cell described in Chapter 2 was employed with 0.1 M $NaNO_3$ electrolyte, a Pt mesh counter electrode and Ag/AgCl reference electrode.

4.2.3.1 Determination of Pt-PVDF electroactive surface area

The electroactive surface area of Pt-PVDF membrane was determined using cyclic voltammetry between +0.6 and -0.8 V in a solution of 5 mM $K_3[Fe(CN)_6]$ and 0.1 M $NaNO_3$ at varying scan rates. The electroactive surface area of a piece of platinised membrane (1 cm^2 geometric area) was determined by the Randles-Sevcik equation (Equation 1):

Equation 1
$$A = \frac{I_p}{kn^{\frac{3}{2}}D^{\frac{3}{2}}Cv^{\frac{1}{2}}}$$

where: A = area of the electrode in cm^2; I_p = average of anodic and cathodic peak current in mA; k = 2.72 x 10^5; n = number of mole of electrons per mole of electroactive species; D = diffusion coefficient in cm^2/s; which is 7.6 x 10^{-6} cm^2/s for $K_3[Fe(CN)_6]$ at 25 ^oC; and v = scan rate in V/s. The validity of the results was ascertained by comparison to Pt disk electrode, which has a well defined area (0.0176 cm^2).

4.2.4 *In-situ* electrochemical contact angle measurements

In-situ electrochemical contact angle measurements were carried out using the DataPhysics goniometer described in Chapter 2 and a modified electrochemical cell (Figure 2). The working electrode (polypyrrole on Pt-PVDF when using the trilayer integrated membrane, or Pt sheet or Pt-glass otherwise) was adhered to the bottom of a 2 x 2 x 2 cm^3 glass cell using double-sided adhesive tape. The counter electrode was either the integrated PPy.DBS counter electrode when using the trilayer configuration, or a Pt mesh positioned at the opposite end of the cell to the working electrode connection. A Ag/AgCl reference electrode was positioned at the opposite end of the cell to the working electrode connection.

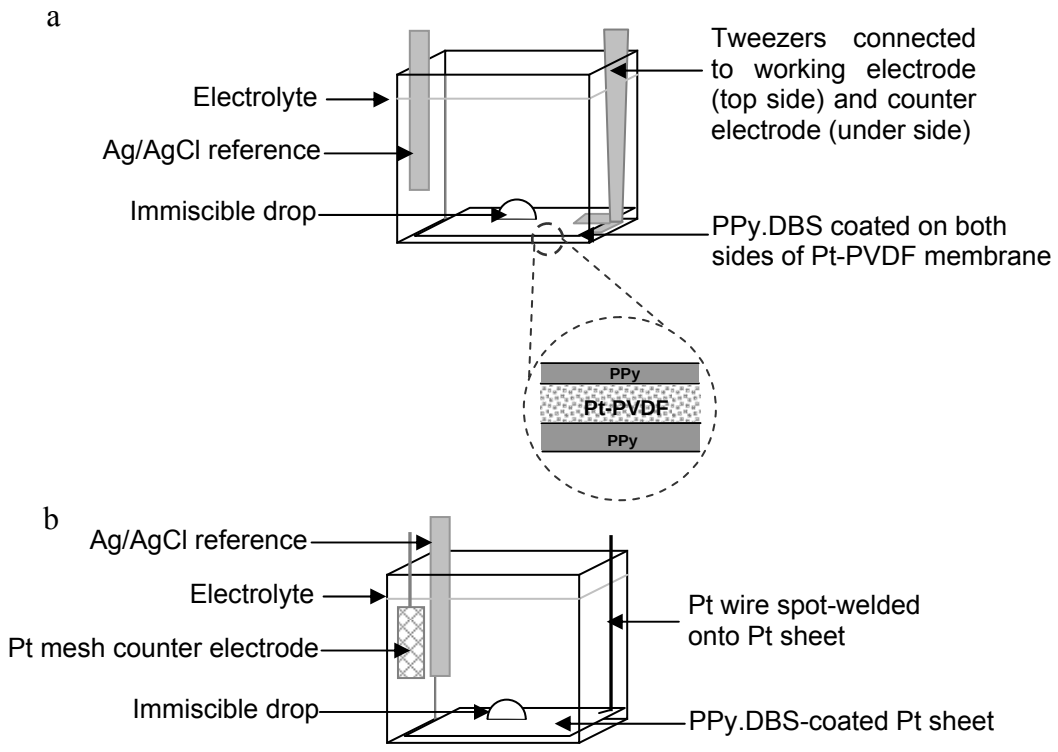

Figure 2. Set-up for *in-situ* electrochemical contact angle measurement. a) Integrated trilayer PPy.DBS-coated Pt-PVDF working electrode and counter electrodes and b) Pt sheet working electrode with Pt mesh counter electrodes. Working electrodes were held horizontally in a glass cell containing aqueous electrolyte (typically 0.1 M $NaNO_3$) in a three-electrode cell configuration (*vs*. Ag/AgCl). Syringe (not shown) introduced immiscible drop (typically DCM) to the surface of the working electrode. The potential was switched between oxidising and reducing (+0.6 V and -0.8 V *vs*. Ag/AgCl, respectively).

A range of aqueous electrolytes ($NaNO_3$, KCl and KNO_3) with a concentration of 0.1 M were employed, with the concentration of $NaNO_3$ varied to 0.01 M and 1.0 M in relevant experiments.

4.3 Results and discussion

4.3.1 Preparation of PPy.DBS on Pt-PVDF and Pt sheet

Galvanostatic polymerisation was used for the preparation of PPy.DBS as this method enabled a standard amount of polymer to be deposited for every film. Also, galvanostatic methods have been found to yield more controlled depositions with more reproducible deposition voltages compared with the variation in current when using potentiostatic methods [36]. Electrodeposition of PPy.DBS proceeded at a constant potential of ca. +0.55 V (*vs*. Ag/AgCl) and ca. +0.61 V (*vs*. Ag/AgCl) on Pt-PVDF and Pt sheet, respectively, indicative of the formation of conducting films. The thickness of PPy.DBS films deposited using a charge density of 90 mC/cm^2 was estimated to be ca. 560 nm, based on the relationship between charge consumed during deposition and film thickness, calculated by Bay *et al*. to be 160 mC/cm^2 per μm [28]. Various potential ranges were tested potentiodynamically in order to determine the optimum potentials of oxidation and reduction using 0.1 M $NaNO_3$ electrolyte (i.e. small, mobile cation and anion). At potential ranges narrower than +0.6 to -0.8 V, defined redox peaks were not present, whereas wider potential ranges caused a decrease in current on successive cycling. Hence +0.6 V and -0.8 V (*vs.* Ag/AgCl) were determined to be the optimum potentials for oxidation and reduction, respectively, and were used in all further studies.

4.3.2 Initial characterisations of PPy.DBS

Initial characterisations of the morphology and wettability of films in air of PPy.DBS on Pt sheet and Pt-PVDF substrates were carried out prior to investigation of the polymer for *in-situ* dynamic fluid control. These substrates have vastly different morphologies

and roughness, which was found to be an important factor in determining the wetting behaviour of polyterthiophene as reported in the previous chapter. Pt sheet can be polished to a smooth finish and has been widely used as an electrode substrate, while Pt-PVDF possesses a highly microstructured morphology, introducing the possibility of Wenzel or Cassie states and contact line pinning, as described in Chapter 1, Section 1.1.2.3. The use of Pt-PVDF membrane also facilitated the design of an integrated electrochemical cell where the working and counter electrodes were on opposing sides of the PVDF membrane (described in Chapter 2, Section 2.3.1).

4.3.2.1 Optical characterisation of PPy.DBS-coated substrates

Visual inspection of PPy.DBS-coated substrates revealed the substrate employed had an effect on the colour of the polymer. PPy.DBS films deposited on Pt sheet were found to be shiny and green in colour in the as-deposited state, while films deposited on Pt-PVDF in the as-deposited state were dull and brown in colour, despite the same charge density being used for both substrates during deposition. Scanning electron microscopy (SEM) revealed a dramatic difference in the films morphologies. PPy.DBS on Pt-sheet exhibited the familiar 'cauliflower'-type morphology, whereas PPy.DBS on Pt-PVDF predominantly exhibited the structure of the underlying membrane (Figure 3).

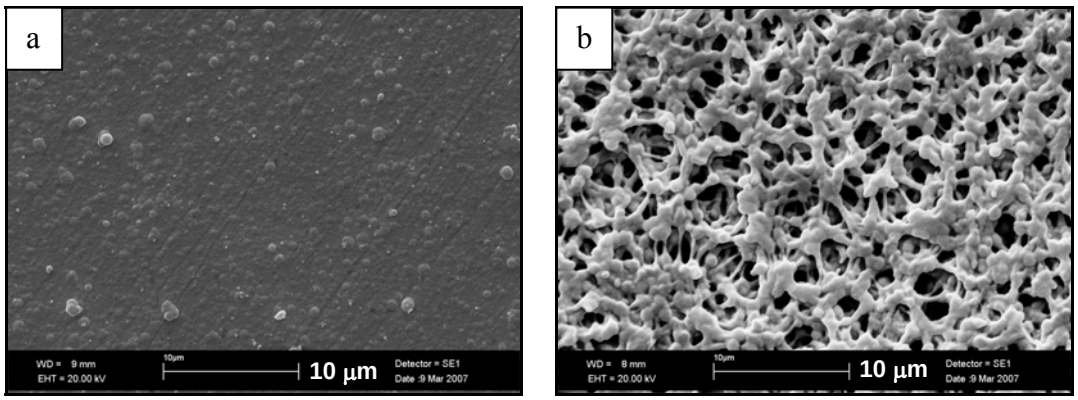

Figure 3. SEM images of PPy.DBS, deposited using a charge density of 90 mC/cm^2 in a three-electrode cell *vs*. Ag/AgCl, on a) platinum sheet; and b) platinised PVDF membrane. Scale bar = 10 µm.

4.3.2.2 Wettability characterisations of PPy.DBS-coated substrates *in air*

Initial investigations into the water wettability of PPy.DBS on Pt sheet and Pt-PVDF were undertaken after removal from the electrochemical cell. The contact angle of water on as-deposited and reduced PPy.DBS and Pt-PVDF and Pt sheet is shown in Table 1. Reduced films were prepared as per Section 4.2.2. The water contact angles for the uncoated substrates (detailed in Chapter 3) are shown for comparison. The results are described in Sections 4.3.2.2.1 and 4.3.2.2.2 below.

Table 1. Water contact angles (°) of PPy.DBS deposited on Pt sheet and Pt-PVDF in the as-deposited (oxidised) and reduced states, along with water contact angles of the uncoated substrates.

	Oxidised	**Reduced**	**Uncoated**
Pt sheet	72 ± 7	18 ± 6	~5
Pt-PVDF	~0	~0	120 ± 2

4.3.2.2.1 *PPy.DBS on Pt sheet*

PPy.DBS deposited on Pt sheet was found to have average water contact angles of 72 ° in the as-deposited (oxidised) state and 18 ° in the reduced state. The result for oxidised PPy.DBS (72 °) was on the order of previously reported results [30]. The increased wettability of the reduced film compared to the oxidised film was consistent with observations made by Isaksson *et al*. for PAn.DBSA [25]. This dramatic increase in wettability upon reduction of the polymer was in contrast to the observations in the previous chapter for polyterthiophene doped with perchlorate (PTTh.ClO_4), where films were observed to become more hydrophobic upon reduction. The variation is due to the different methods of charge balancing upon redox switching inherent to the two polymers. In the case of PTTh, the ClO_4^- dopant anions were expelled from the polymer

upon reduction due to their small size and mobility. However, a different mechanism exists for polymers doped with large immobile anions such as DBS. The major change in mass upon oxidation and reduction of PPy.DBS has been found to be associated with cation movement, rather than the insertion and expulsion of the dopant anion generally seen for small mobile dopant anions such as SO_4^-, NO_3^- and Cl^-. The large DBS anions remain enmeshed in the polymer matrix upon redox cycling, even in electrolyte where DBS was not present, leading to the incorporation of cations from the electrolyte solution for charge neutrality [27, 28, 37-39]. The increased wettability of reduced PPy.DBS films was thus consistent with the increased charge in the polymer associated with cation insertion upon reduction, according to the following equation [40, 41]:

Equation 2 $$\left(PPy^0 DBS_x^- Na_x^+\right)_n \longleftrightarrow \left(PPy^{x+} DBS_x^-\right)_n + nxNa + nxe^-$$

An increase in wettability of reduced polypyrrole in comparison to the oxidised state has also been reported by Xu *et al.* [42] for polypyrrole doped with the low surface energy dopant tetraethylammonium perfluorooctanesulfonate (TEA.PFOS) prepared by galvanostatic deposition. Using a method analogous to the present investigation, the films were oxidised or reduced then washed and dried prior to carrying out contact angle measurements in air (removed from the electrochemical cell). Smooth compact films, formed in the absence of $FeCl_3$ catalyst, were found to have contact angles of 105 ± 2 ° and 48 ± 2 ° for oxidised and reduced films, respectively; that is, the reduced films were more wettable, as was observed in the present study. When a $FeCl_3$ catalyst was present, porous structures were formed leading to superhydrophobic oxidised polymer (152 ± 2 °) and superhydrophilic reduced polymer (~0 °). The mechanism by which reduced films were more wettable than oxidised films was different to the mechanism in the present study. The neutral PPy.PFOS film in Xu's study was found to contain only

trace amounts of dopant, suggesting the majority was expelled upon reduction. This is in contrast with the predominant cation motion observed for PPy.DBS [27]. It is proposed that upon oxidation of PPy, the DBS anions are oriented so the hydrophilic charged sulfonate groups are buried into the polymer upon doping. The hydrophobic tail groups concurrently align at the polymer-air interface, increasing the apparent hydrophobicity, whereas the decreased wettability of the oxidised state in the study by Xu was due to the incorporation of low energy dopant.

4.3.2.2.2 *PPy.DBS on Pt-PVDF*

Dramatically different wetting behaviour was observed for PPy.DBS when platinised PVDF was used as the substrate. Water drops placed on both oxidised and reduced PPy.DBS in ambient conditions were observed to quickly soak into films, resulting in a contact angle of ca. 0 ° for films of both oxidation states. Initial contact angles recorded at the moment of contact, using the video capability of the goniometer software, ranged from 10 – 80 °, however these angles quickly became 0 ° as the droplets spontaneously spread and soaked into the membrane. The extreme wetting behaviour of PPy.DBS was vastly different to that of non-polymer coated Pt-PVDF, which had a contact angle of ca. 120 ° (Table 1). The porous nature of the membrane and the inherent hydrophilicity of the films were consistent with capillary action causing the water to move into the membrane, indicating drops were in the Wenzel state and suggested the microstructured roughness of the membrane enhanced the polymers wetting properties.

Hence it can be seen that different substrate morphologies had a significant impact upon the resulting wettability of the polymer. Pt-PVDF, while initially hydrophobic, became superhydrophilic when coated with PPy.DBS in both the as-deposited and reduced states of the polymer, presumably due to capillary action wicking the water into the

nanostructured surface. Conversely, PPy.DBS on Pt sheet, which was superhydrophilic when uncoated, was significantly less wettable in the oxidised state than when reduced. The Pt sheet was believed to give a truer indication of PPy.DBS wettability, as the smooth Pt sheet morphology did not interfere with wettability measurements. The impact of the substrate upon the fluid movement capability of PPy.DBS upon *in-situ* redox switching is considered in Section 4.3.4.

Surface energy measurements of PPy.DBS-coated substrates were not pursued due to experience described in the preceding chapter, where the apolar surface energy test liquid diiodomethane was observed to spread spontaneously on the surface of polyterthiophene and rarely formed measurable contact angles. Since PPy.DBS films were found to be predominantly hydrophilic, it was surmised that the films would have been reasonably polar with surface energies greater than that of diiodomethane (50.8 mN/m), as was the case for PTTh.ClO_4 films. Given the criterion that the surface tension of the liquid should be greater than that of the solid for a discrete, measurable contact angle to form (i.e. $\gamma_l > \gamma_s$; [43]), surface energy measurements of PPy.DBS were not pursued.

4.3.3 Electrochemical characterisations

The electrochemistry of the integrated trilayer Pt-PVDF membrane configuration (described in Chapter 2, Section 2.3.1) was investigated prior to its implementation as a substrate for PPy.DBS in fluid movement studies.

4.3.3.1 Electrochemical characterisation of uncoated Pt-PVDF

The effectiveness of Pt-PVDF as an electrode was determined by using the well known ferrocyanide-ferricyanide couple in comparison to the electrochemistry of Pt wire. The

resulting curves were of the general shape to be expected (Figure 4), with peaks occurring at +0.46 V (anodic) and +0.018 V (cathodic) for Pt-PVDF, and +0.30 V (anodic) and +0.15 V (cathodic) for Pt wire. The shifting of peaks for Pt-PVDF to a higher anodic potential and a lower cathodic potential may be attributed to the increased surface area and more resistive nature of the platinised membrane in comparison to the platinum wire.

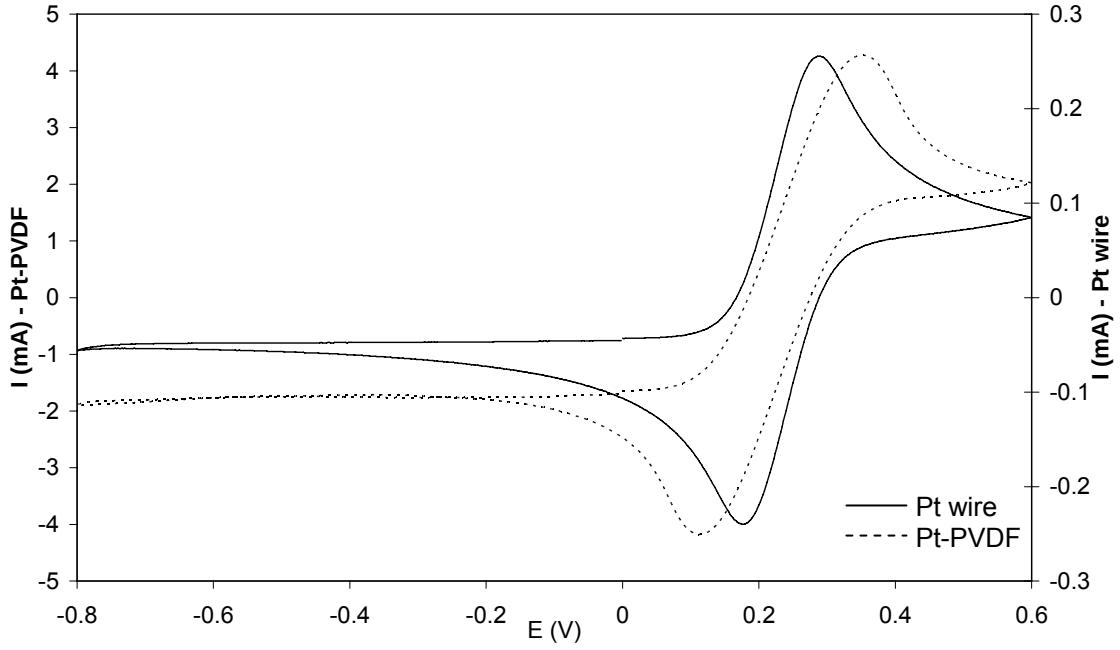

Figure 4. Cyclic voltammogram of Pt-PVDF (film area = 2 cm^2) and Pt wire (area approx. 16 mm^2), cycled from -1 to +1 V (*vs.* Ag/AgCl) at 50 mV/s for 3 cycles each in a solution containing 0.2 M $NaNO_3$, 0.04 M $K_3[Fe(CN)_6]$ and 0.04 M $K_4[Fe(CN)_6]$.

The electroactive surface areas of Pt-PVDF and Pt disk were determined using the Randles-Sevcik equation (detailed in Section 4.2.3.1) applied to data collected at varying scan rates. The surface areas of both substrates were determined to be scan rate dependent (Table 2), with the deviation in surface area significantly higher for Pt-PVDF. Interestingly, the surface areas determined using the 50 mV/s scan rate for both substrates (0.714 cm^2 and 0.0172 cm^2 for Pt-PVDF and Pt-disk, respectively) and the 20 mV/s scan rate for Pt-PVDF (0.818 cm^2) were found to be less than the known

geometric area of the substrate (i.e. 1 cm^2 for Pt-PVDF and 0.0176 cm^2 for Pt-disk). These results were somewhat unexpected, especially for Pt-PVDF membrane, as one would predict that the surface area calculated would be at least that of the geometric area (i.e. 1 cm^2), if not higher due to the porous nature of the membrane structure. It is possible that at the higher scan rates there was not sufficient time for the electrolyte to enter the pores of the membrane, whilst at slower scan rates the electrolyte was able to diffuse into the pores more effectively. Plots of the peak current *vs*. the square root of the scan rate using the Randles-Sevcik equation (Equation 1) revealed the cathodic and anodic reactions of uncoated platinum disk electrodes were diffusion controlled (see Appendix A for plots), whereas uncoated Pt-PVDF experienced a greater peak separation and deviation from ideality (see Appendix B for plots), indicating Pt-PVDF was less ideal as an electrode substrate than Pt disk.

Table 2. Electroactive surface area of Pt-PVDF (1 cm^2 geometric area) and Pt disk (0.0176 cm^2 geometric area) calculated from cyclic voltammograms in 5 mM $K_3[Fe(CN)_6]$/0.1 M $NaNO_3$. The dashed line represents the actual geometrical substrate surface area.

	Electroactive surface area (cm^2)	
Scan rate (mV/s)	**Pt-PVDF**	**Pt-disk**
50	0.714	0.0172
20	0.818	0.0180
10	1.154	0.0182

4.3.3.2 Electrochemical characterisation of PPy.DBS-coated substrates

4.3.3.2.1 *Electrochemistry of PPy.DBS on Pt-disk*

The electrochemistry of PPy.DBS was initially characterised using a standard substrate, namely Pt disk. A reversible conversion between oxidised and reduced forms was

observed for PPy.DBS-coated Pt disk electrodes using cyclic voltammetry in 0.1 M $NaNO_3$ (Figure 5). A redox couple at -0.5 V and -0.35 V (*vs.* Ag/AgCl) corresponds to the incorporation of Na^+ into the polymer and expulsion of Na^+ into the electrolyte, respectively [27]. The peak at -0.5 V has also been attributed to the expulsion of small anions (NO_3^-) into the electrolyte, while a shoulder in the anodic scan at ca. 0 V (*vs.* Ag/AgCl) has been reported to be associated with the insertion of anions into the polymer from the electrolyte [27]. Cyclic voltammograms were analogous to those previously reported for PPy.DBS [38].

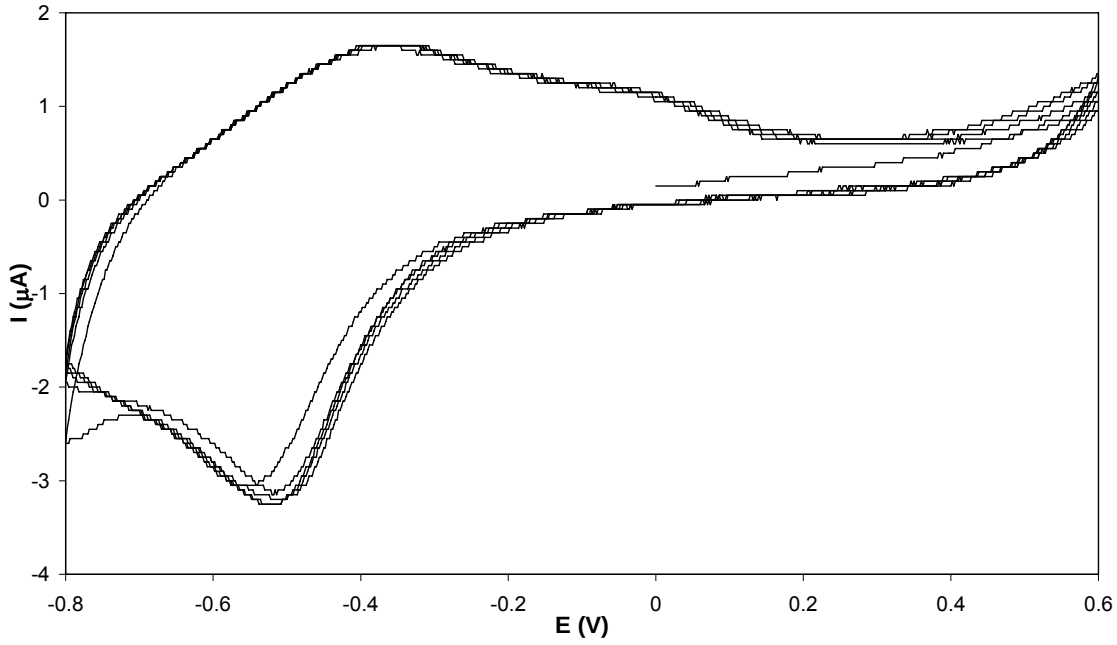

Figure 5. Cyclic voltammogram of PPy.DBS on Pt disk working electrode with Pt mesh counter electrode *vs.* Ag/AgCl in 0.1 M $NaNO_3$. The potential was scanned between -0.8 to +0.6 V using a scan rate = 50 mV/s and 5 cycles.

4.3.3.2.2 *Electrochemistry of PPy.DBS on Pt-PVDF*

The electrochemistry of PPy.DBS was investigated using Pt-PVDF as a substrate. Both the integrated trilayer PPy.DBS counter electrode and a standard Pt mesh counter electrode were employed, in order to test the functioning of the trilayer counter electrode. Electrochemical characterisation of PPy.DBS-coated Pt-PVDF was carried

out using cyclic voltammetry using analogous conditions to those used for PPy.DBS on Pt disk. The cyclic voltammograms (Figure 6) were similar to that of PPy.DBS on Pt disk (Figure 5); however both the cathodic and anodic peaks were significantly broadened. This effect may be attributed to the increased surface area of the Pt-PVDF membrane in comparison to the Pt disk electrode, leading to less well-defined oxidation and reduction peaks. The cathodic peak occurred at ca. -0.6 V (vs. Ag/AgCl) and the anodic peak at ca. -0.33 V (*vs*. Ag/AgCl) when using both the external Pt mesh and integrated PPy.DBS counter electrodes, which were similar to those for PPy.DBS on Pt disk (i.e. -0.5 V and -0.35 V, respectively).

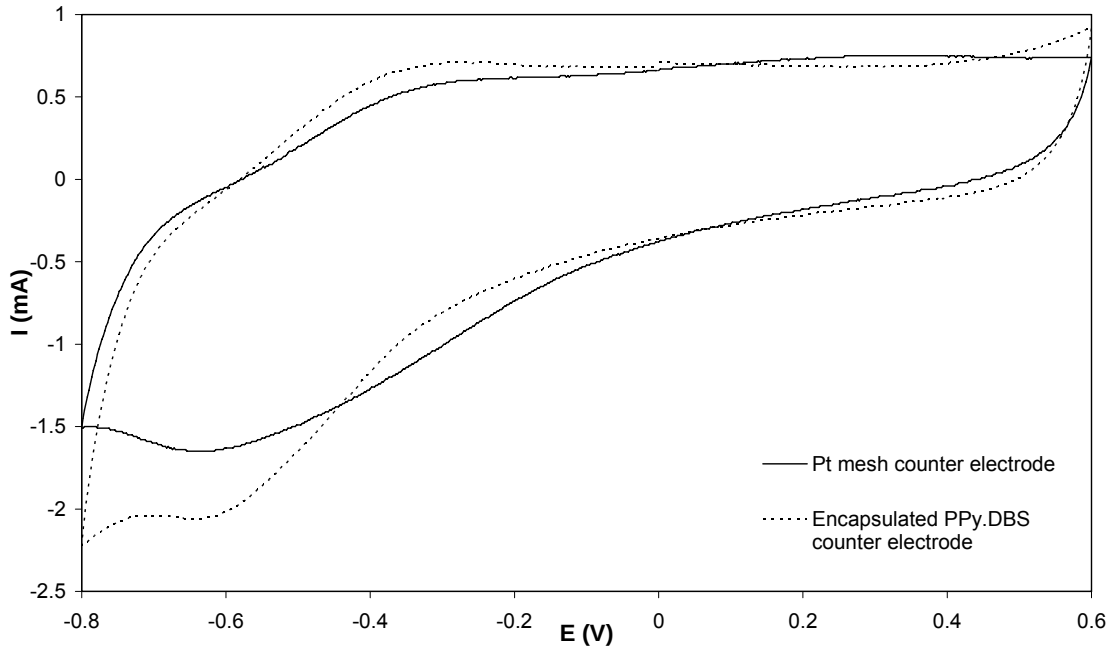

Figure 6. Cyclic voltammograms of PPy.DBS on Pt-PVDF working electrode in 0.1 M $NaNO_3$. A comparison of the electrochemistry of the integrated trilayer PPy.DBS counter electrode (dashed line) with a standard Pt mesh counter electrode (solid line) is shown. The potential was scanned between -0.8 to +0.6 V Ag/AgCl using a scan rate = 50 mV/s; 5^{th} cycle shown.

The use of the integrated counter electrode was found to enable more efficient transfer of ions between working and counter electrodes during redox switching. This was evidenced by an increase in the average charging current upon application of a square

wave potential for the integrated trilayer PPy.DBS/Pt-PVDF counter electrode in comparison to the external Pt mesh counter electrodes (from ca. 5 mA to ca. 70 mA, respectively; not shown here). PPy.DBS-coated electrodes behaved in a fashion analogous to uncoated substrates, in that reactions at PPy.DBS-coated Pt disk were diffusion controlled (see Appendix C for plots of peak current *vs*. the square root of the scan rate, as determined using the Randles-Sevcik equation - Equation 1) while PPy.DBS on Pt-PVDF deviated from ideality (see Appendix D for plots). Hence the integrated trilayer Pt-PVDF configuration was found not to compromise the electroactivity of PPy.DBS, rendering it suitable for investigating fluid control properties.

4.3.4 Investigation of fluid movement using PPy.DBS

The investigation of PPy.DBS for controlling the position of fluids upon redox switching was one of the primary aims of this thesis. This section explores the possibility of translating the change in wettability of PPy.DBS into movement of drops of the organic solvent, dichloromethane (DCM). DCM was investigated due to its immiscibility in and greater density than the surrounding aqueous electrolyte solution, meaning droplets could rest on the polymer surface. The control of DCM droplets in microfluidic devices may prove useful for digital micro-chemical reactors, where reactants are laterally translated and combined in droplets of DCM. Importantly, the use of aqueous liquids affords more freedom than organic electrolytes required for redox switching conducting polymers such as polythiophenes. The knowledge gained in the Sections 4.3.2 and 4.3.3 by characterising the wettability in ambient conditions, polymer morphology and electrochemistry of PPy.DBS-coated Pt sheet and Pt-PVDF electrodes was utilised when implementing PPy.DBS for fluid control upon *in-situ* electrochemical redox switching.

4.3.4.1 Fluid movement using integrated trilayer PPy.DBS-coated Pt-PVDF configuration

The initial design for the fluid control device was modelled on the structure of trilayer actuators reported by Alici and co-workers [31-35], which was described in Chapter 2, Section 2.3.1. The close proximity of the working and counter electrodes was found to enable efficient ion transfer during redox switching. This configuration was investigated using an external aqueous electrolyte, prior to the adaptation of this set-up as an integrated self-contained electrochemical cell aimed at dynamically controlling fluid movement of various liquids in air (discussed in Chapter 5).

The monomer-free polymerisation electrolyte i.e. 0.2 M NaDBS, was initially used as supporting electrolyte for fluid movement experiments, since this has been found to result in long term switching ability [44]. However, DCM was observed to spontaneously disperse into many little droplets prior to the application of a potential, rendering NaDBS unsuitable as an electrolyte for redox switching. Hence other aqueous electrolytes, primarily 0.1 M $NaNO_3$, were employed in subsequent investigations.

Droplets of dichloromethane, generally 1 – 2 μL in volume, were placed on the surface of the integrated trilayer PPy.DBS-coated working electrode, which was connected in a three-electrode cell configuration employing the integrated PPy.DBS counter electrode and a Ag/AgCl reference electrode (Figure 2a). The application of a reducing potential (-0.8 V *vs.* Ag/AgCl) to the working electrode caused DCM droplets to spread across the surface of the polymer (Figure 7b). Subsequent oxidation (+0.6 V *vs.* Ag/AgCl) of the polymer caused the immediate contraction of DCM drops to their original shape

(Figure 7a). This behaviour was reproducible and reversible upon application of a square wave potential, commonly using 1 - 5 sec pulse width.

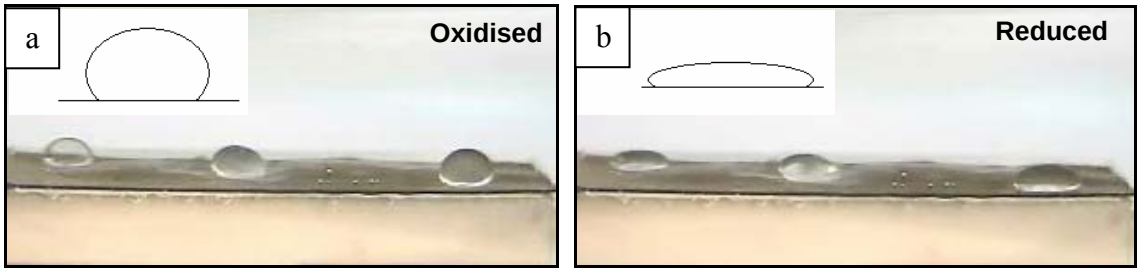

Figure 7. Image taken from video footage showing the shape change of DCM drops resting on the trilayer integrated PPy.DBS-coated electrode, utilising the integrated PPy.DBS counter electrode on the opposite side of the membrane, in 0.1 M $NaNO_3$ external electrolyte upon a) oxidation (+0.6 V *vs.* Ag/AgCl) and b) reduction (-0.8 V *vs.* Ag/AgCl); 1 sec pulse width.

The observed change in DCM drop shape upon *in-situ* redox switching was generally immediate; however, on certain occasions a change in DCM shape was not observed until several minutes of repeated redox cycling of the polymer. On other films, drops resting on one area changed shape immediately, while others adjacent to them only exhibited a slight change in contact angle upon redox switching. This behaviour was believed to be due to the non-homogeneity of the PPy.DBS layer, brought about by the unevenness of the platinising step causing local variations in film conductivity.

Using visual inspection, drops were initially believed to be spreading upon reduction in a hemispherical-type (spherical cap) fashion, as is observed for conventional wetting and electrowetting studies of liquids on surfaces. However, upon further examination using a goniometer with a video camera zoom capability and image capture software, it was realised that the drops were actually collapsing, adopting a 'pancake'-type shape (Figure 7b). Interestingly, the DCM drop contact angle was observed to increase upon

spreading, rather than the decrease in contact angle which is generally indicative of wetting by a liquid. This result indicated that even though the DCM spread over the PPy.DBS surface, there was less of an interaction at the triple phase line.

4.3.4.1.1 *Mechanism of DCM shape change*

Hypothetical surface energy-based mechanism explanation

The mechanism of DCM spreading was hypothetically considered from the perspective of a surface energy change in PPy.DBS upon oxidation and reduction, reported for conducting polymers in the literature (Section 1.2.5): Upon oxidation of the polymer, the charged sulfonate heads of DBS at the polymer-electrolyte interface reorient so they are doping the polymer, causing the hydrophobic portion of the DBS to be presented to the polymer-electrolyte interface, as in Figure 8a. The apolar DCM should interact more strongly with the dopant alkyl chains at the oxidised polymer surface through hydrophobic interactions, causing the drop to spread across the film surface. Upon reduction of PPy.DBS, the polar groups would reorient to face away from the polymer at the polymer-electrolyte interface (Figure 8b), in addition to the migration of charged sodium ions into the polymer for charge neutrality. The increased hydrophilicity of the reduced polymer should cause the DCM drop to be repelled from the polymer surface, thereby increasing the drop contact angle. In fact, the opposite trend in drop spreading was observed, in that DCM on reduced polymer spread out, while DCM on oxidised polymer was in a contracted spherical-cap shape. These observations suggest a different mechanism was responsible for the observed shape change.

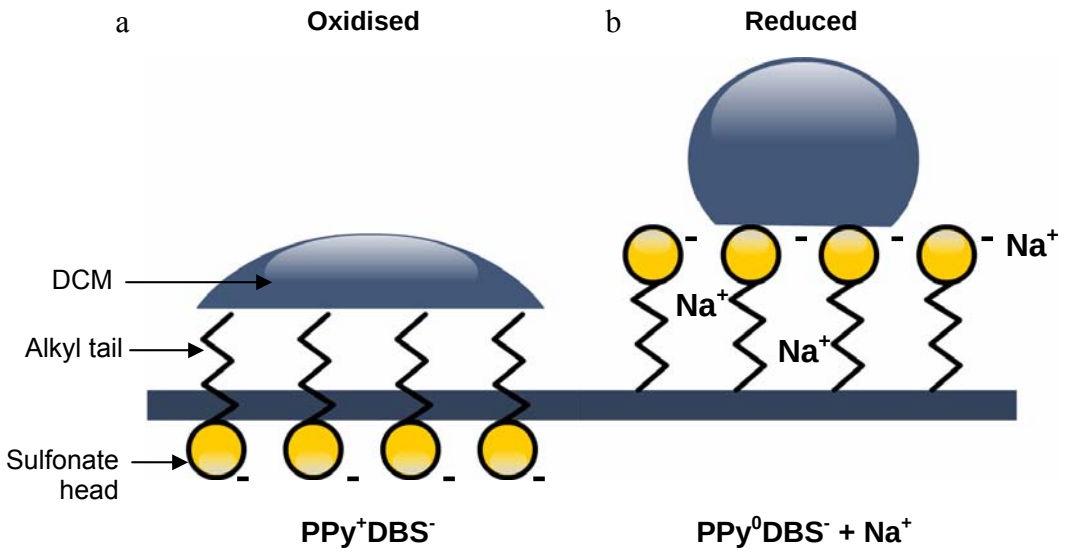

Figure 8. Schematic of interaction of DBS dopant with DCM drop at polymer-electrolyte interface, based on theoretical surface energy change of PPy.DBS upon a) oxidation (+0.6 V *vs*. Ag/AgCl) states) and b) reduction (-0.8 V *vs*. Ag/AgCl) in 0.1 M $NaNO_3$. The opposite trend in DCM drop spreading was actually observed experimentally.

Proposed mechanism for DCM shape change

The incongruity of the surface energy model with the experimentally observed results led to the following model to explain the shape change observed in DCM drops upon *in-situ* PPy.DBS redox switching. It is proposed that the change in DCM drop shape in the present study may be due to a change in DCM-electrolyte interfacial tension resulting from the expulsion of minute amounts of the surfactant dopant DBS into the DCM during reduction of the polymer. Figure 9 illustrates the processes involved during redox switching of PPy.DBS in contact with the DCM drop. The DCM droplet is applied to the oxidised PPy.DBS surface, which was shown to be very hydrophilic when a Pt-PVDF substrate was used (Table 1). Consequently, the DCM forms a drop in the shape of a spherical cap with a high contact angle (determined to be ca. 120 ° in subsequent detailed studies in Section 4.3.4.2.1) due to the balancing of interfacial energies (electrolyte-PPy.DBS; electrolyte-DCM and DCM-PPy.DBS). When the polymer was reduced, it is known that Na^+ ions move from the aqueous electrolyte into

the polymer to form ion pairs with the DBS. However, it is proposed that where the PPy is in contact with the DCM drop, small amounts of DBS are released from the polymer into the DCM, rather than remaining trapped in the polymer. The surfactant nature of the DBS then ensures that the DBS migrates to the DCM-aqueous electrolyte interface. It is further proposed that the DBS assembly at the DCM-aqueous electrolyte interface produces a scenario where an increase in the area of contact between the DCM and the surrounding aqueous electrolyte is required in order to minimise the energy of the system. This 'spreading pressure' causes the droplet to spread, but the hydrophilic nature of the reduced PPy outside the DCM drop restricts the spreading, causing an increased DCM drop contact angle and a new equilibrium drop shape to be attained.

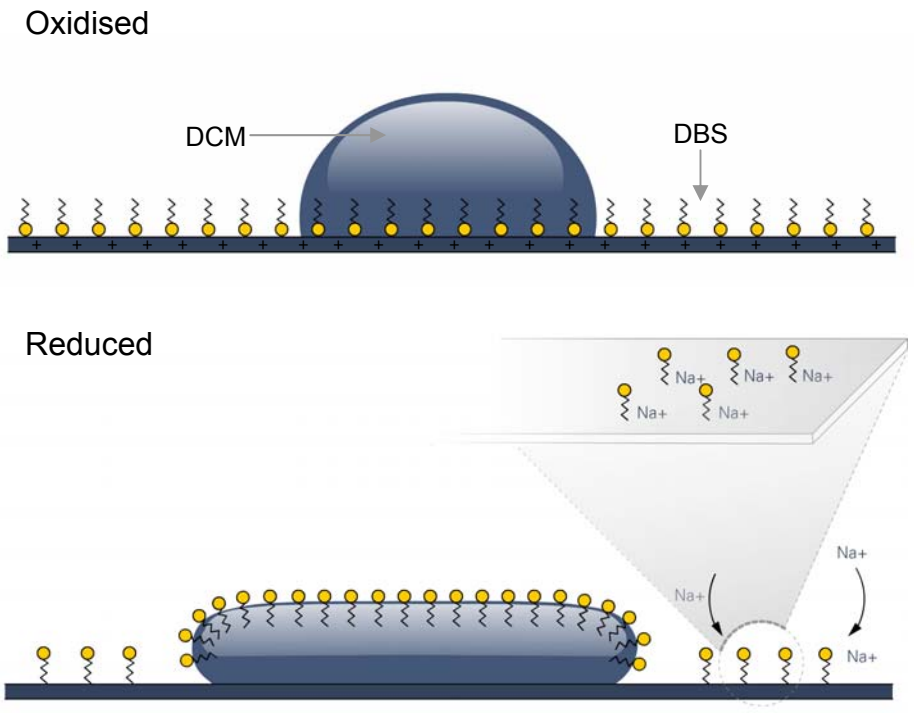

Figure 9. Schematic showing the change in DCM drop shape upon reversible incorporation and expulsion of minute amounts of DBS dopant into and from PPy.DBS upon oxidation and reduction, respectively. Upon reduction, sodium ions are incorporated in the polymer for charge neutrality, increasing the polymer wettability and decreasing the affinity of DCM for the polymer, leading to an increase in contact angle, while the presence of the surfactant causes the DCM-electrolyte interfacial tension to decrease and the droplet to spread.

The 'pancake' shape of the DCM droplets supports the proposed mechanism. Gravity effects tend to flatten out sessile drops, while the DBS migration to the interface causes droplet spreading. However, the hydrophilic nature of the PPy tends to reduce the DCM-PPy interfacial area. The result is the pancake shape with a high contact angle (determined to be ca. 150 ° in subsequent detailed studies in Section 4.3.4.2.1). Note that the higher contact angle of reduced films as compared to oxidised films is what would be predicted according to the surface energy model (Figure 8). This indicates that the inherent change in wettability of the polymer upon oxidation and reduction is still present; however, the surfactant-induced change in DCM-electrolyte interfacial tension is the dominant effect in controlling the DCM drop shape.

The effect of gravity on the shape of drops immersed in immiscible liquids has been discussed by Chatterjee [45]. Cases where the droplet was both heavier and lighter than the surrounding fluid were considered. The dimensionless Eötvös number was used to predict the deviation of contact angle and drop profile from a spherical cap upon the change in interfacial tension of the drop. The contact angle of drops which were heavier than the surrounding medium was found to increase with a decrease in interfacial tension, supporting the proposed mechanism in the present study.

It was noted that several redox switching cycles were often needed to induce the droplet shape change. It is possible that the delay in switching may have been due to ingression of DCM into the pores of the polymer upon prolonged contact, releasing small amounts of dopant into the drop. DCM drops were often observed to become opaque after prolonged redox switching. This may be explained by the polar heads of the small amount of DBS expelled into the DCM forming a microemulsion with the $NaNO_3$ electrolyte. The hydrophobic alkane chain of DBS would then face inwards towards the

DCM, minimising the energy of the system. This alignment of DBS at the DCM-electrolyte interface would act to decrease interfacial tension, causing the drop to collapse upon reduction.

The hypothesis of surfactant-induced change in interfacial tension being responsible for the observed change in DCM drop profile upon redox switching of PPy.DBS was tested by the addition of excess (ca. 2 M) NaDBS to DCM prior to placement on a PPy.DBS film under no applied potential. These drops were observed to immediately spread out like a 'pancake', prior to the application of a potential. The application of a pulsed potential applied between –0.8 and +0.6 V did not have any affect on the shape of the drops and they remained spread across the film surface, even upon application of an oxidising potential. After several minutes, the drops became opaque, again suggesting DBS had induced the formation of a microemulsion.

The role of DBS in the shape change observed for DCM was further tested by the addition of a much smaller amount (1×10^{-4} M) of NaDBS to the DCM, prior to placement on the polymer surface. Droplets were immediately observed to spread on reduction (as in Figure 7b) and return to a spherical shape (as in Figure 7a) upon oxidation, circumventing the need for any extended periods of redox switching prior to the observation of any fluid movement. This observation strongly supported the idea that the presence of DBS in the droplet was integral in facilitating a change in the DCM drop profile.

Successful change in DCM drop shape was observed when alternate electrolytes were used, namely 0.1 M KCl, 0.1 M NaCl and 0.1 M KNO_3, although the extent of contact angle and drop dimension change was variable in different electrolytes. Alternate chlorinated solvent droplets, including trichloroethane, chloroform and dichloroethane,

were all tested for fluid movement using an analogous set-up to that previously described for DCM. All exhibited shape changes to varying extents upon redox switching of PPy.DBS. Other immiscible liquids tested, namely silicone oil, ethylene glycol, glycerol and some ionic liquids, exhibited no change in shape upon redox switching of PPy.DBS, although no particular trend was evident. This may have been due to a lack of release of DBS from polymer into drop upon reduction, perhaps as a result of lower solubility of DBS in organic liquids other than chlorinated solvents.

This is the first example to the author's knowledge where the interfacial tension of an immiscible drop was dynamically controlled using electrochemical expulsion and insertion of surfactant into and out of a conducting polymer. Abbott and Gallardo [4] have used redox active surfactants to induce fluid movement in drops by controlling the surface tension at opposite ends of the drop; however, the surface tension change in their case was at the solid-drop interface rather than the liquid-liquid interface. The change in solid-liquid interfacial tension (i.e. solutocapillary generated Marangoni flow) was the phenomenon that was being pursued in this work; however the change in liquid-liquid interfacial tension appeared to be the dominant effect. Santiago *et al.* [46] modelled the change in contact angle of an oil drop resting on a metal surface submerged in aqueous surfactant with respect to the applied voltage difference and cell geometry. The model described was similar to the proposed mechanism in the present study, except the surfactant solution was in the external electrolyte in Santiago's study. Dramatic changes in the wetting behaviour of the system were observed with only millimolar amounts of surfactant, while no contact angle change was observed in the absence of the surfactant, as in the present case. However, only spherical droplets were observed throughout their investigation, possibly because the amount of surfactant in solution remained constant unlike in the present study.

The integral nature of the DBS dopant to the observed DCM shape changes was highlighted when polypyrrole doped with chloride (PPy.Cl) was tested for fluid control properties. No shape change was observed in the DCM drop, despite a dramatic colour change of the polymer from bright pink (reduced) to green (oxidised), confirming oxidation and reduction of PPy.Cl was occurring on Pt sheet in 0.1 M KCl. A very slight adjustment in the shape of the drop was observed, but this was considered negligible and due to electrostatic effects. These observations confirm both the role of the DBS dopant as integral in facilitating the observed shape changes of DCM upon *in-situ* redox switching.

There are precedents in the literature which indicates polypyrrole undergoes a change in surface energy upon oxidation and reduction [47, 48]. In addition to this, PAn.DBSA has been shown to undergo change in wettability during redox switching [25, 26]. Hence it was logical to predict PPy.DBS would undergo a similar change in surface energy upon oxidation and reduction in the present study. However, the investigation of wetting using an immiscible organic droplet was found to add an extra level of complexity compared to *in-situ* redox-switching of the polymer in air, such as in the study in air by Isaksson *et al*. [25, 26]. The controllable change in interfacial tension at the droplet-electrolyte interface in this study was found to be of greater importance in determining the overall dimension change of DCM drops than any change observed at the polymer-droplet or polymer-electrolyte interface.

In their similar study, Isaksson and co-workers addressed the possibility that the change in wettability observed for PAn.DBSA upon reduction, evidenced by the motion of a water drop spreading towards reduced polymer, was due to DBSA released from the polymer decreasing the surface tension of the drop [25]. They tested this by comparing the contact angles of water with millimolar quantities of NaDBSA added and found

negligible difference to that of pure water, concluding that the spreading of the water drop was not due to a surfactant-enabled decrease in surface tension upon polymer reduction. In the present case, we believe the small amounts of DBS released from the polymer on reduction are responsible for the dramatic changes in DCM drop shape observed. Na^+ motion is predominant between PPy.DBS and the aqueous electrolyte, while DBS reversibly switched between doping the polymer and moving into the DCM drop. These results point to the complex interplay between PPy.DBS, the DCM drop and the electrolyte.

4.3.4.1.2 *Lateral translation of DCM drops*

Given the successful control of DCM drop shape in one position, attempts were made to induce lateral translation of DCM drops resting on integrated trilayer PPy.DBS-coated Pt-PVDF electrodes. Several approaches were investigated. In one approach, the connection to the working and counter electrodes (on alternate sides of the trilayer structure) were made at opposite ends of the 1 x 2 cm films, rather than connecting to the same end of the films, as in previous studies. Some droplets were observed to spread in the direction away from the working electrode connection, but this effect was inconsistent.

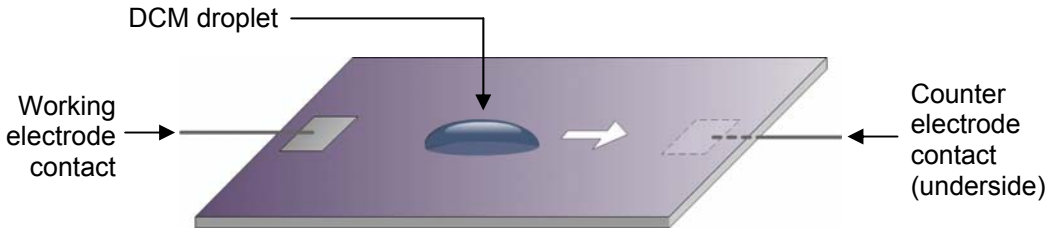

Figure 10. Schematic of integrated trilayer PPy.DBS-coated PVDF membrane configuration for lateral fluid movement attempts of DCM. Gradient in oxidation state generated by connecting electrical contacts of PPy.DBS working electrode (top side) and PPy.DBS counter electrode (underside) at opposite ends of membrane. DCM spread upon application of reducing potential (-0.8 V *vs.* Ag/AgCl) in 0.1 M $NaNO_3$ electrolyte.

In another approach, the working and counter electrodes were directly connected to the same surface of the polymer using multimeter probes attached to the positive and negative terminals of a 1.5 V battery (Figure 11). A gradient in polymer oxidation state was evident by the change of film colour from purple (oxidised) to yellow (reduced), which dynamically changed depending on the position of the electrode contacts. Drops were observed to contract and spread reversibly on the spot, as per Figure 7, but no directionality of motion could be achieved. PPy.DBS deposited on Pt-coated plastic was investigated in an attempt to move DCM droplets sitting at an interface between two segments of polymer (formed by scratching the film off to produce electrically isolated areas). This method showed promise, as drops were observed to spread towards the reduced segment, however the roughness induced by the scratch caused the drops to be significantly pinned and unable to move between segments with varying oxidation state.

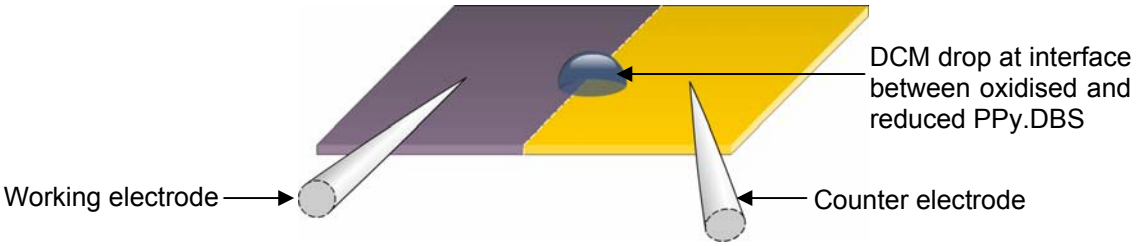

Figure 11. Schematic of integrated trilayer PPy.DBS-coated PVDF membrane configuration for lateral fluid movement attempts of DCM. Working and counter electrode probes connected to a 1.5 V battery in contact with the same side of PPy.DBS-coated Pt-PVDF, immersed in 0.1 M $NaNO_3$ in a two electrode cell configuration. The dashed line represents the gradient in the colour of the film as a result of the variation in oxidation state of the polymer.

Thus despite various attempts to gain directionality of motion, DCM droplets remained pinned to the polymer at one edge of the drop using the approaches mentioned thus far. This phenomenon, known as contact line pinning, is widely recognised as one of the critical issues to overcome when attempting fluid movement in microfluidic devices

[22]. Contact line pinning results when an impediment to the motion of the contact line exists, by either mechanical or chemical hystereses, as discussed in Chapter 1. The rough nature of the underlying PVDF membrane (SEM image, Figure 3b) presumably contributed to inhibiting the motion of dichloromethane droplets subjected to various techniques to induce surface energy gradients and thus fluid motion. Platinum sheet was therefore explored as a substrate for the control of DCM position. The smoother morphology should reduce droplet line pinning, while the homogeneous conductivity would address the issue of reproducibility in film conductivity and DCM droplet shape change present when using Pt-PVDF membrane. The use of Pt sheet as a substrate also coincided with the purchase of a more sophisticated contact angle goniometer with high quality video imaging and drop shape analysis capability, thereby enabling a more in-depth characterisation of the change in contact angles and dimensions of DCM drops upon PPy.DBS oxidation and reduction. Thus the integrated trilayer Pt-PVDF configuration will not be discussed further in this chapter; however, its implementation as a flow valve is described in Chapter 5, along with a brief investigation using the trilayer configuration to control the position of liquids upon redox switching the polymer in air.

4.3.4.2 Fluid movement using PPy.DBS-coated Pt sheet

PPy.DBS on Pt-sheet was tested for fluid movement capabilities using an analogous set-up to that of the integrated trilayer configuration described in Section 4.3.4.1, except Pt mesh was used in place of the integrated trilayer counter electrode. The Pt mesh was positioned at the opposite side of the cell to the working electrode connection in an attempt to generate a gradient of oxidation state and surface energy along the polymer surface upon redox switching (shown in Figure 2b).

4.3.4.2.1 *Contact angle and dimension change of DCM drops*

Drops of DCM placed on PPy.DBS-coated Pt sheet were found to change shape immediately and reversibly upon the application of square wave oxidation (+0.6 V *vs.* Ag/AgCl) and reduction (-0.8 V *vs.* Ag/AgCl) pulses. The change in drop dimensions upon redox switching was notably greater than when Pt-PVDF was used as a substrate. Video images representative of the contact angle and dimension changes observed are shown in Figure 12. Interestingly, DCM drops were observed to change immediately in all cases where Pt sheet was used as a substrate, eliminating the need for the repeated switching often necessary when Pt-PVDF was used as the substrate.

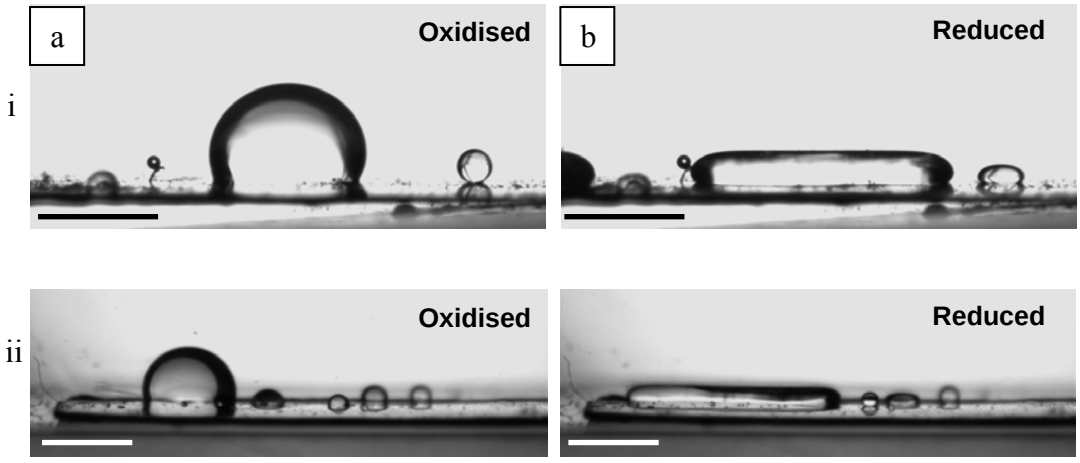

Figure 12. Video images of DCM drops on two different PPy.DBS-coated Pt-sheets (i and ii) in a) oxidised (+0.6 V) and b) reduced (-0.8 V) state in 0.1 M $NaNO_3$ *vs.* Ag/AgCl. Scale bar = 2 mm.

The DCM contact angle was observed to be reversibly switched between ca. 120 ° in the oxidised state to ca. 150 ° in the reduced state, i.e. an increase in contact angle upon reduction DCM drops of various sizes were observed to spread dramatically upon reduction. An average increase in width of 66 ± 2 % and a decrease in height of 196 ± 14% were observed for the switching of droplets on one film. The volume of the drop was not believed to change on redox cycling. These dimension and contact angle changes were reproducible over hundreds of cycles.

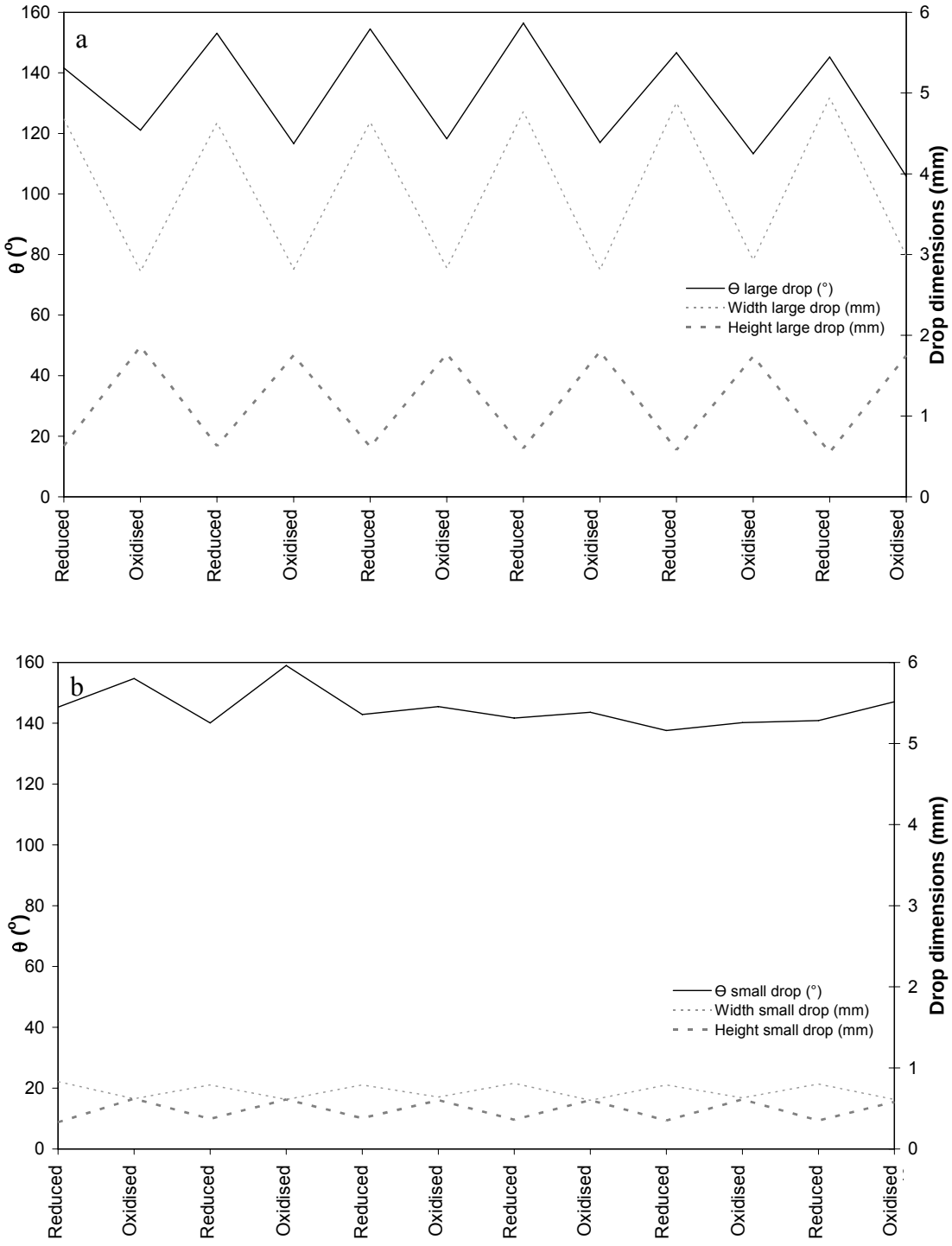

Figure 13. Graph showing the change in a) large and b) small DCM drop dimensions and contact angles upon oxidation and reduction of PPy.DBS-coated Pt sheet in external 0.1 M $NaNO_3$ electrolyte using a Pt mesh counter electrode and Ag/AgCl reference electrode. The change in contact angle is represented by the solid line; change in drop width is represented by the thin dashed line; and change in drop height represented by the thick dashed line. Contact angles (solid lines) are shown on the left-hand side axes and drop dimensions are shown on right-hand side axes. Drop dimensions were measured at the widest point of the profile.

A representative data set is shown for the first 12 redox cycles of large and small drops in Figure 13. This data relates to the drops shown in Figure 12i. The large drop in the middle of the image is denoted 'large drop' (Figure 13a) and the smaller drop on the right hand side of the image is denoted 'small drop' (Figure 13b). The large drop (ca. 2 μL in volume; Figure 13a) was observed to spread upon reduction of PPy.DBS, increasing in width to ca. 4.6 mm and decreasing in height to ca. 0.6 mm, while increasing in contact angle to ca. 155 °. Upon oxidation of the polymer, a decrease in width to ca. 2.8 mm and an increase in height to ca. 1.8 mm was observed, while the contact angle decreased to ca. 120 °. Drop dimensions were measured at the most extreme points on the drop profile by an on-screen ruler. The change in drop dimensions was reversible and reproducible for both large and small drops. A comparison of the contact angle and dimension change of drops revealed a dependence on drop size. Smaller drops (~ ca. 0.1 μL) were observed to spread and contract in the same fashion as larger drops (i.e. spread on reduction and contract on oxidation), albeit to a less significant amount, with a ca. 34 % increase in width and a ca. 88 % decrease in height upon reduction. Interestingly, smaller droplets were observed to *increase* in contact angle upon oxidation and *decrease* upon reduction, which is the reverse of what was observed for larger drops. This suggests that the amount of DBS that enters the DCM drop depends on the size of the drop. Smaller drops would have a higher ratio of DCM-aqueous electrolyte area to DCM-PPy area, leading to less of a 'spreading pressure' in smaller DCM droplets.

4.3.4.2.2 *Speed of pulsing DCM drops*

The speed for which a change in DCM drop shape was observable was tested by changing the duration of the oxidation and reduction pulse of PPy.DBS. DCM drops on PPy.DBS-coated Pt sheet responded immediately to a change in the applied potential

from oxidising and reducing. Pulse lengths were varied from greater than 10 s, down to 0.5, 0.25 and 0.06 s. Very little change in DCM drop dimensions (less than 6 % for both drops in both dimensions) or contact angle was observed at these faster oscillation speeds, consistent with the low amount of current that was passed during rapid pulsing. The change in shape of ca. 1 μL drops are shown below for 0.25 sec pulses in Figure 14. The rapid response of the droplet may be exploited for a microscale pump or micro-mixer in potential applications.

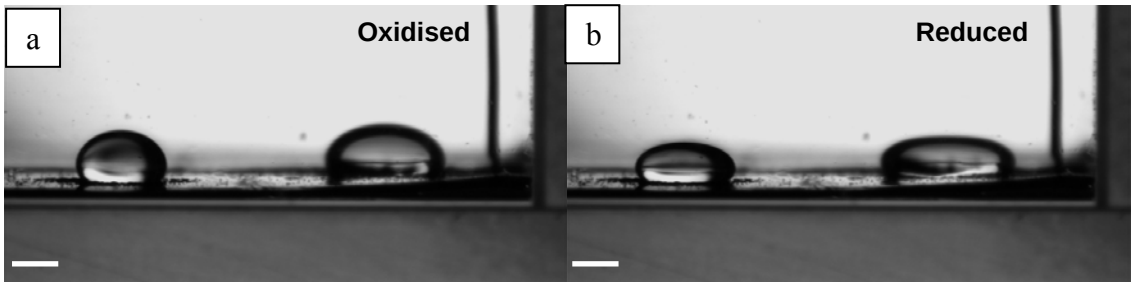

Figure 14. Video images showing the change in shape of DCM drops on PPy.DBS-coated Pt sheet in 0.1 M $NaNO_3$ during rapid pulsing (0.25 sec) upon application of a) oxidation (+0.6 V) and b) reduction (-0.8 V) pulses (*vs* Ag/AgCl). Scale bar = 2 mm.

4.3.4.2.3 *Effect of tilt on DCM droplet motion*

An interesting effect was observed when a slight tilt of 3 ° was introduced into the PPy.DBS-coated Pt sheet substrate. Drops of DCM were observed to roll freely down the slope during the application of a reducing potential, moving up to 7 mm during the duration of a 5 sec pulse (Figure 15).

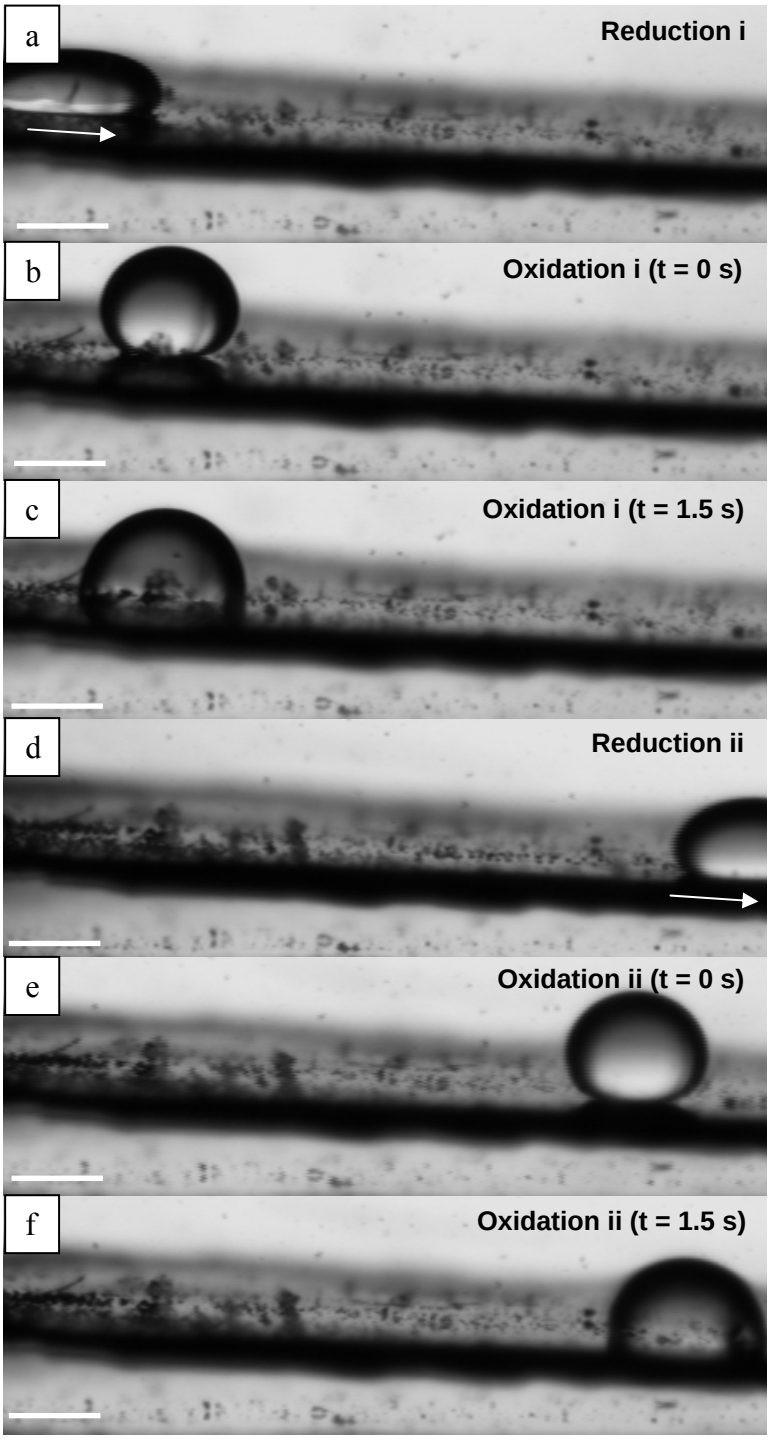

Figure 15. Sequential still images captured from a video of DCM drops rolling down a slight incline on PPy.DBS-coated Pt sheet during switching of the polymer from oxidised to reduced in external 0.1 M $NaNO_3$ (Pt mesh counter electrode *vs.* Ag/AgCl); where a) DCM drop in motion, rolling down slight incline upon reduction pulse; b) DCM drop stationary, immediately upon oxidation pulse; c) DCM drop stationary, 1.5 s after oxidation pulse; d) DCM drop in motion, rolling again down slight incline on reduction pulse; e) DCM drop stationary, immediately upon oxidation pulse; and f) DCM drop stationary 1.5 s after oxidation pulse. Scale bar = 2 mm.

Of particular note, drops ceased rolling and became attached to the spot upon oxidation of the polymer, in spite of the downhill force to which they were subjected. Interestingly, drops were observed to increase dramatically in contact angle the moment that the oxidation pulse was applied (i.e. t = 0 s; Figure 15b and e), followed by a sudden decrease in contact angle as the DCM drop attached to the film moments later (as shown at time points, t = ~1.5 s; Figure 15 c and f). Upon the application of further reducing potentials, DCM drops were again observed to roll freely down the slope (Figure 15d). In a typical example, rolling drops on reduced PPy.DBS had contact angles of 155 ° at the leading edge of the drop. This was observed to decrease to 142 ° at the moment of oxidation, then decrease to 91 ° as the DCM became hemispherical in shape moments later (~1.5 s after oxidation pulse applied). The slight decrease in contact angle immediately upon oxidation (t = 0 s) indicated an initial repulsion from the surface, followed by an attractive force as the drops became fixed on the spot. This most interesting effect indicated the interfacial tension and/or the attractive electrostatic force, between the polymer and the dichloromethane in the oxidised state, were sufficient to overcome the force of gravity acting upon the drop. Further investigation into the force the maximal tilt that the DCM-PPy.DBS interfacial tension could withstand in the oxidised state should elucidate more about the mechanism and reveal interesting applications where this phenomenon may prove useful.

4.3.4.2.4 *Lateral translation of DCM drops on PPy.DBS-coated sheet*

Several approaches were used to achieve lateral motion of DCM drops on PPy.DBS-coated Pt-sheet by dynamically controlling the DCM-electrolyte interfacial tension through redox switching of the polymer. It was hoped a gradient in polymer surface energy would cause a difference in surfactant concentration and thus surface tension at opposite ends of the DCM drop, thereby causing droplet motion. Positioning the

working and counter electrode connections at opposite ends of the 2cm wide cell did not generate a strong enough potential (and thus surface energy) gradient in the polymer to cause DCM drops to move along the distance of the working electrode. DCM drops moved up and down on the spot reproducibly while sitting on a flat surface, though they were not observed to spread in any particular direction. Drops appeared to be significantly less affected by contact line pinning when using platinum sheet rather than Pt-PVDF membrane as a substrate. This was as predicted, due to the vast difference in substrate morphology (SEM images, Figure 3). However it became apparent that some pinning still occurred upon attempts to generate lateral droplet motion, in addition to a lack of surface tension gradient strength in the polymer.

A brief attempt at lateral fluid of DCM drops was carried out using platinum-coated glass (Pt-glass) as a substrate for PPy.DBS. Pt-glass was pursued as an electrode as its smooth surface and higher resistivity than Pt sheet (ca. 40 Ω over 2.5 cm using 2-point probe multimeter, compared to 1 Ω over 2.5 cm for Pt sheet) would hopefully allow a greater surface energy gradient to develop between the working electrode contact and the counter electrode, thereby stimulating an appropriately positioned droplet to move in the direction of lower surface energy. DCM drops were again observed to change shape dramatically and reversibly on the spot upon redox cycling, but complete lateral translation and unpinning of droplets was not achieved (Figure 16). Films became roughened after switching for a short time and the PPy.DBS-Pt coating began to detach from the glass, which presumably impacted the DCM contact angle and impeded fluid movement. In one study, a large drop of DCM on PPy.DBS-Pt-glass was observed to spread dramatically across the surface of the film upon reduction, returning to its initial position upon oxidation. This process was repeated many times and was reversible. The

droplet flattened out significantly upon reduction, moving at least 6 mm across the width of the film; however the drop was not able to detach from where it was pinned.

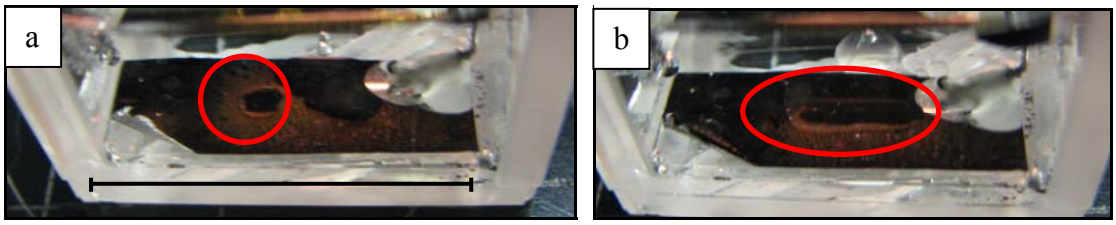

Figure 16. Change in shape of a DCM drop resting on PPy.DBS-Pt glass upon redox switching in external 0.1 M $NaNO_3$ electrolyte, using a Pt mesh counter electrode and a Ag/AgCl reference electrode. a) DCM drop on PPy.DBS in oxidised state (+0.6 V *vs*. Ag/AgCl); b) spreading of DCM drop on reduction of PPy.DBS (-0.8 V *vs*. Ag/AgCl). The detaching of the PPy.DBS/Pt-coating from the glass can be observed in the lower left-hand corner of the images. The electrical contact to the Pt-coating using Pt wire and conducting epoxy, coated with insulating sealant spray, can be observed in the upper right hand corner of the images. Scale bar is 2 cm.

Decreasing the concentration of the supporting electrolyte from 0.1 M to 0.01 M $NaNO_3$ was found to increase the potential gradient across the film due to the reduced ionic conductivity of the electrolyte. A yellow front, indicative of reduced PPy.DBS, was observed to move from one end of the film to the other upon the application of -0.8 V potential. However there was no conclusive evidence of directional movement of DCM droplets. An increase in $NaNO_3$ electrolyte concentration to 1.0 M was found to bring about an instantaneous colour change in the film upon reduction, however no advantageous effect on fluid movement was observed. Careful planning of an electrode with sufficient resistance and electrolyte with appropriate ionic conductivity may realise lateral fluid movement of discrete DCM drops on PPy.DBS in the future.

Hence, while DCM drops were observed to spread and contract repeatedly upon redox switching, unpinning and lateral translation of DCM drops on a flat surface were

unsuccessful. In some configurations, the DCM was observed to spread in the direction of the reduced polymer reversibly upon redox switching the polymer, however there was not a significant force to over come droplet pinning. It is also possible the attempts at lateral droplet translation were unsuccessful as the surfactant spontaneously spread around the droplet-electrolyte interface upon reduction of the polymer. In such a case, a gradient in surfactant concentration would not be able to form and hence the hysteresis in contact angles at either end of the DCM was not able to be translated into droplet motion. Propulsion of droplets in microfluidic devices relies on the hysteresis between the advancing and receding edge of the droplet [17], which has been reported to be ca. 30 ° to induce fluid movement of drops [22]. This amount may be decreased by the reduction in frictional force when working in external liquids. Further investigation into the effects of contact line pinning and advancing and receding contact angle measurements should reveal the conditions necessary for successful translation of discrete droplets using PPy.DBS.

4.4 Conclusions

The development of simple, *in-situ* electrochemical fluid control devices using polypyrrole has been demonstrated. The electrochemistry of PPy.DBS-coated PVDF in an integrated trilayer configuration was compared to that of PPy.DBS on standard Pt disk electrodes, and was found to be suitable for use in *in-situ* wettability studies. The surfactant DBS was used as dopant for polypyrrole, as significant changes in polymer wettability upon redox switching were expected due to a reorientation of the surfactant at the polymer-droplet interface. Dramatic and reversible changes in DCM shape and dimensions upon redox switching PPy.DBS were observed when both Pt sheet and Pt-PVDF were used as substrates. However, the wettability and/or surface energy change of the polymer was not believed to be the primary source of this phenomenon, and a

different mechanism of fluid interaction was proposed. The contact angle and dimension changes observed in DCM were believed to be due to movement of minute amounts of DBS out of the polymer into the DCM upon reduction and incorporation back into the polymer during oxidation. Any surface energy changes of the polymer were believed to be outweighed by the surfactant-induced changes in DCM-electrolyte interfacial tension. Attempts to exploit this phenomenon for solutocapillary flow were based on establishing a surface tension gradient in the polymer; however, contact line pinning and spontaneous spreading of the surfactant across the DCM-electrolyte interface were believed to be responsible for impeding the unhinging of DCM drops. This factor must be overcome in future devices if lateral translation across horizontal PPy.DBS surfaces is to be attained.

The introduction of a slight tilt into the substrate revealed a different interaction of DCM with the polymer, depending on its oxidation state. The DCM rolled freely down the tilt upon reduction of the polymer, while application of an oxidised potential caused the drop to attach strongly to the polymer. This indicated there was an increased interaction between the PPy.DBS and DCM in the oxidised state, due to hydrophobic interactions between the inherently more hydrophobic oxidised PPy.DBS and the DCM.

Further investigation could include testing the extent to which the oxidised PPy.DBS-DCM is able to overcome the force of gravity by adjusting the tilt in the substrate. Another interesting study could investigate the wettability of PPy.DBS with electrolyte (i.e. 0.1 M $NaNO_3$), removed from the electrochemical cell (i.e. in air), as well as studying a range of electrolyte concentrations to determine the effect on polymer-droplet contact angles. Measurement of hysteresis data of PPy.DBS both in air and *in-situ* during electrochemical redox switching on Pt sheet and Pt-PVDF should elucidate

information about the contact line pinning constraint when attempting lateral droplet translation. Careful planning of the ionic strength of the surrounding electrolyte with a gradient in oxidation state in the polymer in future studies is expected to reveal the conditions necessary to overcome droplet pinning and facilitate lateral droplet translation.

Despite the lack of lateral motion of discrete droplets, the phenomena presented in this chapter may be suitable for microvalves or mixers, valves and gates or liquid lenses in microdevices. The implementation of the integrated trilayer configuration presented here will be explored for fluid control in Chapter 5. With further investigation, it is believed that the principles outlined in this chapter will provide the basis for the future development of fluid movement strategies in microfluidic devices.

4.5 References

1. Squires, T.M. and Quake, S.R., *Rev. Mod. Phys.*, 2005. **77** p. 977.
2. Shin, J.Y. and Abbott, N.L., *Langmuir*, 1999. **15** p. 4404.
3. Lee, H.J., Fermin, D.J., Corn, R.M., and Girault, H.H., *Electrochem. Commun.*, 1999. **1** p. 190.
4. Gallardo, B.S., Gupta, V.K., Eagerton, F.D., Jong, L.I., Craig, V.S., Shah, R.R., and Abbott, N.L., *Science*, 1999. **283** p. 57.
5. Luk, Y.Y. and Abbott, N.L., *Science*, 2003. **301** p. 623.
6. Abbott, N.L., *AICHE Journal*, 2001. **47** p. 2634.
7. Datwani, S.S., Truskett, V., Rosslee, C.A., Abbott, N.L., and Stebe, K.J., *Langmuir*, 2003. **19** p. 8292.
8. Luk, Y.Y. and Abbott, N.L., *Curr. Opin. Colloid Interface Sci.*, 2002. **7** p. 267.
9. Aydogan, N. and Abbott, N.L., *Langmuir*, 2001. **17** p. 5703.

10. Bai, G.Y., Abbott, N.L., and Graham, M.D., *Langmuir*, 2002. **18** p. 9882.

11. Rosslee, C.A. and Abbott, N.L., *Curr. Opin. Colloid Interface Sci.*, 2000. **5** p. 81.

12. Fair, R.B., *Microfluid. Nanofluid.*, 2007. **3** p. 245.

13. Bezuglyi, B. and Ivanova, N., *Fluid Dynamics*, 2007. **42** p. 91.

14. Daniel, S., Chaudhury, M.K., and Chen, J.C., *Science*, 2001. **291** p. 633.

15. Chen, J.Z., Troian, S.M., Darhuber, A.A., and Wagner, S., *J. Appl. Phys.*, 2005. **97** p. 014906.

16. Kuo, J.S., Spicar-Mihalic, P., Rodriguez, I., and Chiu, D.T., *Langmuir*, 2003. **19** p. 250.

17. Pollack, M.G., Fair, R.B., and Shenderov, A.D., *Appl. Phys. Lett.*, 2000. **77** p. 1725.

18. Krupenkin, T.N., Taylor, J.A., Schneider, T.M., and Yang, S., *Langmuir*, 2004. **20** p. 3824.

19. Krupenkin, T., Taylor, J.A., Kolodner, P., and Hodes, M., *Bell Labs Tech. J.*, 2005. **10** p. 161.

20. Stone, H.A., Stroock, A.D., and Ajdari, A., *Annu. Rev. Fluid Mech.*, 2004. **36** p. 381.

21. Wong, P.K., Wang, T.H., Deval, J.H., and Ho, C.M., *IEEE-ASME T. Mech.*, 2004. **9** p. 366.

22. Darhuber, A.A. and Troian, S.M., *Annu. Rev. Fluid Mech.*, 2005. **37** p. 425.

23. Chen, T.-H., Chuang, Y.-J., Chieng, C.-C., and Tseng, F.-G., *J. Micromech. Microeng.*, 2007. **17** p. 489.

24. Dubois, P., Marchand, G., Fouillet, Y., Berthier, J., Douki, T., Hassine, F., Gmouh, S., and Vaultier, M., *Anal. Chem.*, 2006. **78** p. 4909.

25. Isaksson, J., Tengstedt, C., Fahlman, M., Robinson, N., and Berggren, M., *Advanced Materials*, 2004. **16** p. 316.

26. Isaksson, J., Robinson, N.D., and Berggren, M., *Thin Solid Films*, 2006. **515** p. 2003.

27. Skaarup, S., Bay, L., Vidanapathirana, K., Thybo, S., Tofte, P., and West, K., *Solid State Ionics*, 2003. **159** p. 143.

28. Bay, L., Mogensen, N., Skaarup, S., Sommer-Larsen, P., Jorgensen, M., and West, K., *Macromolecules*, 2002. **35** p. 9345.

29. Omastová, M., Trchová, M., Kovárová, J., and Stejskal, J., *Synth. Met.*, 2003. **138** p. 447.

30. Liu, M., Zhang, Y., Wang, M., Deng, C., Xie, Q., and Yao, S., *Polymer*, 2006. **47** p. 3372.

31. Wu, Y., Alici, G., Spinks, G.M., and Wallace, G.G., *Synth. Met.*, 2006. **156** p. 1017.

32. Alici, G. and Huynh, N.N., *Sens. Actuators, A*, 2006. **132** p. 616.

33. Alici, G., Mui, B., and Cook, C., *Sens. Actuators, A*, 2006. **126** p. 396.

34. Fang, Y., Tan, X., Shen, Y., Xi, N., and Alici, G., *Submitted to Mater. Sci. Eng., C*, 2007.

35. Alici, G., Spinks, G., Huynh, N., Sarmadi, L., and Minato, R., *Bioinspir. Biomim.*, 2007. **2** p. S18.

36. Maw, S., Smela, E., Yoshida, K., Sommer-Larsen, P., and Stein, R.B., *Sens. Actuators, A*, 2001. **89** p. 175.

37. Khalkhali, R.A., Price, W.E., and Wallace, G.G., *React. Funct. Polym.*, 2003. **56** p. 141.

38. Matencio, T., Depaoli, M.A., Peres, R.C.D., Torresi, R.M., and Detorresi, S.I.C., *Synth. Met.*, 1995. **72** p. 59.

39. Torresi, R.M., Detorresi, S.I.C., Matencio, T., and Depaoli, M.A., *Synth. Met.*, 1995. **72** p. 283.

40. Gandhi, M.R., Murray, P., Spinks, G.M., and Wallace, G.G., *Synth. Met.*, 1995. **73** p. 247.

41. Bay, L., Jacobsen, T., Skaarup, S., and West, K., *J. Phys. Chem. B.*, 2001. **105** p. 8492.

42. Xu, L.B., Chen, W., Mulchandani, A., and Yan, Y.S., *Angew. Chem. Int. Ed.*, 2005. **44** p. 6009.

43. van Oss, C.J., *J. Adhes. Sci. Technol.*, 2002. **16** p. 669.

44. Pyo, M., Reynolds, J.R., Warren, L.F., and Marcy, H.O., *Synth. Met.*, 1994. **68** p. 71.

45. Chatterjee, J., *J. Colloid Interface Sci.*, 2003. **259** p. 139.

46. Santiago, J.M., Keffer, D.J., and Counce, R.M., *Langmuir*, 2006. **22** p. 5358.

47. Lee, M.-H., *Mol. Cryst. Liq. Cryst.*, 1998. **316** p. 329.

48. Liu, M.J., Tzou, K., and Gregory, R.V., *Synth. Met.*, 1994. **63** p. 67.

CHAPTER 5

IMPLEMENTATION OF POLYPYRROLE INTO MICRODEVICES FOR FLUID CONTROL

5.1 Introduction

The previous chapter investigated the use of polypyrrole doped with dodecylbenzenesulfonate (PPy.DBS) for controlling the shape and dimensions of dichloromethane droplets. This shape change was based on dynamically controlling the expulsion and incorporation of surfactant into and from the polymer, respectively, upon redox switching. This chapter investigates implementing PPy.DBS into practical applications for controlling the flow of fluid on the microscale, using both continuous flow channel-based configurations and discrete droplet-based microdevices.

5.1.1 Fluid movement in microdevices

Microfluidic devices have found application in many sectors, ranging from biopharmaceutical analysis, environmental and food monitoring, clinical diagnostics and biomedical research. One of the long term goals in the field of microfluidics is to create low power, portable/autonomous analytical devices that can be used at point-of-need, thereby eliminating time consuming sample transport for laboratory analysis procedures at centralised facilities. A key challenge in the realisation of these devices is the ability to control the movement of fluids and fluid components within the microfluidic device. This has been discussed in detail in Chapter 1, Section 1.4. Conducting polymers have proved useful for fluid control on the microscale due to a significant change in their properties upon application of a small potential (ca. 5 V) [1-3], as discussed in Chapter 1, Section 1.4.3.2.

5.1.2 Dynamic contact angle analysis of polypyrrole

Wilhelmy balance tensiometry is a useful characterisation method which is sensitive to minute changes in surface composition. It has been found to be the most accurate and reproducible method for determining advancing and receding contact angles [4, 5] and

has been described in detail in Chapter 1, Section 1.1.2.4.2. Surprisingly, there has been relatively little reported on the use of the Wilhelmy technique for characterisation of conducting polymers, despite its widespread usage for analysis of conventional polymers and materials (see Chapter 1, Section 1.2.5 for a summary of wettability studies on conducting polymers). Hence further investigation of the dynamic wettability properties of polypyrrole in the doped and de-doped states is warranted.

5.1.3 Chapter Aims

This work was carried out with the intention of designing simple, proof-of-concept devices illustrating the use of conducting polymers to induce and control fluid movement in microfluidic devices by manipulating the surface wettability of PPy-coated substrates using *in-situ* electrochemical redox switching. The designs utilise the two main paradigms in microfluidic device configurations; that is, channel-based and droplet-based fluid control. The initial goal of this work was to demonstrate that altering the oxidation state of a conducting polymer induced a change in its wettability which could be exploited for fluid movement. To investigate this aim, electrochemical redox switching of polypyrrole deposited in microchannels was carried out in a three-electrode cell configuration where the PPy-coated channel was the working electrode and the electrolyte was the fluid to be moved. Polypyrrole was employed due to its stability in air [6] and environmentally-benign nature. Dynamic contact angle analysis of polypyrrole was carried out using Wilhelmy balance tensiometry to determine polymers suitable for fluid movement in microfluidic channels. Two different dopants were investigated, namely sodium dodecylbenzenesulfonate (NaDBS; Figure 1) and sodium *para*-toluenesulfonate (NapTS; Figure 2). Interesting wetting properties of DBS have been observed to arise in a similar wettability-switch based on polyaniline doped with dodecylbenzenesulfonic acid (PAn.DBSA), as a result of the surfactant nature of

the dopant [1, 2]. PPy.pTS was investigated for comparison of electrochemical and wettability characteristics, due to the similarity in molecular structure of the dopants.

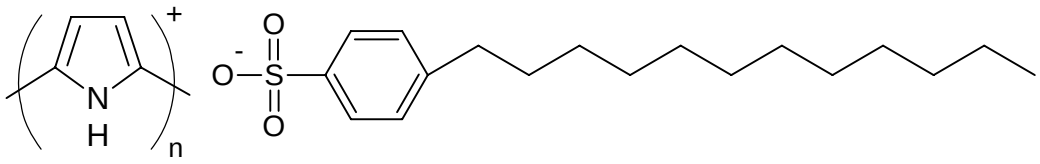

Figure 1. Structure of polypyrrole doped with dodecylbenzenesulfonate (PPy.DBS).

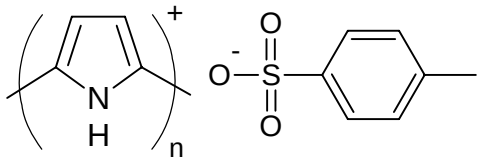

Figure 2. Structure of polypyrrole doped with *p*-toluenesulfonate (PPy.pTS).

An attempt to control the position of liquids on the surface of PPy.DBS *in air* was briefly pursued, using the integrated trilayer PPy.DBS-coated PVDF membrane device described in Chapter 4, with the aim of fully integrating the electrochemical cell by incorporation of electrolyte into the pores of the PVDF membrane. Subsequent research into controlling the flow of electrolyte through the same integrated trilayer membrane in surrounding external electrolyte was carried out by employing dichloromethane drop as a valve upon *in-situ* redox switching of PPy.DBS.

The objectives of this chapter may therefore be summarised as follows:

- To characterise and compare the dynamic wetting properties of PPy.DBS and PPy.pTS in the oxidised and reduced states with a view to identifying suitable polymers for controlling the position of fluids in microdevices using channel-based and droplet based configurations.
- To test the effectiveness of platinum-coated microchannels as substrates for polypyrrole by electrochemical characterisation.

- To implement polypyrrole into microchannels using a three-electrode cell configuration where the polymer is the working electrode for *in-situ* electrochemically-induced movement of the electrolyte upon reduction of the polymer.
- To investigate the integrated trilayer PPy.DBS-coated Pt-PVDF membrane configuration using an electrolyte which enables *in-situ* electrochemical redox switching and thus fluid control in air.
- To investigate the usefulness of PPy.DBS-coated Pt-PVDF membrane coupled with the dramatic surfactant-induced dimension change of dichloromethane droplets upon redox-switching the polymer for a simple flow-through valve, using the insight gained in the previous chapter.

A brief experimental section will be followed by a presentation of a combined results and discussion section. A summary of the simple, proof-of-concept devices presented and suggestions for future work will follow.

5.2 Experimental methods

5.2.1 Reagents and materials

Additional materials and reagents are described in Chapter 2, Section 2.2. NaDBS and NapTS were used as electrolytes and provided the anionic dopants for polypyrrole (PPy), forming PPy.DBS and PPy.pTS, respectively. Platinum wire (Goodfellow Metals Ltd.) of 500 μm diameter was cut into 5 cm pieces for use in dynamic contact angle measurements. The wires were heated under a Bunsen flame prior to deposition of polypyrrole, in order to remove any excess polymer or organic material and ensure a clean surface was obtained.

The substrate used for microchannel fabrication was 1.5 mm thick polymethylmethacrylate (PMMA) sheets (Radionics, Ireland). PMMA chips were cut to size (10 x 33 mm) using a CO_2 laser and microchannels were milled to 700, 500 and 300 μm in width and 2.5 cm in length. Channel depths of both 350 μm and 100 μm were investigated. Channels were platinised using the Dynavac sputter coater described in Chapter 2, to enable electrochemical deposition of polypyrrole directly into the microchannel and to establish electrical contact to the deposited polymer. A sputtering current of 30 mA and an Argon pressure of 2×10^{-3} mbar were applied for 10 min. The resistance of the platinised channel was found to be approximately 150 Ω over a 1 cm length. PMMA chips without channels were also platinised on all surfaces (denoted Pt-PMMA) to form substrates for the dynamic contact angle analyses of PPy.DBS and PPy.pTS.

5.2.2 Electrochemical deposition

The electrochemical deposition cell is described in Chapter 2. Deposition solutions containing 0.2 M Py in 0.2 M NaDBS or 0.2 M NapTS dopant were degassed for 10 min prior to use and a blanket of nitrogen maintained over the solution during deposition. Polymer films were thoroughly washed under a stream of deionised water and dried under a gentle nitrogen stream. PPy.DBS and PPy.pTS were prepared in the oxidised state by potentiostatic methods. A constant potential of +0.9 V was used for preparing polymer for dynamic contact angle analyses and a potential of +0.55 V was used to prepare smoother polymers for channel-based fluid movement. A platinum counter electrode and Ag/AgCl reference electrode (in 3.0 M KCl) were used, against which all potentials in this chapter are reported. The thickness of the films were quantified by the amount of charge passed during the polymerisation per surface area

unit and was expressed in C/mm^2. Polymers were typically deposited on all substrates until 0.5 mC/mm^2 of charge was passed, corresponding to a thickness of approximately 300 nm [7].

5.2.3 Preparation of solid polymer ionic liquid electrolyte for fluid movement using trilayer devices

The formation of solid polymer ionic liquid electrolyte (PILE) in the pores of Pt-PVDF membrane for the investigation of droplet movement using an integrated solid polymer electrolyte was achieved as follows. Ionic liquid 1-ethyl-3-methylimidazolium bis(trifluoromethyl) sulfonylimide (EMI.TFSI) was produced in our laboratories according to previously published procedures [8]. Methyl methacrylate (MMA), tetraethylene glycol diacrylate (TEGDA) and benzoyl peroxide (BPO) were used as received from Sigma. 0.3 g MMA plus 0.03 g TEGDA was added to 2.3 mL of EMI.TFSI and stirred well. 0.01 g BPO inhibitor was added to the mixture, which was poured over a piece of platinised PVDF membrane and sealed between two glass plates to keep the membrane flat and PILE production even. The glass plate-membrane-electrolyte unit was placed in metal container filled with water, which was heated at 80 ° C for 2 hours in order for polymerisation of the methyl methacrylate to occur. PPy.DBS was subsequently deposited on either side of the platinised PVDF membrane by application of 1.0 mA/cm^2 for 90 s on the working electrode side (with known pore sizes) and 180 s on the counter electrode side from an aqueous solution containing 0.2 M Py and 0.2 M NaDBS, forming the trilayer structure shown in Figure 3; namely PPy.DBS-Pt-PVDF/PILE-Pt-PPy.DBS. MilliQ water was used to rinse the films after deposition as acetonitrile was found to dry out the electrolyte.

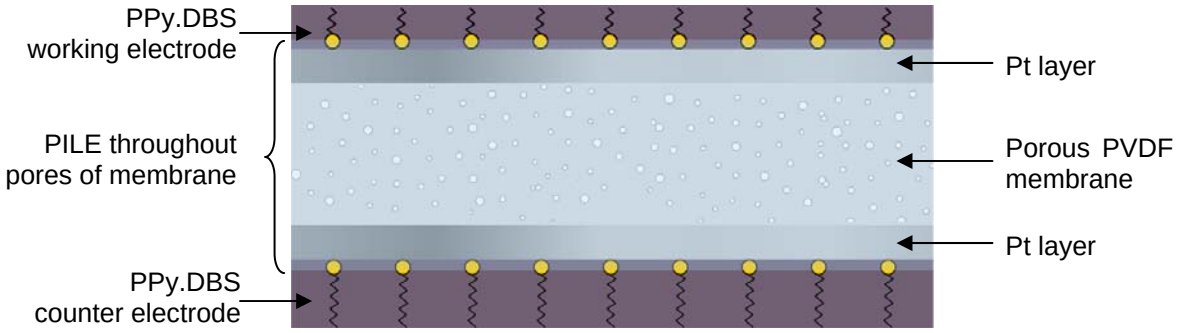

Figure 3. Integrated trilayer electrochemical cell configuration: PPy.DBS deposited on both sides of Pt-PVDF membrane to form a working electrode (1 mA/cm^2, 90s) and a thicker counter electrode (1 mA/cm^2, 180s). The pale blue square over the pores of the membrane and the Pt layers is indicative of the solid polymer ionic liquid electrolyte (PILE), which enables the cell to operate without an external aqueous electrolyte.

5.2.4 Electrochemical characterisations

The electrochemical instrumentation employed for the majority of the channel-based work was detailed in Chapter 2. Additionally, electrochemical polymerisation and characterisations of polymers for dynamic contact angle analyses as well as the integrated trilayer PPy.DBS-coated PVDF membrane for flow-control were performed using a CH Instruments Model 660 Electrochemical Workstation and a conventional three-electrode cell. These studies were carried out in the laboratories of Prof. Dermot Diamond at the National Centre for Sensor Research, Dublin City University, Ireland, in conjunction with Dr. Shannon Stitzel and Sarah Brady (channel-based studies) and Dr. Yanzhe Wu (droplet-valve studies).

Platinised microchannels were characterised by cyclic voltammetry between 0 V and +0.65 V in a solution containing 5 mM $K_3Fe(CN)_6$ and 0.5 M KCl. Polypyrrole-coated microchannels were subsequently characterised by cyclic voltammetry between –1.0 V to +0.65 V in a 0.1 M KCl. The scan rates used for the afore-mentioned characterisations were 50 and 100 mV/s, respectively.

5.2.5 Dynamic contact angle measurements

Advancing and receding contact angle measurements were carried out using a Cahn DCA-315 dynamic contact angle analyser employing Win-DCA software. A stage speed of 24.5 μm/s and an immersion depth of 10 mm were utilised with a dwell time of 3 minutes in between immersion cycles. The water probe was replaced with fresh MilliQ water between cycles, to ensure the surface tension of the water had not been altered by any migration of the dopant upon immersion. A water surface tension value of 72.8 mJ/m^2 was used for all measurements of polypyrrole in the oxidised state. Contact angles of polypyrrole films on Pt-PMMA were measured in water in the oxidised (as-deposited) state. Analysis of reduced films, prepared by electrochemically reducing the polymer for 180 s at -1.0 V, were attempted; however the platinum coatings were observed to lift off the smooth PMMA surface at these potentials, rendering the electrochemically reduced films unsuitable for contact angle measurement. Dynamic contact angle measurements of PPy in the oxidised and reduced state were subsequently carried out on Pt wire. For oxidised films, water was used as the liquid probe for freshly deposited polymer. For reduced films, polypyrrole was chemically reduced in a concentrated solution of hydrazine monohydrate then dried under a nitrogen stream. The liquid probe used for contact angle measurements was a 1.0 M solution of hydrazine monohydrate (surface tension of 72.7 mJ/m^2), to ensure the polymer remained in a reduced state throughout the measurement.

5.2.6 Water head of pressure measurement

The water head of pressure (measured in mm) required to move fluid through a 700 μm wide, 100 μm deep platinised microfluidic channel was measured. The channel was sealed with a PMMA covering lid with two holes at either end of the channel for the inlet and outlet of water. The lid was sealed tightly to the channel using clamps. High

vacuum grease was used around the channel to ensure a water-tight seal. A rubber hose with one end submerged in a vial of water was connected to the channel via one of the holes in the PMMA lid. The vial of water was lifted using a z-stage and the height at which water flowed out the end of the channel recorded.

5.2.7 Cell configurations for electrochemically-induced fluid movement using polypyrrole-coated microchannels

The movement of electrolyte fluid along polypyrrole-coated microfluidic channels was initially investigated using a vertical configuration (350 μm deep), where the open microchannel (i.e. no covering lid) working electrode was held vertically in a cell containing electrolyte (i.e. the fluid to be moved), a Ag/AgCl reference electrode (in 3.0 M KCl) and a platinum mesh counter electrode. Subsequently, a configuration where the working electrode was held horizontally was investigated, as shown in Figure 4. Channel depths of 350 μm were used for vertically-configured fluid movement, while 100 μm deep channels were used for horizontally-configured studies, with the effect of channel aspect ratio on resulting fluid movement noted.

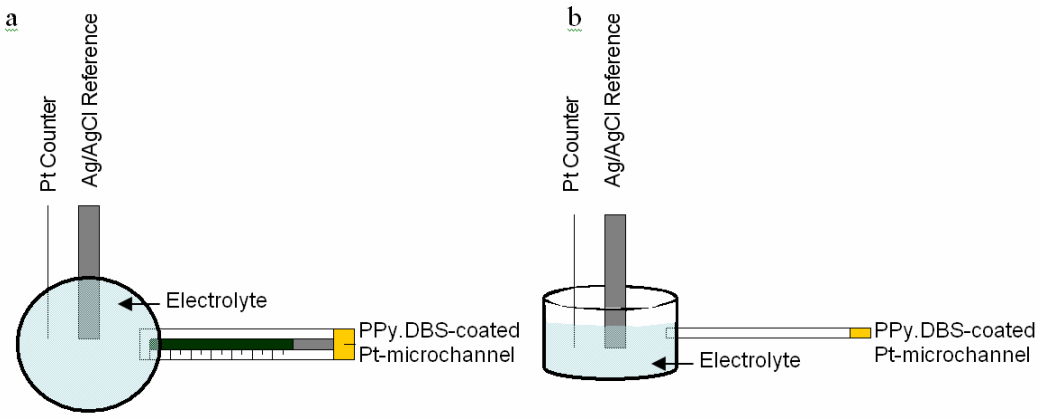

Figure 4. Schematic of three-electrode cell for studying fluid control in the horizontal configuration: a) top view and b) side view. The working electrode was a PPy.DBS-coated microchannel milled in PMMA (700 μm wide, 100 μm deep and 2.5 cm long). Fluid movement of KCl electrolyte along the microchannel was investigated upon application of a reducing potential (-0.8 V *vs*. Ag/AgCl).

5.2.8 Flow control using PPy.DBS-coated Pt-PVDF membrane

The flow of electrolyte through the porous integrated trilayer PPy.DBS-coated Pt-PVDF membrane was controlled by the dimension change of immiscible dichloromethane drops upon *in-situ* redox switching using the instrumentation shown in Figure 5. The trilayer device was secured above a platform with a 2 mm diameter hole. The platform was mounted on a microbalance in a three-electrode cell configuration and the potential was switched, causing the dichloromethane droplet (~ 3 μL) to spread (-0.8 V *vs*. Ag/AgCl) and contract (+0.6 V *vs*. Ag/AgCl). The change in the amount of electrolyte passing through the membrane was measured using a microbalance as the droplet valve was opened or closed.

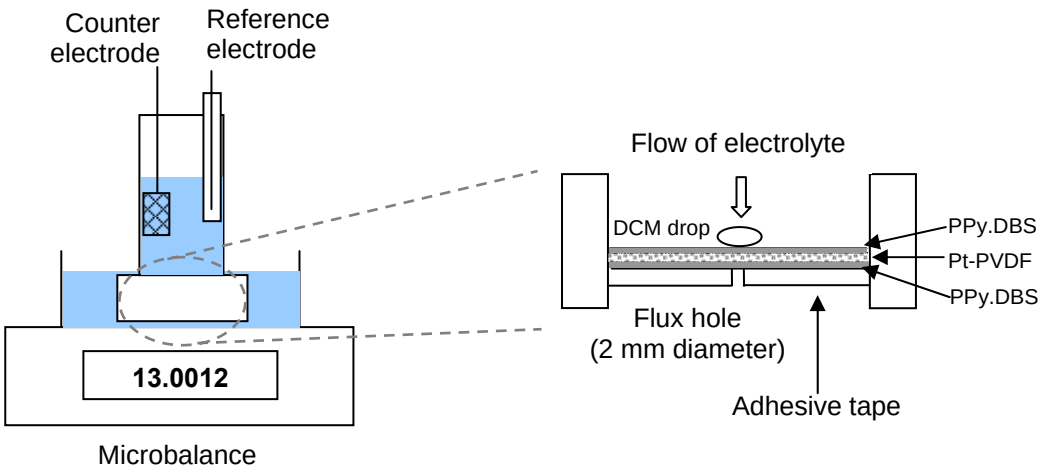

Figure 5. Schematic of configuration to measure flow control of electrolyte through a PPy.DBS-coated PVDF membrane through a 2 mm diameter hole using a dichloromethane droplet (~3 μL) as a valve. The PPy.DBS-coated PVDF membrane working electrode was connected in a three-electrode cell configuration with a Pt mesh counter electrode and Ag/AgCl reference electrode in 0.1 M KCl electrolyte. The cell was placed on a microbalance which measured the change in flow rate of electrolyte upon switching the potential from +0.60 V (drop contracted, flow permitted) and –0.80 V (drop spread, flow blocked).

5.3 Results and Discussion

Two configurations for controlling fluid flow in microdevices are presented in this chapter, namely channel-based and droplet-based fluid control. These two paradigms each have their associated benefits and disadvantages. Channel-based microfluidics, widely used due to their simplicity in design, manufacture and wide applicability, will be discussed in Section 5.3.1. This work was aimed at designing a simple, proof-of-concept device capable of moving microliters of fluids in microchannels at low voltages. PMMA was used as the channel substrate due its low-cost and ease with which channels may be fabricated in it. Droplet-based microfluidics, often referred to as digital microfluidics [9-12], have found increasing use in recent years due to the benefits associated with being reconfigurable as well as having scalable architecture, and will be discussed in Sections 5.3.2 and 5.3.3.

5.3.1 Fluid movement using polypyrrole-coated microchannels

5.3.1.1 Optical and electrochemical characterisations

5.3.1.1.1 Pt-coated microchannels

The microfabricated channels were coated with a thin layer of platinum in order to establish electrical contact to the entire polymer and ensure the preparation of an even polymer layer with consistent morphology. Channels with small dimensions (< 10 μm) are frequently used in microfluidic devices to exploit the advantageous forces which exist upon miniaturisation. However, to ensure the electrochemistry of the conducting polymer in this proof-of-concept device was not compromised by the lack of diffusion into the channel at smaller dimensions and for ease of fluid motion detection, larger channel widths were investigated, namely 700, 500 and 300 μm.

The ability of the platinised channel to function as an effective working electrode was tested using cyclic voltammetry of the well-known $Fe(CN)_6^{4-}/Fe(CN)_6^{3-}$ redox couple. The resulting curves were of the general shape to be expected (Figure 6). Peaks occurred at +0.231 V (cathodic) and +0.302 V (anodic) for Pt wire; +0.184 V (cathodic) and +0.341 V (anodic) for 700 μm width channels; +0.169 V (cathodic) and +0.348 V (anodic) for 500 μm width channels and +0.063 V (cathodic) and +0.443 V (anodic) for 300 μm width channels, as detailed in Table 1. Slower scan rates (1 – 10 mV/s) were found to result in more idealised responses, whereas faster scan rates resulted in peak broadening. Cyclic voltammograms for channels of all widths in comparison to Pt wire using a scan rate of 50 mV/s are shown in Figure 6. 700 μm wide Pt-channels were found to have similar electrochemical properties to the ideal Pt-wire, while 500 μm and 300 μm wide channels deviated more significantly from ideality (Figure 6 inset).

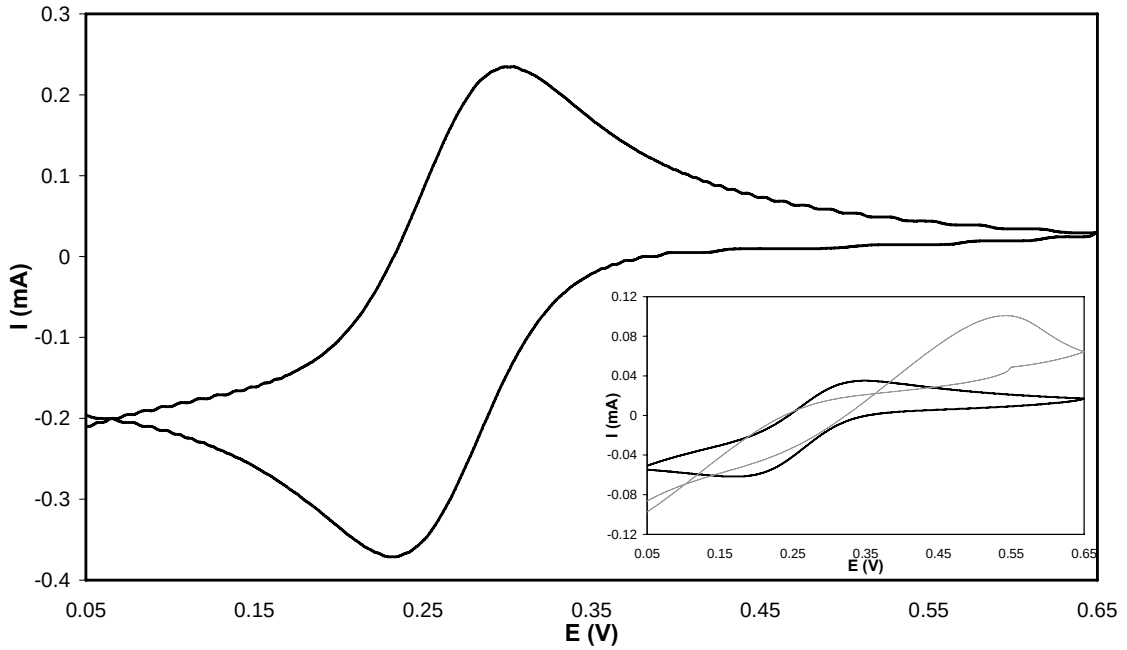

Figure 6. Main figure*:* Cyclic voltammogram of a 500 μm diameter platinum wire (heavy line) and a 700 μm width platinised channel (light line) in 5 mM $K_3Fe(CN)_6$ and 1.0 M KCl *vs*.Ag/AgCl using a scan rate of 50 mV/s. Inset: Cyclic voltammograms of 500 μm (heavy line) and 300 μm (light line) width channels in 5 mM $K_3Fe(CN)_6$ and 1.0 M KCl *vs*.Ag/AgCl using a scan rate of 50 mV/s.

The broadening and shifting of peaks to higher anodic/lower cathodic potentials upon investigating narrower channel dimensions is believed to be due to the lack of diffusion into narrower channels leading to non-ideal responses. The peak separation of approximately 150 mV for the 700 μm width channel suggested that this coating was more resistive than the solid platinum wire (peak separation of ~70 mV). The 500 and 300 μm width channels deviated from the response of the platinum wire, evidenced by increased peak separation and broadened, less well-defined peaks (Figure 6). Hence the 700 μm channels were used in all further fluid movement investigations.

Table 1. Oxidation (E_{ox}) and reduction (E_{red}) potentials for Pt wire and Pt-coated microchannels of varying widths cycled in 5 mM $K_3Fe(CN)_6$ in 0.5 M KCl at 50 mV/s.

	E_{ox} (V)	E_{red} (V)	Peak separation (mV)
Pt wire	0.302	0.231	71
700 μm channel	0.341	0.184	157
500 μm channel	0.348	0.169	179
300 μm channel	0.443	0.063	380

5.3.1.1.2 PPy-coated Pt-microchannels

Polypyrrole was electrodeposited into 700 μm wide Pt-microchannels using a potentiostatic method, which has been found to yield polymers with more reproducible wetting properties in dynamic contact angle studies [13]. Chronoamperograms recorded during growth of both PPy.DBS and PPy.pTS used in these initial wettability and contact angle characterisations at +0.9 V *vs*. Ag/AgCl revealed a gradual increase in current with time, indicating the deposition of a conducting layer. Subsequent detailed fluid movement studies employed PPy.DBS which had been deposited into Pt-

microchannels at a lower potential (+0.55 V *vs*. Ag/AgCl) in order to obtain a smoother polymer layer. Visual inspection using an optical microscope revealed a thin green layer of PPy deposited along the length of the channel (shown for PPy.DBS in Figure 7).

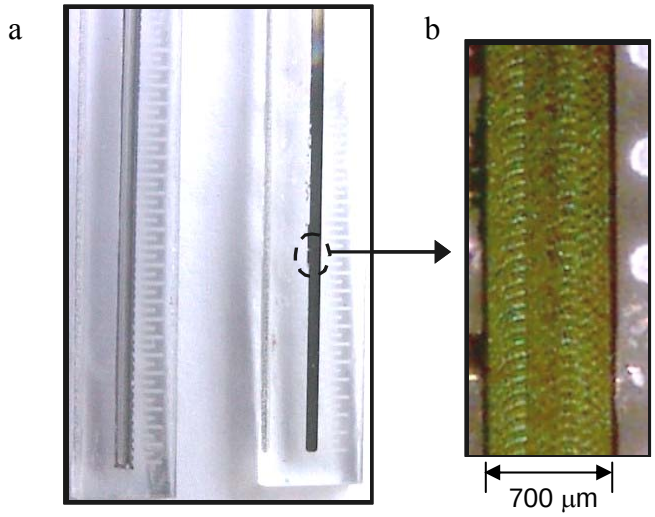

Figure 7. a) Optical image of platinised channel (left) and PPy.DBS-coated channel (right) of width 700 μm depth ca. 100 μm. Graduated markings in left-hand side image are 0.5 mm. b) Zoomed image of PPy.DBS-coated channel.

Scanning electron microscopy (SEM) images revealed an even coating of the polymer on the platinised microchannel (Figure 8). The surface was roughened due to the milling process, with the machined grooves evident in the Inset of Figure 8.

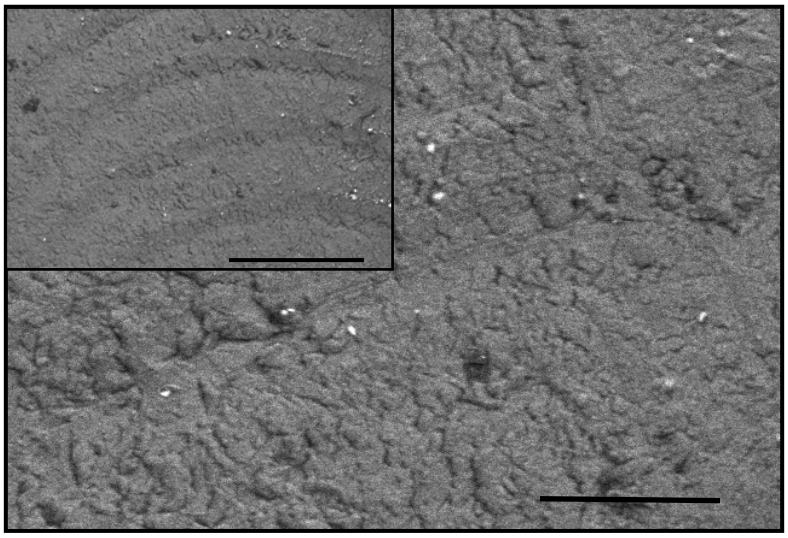

Figure 8. Main image: SEM images of PPy.DBS-coated microchannel. Main image: 12000 x zoom; scale bar represents 25 μm. Inset: 450x zoom; scale bar represents 100 μm.

Cyclic voltammetry was used to investigate the electrochemistry of polypyrrole-coated microchannels. Cyclic voltammograms of PPy.DBS-coated microchannels in 0.1 M KCl (Figure 9) revealed the polymer underwent well-defined and reversible oxidation and reduction processes, attributable to the predominant cation motion into and out of the polymer as a result of the immobile nature of the large DBS anion. The redox couple at -0.65 V and -0.35 V (*vs*. Ag/AgCl) corresponds to both the insertion of cations into the polymer and expulsion of cations into the electrolyte, respectively, as has been previously observed for PPy.DBS [14, 15], and indicated the microchannel did not compromise the electrochemistry of the polymer.

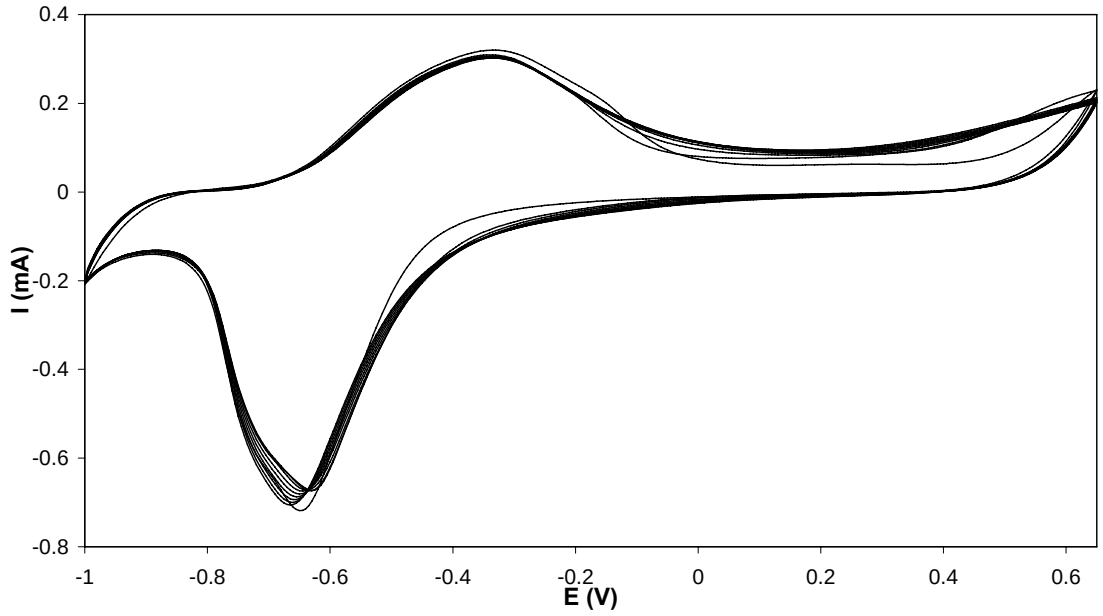

Figure 9. Cyclic voltammogram of 700 μm channel coated with PPy.DBS in 0.1 M KCl; potential limits: -1.0 to +0.65 V; scan rate = 100 mV s^{-1} *vs.* Ag/AgCl; 10 cycles.

Cyclic voltammetry of PPy.pTS-coated microchannels in 0.1 M KCl (Figure 10) revealed a well-defined cathodic peak at -0.75 V (*vs*. Ag/AgCl) and an anodic peak at ca. -0.35 V (*vs*. Ag/AgCl). PPy.pTS has been reported to undergo two reduction processes in aqueous solutions, corresponding to two doping sites in the polymer; one

associated with the doping of counter-ions located between PPy layers and another associated with the insertion of cations from solution to balance the charge on anions in the PPy layers [16]. The shape of the cyclic voltammograms was found to depend on the nature of the electrolyte and the solution pH. Only one redox couple was clearly evident in the present study, corresponding to the motion of solution cations into and out of the polymer located in the PPy layers (as opposed to in between the polymer layers).

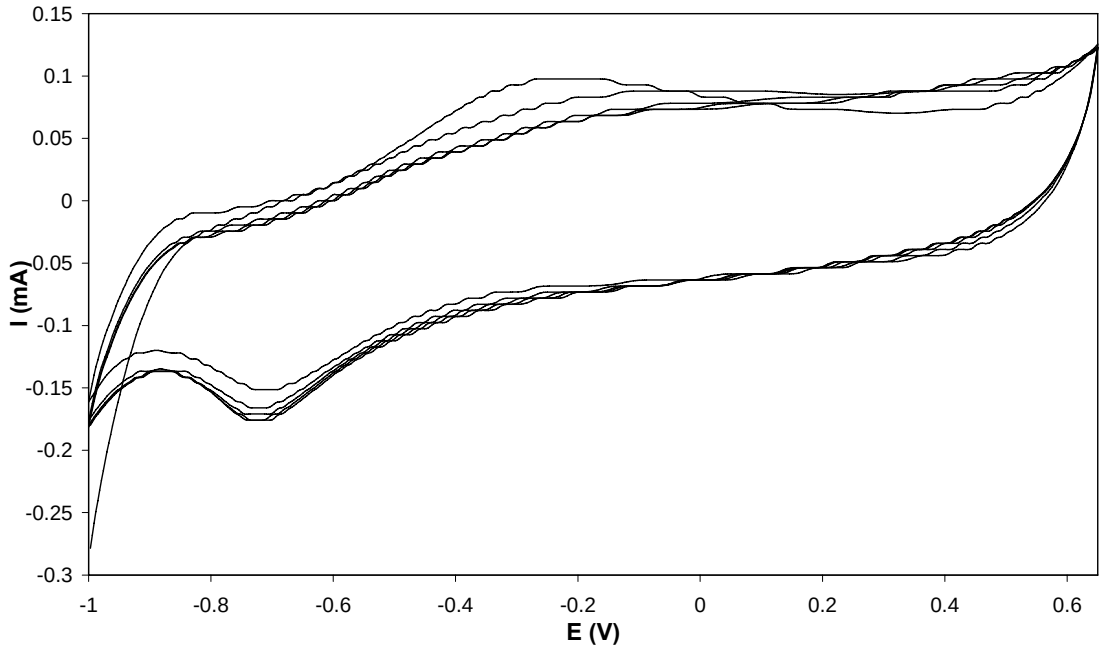

Figure 10. Cyclic voltammogram of 700 μm channel coated with PPy.pTS in 0.1 M KCl; potential limits: -1.0 to +0.65 V; scan rate = 100 mV s^{-1} *vs.* Ag/AgCl; 5 cycles shown.

Thus cyclic voltammetry revealed that the electrochemical integrity of PPy.DBS and PPy.pTS was not compromised by fabrication in microchannels, suggesting that they should function well as working electrodes when subsequently investigated for fluid movement capability (Section 5.3.1.3). The change in polypyrrole wettability upon varying the oxidation state was characterised by dynamic contact angle analyses.

5.3.1.2 Characterisation of polypyrrole by dynamic contact angle analyses

In order to study wettability changes associated with redox switching the polymer, dynamic contact angle analysis using Wilhelmy balance tensiometry was performed. Advancing (θ_a) and receding (θ_r) contact angles were used as a measure of the polymers' wettability and the tendency of the liquid to adhere to the polymer, respectively. Two immersion/emersion cycles were carried out, as the θ_a and θ_r measured have been found to vary significantly depending on whether the surface was dry or had been previously wet [13]. Results were the average of at least three films for each polymer, oxidation state and substrate. The as-deposited films were taken to be indicative of oxidised polymer, as PPy has been found to auto-oxidise in ambient conditions [6].

5.3.1.2.1 PPy-coated Pt-PMMA

Advancing and receding contact angles were initially measured on bare PMMA surfaces (i.e. with no channel milled) which had been platinised on all faces and coated with polypyrrole. The Pt-coating was observed to be compromised upon application of a reducing potential, rendering it unsuitable for contact angle analyses. Hence dynamic wetting data for oxidised polypyrrole on Pt-PMMA will be discussed in this section. Contact angles for oxidised PPy.DBS and PPy.pTS deposited on Pt-PMMA are presented in Table 2, namely the first (θ_{a1}) and second (θ_{a2}) immersion cycles, first (θ_{r1}) and second (θ_{r2}) emersion cycles, and the hysteresis ($\Delta\theta = \theta_a - \theta_r$) values. Oxidised PPy.DBS and PPy.pTS were both found to have high water θ_{a1} and θ_{a2} values, ranging from 80 – 89 ° (Table 2). The hydrophobic nature of these data may be understood by consideration of the dopant structures and orientation when the polymer is oxidised. The polar sulfonate heads should be buried in the PPy layers upon oxidation to maintain charge neutrality. This in turn would cause the non-polar methyl and dodecyl groups of

pTS and DBS, respectively, to reorient so that they were facing the polymer-solution interface, leading to the high advancing contact angles observed.

The receding angles were similar for both emersion cycles of each polymer (i.e. 39 ° and 33 ° for PPy.pTS; 16 and 23 ° for PPy.DBS), indicating the water adhered to the polymer reasonably well. This behaviour may be explained by the pTS and DBS anions changing orientation upon wetting so that the polar sulfonate head faced outwards, increasing the hydrophilicity of the polymer during the emersion cycle. The greater adhesion (i.e. lower θ_r values) of water to oxidised PPy.DBS than to PPy.pTS may be due to differences such as the degree of doping, polymer morphology, density and porosity.

Table 2. Dynamic water contact angle (°) of PPy.DBS and PPy.pTS films on platinised PMMA in as-deposited (oxidised) states.

	Cycle 1 Avg θ_{a1}	**Cycle 1 Avg θ_{r1}**	**$\Delta\theta_1$**	**Cycle 2 Avg θ_{a2}**	**Cycle 2 Avg θ_{r2}**	**$\Delta\theta_2$**
PPy.DBS (ox)	80 ± 16	16 ± 5	64	88 ± 7	23 ± 3	65
PPy.pTS (ox)	89 ± 1	39 ± 2	50	84 ± 1	33 ± 4	51

The hystereses between the advancing and receding angles was almost identical for the first and second cycles for both dopants, and were similar to each other in value, i.e $\Delta\theta_1$ and $\Delta\theta_2$ ca. 65 ° for PPy.DBS, and $\Delta\theta_1$ and $\Delta\theta_2$ ca. 51 ° for PPy.pTS. These observations indicated that there was little change in the polymer composition between the first and second immersion cycles for both PPy.DBS and PPy.pTS. This consistency was in contrast to observations for polyterthiophene (PTTh) in Chapter 3, where the oxidised polymer was found to interact strongly with water upon repeated wetting (i.e.

the 'watermark effect'). This difference was believed to be due to the tendency of PTTh to auto-reduce, while PPy is more stable in the oxidised state.

It is worth noting that the water probe into which the polymer samples were dipped was replaced with fresh MilliQ water during the dwell time in the program cycle, as it had been observed that the instrument was often unable to calculate the zero depth of immersion when measuring the second cycle. This was presumably due to small amounts of dopant molecules entering the water during the force measurement and locally changing the water surface tension. Significantly better reproducibility was obtained when fresh water was used as the liquid probe for the second immersion cycle.

As previously mentioned, attempts to measure the contact angle of electrochemically reduced polypyrrole on Pt-PMMA were thwarted by the fact that the platinum coating was observed to crack and lift off at the potentials applied, prior to dynamic contact angle analysis being carried out. Since dynamic contact angle techniques are extremely sensitive to heterogeneities in surface composition, Pt wire was pursued as an alternative substrate for wettability analyses for oxidised and reduced polypyrrole.

5.3.1.2.2 PPy-coated Pt wire

Dynamic contact angle measurements of PPy.DBS and PPy.pTS were carried out on Pt wire with a diameter of 500 μm, similar to the width of the microchannels (700 μm). Measurements on oxidised polypyrrole were again carried out using water as a probe liquid as this should maintain the oxidised state. For the reduced films, fresh as-deposited polymer was dipped in a solution of concentrated hydrazine to ensure the complete reduction, then contact angle analyses were carried out in 1.0 M hydrazine solution to maintain the reduced state of the polymer throughout the measurement. The

similarity in surface tension of the reductant solution (72.7 mJ/m^2) to pure water (72.8 mJ/m^2) indicated that the presence of the reductant had little effect on the surface tension value and enabled a direct comparison of the oxidised and reduced polymers. Contact angles for the reduced and oxidised forms of PPy.DBS and PPy.pTS deposited on Pt wire for immersion and emersion cycles are presented in Table 3, along with hysteresis values. These results are discussed below for PPy.DBS, followed by PPy.pTS. The results for oxidised PPy.DBS and PPy.pTS on Pt wire (θ_{a1} and θ_{a2} all between 91 – 95 °) were very similar to those on Pt-PMMA (80 – 89 °; Table 2), confirming the relevance of these measurements on Pt wire for implementation of polymers into Pt-PMMA microchannels.

Table 3. Dynamic contact angle (°) of PPy.DBS and PPy.pTS films on platinum wire in as-deposited (oxidised) and reduced states.

	Cycle 1 Avg θ_{a1}	**Cycle 1 Avg θ_{r1}**	**$\Delta\theta_1$**	**Cycle 2 Avg θ_{a2}**	**Cycle 2 Avg θ_{r2}**	**$\Delta\theta_2$**
PPy.DBS (ox)	95 ± 0	14 ± 8	81	95 ± 0	16 ± 1	79
PPy.DBS (red)	69 ± 8	35 ± 4	34	82 ± 1	35 ± 4	47
PPy.pTS (ox)	91 ± 1	38 ± 12	53	93 ± 4	32 ± 6	61
PPy.pTS (red)	89 ± 7	47 ± 0	42	88 ± 3	42 ± 2	46

N.B. Water was used as a probe for oxidised films. 1.0 M hydrazine monohydrate was used as a probe liquid for reduced films to ensure the polymer stayed in the reduced state throughout the measurement.

PPy.DBS

The high contact angle of oxidised PPy (95 °) was again attributable to the orientation of the DBS dopant causing the hydrophobic tail to be exposed to the polymer–water interface (Figure 11 a). Reduction of PPy.DBS resulted in a decrease in the first cycle advancing angle of PPy.DBS (95 to 69 °). This value increased during the dwell time between cycles (180 s) to 82 °, suggesting a gradual re-oxidation of the polymer in air was occurring. The increased wettability of PPy.DBS upon reduction may be explained by a combination of the reorientation of DBS chains at the polymer-water interface as a result of expulsion of the charged sulfate group, as well as cation ingression of NH_4^+ from the reductant solution into the polymer to maintain charge neutrality for immobile DBS groups (Figure 11 b), as was observed in Chapter 4, Section 4.3.1.2.1. The charged nature of the polymer backbone increases the polymers' affinity for water and results in a more hydrophilic surface, as evidenced by the lower contact angle (69 °). This mechanism is supported by *ex-situ* contact angle measurements of reduced and oxidised PPy.DBS reported in the previous chapter, which followed a similar trend, although the values for reduced (18 °) and oxidised (72 °) PPy.DBS on Pt-sheet in Chapter 4 were somewhat lower than the present results. This difference may be due to the different contact angle analysis technique used, as the previous chapter employed sessile drop goniometry, in addition to electrochemical methods used for reduction, rather than chemical reduction in the present study. A similar increase in polymer wettability was observed for the analogous polymer PAn.DBSA upon reduction in studies by Isaksson *et al*. [1, 2].

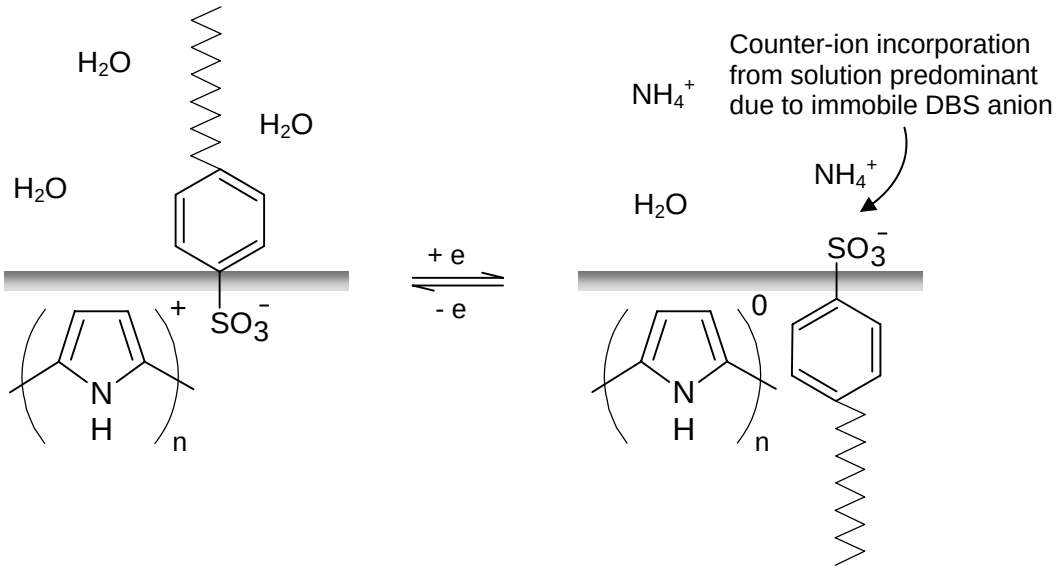

Figure 11. Idealised schematic of DBS configuration at polymer-water interface under oxidising and reducing conditions. Incorporation of NH_4^+ counter-ion from the reductant solution (1.0 M N_2H_4) to main charge neutrality due to the immobile DBS anion enmeshed in the polymer was expected.

The hysteresis was significantly smaller for reduced PPy.DBS ($\Delta\theta_1$ = 34° and $\Delta\theta_2$ = 47 °) as compared to oxidised PPy.DBS ($\Delta\theta_1$ = 81 °and $\Delta\theta_2$ = 79 °), indicating water adhered less to the reduced polymer. The low θ_r observed for the oxidised form (θ_{r1} = 14 °, θ_{r2} = 16 °) indicated that once wet, this material adhered more strongly to the water molecules – this was not surprising given the dynamic nature of these polymer surfaces and the charged nature of the polymer backbone in the oxidised state. The uncharged nature of the reduced polymer presumably contributes to the higher θ_r recorded in the reduced state.

Force-distance curves recorded during advancing and receding contact angle measurements are a visual representation of the change in surface composition during immersion cycles. They are shown for PPy.DBS in the oxidised and reduced states in Figure 12 and Figure 13, respectively, where the force reported is the weight force.

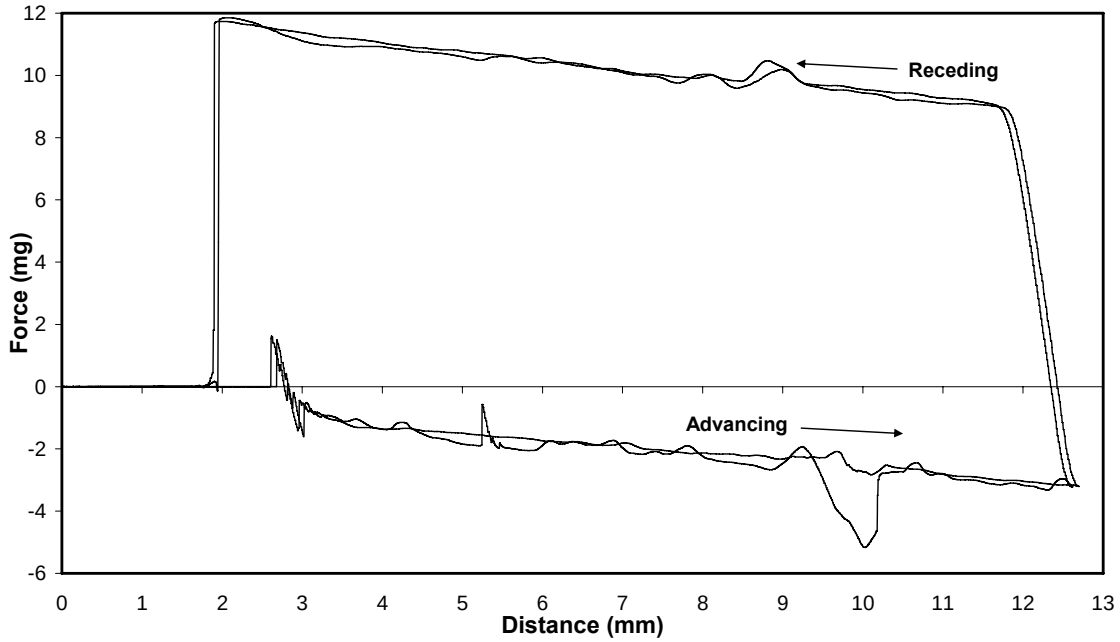

Figure 12. Weight force-distance curve for as-deposited (oxidised) PPy.DBS using water as a probe liquid. The first and second cycles are overlaid as shown.

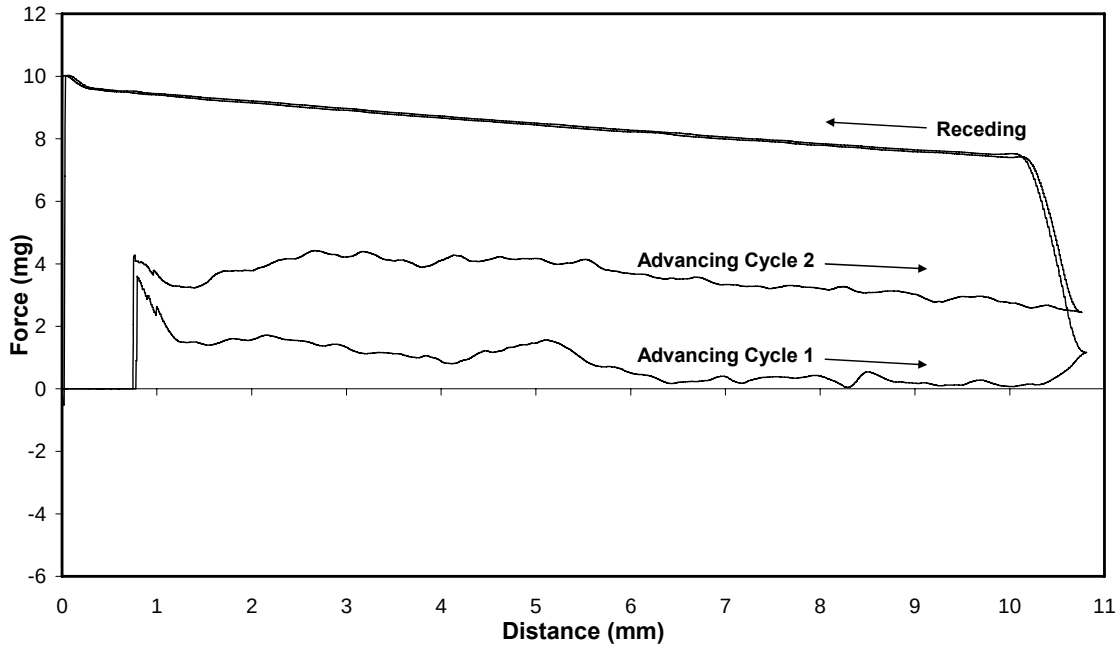

Figure 13. Weight force-distance curve for chemically reduced PPy.DBS (pre-reduced in concentrated hydrazine), using 1.0 M hydrazine as a probe liquid. The first and second cycles are as shown.

The advancing curve of both the oxidised and chemically reduced polymer was more variable than the receding curve. This variability may be attributed to local variations in

surface roughness or chemical inhomogeneity due to the nature of the surfactant dopant pinning the liquid as the polymer was immersed. The receding curves were smoother as a consequence of the pulling motion upon emersion. Also of note is the variation in the plots between the first and second cycles, which is of use in determining the difference in wetting behaviour of completely dry and previously wet surfaces. The force-distance curves for oxidised PPy.DBS (Figure 12) were overlaid for both the advancing and receding edge, a point which is reflected in the similar contact angles (θ_{a1} and θ_{a2} were both 95 °, while θ_{r1} and θ_{r2} were 14 and 16 °, respectively). Conversely, the difference in the advancing contact angle for reduced PPy.DBS (68 and 82 ° for the first and second cycles, respectively) was a result of the polymer re-oxidising in air between cycles, as previously mentioned.

PPy.pTS

PPy.pTS exhibited different wetting behaviour from PPy.DBS in that the reduction of the polymer appeared to have little effect on the contact angles observed. Both oxidised and reduced films possessed similar advancing contact angles (ranging from 88 – 93 ° for all films) while the receding contact angles were slightly higher for the reduced films compared to the oxidised PPy.pTS (Table 3). Force-distance curves for PPy.pTS were overlaid (not shown here), reflecting the similar wetting properties of the oxidised and reduced films. The similar wetting hysteresis values for PPy.pTS, (i.e. $\Delta\theta_1$ = 53 ° and $\Delta\theta_2$ = 61 ° for oxidised PPy.pTS; $\Delta\theta_1$ = 42 ° and $\Delta\theta_2$ = 46 ° for reduced PPy.pTS) suggested water interacted similarly with both oxidised and reduced PPy.pTS. It is known that pTS does not completely leave the polymer during reduction, so the orientation of pTS molecules and the formation of cation-pTS pairs both contribute to the similarity of the reduced PPy.pTS contact angle data compared to the oxidised form.

Comparison of dynamic wetting data to literature

The dynamic wetting data obtained for PPy.DBS and PPy.pTS were compared to those reported by Teasdale [13] and Azioune *et al*. [17] for polypyrrole doped with the similarly structured dodecylsulfate anion (PPy.DS) and PPy.pTS, as shown in Table 4. Dynamic contact angle analyses were performed using Wilhelmy balance tensiometry in the study by Teasdale, as in the present chapter, while Azioune employed captive drop goniometry to determine dynamic wetting data (as described in Chapter 1, Section 1.1.2.4.1), as was used in Chapter 3 for the determination of PTTh dynamic wetting properties. Only the oxidised polymers were reported in their publications. The contact angles from the oxidised films in the present study are repeated in Table 4 for ease of reference.

Table 4. Comparison of dynamic water contact angles (°) of as-deposited (oxidised) PPy.DBS and PPy.pTS as-deposited (oxidised) state from the present study with PPy.DS and PPy.pTS from Teasdale [13] and Azioune *et al.* [17].

	Cycle 1 Avg θ_{a1}	Cycle 1 Avg θ_{r1}	$\Delta\theta_1$	Cycle 2 Avg θ_{a2}	Cycle 2 Avg θ_{r2}	$\Delta\theta_2$	Thick (μm)	Ref
PPy.DBS (ox)	95 ± 0	14 ± 8	81	95 ± 0	16 ± 1	79	0.3[a]	[b]
PPy.DS (ox)	81	12	69	72	10	62	~2[c]	[13]
	59 ± 3	43 ± 7	16	*x*	*x*	*x*	0.1[d]	[17]
PPy.pTS (ox)	91 ± 1	38 ± 12	53	93 ± 4	32 ± 6	61	0.3[a]	[b]
	74	12	62	50	10	40	~2[c]	[13]
	77 ± 4	50 ± 6	27	*x*	*x*	*x*	0.1[d]	[17]

a: Potentiostatic deposition onto Pt wire to a thickness of ca. 300 nm was used; b: the present study; c: galvanostatic deposition onto Pt sheet. Thickness was not reported but was estimated to be ~ 2 μm using relation from Bay *et al*. [7] whereby 160 mC/cm^2 charge was passed per micron thickness of polymer; d: galvanostatic deposition onto Pt-coated glass slides to a thickness of 100 nm; *x:* indicates measurement was not reported.

The wetting data obtained for oxidised PPy.DBS in this study (θ_{a1} = 95 °, θ_{r1} = 14 °) corresponds well to those reported by Teasdale [13] for PPy.DS on Pt sheet (θ_{a1} = 81 °, θ_{r1} = 12 °). A comparison with contact angles reported by Azioune *et al*. [17] (θ_{a1} = 59 °, θ_{r1} = 43 °) reveal markedly different wetting properties. This may be due to the use of captive drop goniometry, as opposed to Wilhelmy balance tensiometry, which is thought not to fully probe the extent of the wetting properties of a material [4, 5]. There is less of a correlation of the present results (θ_{a1} = 91 °, θ_{r2} = 38 °) with literature values for PPy.pTS, namely θ_{a1} = 74 ° and θ_{r2} = 12 ° in Teasdale's study [13] and θ_{a1} = 77 ° and θ_{r2} = 49 ° in the work of Azioune *et al*. [17]. The source of these discrepancies is not known, but is indicative of the complex interplay present between dopant, substrate, species concentration and thickness.

The current study investigated pre-oxidised or pre-reduced polymer using a probe liquid that would maintain the polymer's oxidation state (i.e. water for oxidised polypyrrole and hydrazine for reduced polypyrrole). Perhaps a more relevant method to probe the wetting characteristics of the oxidised or reduced polymer is to perform *in-situ* dynamic contact angle analyses. There are several reports of using this technique for conducting polymers in the literature. Dynamic contact angle analyses by Lee *et al*. [18-20] of polypyrrole with various dopants ($LiClO_4$, $(C_2H_5)_4NBF_4$, $LiCF_3SO_3$ and $LiBF_4$) were carried out using Wilhelmy balance tensiometry during *in-situ* electrochemical oxidation. An immediate increase in the force measured was observed, indicative of the increased interaction between the liquid and the polymer upon doping as the polymer became more polar, although this was found to be dependent on dopant. Reduction of polypyrrole resulted in a slow decrease in the wetting force observed, which may be explained by the expulsion of dopant being the limiting time factor. Similar *in-situ*

electrochemical contact angle measurements were carried out for poly-3-hexylthiophene (P3HT) and poly-(3,4-ethylenedioxythiophene) (PEDOT) in a study by Wang and co-workers [21]. The contact angle for P3HT decreased upon oxidation and increased upon reduction, whereas vapour phase polymerised PEDOT behaved in the reverse fashion, decreasing in contact angle upon reduction. These trends were consistent with the overall hydrophobicity of the polymer backbones and the movement of charge during doping and dedoping. A similar dependence of polymer wettability on oxidation state was observed for polyaniline doped with hydrochloric acid (PAn.HCl) [22] using potential-controlled tensiometry. The application of a reducing potential caused an increase in the contact angle (i.e. decrease in wettability), whereas an oxidising potential saw a decrease in contact angle (increase in wettability). This effect was reversible and observable in the change of the solution meniscus height at the working electrode. These observations confirm the change in wettability of conducting polymers during *in-situ* electrochemical redox switching. This knowledge, coupled with the change in wettability of PPy.DBS upon reduction of the polymer in the present study, indicated PPy.DBS was suitable for investigating fluid control capabilities on the microscale. PPy.pTS was not investigated for fluid control capabilities as there was negligible change in the wetting properties between the oxidised and reduced polymers.

5.3.1.3 Electrochemically-induced fluid movement of electrolyte in PPy.DBS-coated microchannels

The wettability changes observed during dynamic contact angle analyses between the oxidised and the reduced form of PPy.DBS were translated into fluid movement of electrolyte solution by the application of a reducing potential to PPy.DBS-coated Pt-microchannels in a three-electrode cell configuration (detailed in Section 5.2.7).

5.3.1.3.1 Initial studies

Initial attempts at fluid movement involved a vertical configuration of the PPy.DBS-working electrode microchannel. The electrolyte was allowed to equilibrate in the channel prior to the application of a reducing potential, to ensure that any subsequent fluid movement observed was due to a change in PPy.DBS wettability. The electrolyte solution was observed to move up the channel upon application of -1.0 V (*vs*. Ag/AgCl) for 180 s pulse duration (Figure 14).

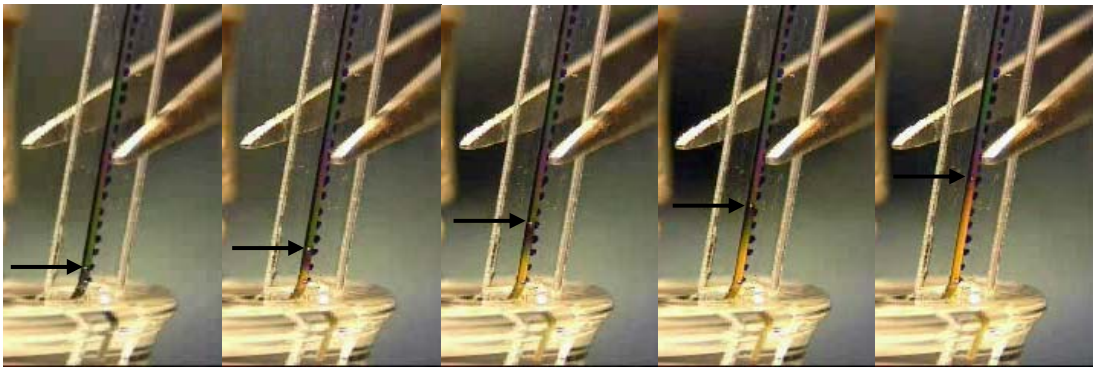

Figure 14. Sequential video images showing movement of 0.1 M KCl electrolyte along PPy.DBS-coated microchannel (700 μm width and 350 μm depth) under application of reducing potential (-1.0 V *vs*. Ag/AgCl for 180 s). Marking on channel edges represents 1 mm increments. Fluid position is indicated by arrow in consecutive images at t = 0, 2, 5, 10 and 30 s.

More rapid electrolyte motion was observed at first, followed by a significant slowing down towards the end of the 180 s reduction pulse. Electrolyte was observed to move over a distance of 9.5 ± 2.1 mm in 180 s when this experiment was carried out on several different microchannels, although the majority of the fluid motion was in the first 30 s. The yellow polymer film underneath the electrolyte in the channel was indicative of the reduced form of PPy.DBS. This fluid movement was believed to be a result of the increased wettability of reduced PPy.DBS, as predicted from the dynamic contact angle measurements in Section 5.3.1.2.2. Analogous control experiments

carried out with platinised microchannels (i.e no polypyrrole layer) also revealed electrolyte motion upon the application of a reducing potential. The distance moved by the electrolyte (ca. 7 mm) was slightly less than for PPy.DBS-coated channels. The electrolyte motion on the bare platinum channel was believed to be due to the electrocapillary effect, that is, the tendency of a liquid to increase its surface area with a metal upon the application of an electrical potential at an interface (shown for a metallic rod immersed in electrolyte solution in Figure 15) [23, 24]. The potential of zero charge (PZC) has been found to be 0.06 V (vs. Ag/AgCl) for PPy doped with $LiClO_4$ [20]. Therefore at potentials above and below this, such as when a negative reducing potential is applied during fluid movement, the relative surface tension decreases due to the existence of excess surface charge, and may have been partially responsible for the electrolyte movement observed on polymer-coated channels [20]. Satoh *et al*. [25] have used a similar approach to the present study to facilitate fluid movement in a 1 mm wide open-flow channel by application of a negative potential to the gold electrode. Through direct manipulation of the liquid interfacial tension using a three-electrode cell with auxiliary and counter electrodes, the advancing liquid front was observed to spread and move, as it attempted to establish a new equilibrium. An analogous effect is believed to be responsible for the electrolyte movement observed in uncoated Pt-microchannels in the present study.

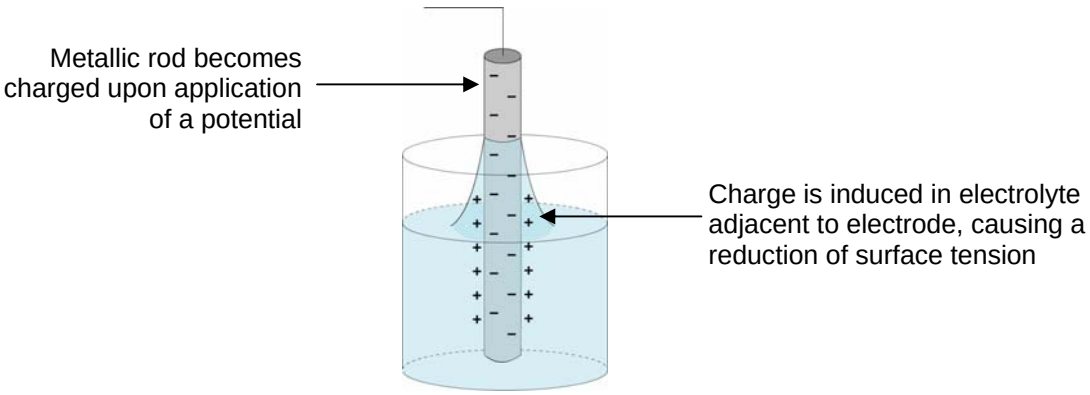

Figure 15. Schematic depicting the electrocapillary effect. Application of a negative potential to a metallic electrode reduces the surface tension of electrolyte adjacent, increasing the area of contact.

5.3.1.3.2 Quantitative study of electrolyte movement in PPy.DBS-coated microchannels

A more detailed, quantitative investigation into the extent of electrolyte movement upon PPy.DBS reduction and the factors affecting it, including electrolyte concentration and applied potential, was carried out using a horizontal configuration (detailed in Section 5.2.7, Figure 4). There was difficulty in gaining a clear image of fluid position using the vertical configuration, due to shadow masking the position of the fluid. This more in-depth study also coincided with utilising channels with a depth of 100 μm, as opposed to 350 μm in initial studies, as well as the use of a reducing potential of -0.8 V *vs*. Ag/AgCl. The pressure (in terms of water-head) required to move fluid through a platinised channel 700 μm wide and 100 μm deep was determined to be approximately 20 mm, suggesting there was little resistance to fluid flow through the channels.

Effect of electrolyte concentration

The effect of electrolyte concentration on the distance of fluid movement was investigated using 0.01 M, 0.1 M and 0.5 M KCl in both PPy.DBS-coated microchannels and control (uncoated) Pt-microchannels (Figure 16a and b, respectively). The greatest distance of fluid movement was achieved using 0.1 M KCl, which was observed to move 11.3 ± 2.9 mm along the horizontally-aligned channel. A concentration of 0.1 M KCl was therefore used in subsequent fluid movement characterisations. A small amount of fluid movement was observed using 0.1 M KCl for the platinised channels 3.8 ± 0.8 mm. This decrease in fluid movement distance on Pt-coated microchannels as compared to the 350 μm deep channels may been influenced by the decrease in channel aspect ratios [26]; however, the comparison between the distance of electrolyte movement for PPy.DBS-coated microchannels (11.3 ± 2.9 mm) and Pt-coated microchannels (3.8 ± 0.8 mm) using 100 μm deep channels

indicates the majority of the electrolyte movement was due to the change in wettability of PPy.DBS upon reduction, rather than the effect of the Pt coating (Figure 16).

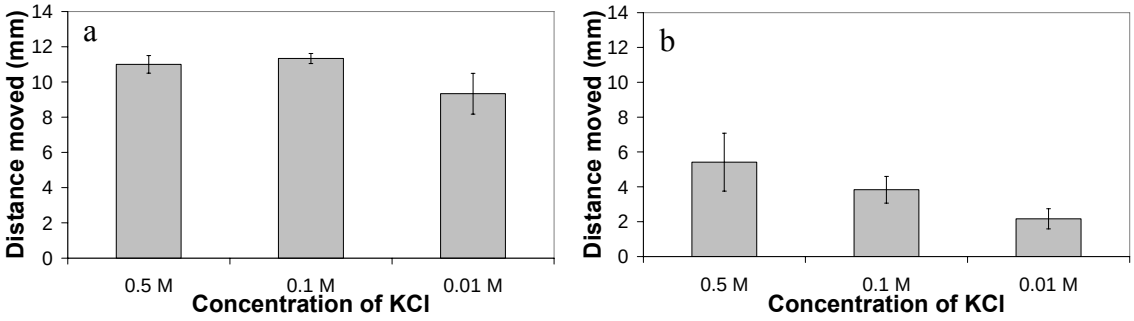

Figure 16. Distance of fluid movement (mm) with respect to KCl concentration on a) PPy.DBS-coated 700 μm wide, 100 μm deep platinised PMMA channels and b) control (non-polymer-coated) 700 μm wide, 100 μm deep platinised PMMA channels upon application of -0.8 V *vs.* Ag/AgCl.

The increase in distance of fluid movement upon increasing the concentration of the electrolyte (Figure 16b) is consistent with observations made by Sato and co-workers [27] that an increase in ionic concentration causes a reduction in liquid surface tension. This reduction in surface tension enabled an increase in the distance of fluid moved in Pt-coated channels. The fact that PPy.DBS-coated channels were not observed to exhibit a similar trend (Figure 16a) is indicative of the different mechanism responsible for electrolyte movement, namely the redox-induced wettability change.

Effect of applied potential

The effect of applied potential on the distance of fluid movement was also investigated. Using 0.1 M KCl, different potentials were applied to the polymer and the distance of fluid movement as well as the charge passed was determined (Figure 17). With potentials more positive or equal to -0.2 V the amount of charge passed and fluid movement was minimal. However at -0.5 V, where the onset of polymer reduction is expected (refer to cyclic voltammogram in Figure 9), a significant increase in charge

generation and fluid flow was observed. This movement is attributed to the increase in PPy.DBS hydrophilicity, as discussed in Section 5.3.1.2.2.

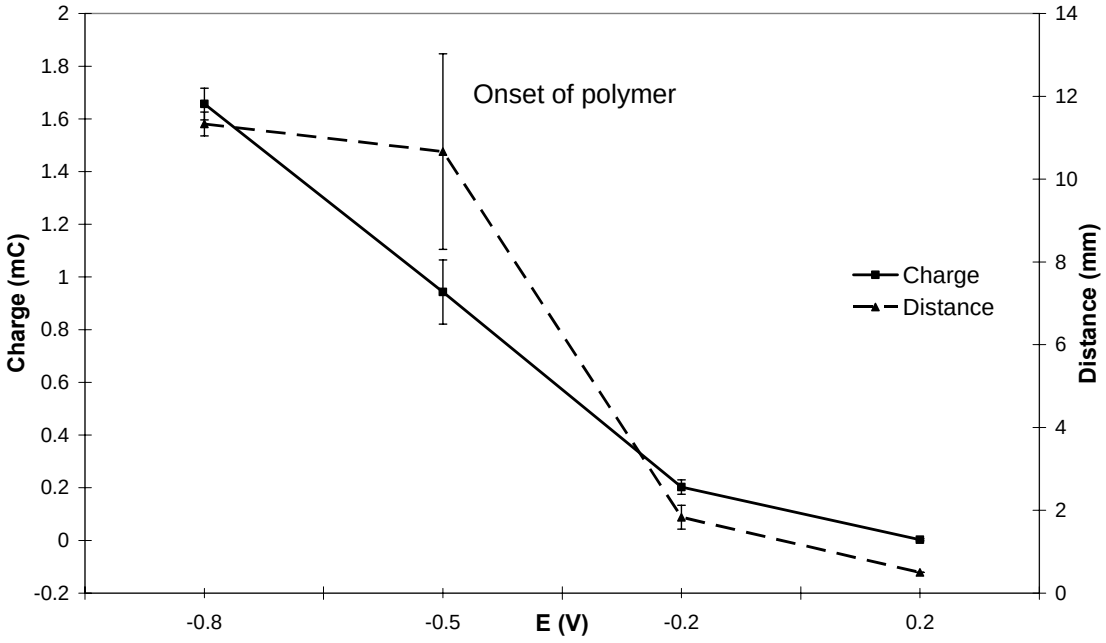

Figure 17. Plot of distance of fluid (0.1 M KCl) moved and charged passed over a 120 s period vs. applied potential in PPy.DBS coated channel. Results were carried out in at least triplicate with standard deviations shown.

It was noted that fluid movement was not continuous but rather occurred in jumps. This mechanism could be explained by the fluid moving in discrete segments. Presumably sufficient fluid was initially moved along the channel by capillary action to 'wet' the hydrophobic polymer. Upon exposure to electrolyte, the wetted polymer surface was reduced, enabling further fluid to move along the channel via capillary action. The sequential exposure of new polymer to the electrolyte and electrochemical transformation moved the hydrophobic/hydrophilic barrier along the channel. It is also possible that minute amounts of dopant were expelled from the polymer, as observed in Chapter 4 for the *in-situ* redox switching of PPy.DBS with dichloromethane drops on the surface. This release would cause a local reduction in the liquid surface tension, causing it to spread and contact the next segment of polymer, thereby translating the

liquid along the channel. The application of a positive potential stopped fluid flow but did not reverse it, as the dynamic contact angle data have shown that once wet, the water molecules adhere well to the polymer surface (Table 3). Application of potentials more negative than -0.8 V were found to damage the channel, with the coating lifting off the channel surface.

5.3.1.4 Drawbacks of the open channel configuration for fluid movement

Despite providing a convincing example of fluid control using PPy.DBS in microchannles, the methods presented in this work were subject to some short-comings. The open channel configuration, which was necessary to enable a complete electrochemical cell with the external Pt mesh counter electrode and reference electrode in the current design, would not be widely applicable to many applications. Incorporation of the electrochemical components of the cell into the microchannels itself may realise true encapsulation of the electrochemistry driving the fluid movement. The nature of the air-liquid interface and adhesion of the liquid being moved by the polymer once it is wet, means that this type of fluid control is best suited for microdevices where once-off filling is required. Flows of electrolyte 'fingers' along the corners of microchannels preceding the bulk flow was also observed on occasion, which would cause problems for the accurate delivery of liquids. Despite their lack of applicability in the current configuration, it is hoped that the principles presented in this simple proof-of-concept device form the platform for future studies utilising the tuneable wettability of conducting polymers upon the application of a small potential, for low power, low voltage fluid control so that microfluidic devices may be truly miniaturised. Similar to these aims, but using the cell configuration discussed in Chapter 4, the use of PPy.DBS-coated membranes to control the flow of liquids will be discussed in Sections 5.3.2 and 5.3.3.

5.3.2 Integrated electrochemical device for fluid movement *in air*

The realisation of a device for fluid control in air (i.e. without surrounding electrolyte) was one of the major objectives of this study. Evidence of the change in wettability of conducting polymers upon redox switching from ex-situ studies (Chapter 4, Section 4.3.1.2) and Wilhelmy balance tensiometry (present chapter, Section 5.3.1.2) was the driving force to design a device capable of fluid control without the need for external electrolyte. The PPy.DBS/Pt-PVDF membrane trilayer device described in Chapter 4 was adapted for the control of liquids resting on the polymer surface. The fabrication of the integrated trilayer configuration was described in Chapter 2 and was based on PPy trilayer actuators, where PPy.DBS layers coated on either side of the membrane acted as the working and counter electrodes [28-32]. The capacity of the membrane pores to hold electrolyte enabled a fully integrated electrochemical cell capable of working in air. The aim of this work was to generate a significant change in polymer wettability to control fluid movement on the polymer surface.

The ionic liquid EMI.TFSI was first chosen as an electrolyte for these studies, based on its suitability as an electrolyte for conducting polymer actuators [33]. The low volatility of EMI.TFSI meant that the electrochemical cell could potentially operate in air (without the need for the inert atmosphere of a glove box) for up to 1 million cycles without needing to replenish the electrolyte, due to the decreased incidence of nucleophilic attack on, and hydrolysis of, the polymer [34]. A potential difference of ±1.5 V applied in a two-electrode cell configuration enabled an analogous amount of charge to be passed as when a conventional three-electrode cell configuration with an external reference electrode and electrolyte were used; however at ±1.5 V for pulse lengths greater than a few seconds, the EMI.TFSI electrolyte was observed to electrolyse and over-oxidise the polymer. Hence a ±1.0 V potential was employed for

redox switching the polymer in air. Cyclic voltammograms of PPy.DBS-coated working and counter electrodes in the two-electrode configuration between -1 and +1 V revealed a lack of distinct redox couples present (Figure 18), despite the colour change of the working and counter electrodes indicating successful redox switching was occuring. This is believed to be due to the inherent difference in shape between two- and three-electrode cell configurations as a result of the absence of a reference electrode which monitored the actual potentials during redox switching [35].

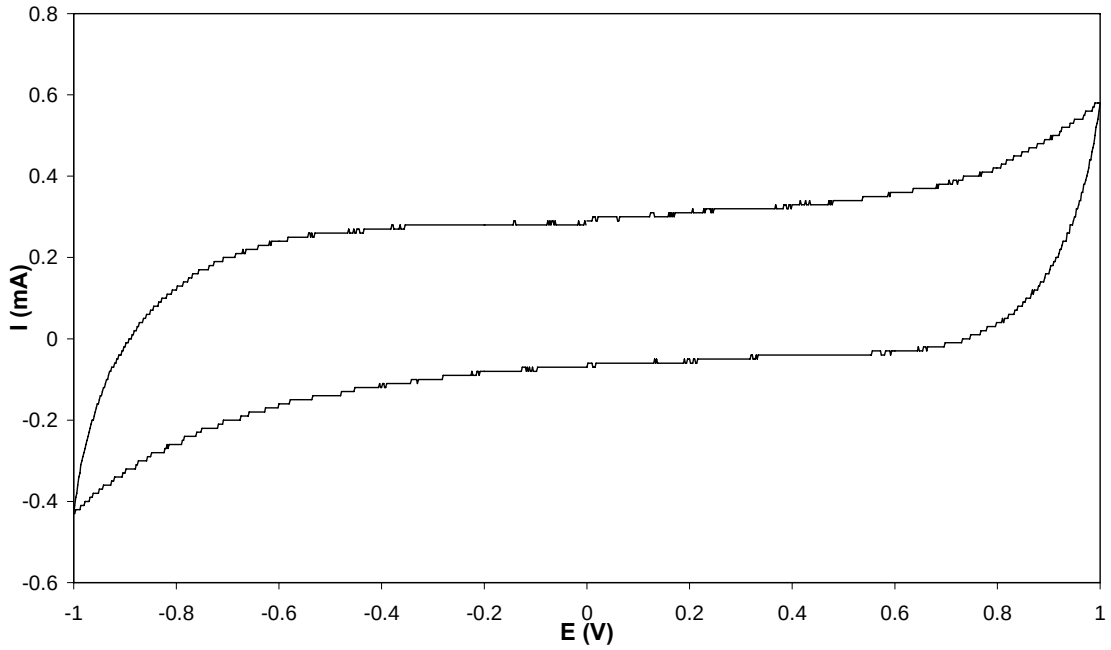

Figure 18. Cyclic voltammogram of integrated trilayer PPy.DBS-coated Pt-PVDF configuration, with PPy.DBS working electrode and counter electrodes (2-electrode cell) and ionic liquid electrolyte (EMI.TFSI). Scan between -1.0 to +1.0 V; scan rate = 50 mV/s. 5th cycle shown.

The power consumption of the integrated trilayer PPy.DBS-coated Pt-PVDF membrane configuration has been determined to be 0.359 mW/cm^2 [36]. This equates to ca. 50 μW when scale to the dimensions of a microchannel 700 μm in width and 2 cm in length, indicating this configuration should operate with low power consumption when implemented into practical devices.

Various liquids were tested on the surface of the integrated trilayer PPy.DBS-coated PVDF membrane/EMI.TFSI for fluid movement upon redox switching the integrated electrochemical cell in air. Interestingly, a water drop placed on the film surface while the PPy.DBS working electrode remained sessile while the polymer was in the oxidised state, then spread instantly upon the application of a reducing potential to the polymer. Further to this, a water drop was observed to spread and contract for at least 20 cycles on one occasion, although the contact angle of the water drop was extremely low and a 'pulsating' type motion was observed. However, these effects were typically inconsistent and irreproducible, and unpinning of drops from their original positions was not observed. This lack of unpinning was not surprising given the difficulty in gaining lateral droplet motion with an analogous configuration when the trilayer membrane configuration was immersed in surrounding electrolyte in Chapter 4, where the lower friction present in liquid-liquid systems would have acted to assist droplet unpinning [37]. As has been noted for polypyrrole in Section 5.3.1.2, once the polymer has been wet, water molecules adhere strongly to the polymer [38]. A similar phenomenon of droplet spreading was also observed in the wettability switch reported by Isaksson *et al*. [1] using PAn.DBSA, where water was observed to spread in the direction of the reduced polymer; although the spreading was not reported to be reversible.

The difficulty in fluid control was primarily due to the miscibility of the many fluids tested with the EMI.TFSI electrolyte. DCM (the fluid investigated in the previous chapter) was found to evaporate too quickly for a response upon redox-switching to be determined, as may have been predicted. Glycerol, silicone oil and ethylene glycol all exhibited no change in shape upon redox switching of the integrated trilayer cell in air, despite a colour change observed in the polymer indicating successful oxidation and

reduction was occurring. The thin layer of ionic liquid electrolyte could not be removed from the outer surface of the membrane and hence interacted with test liquids, which spread spontaneously and were unable to form discrete droplets on the polymer surface.

An alternative solid polymer ionic liquid electrolyte (PILE) was investigated with the aim of isolating the electrolyte from the fluid being moved. A schematic of the configuration is shown in Figure 3 and its fabrication was described in Section 5.2.3. The membrane was flexible and the presence of the PILE did not compromise the mechanical properties of the PVDF. Cyclic voltammetry was used to ascertain the stability of the PILE, prior to the deposition of PPy.DBS on the membrane surface for fluid movement studies (Figure 19). Stable and reproducible current responses indicated there was no decomposition of the electrolyte over many cycles, while the capacitive behaviour of the two-electrode integrated Pt-PVDF-PILE-PVDF-Pt configuration suggested the configuration should operate successfully as an electrolyte upon deposition of the polymer. PPy.DBS was thus electrodeposited on the working and counter electrodes of integrated membrane using a standard three-electrode cell, to test for fluid movement capabilities of this configuration. However, upon deposition of the PPy.DBS, the PVDF membrane became brittle, exhibiting poor mechanical properties and resistive behaviour. The cause for this was not known, however it rendered the device unable to be tested for fluid control in air. Further work carried out in this area would involve the incorporation of an electrolyte capable of producing successful redox switching of the polymer in air, as well as identifying a suitable substrate which may assist in overcoming droplet pinning, to gain translational motion of liquids resting on the electrode surface.

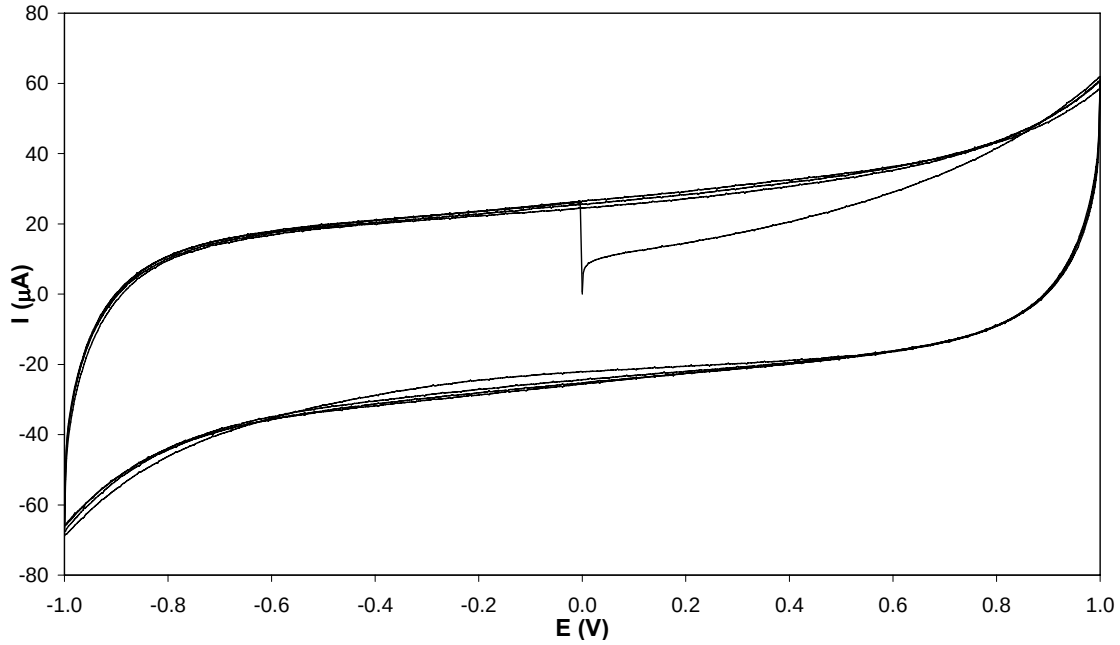

Figure 19. Cyclic voltammogram of Pt-PVDF membrane with polymer-ionic liquid electrolyte (PILE) in a two-electrode cell configuration, prior to the deposition of PPy.DBS on the electrodes. Potential scanned between -1.0 V to +1.0 V; scan rate 50 mV/v, 5 cycles.

The development of a device capable of moving any liquid upon application of a small voltage and with low power consumption, without the need for surrounding external electrolyte continues to be an interesting area of research, and is appealing due to its wide applicability in microfluidic devices for various applications. Such a device would prove to be an exciting contribution to the area of fluid control in microdevices. However, electrochemically-controlled changes in the properties of dichloromethane on PPy.DBS upon conventional redox switching in surrounding aqueous electrolyte also affords an alternate method of flow control in microdevices, and will be discussed in the following section.

5.3.3 Use of PPy.DBS-coated Pt-PVDF membrane and DCM drop as flow control valve

The trilayer *in-situ* electrochemical switching configuration described in Chapter 4, Section 4.3.3.1 for controlling DCM shape and dimensions was investigated as a simple valve in a proof-of-concept device for controlling the flow of electrolyte through PVDF

membrane. This work was pursued in light of the large change in dimensions of DCM droplets upon redox switching in external aqueous electrolyte. The idea was based on the hydrophobic DCM being able to block the flow of liquid under gravity through the PVDF membrane when the polymer was in the reduced state, while allowing liquid to pass through the porous membrane when the polymer was in the oxidised state. The instrumentation used to measure the flow is depicted in Figure 5 (Section 5.2.8). PPy.DBS-coated Pt-PVDF membrane connected as the working electrode in a three-electrode cell, where the counter electrode was either the integrated trilayer PPy.DBS counter electrode or an external Pt mesh in 0.1 M KCl (*vs.* Ag/AgCl).

Upon oxidation of the PPy.DBS working electrode, the immiscible DCM drop was in its original spherical-cap shape (Figure 20a) and electrolyte was able to flow through the membrane freely under pressure of the electrolyte (ca. 30 mm fluid-head). Upon reduction, the DCM droplet spread and blocked the flow of electrolyte through the membrane, as shown in Figure 20b.

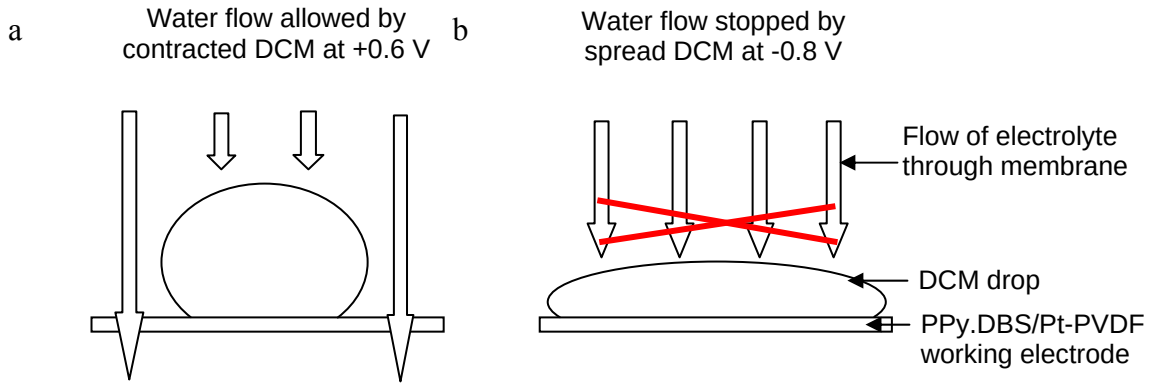

Figure 20. Schematic showing the change in flow of electrolyte under gravity through the porous PPy.DBS-Pt-PVDF membrane switching device detailed in Chapter 4. a) Application of an oxidising potential (+0.6 V *vs.*Ag/AgCl) to the PPy.DBS working electrode caused the DCM drop to contract and allow electrolyte to pass through the membrane under pressure of the electrolyte (ca. 30 mm fluid-head). b) Application of a reducing potential (-0.8 V *vs.*Ag/AgCl) to the PPy.DBS working electrode caused the DCM drop to spread and stop the flow of electrolyte through the membrane. Pt mesh counter electrode, Ag/AgCl reference electrode and microbalance not shown.

The flow rate of electrolyte through the membrane was reversibly controlled from 56 μg/s when the polymer was oxidised to 1 μg/s when the polymer was reduced, highlighting the effectiveness of this device to control electrolyte flow through the membrane (Figure 21). The results presented in Figure 21 were obtained by Dr. Yanzhe Wu in the laboratories of the National Centre for Sensor Research, Dublin City University.

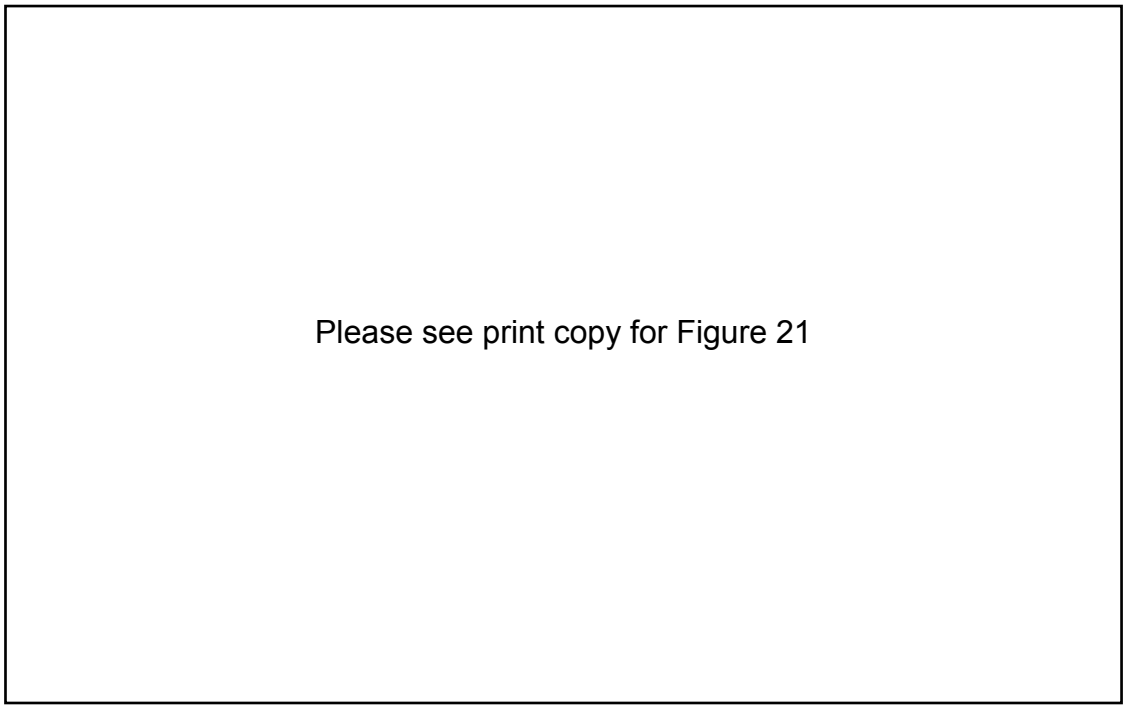

Figure 21. The change of electrolyte flow through PPy.DBS-coated Pt-PVDF membrane working electrode upon application of oxidising (+0.60 V *vs*. Ag/AgCl) and reducing (–0.80 V *vs*. Ag/AgCl) potentials using a dichloromethane droplet valve (weight of water evaporation: 0.05 mg/s)

Valves such as these may be employed in a microchannel configuration, providing a simple means of controlling fluid flow at a channel junction under a small potential (1.4 V *vs* Ag/AgCl) using a three-electrode cell. The presence of the integrated trilayer PPy.DBS counter electrode on the opposite side of the membrane to the working electrode may facilitate a fully-integrated device, without an external counter electrode or reference electrode, in future applications. A liquid microvalve has been recently shown to regulate the flow at a T-junction through electrowetting-induced surface

tension change in the droplet [39]. The control of flow through a porous membrane is also of interest in studies where the transport and separation of molecules through a membrane is required [40]. Hence the PPy.DBS-coated Pt-PVDF membrane DCM droplet valve holds great promise for devices where a low voltage means of controlling aqueous flow through a membrane is required. In future devices, the use of many drops carefully placed in an array-type configuration covering a greater area should allow a higher volume of fluid to be processed. Further research is being carried out in this area.

5.4 Conclusions

Exploitation of the change in wettability of PPy.DBS that exists upon *in-situ* electrochemical oxidation and reduction was carried out with the aim of developing simple, proof-of-concept devices demonstrating fluid control that may be employed in microfluidic devices. Wilhelmy balance tensiometry was used to assess the wettability of oxidised (as-deposited) and chemically reduced PPy.DBS and PPy.pTS on Pt wire. Dynamic contact angle analyses of PPy.pTS revealed little change in wettability upon reduction of the polymer (both oxidised and reduced films had contact angles of ca. 90°; Table 3), and was not investigated for fluid control capabilities. PPy.DBS however was observed to undergo an increase in wettability upon reduction, with the advancing water contact angle decreasing from ca. 95 ° to 69 °. This increase in PPy.DBS wettability was explained by the increased polarity of the polymer backbone upon cation immersion for charge neutrality in the reduced state, as well as reorientation of the surface-bound DBS groups. This principle was extended to investigate surface tension-induced fluidic movement in a 700 μm wide polymethylmethacrylate (PMMA) channel, sputter-coated with platinum and coated with electrochemically-deposited PPy.DBS on the surface. By applying a reducing potential to the channel, which was held both

perpendicularly and parallel to the liquid surface, electrolyte solution was seen to move along the polymer-coated channel. This mechanism may be useful to induce sample reagent mixing, and sample movement through a single-shot analytical device (e.g. clinical diagnostic test) using very low voltages. Continuing investigations will endeavour to utilise this principle to develop an electrochemically-actuated microfluidic pumping system.

During testing of the channel-based configuration, some of the considerations and factors involved when using conducting polymers for fluid movement on smaller scales became apparent. Electrode placement and removal of the electrochemistry from the fluid being moved was deemed to be important in the development of devices for moving non-specific liquids along polymer surfaces. An attempt to enable fluid movement without surrounding aqueous electrolyte was carried out using the integrated trilayer PPy.DBS-coated Pt-PVDF membrane configuration presented in Chapter 4, which was successfully used for changing the shape of immiscible DCM drops. Ionic liquid electrolyte and solid PILE composite were investigated, with both found to function successfully in the two-electrode cell configuration. Spreading of water drops upon the application of a reduced potential was observed when using EMI.TFSI electrolyte, although difficulty associated with droplet pinning and irreproducibility of drop motion were still an issue. The use of EMI.TFSI as an electrolyte was subject to shortcomings related to the miscibility of the fluid to be moved, as droplets typically spread spontaneously upon the ionic liquid and did not form discrete droplets with measurable contact angles on the polymer surface. Deposition of PPy.DBS onto the trilayer Pt-PVDF membrane containing PILE led to undesirable mechanical properties in the membrane, rendering the device unable to be explored for PPy.DBS-induced fluid movement. Further research into this area would involve identifying fully-integrated

electrolytes which would enable the positioning of liquids placed on the device surface in combination with a surface energy gradient in the polymer, controlled with the application of only a small voltage and with low power consumption.

Finally, PPy.DBS-coated Pt-PVDF membrane coupled with immiscible DCM droplets resting on the film surface, in a three-electrode cell configuration with surrounding aqueous electrolyte, were implemented as a simple valve for controlling the flow of electrolyte through the PVDF membrane. The amount of electrolyte passing through the porous membrane was controlled by exploiting the dramatic surfactant-induced change in DCM drop dimensions upon the application of oxidising and reducing pulses, detailed in Chapter 4. Such a microvalving system may prove useful for the control of liquids through membranes in transport studies, in addition to liquid valves and gates in microchannels that operate under the application of only a small potential. The integrated trilayer PPy.DBS counter electrode (on the opposite side of the membrane to the working electrode) may facilitate the complete integration of this configuration for use in future applications.

The demonstrations of fluid control using polypyrrole-coated substrates presented in this chapter should form the basis of devices which exhibit a substantial change in fluid position or flow upon the application of a small potential and with low power consumption. The interesting change in properties of PPy.DBS and indeed conducting polymers in general upon redox switching should lead to the realisation of interesting solutions to improve flow control on the microscale.

5.5 References

1. Isaksson, J., Tengstedt, C., Fahlman, M., Robinson, N., and Berggren, M., *Advanced Materials*, 2004. **16** p. 316.
2. Isaksson, J., Robinson, N.D., and Berggren, M., *Thin Solid Films*, 2006. **515** p. 2003.
3. Robinson, L., Hentzell, A., Robinson, N., Isaksson, J., and Berggren, M., *Lab Chip*, 2006. **6** p. 1277.
4. Lander, L.M., Siewierski, L.M., Brittain, W.J., and Vogler, E.A., *Langmuir*, 1993. **9** p. 2237.
5. Krishnan, A., Liu, Y.H., Cha, P., Woodward, R., Allara, D., and Vogler, E.A., *Colloids Surf., B*, 2005. **43** p. 95.
6. Maksymiuk, K., *Electroanalysis*, 2006. **18** p. 1537.
7. Bay, L., Mogensen, N., Skaarup, S., Sommer-Larsen, P., Jorgensen, M., and West, K., *Macromolecules*, 2002. **35** p. 9345.
8. Dong, Z., Mazurkiewicz, J., Kane-Maguire, L.A.P., and Wallace, G.G., *Green Chemistry (Submitted)*, 2007.
9. Fair, R., *Microfluid. Nanofluid.*, 2007. **3** p. 245.
10. Cho, S.K., Moon, H.J., and Kim, C.J., *J. Microelectromech. Syst.*, 2003. **12** p. 70.
11. Dubois, P., Marchand, G., Fouillet, Y., Berthier, J., Douki, T., Hassine, F., Gmouh, S., and Vaultier, M., *Anal. Chem.*, 2006. **78** p. 4909.
12. Fair, R.B., Khlystov, A., Tailor, T.D., Ivanov, V., Evans, R.D., Griffin, P.B., Srinivasan, V., Pamula, V.K., Pollack, M.G., and Zhou, J., *IEEE Des. Test Comput.*, 2007. **24** p. 10.

13. Teasdale, P.R., *Characterisation of the chemical properties of polypyrrole and polyaniline*, in *Intelligent Polymer Research Institute*. 1993, University of Wollongong: Wollongong.

14. Vidanapathirana, K.P., Careem, M.A., Skaarup, S., and West, K., *Solid State Ionics*, 2002. **154-155** p. 331.

15. Matencio, T., Depaoli, M.A., Peres, R.C.D., Torresi, R.M., and Detorresi, S.I.C., *Synth. Met.*, 1995. **72** p. 59.

16. Li, Y.F., Deng, B.H., He, G.F., Wang, R.Q., and Yang, C.H., *J. Appl. Polym. Sci.*, 2001. **79** p. 350.

17. Azioune, A., Chehimi, M.M., Miksa, B., Basinska, T., and Slomkowski, S., *Langmuir*, 2002. **18** p. 1150.

18. Lee, M.-H., Kim, S.S., Rhee, J.M., and Kang, Y., *Polymer (Korea)*, 1998. **22** p. 619.

19. Lee, M.-H., *Mol. Cryst. Liq. Cryst.*, 1998. **316** p. 329.

20. Lee, M.H., Kim, S.S., and Kang, Y., *Synth. Met.*, 1999. **101** p. 442.

21. Wang, X.J., Ederth, T., and Inganas, O., *Langmuir*, 2006. **22** p. 9287.

22. Hato, M., *Chem. Lett., Chem. Soc. Japan*, 1988 p. 1959.

23. Quilliet, C. and Berge, B., *Curr. Opin. Colloid Interface Sci.*, 2001. **6** p. 34.

24. Kedzierski, J. and Berry, S., *Langmuir*, 2006. **22** p. 5690.

25. Satoh, W., Loughran, M., and Suzuki, H., *J. Appl. Phys.*, 2004. **96** p. 835.

26. Ichikawa, N., Hosokawa, K., and Maeda, R., *J. Colloid Interface Sci.*, 2004. **280** p. 155.

27. Sato, M., Kudo, N., and Saito, M., *IEEE T. Ind. Appl.*, 1998. **34** p. 294.

28. Wu, Y., Alici, G., Spinks, G.M., and Wallace, G.G., *Synth. Met.*, 2006. **156** p. 1017.

29. Alici, G. and Huynh, N.N., *Sens. Actuators, A*, 2006. **132** p. 616.

30. Alici, G., Mui, B., and Cook, C., *Sens. Actuators, A*, 2006. **126** p. 396.

31. Fang, Y., Tan, X., Shen, Y., Xi, N., and Alici, G., *Submitted to Mater. Sci. Eng., C*, 2007.

32. Alici, G., Spinks, G., Huynh, N., Sarmadi, L., and Minato, R., *Bioinspir. Biomim.*, 2007. **2** p. S18.

33. Ding, J., Zhou, D.Z., Spinks, G., Wallace, G., Forsyth, S., Forsyth, M., and MacFarlane, D., *Chem. Mat.*, 2003. **15** p. 2392.

34. Lu, W., Fadeev, A.G., Qi, B.H., Smela, E., Mattes, B.R., Ding, J., Spinks, G.M., Mazurkiewicz, J., Zhou, D.Z., Wallace, G.G., MacFarlane, D.R., Forsyth, S.A., and Forsyth, M., *Science*, 2002. **297** p. 983.

35. Lewis, T.W., Spinks, G.M., Wallace, G.G., Mazzoldi, A., and De Rossi, D., *Synth. Met.*, 2001. **122** p. 379.

36. Wu, Y., *Unpublished results*, 2006.

37. Good, R.J., *Contact angle, wetting and adhesion: a critical review*, in *Contact angle, wettability and adhesion*, K.L. Mittal, Editor. 1993, VSP: Utrecht, The Netherlands. p. 3.

38. Teasdale, P.R. and Wallace, G.G., *Reactive Polymers*, 1995. **24** p. 157.

39. Mohseni, K. and Dolatabadi, A., *An electrowetting microvalve - Numerical simulation*, in *Interdisciplinary Transport Phenomena In The Space Sciences*. 2006. p. 415.

40. Zhou, D., Too, C.O., Wallace, G.G., Hodges, A.M., and Mau, A.W.H., *React. Funct. Polym.*, 2000. **45** p. 217.

CHAPTER 6

GENERAL CONCLUSIONS

The preceding chapters of this thesis aimed to explore the change in wettability of conducting polymers upon *in-situ* electrochemical redox switching, coupled with the favourable scaling effects of surface tension forces on the microscale, for interesting solutions to fluid control in microfluidic devices. In order to fulfil these aims, the factors influencing the wettability of conducting polymers were first investigated, and then polymers were implemented for fluid control in simple, dynamically-controlled microfluidic devices.

Wettability and surface energy measurements of polyterthiophenes were detailed in Chapter 3. The impact of various factors, including deposition substrate, polymer thickness, oxidation state and functionalisation of the polymer backbone were found to be important in determining the wetting properties of polyterthiophene. Dramatic differences in the wettability of as-deposited and reduced thick polyterthiophene films were evident across all substrates, attributable to the increased polarity of the oxidised polymer. Polymer thickness was also found to be important in determining polymer wetting properties, with thicker films being observed to be significantly rougher, which acted to enhance the wettability of the polymer. Chemical interaction of surface energy test liquids with polyterthiophene resulted in a lack of valid surface energy data, and as such a comparison into the effect of various factors on surface energy could not be carried out. Functionalisation of the polyterthiophene backbone with hydrophobic alkyl substituents caused a dramatic decrease in polymer wettability in comparison to unfunctionalised polyterthiophene, particularly for as-deposited films. The microstructured roughness of the polymer, coupled with the inherent hydrophobicity of the alkyl chains, acted to greatly decrease the polymer wettability. The interaction of water with polyterthiophene was of particular interest. The reduction potential pf this material was found to vary with film thickness, enabling atmospheric water to reduce

the surface layers of thicker polymers, while thinner polymers were maintained in the oxidised state due to their similar reduction potential to water. Some generalised considerations for characterising the wetting properties of conducting polymers were proposed, including the use of smooth polymers to avoid roughness-enhanced wettability as well as the use of surface energy test liquids which do not interact with the polymer.

Chapter 4 detailed the development of simple, *in-situ* electrochemical fluid control systems using polypyrrole doped with the surfactant dodecylbenzenesulfonate (PPy.DBS). A dramatic increase in the wettability of polymer removed from the electrochemical cell was observed upon reduction, attributable to dopant reorientation and cation incorporation during the *in-situ* electrochemical reduction process. This effect was translated into surfactant-controlled surface energy gradient in the polymer for fluid movement of organic liquids, primarily dichloromethane, on the polymer surface upon in-situ redox switching. Dramatic and reversible changes in DCM shape and dimensions upon redox switching PPy.DBS were observed when both Pt sheet and Pt-PVDF were used as substrates. However, the predominant factor in this observed shape change was believed to be due to movement of minute amounts of DBS out of the polymer into the DCM upon reduction and incorporation back into the polymer during oxidation. Attempts to exploit this phenomenon for solutocapillary flow of DCM droplets were carried out; however, contact line pinning and spontaneous spreading of the surfactant across the DCM-electrolyte interface were believed to be responsible for impeding lateral translation of DCM drops. Further investigation into the factors influencing droplet translation, including substrate and polymer roughness, the ionic strength of the electrolyte and surface energy gradient in the polymer, should reveal the

conditions necessary to overcome droplet pinning and facilitate lateral droplet translation in practical devices

Implementation of polypyrrole into microfluidic devices for fluid control was reported in Chapter 5. Both channel-based and droplet-based configurations were considered. The dynamic wetting properties of oxidised (as-deposited) and chemically reduced PPy.DBS and polypyrrole doped with *p*-toluenesulfonate (PPy.pTS) were investigated using Wilhelmy balance tensiometry. Minimal change in the wetting properties of PPy.pTS were observed upon changing the polymer oxidation state, a fact attributed to the lack of complete expulsion of pTS upon reduction. Conversely, PPy.DBS underwent a significant increase in wettability upon reduction, rendering an investigation of its fluid control capabilities appropriate. The change in wettability of the polymer was exploited for surface-tension induced fluid movement in an open channel configuration. Application of a reducing potential caused the electrolyte to move along the polymer-coated channel, as a result of the increased hydrophobicity of the reduced PPy.DBS. The channel-based configuration allowed insight into some of the factors to be considered when utilising conducting polymers for fluid control in microdevices, such as electrode placement. Some microfluidic applications need to move liquids other than the electrolyte. Hence, a configuration utilising the integrated trilayer PPy.DBS-coated Pt-PVDF membrane investigated in Chapter 4 was modified to incorporate ionic liquid-based electrolytes which enabled the device to operate without the need for external electrolyte. Spreading of water drops resting on the polymer surface was observed upon reduction of PPy.DBS-coated Pt-PVDF employing the ionic liquid 1-ethyl-3-methylimidazolium bis(trifluoromethyl)sulfonylimide (EMI.TFSI) as an electrolyte; however, this effect was inconsistent and lateral translation of droplets was impeded by droplet pinning. PPy.DBS-coated Pt-PVDF membrane was implemented as a valve for

controlling the flow of electrolyte through the porous PVDF membrane by exploiting dramatic surfactant-induced change in DCM drop dimensions upon application of a small potential.

Coupling the interesting wetting properties of polyterthiophene, polypyrrole and indeed conducting polymers in general, with suitable electrolytes and device configurations, should lead to some interesting contributions to flow control techniques on the microscale, and be the source of much stimulating research in the area of fluid control in microfluidic devices in the future.

APPENDIX A

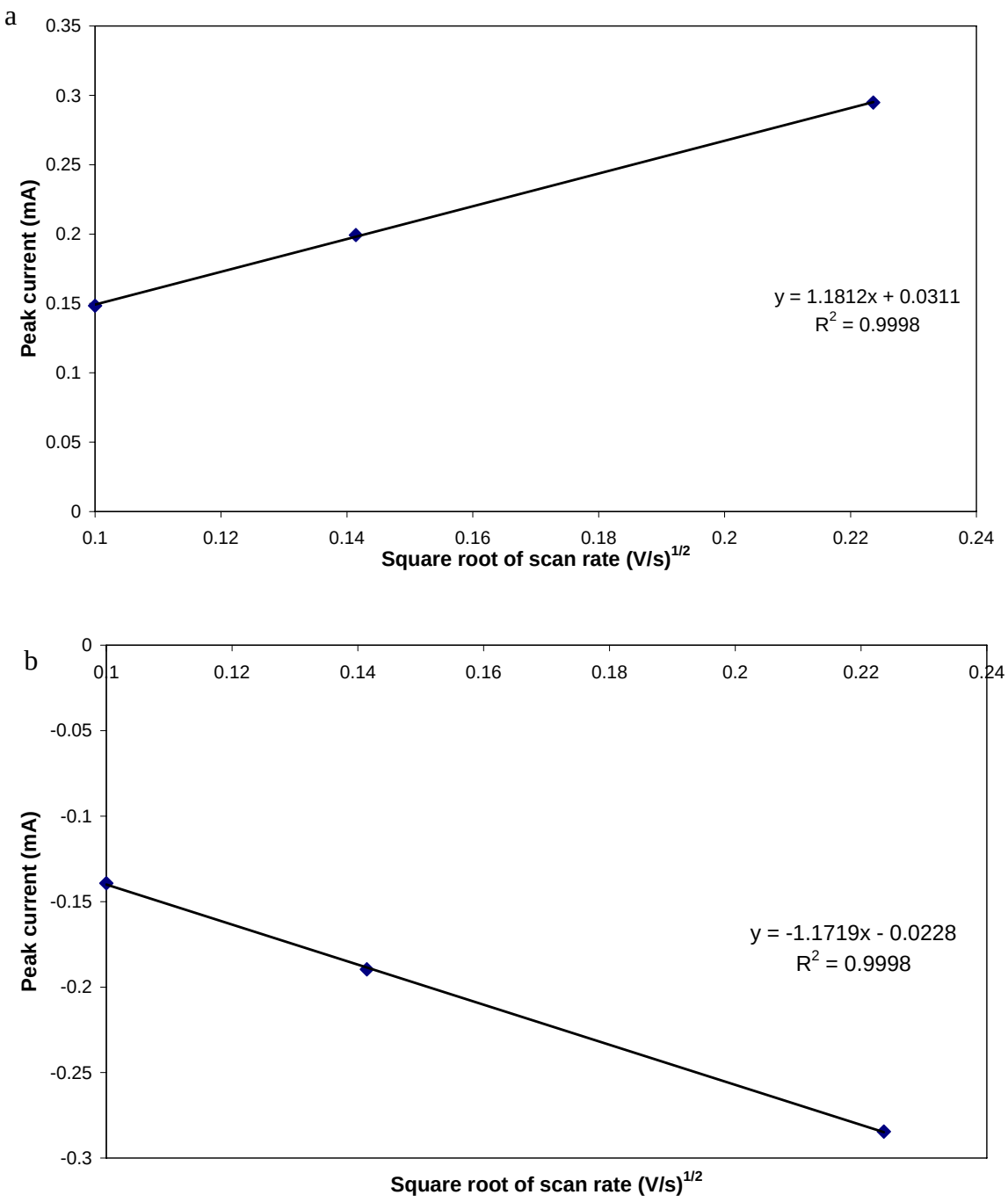

Figure 1. Square root of scan rate *vs* peak current for Pt disk electrode in a solution of degassed 0.2 M $NaNO_3$, 0.04 M $K_3[Fe(CN)_6]$ and 0.04 M $K_4[Fe(CN)_6]$. a. Anodic reaction. b. Cathodic reaction. The linearity of curves indicates the reactions at Pt disk are diffusion controlled.

APPENDIX B

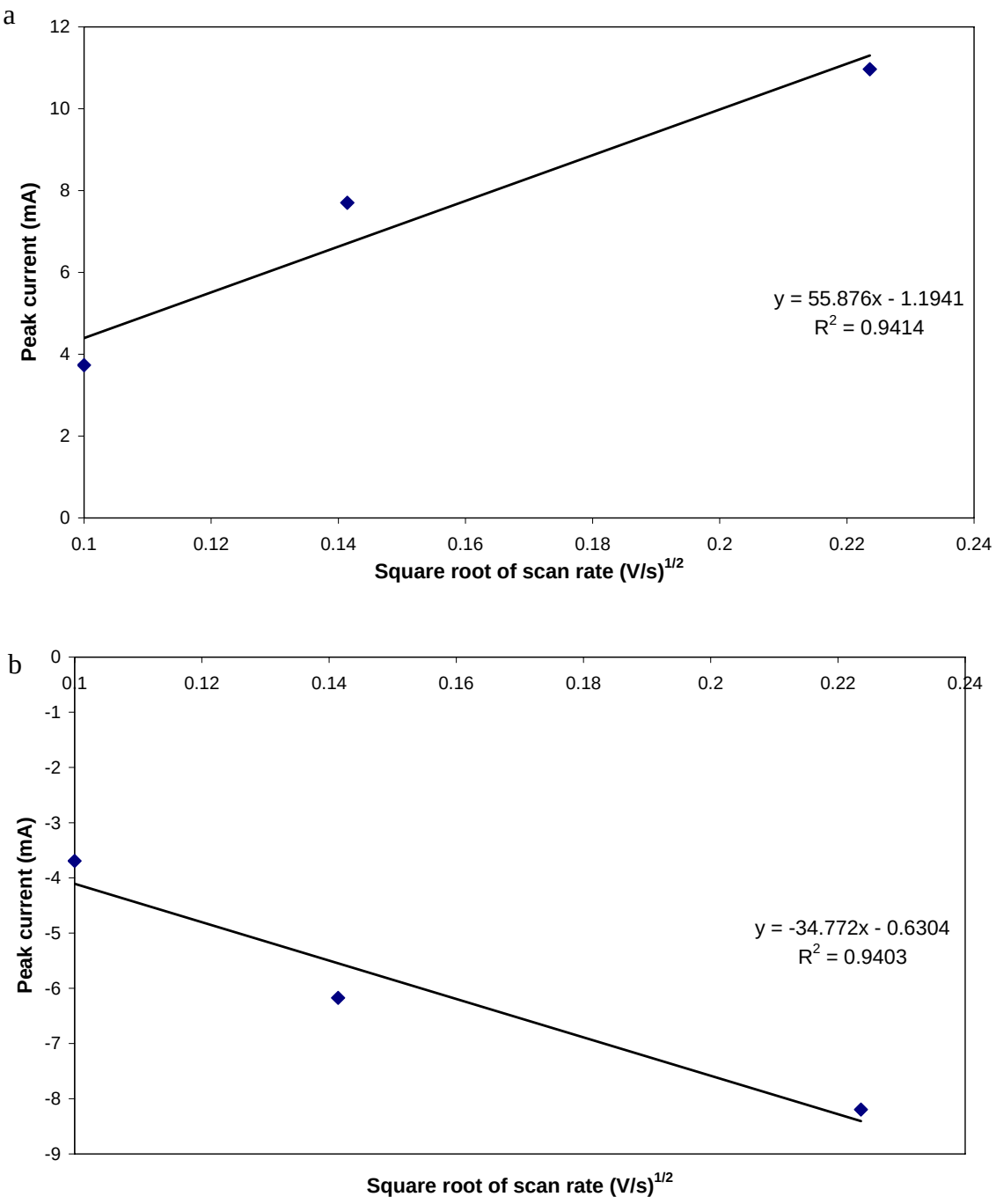

Figure 2. Square root of scan rate *vs* peak current for Pt-PVDF membrane working electrode in a solution of degassed 0.2 M $NaNO_3$, 0.04 M $K_3[Fe(CN)_6]$ and 0.04 M $K_4[Fe(CN)_6]$. a. Anodic reaction. b. Cathodic reaction. The deviation from linearity of the curves indicates the reactions at Pt-PVDF are controlled less significantly by difussion.

APPENDIX C

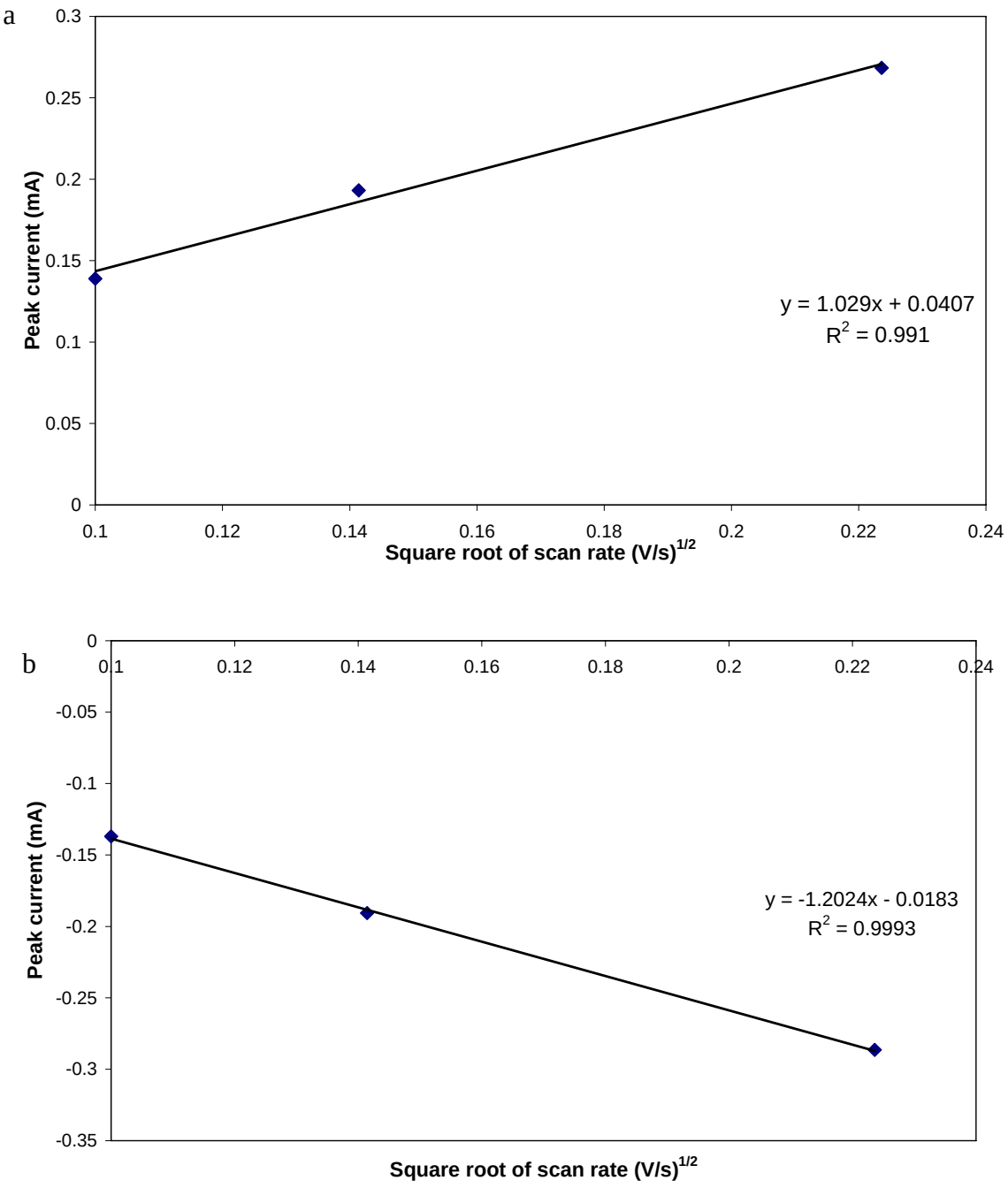

Figure 3. Square root of scan rate *vs* peak current for PPy.DBS-coated Pt disk electrode in a solution of degassed 0.2 M $NaNO_3$, 0.04 M $K_3[Fe(CN)_6]$ and 0.04 M $K_4[Fe(CN)_6]$. a. Anodic reaction. b. Cathodic reaction. The linearity of curves indicates the reactions at PPy.DBS-coated Pt disk are diffusion controlled.

APPENDIX D

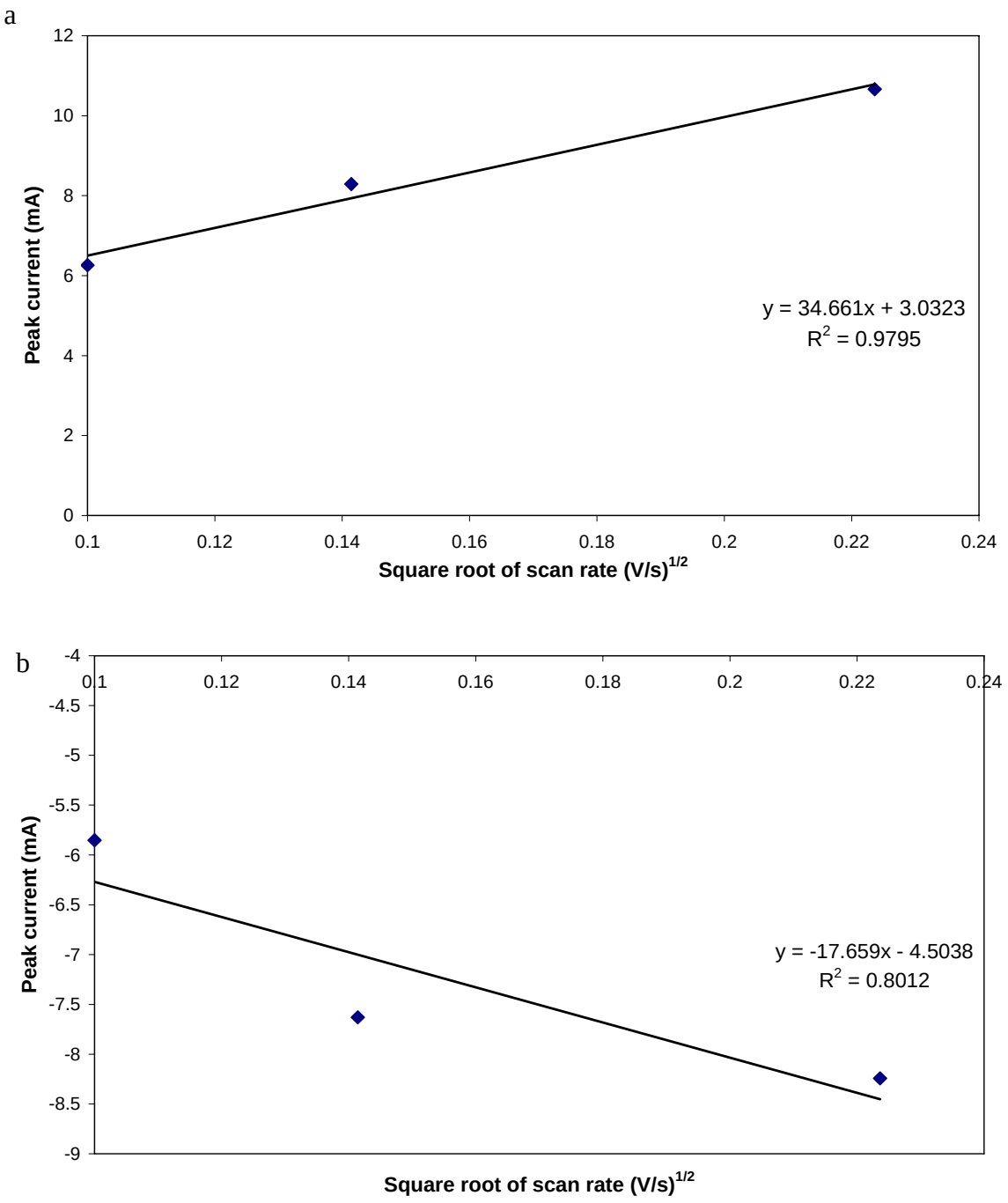

Figure 4. Square root of scan rate *vs* peak current for PPy.DBS-coated Pt-PVDF membrane working electrode in a solution of degassed 0.2 M $NaNO_3$, 0.04 M $K_3[Fe(CN)_6]$ and 0.04 M $K_4[Fe(CN)_6]$. a. Anodic reaction. b. Cathodic reaction. The deviation from linearity of the curves indicates the reactions at PPy.DBS-coated Pt-PVDF are controlled less significantly by diffusion.